

#### **Archive ouverte UNIGE**

https://archive-ouverte.unige.ch

Thèse 2024

**Open Access** 

This version of the publication is provided by the author(s) and made available in accordance with the copyright holder(s).

Finite-Time Processes In Quantum Thermodynamics: The Limits Of Irreversibility

-----

Rolandi, Alberto

#### How to cite

ROLANDI, Alberto. Finite-Time Processes In Quantum Thermodynamics: The Limits Of Irreversibility. Doctoral Thesis, 2024. doi: 10.13097/archive-ouverte/unige:180515

This publication URL: <a href="https://archive-ouverte.unige.ch/unige:180515">https://archive-ouverte.unige.ch/unige:180515</a>

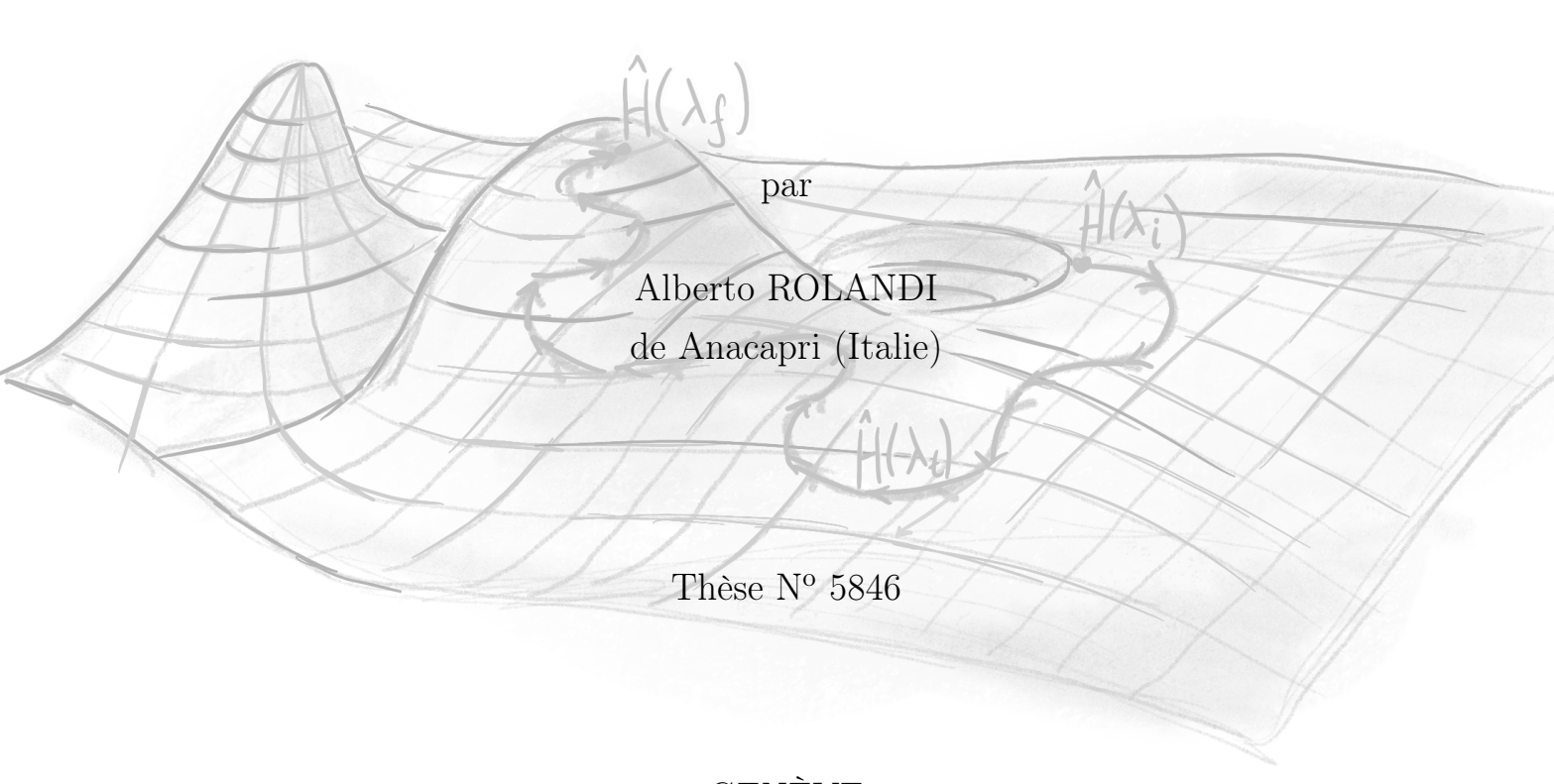
Publication DOI: <u>10.13097/archive-ouverte/unige:180515</u>

© The author(s). This work is licensed under a Creative Commons Attribution (CC BY 4.0) <a href="https://creativecommons.org/licenses/by/4.0">https://creativecommons.org/licenses/by/4.0</a>

# Finite-Time Processes In Quantum Thermodynamics: The Limits Of Irreversibility

#### THÈSE

présentée à la Faculté des sciences de l'Université de Genève pour obtenir le grade de Docteur ès sciences, mention physique



GENÈVE Centre d'impression Uni Mail

2024

Physics is like results, but the			ractical
		— Ric	hard Feyni
Everything we regarded as red	is made o	$f\ things\ t$	$hat\ cannot$
			— Niels E



#### DOCTORAT ÈS SCIENCES, MENTION PHYSIQUE

#### Thèse de Monsieur Alberto ROLANDI

intitulée :

«Finite-Time Processes In Quantum Thermodynamics: The Limits Of Irreversibility»

La Faculté des sciences, sur le préavis de

Monsieur N. BRUNNER, professeur ordinaire et directeur de thèse Département de Physique Appliquée

Monsieur M. PERARNAU-LLOBET, docteur et codirecteur de thèse Département de Physique Appliquée

Monsieur P. LIPKA-BARTOSIK, docteur Département de Physique Appliquée

Monsieur M. HUBER, professeur Faculty of Physics, TU-Wien, Vienna, Austria

Monsieur A. ACIN, professeur ICFO - The Institute of Photonic Sciences, Barcelona, Spain

autorise l'impression de la présente thèse, sans exprimer d'opinion sur les propositions qui y sont énoncées.

Genève, le 27 septembre 2024

Thèse - 5846 -

3. - La thèse doit porter la déclaration précédente et remplir les conditions énumérées dans les "Informations relatives aux thèses de doctorat à l'Université de Genève".

### Soutenue le 27 septembre 2024 devant le jury composé de:

Dr. Martí Perarnau-Llobet Prof. Nicolas Brunner Prof. Antonio Acín Prof. Marcus Huber Dr. Patryk Lipa-Bartosz

## Acknowledgements

First and foremost, I would like to express my unending gratitude to my supervisor Martí Perarnau-Llobet. Thank you for these amazing and formative four years. I cannot overstate how amazing it was to be supervised by someone like you: your planning, guidance, and trust played an ever so important role in making me the person and researcher I am today, for which I can be nothing but thankful.

To a great extent, this thesis is the result of wonderful teamwork and collaborations: Nicolas, Paolo (A), Paolo (E), Harry, Pavel, Kush, Yikai, Vasso, Tiff, and Sjaak; thank you all, you have my deepest gratitude for working with me.

Then I wish to thank my friends and colleagues from Geneva: Ivan, Lorenzo, Gianmichele, Flavio, Ophelia, Rafa, Joey, Mingsong, Maria, Yiorgos, Roope, Victor, Michael, Théo, Patryk, Bora, Alexandre, Giovanni, Rebecka, Sadra, Shishir, Geraldine, Sophie, Towsif, Javier, Davide, and Dmitry; it is difficult for me to express how important you have been in making me feel at home in this city.

I would also like to thank friends and researchers from around the world, from my time in Lausanne to my trips during my PhD, and including timeless friends. Whether it is for the support they gave me, the "good vibes", or the fruitful discussions: Aakash, Alesssandro, Andres, Antonia, Boris, Christian, Edgars, Eloic, Emilio, Evi, Fabian, Florian, Gabriel, Gabriele, Gerry, Hadrien, Hassan, Hendrik, Henrik, Jake, Jeanne, Kai, Kevin, Laetitia, Leonardo, Ludovico, Maja, Mark, Martina, Marzio, Matheus, Mathieu, Matteo, Michael, Nauris, Nicola, Noshin, Pierre, Quentin, Ricard, Tommaso, Victor, and Willem.

Finally, I would like to thank my parents and step-parents. To all of you, thank you for believing in me, thank you for supporting me from the very start. To Ariella and Mike, thank you for teaching me how to be critical of the world and of myself —

and how to be a somewhat practical person. Per Mamma e Papà, grazie per avermi introdotto a tutto quello che so, a come ragiono e come vedo il mondo. Grazie per avermi voluto sempre bene e grazie per avermi sempre guidato in qualsiasi avventura della mia vita. Non bastano parole per esprimere quanto io vi sia riconoscente...

### Abstract

The emergence of irreversibility in physical processes, despite the fundamentally reversible nature of quantum mechanics, remains an open question in physics. This thesis explores the intricate relationship between quantum mechanics and thermodynamics, with a particular focus on minimizing entropy production in finite-time processes. By employing tools from quantum information theory and geometric thermodynamics, we tackle the challenge of deriving irreversible thermodynamic behavior from the reversible microscopic framework of quantum mechanics.

We begin with a comprehensive review of the laws of thermodynamics, setting the stage for the subsequent analyses. We introduce novel developments in quantum thermodynamics through a generalized framework for geometric thermodynamics, which enables the derivation of finite-time corrections beyond the Markovian regime. Building on this foundation, we extend Landauer's principle by incorporating a finite-time correction that highlights the necessity of strong coupling for optimal information erasure processes. This result underscores the emergence of Planckian time as a fundamental speed limit to thermalization. Additionally, we explore how collective effects can be harnessed to reduce energy dissipation in thermodynamic operations, revealing that classical correlations between systems can significantly mitigate dissipation, though this may pose new questions regarding the third law of thermodynamics. Finally, we optimize thermodynamic processes in mesoscopic systems, including quantum dot engines and information engines.

These findings not only enhance our understanding of the fundamental limits of irreversibility but also open new avenues for research. Future works will focus on fully exploiting collective effects, aligning these with the third law of thermodynamics, and understanding the thermodynamic consistency of master equations.

## Résumé

L'émergence de l'irréversibilité dans les processus physiques, malgré la nature fondamentalement réversible de la mécanique quantique, demeure une question ouverte en physique. Cette thèse explore la relation complexe entre la mécanique quantique et la thermodynamique, en se concentrant particulièrement sur la minimisation de la production d'entropie dans les processus thermodynamiques en temps fini. En utilisant des outils de la théorie de l'information quantique et de la thermodynamique géométrique, nous abordons le défi de dériver un comportement thermodynamique irréversible à partir du cadre microscopique réversible de la mécanique quantique. Nous commençons par une revue complète des lois de la thermodynamique, établissant les bases pour les analyses suivantes. Nous introduisons des développements nouveaux en thermodynamique quantique à travers un cadre généralisé pour la thermodynamique géométrique, qui permet la dérivation de corrections en temps fini au-delà du régime Markovien.

En nous appuyant sur cette base, nous étendons le principe de Landauer en incorporant une correction en temps fini qui met en évidence la nécessité d'un couplage fort pour des processus d'effacement de l'information optimaux. De plus, nous explorons comment les effets collectifs peuvent être exploités pour réduire la dissipation d'énergie dans les opérations thermodynamiques, révélant que les corrélations classiques entre systèmes peuvent atténuer substantiellement la dissipation d'énergie. Enfin, nous optimisons les processus thermodynamiques dans les systèmes mésoscopiques, y compris les moteurs à points quantiques et les moteurs d'information. Ces résultats non seulement enrichissent notre compréhension des limites fondamentales de l'irréversibilité, mais ouvrent également de nouvelles pistes de recherche. Les travaux futurs se concentreront sur l'exploitation complète des effets collectifs, leur alignement avec la troisième loi de la thermodynamique, et la compréhension de la cohérence thermodynamique des équations maîtresses.

#### List of Relevant Publications

This thesis is based on the following works (by order of appearance).

- 1. Finite-time Landauer principle beyond weak coupling
  - A. Rolandi, M. Perarnau-Llobet.

```
Quantum 7, 1161 (2023).
```

2. Collective advantages in finite-time thermodynamics

```
A. Rolandi, P. Abiuso, M. Perarnau-Llobet.
```

```
Phys. Rev. Lett. 131, 210401 (2023).
```

3. Pareto-optimal cycles for power, efficiency and fluctuations of quantum heat engines using reinforcement learning

```
P. A. Erdman, A. Rolandi, P. Abiuso, M. Perarnau-Llobet, F. Noé. Phys. Rev. Research 5, L022017 (2023).
```

- 4. Optimal finite-time Szilard quantum dot engine
  - A. Rolandi, K. Aggarwal, Y. Yang, N. Ares, M. T. Mitchison, M. Perarnau-Llobet.

```
(In preparation)
```

Optimal control of dissipation and work fluctuations for rapidly driven systems
 A. Rolandi, M. Perarnau-Llobet, H. J. D. Miller.

```
New J. Phys. 25, 073005 (2023).
```

The following are works in which I took part during my PhD, but are not covered in the thesis.

- 1. Extensive Rényi entropies in matrix product states
  - **A. Rolandi**, H. Wilming. arXiv preprint (2020).
- 2. Proof of entanglement via dynamics exclusion in a quantum dots pair
  - **A. Rolandi**, V. Angelopoulou, T. Brydges, C. J. van Diepen, P. Sekatski. (In preparation)

# Contents

Acknowledgements						
$\mathbf{A}$	Abstract Résumé					
$\mathbf{R}$						
$\mathbf{R}$	eleva	nt Publications	vii			
1	Intr	roduction	1			
	The	sis Outline	3			
2	The	Laws of Thermodynamics	5			
	2.1	Thermodynamic Operations and Work	5			
	2.2	The First Law and the Definition of Heat	7			
	2.3	Equilibrium and the Second Law	9			
	2.4	The Third Law	14			
3	Ma	thematical Tools	17			
	3.1	Evolution of Quantum Systems	17			
	3.2	Geometric Thermodynamics	19			
		3.2.1 General Derivation of the Thermodynamic Metric	19			
		3.2.2 Minimally Dissipating Curves	23			
4	Fin	ite-Time Landauer Principle	25			
	4.1	Framework	27			
	4.2	The Resonant Level Model	28			
	4.3	Special Limits of the Metric	30			
		4.3.1 High Temperature Limit $(\beta \varepsilon, \beta \mu \ll 1)$	30			
		4.3.2 Zero Temperature Limit $(\beta \varepsilon \text{ or } \beta \mu \to \infty) \dots \dots \dots$	31			
		4.3.3 Weak Coupling Limit	32			

	4.4	Optimized Erasure	3
	4.5	Conclusions and Outlook	6
	4.6	Proof of Thermalization	8
		4.6.1 Infinite Time Limit in Absence of Driving	8
		4.6.2 Thermal Expectation Value	9
5	Col	ective Advantages 43	3
	5.1	Framework	4
	5.2	Fundamental Limit of Collective Advantages	6
	5.3	Collective Erasure	7
	5.4	Driven Many-Body Systems	9
	5.5	Conclusions and Discussion	1
6	The	rmodynamic Optimization 53	3
	6.1	Quantum Dot Heat Engine	5
		6.1.1 Multi-Objective Optimization of Heat Engines 5	7
		6.1.2 Optimal Quantum Dot Heat Engine	8
		6.1.3 Violation of Thermodynamic Uncertainty Relation 6.	2
	6.2	Szilard Engine	3
		6.2.1 Experiment	4
		6.2.2 Optimization of a Szilard Engine 6	5
		6.2.3 Results and Discussion 6	7
	6.3	Fast Operations	8
		6.3.1 Excess Work and Fluctuations	0
		6.3.2 Optimality of Instantaneous Jump Protocols	3
		6.3.3 Closed Quantum Systems	6
		6.3.4 Open Quantum Systems	9
	6.4	Conclusions	5
7	Cor	clusion and Outlook 89	9
Bi	ibliog	raphy 93	3

# Chapter 1

### Introduction

The more success the quantum theory has, the sillier it looks.

— Albert Einstein

One of the most puzzling open problems in physics is the emergence of irreversibility. The phenomena that we observe in the world around us are evidently irreversible. This irreversibility is even thought to be the origin of the arrow of time. However, at the microscopic scale the world is described by a reversible theory: quantum mechanics. It is difficult to overstate the success of quantum physics, which has led us to a better understanding of the most fundamental aspects of nature, enabling technological discoveries that revolutionized the world of computing, communication and medicine. Therefore, it is surprising that the irreversible processes that we observe at the macroscopic scale should emerge from the fundamentally reversible microscopic processes described by quantum mechanics – or more precisely, quantum electrodynamics. It is worth noting that, however, the theory of quantum mechanics was born in an attempt to describe a thermodynamic – and fundamentally irreversible – process: black-body radiation. Indeed, the origins of quantum mechanics are deeply rooted in thermodynamics: the quantization of light arises by imposing the thermodynamic consistency of Maxwell's equations [1].

Given this context, it is natural to ask if one can derive irreversibility – and more generally, the laws of thermodynamics – by starting from a microscopic and reversible theory like quantum mechanics. Indeed, foundational insights on the topic date back to the early days of quantum mechanics with the works of Von Neumann [2,3], which extend the works of Boltzmann in classical statistical mechanics to quantum mechanics. A key insight that they brought to our modern understanding of both quantum mechanics and thermodynamics is the role of *information* in

the two theories. Specifically, they illuminate how the lack of information on a system relates to entropy. Perhaps, the role of information for irreversibility is best exemplified by Landauer's principle [4], as it shows that the entropy of the universe increases when information is erased.

Since then, the question of defining entropy production and proving the irreversibility of thermodynamics starting from a reversible classical theory has been a central focus of the field of stochastic thermodynamics, which has developed modern mathematical tools to tackle the topic. Among its most impactful results are the fluctuation theorems [5,6], which generalize the laws of thermodynamics to non-equilibrium processes. These prove the validity of the second law of thermodynamics for a wide variety of scenarios.

In more recent years, with the advent of quantum information and a variety of experimental breakthroughs that have demonstrated an unprecedented level of control over quantum systems – such as trapped ions [7] and optomechanical systems [8] – the focus has increasingly shifted towards quantum thermodynamics. This emerging field, at the intersection of quantum information, stochastic thermodynamics, and many-body physics, has led to a variety of significant advancements ranging from the topic of the equilibration and thermalization of quantum systems to thermodynamic uncertainty relations. For instance, it has been demonstrated that small subsystems of a large pure quantum state can effectively evolve towards a thermal state under certain conditions, highlighting the robustness of thermalization in quantum settings. Moreover, the special role of the observer/external agent in both quantum mechanics and thermodynamics naturally leads to information-theoretic interpretations in quantum thermodynamics. In particular, irreversibility in thermodynamic processes is now understood as the loss of information about the state of the system.

The question of irreversibility is especially relevant for finite-time processes where the system is brought out of equilibrium and entropy production is thought to be always strictly positive. Indeed, the main goal of this thesis is to reach a better understanding on the gap between reversible processes with no entropy production and irreversible processes with finite entropy production. Therefore, it is in this context – and armed with quantum information theoretic tools – that we approach multiple aspects of the minimization of the entropy production of physical tasks.

#### Thesis Outline

In this thesis we start by presenting a self-contained review on the laws of thermodynamics in Chapter 2. We then present the mathematical formalism that is used in the rest of the thesis. In particular, in Sec. 3.2 we generalize the results of [9] to obtain a derivation of the thermodynamic geometry technique that applies to all types of dynamics – i.e. for both open and closed quantum systems; thus giving a formal setting for the work minimization of thermodynamic protocols in the slow-driving regime, which is used multiple times in the rest of the thesis.

In Chapter 4 we apply this extended formalism to obtain a finite-time correction to Landauer's bound on the dissipated energy required to erase information. While previous works obtaining a finite-time correction to the bound already existed, these were limited to the Markovian regime [9–11]. The main result of the chapter eq. (4.2) is valid beyond such approximations [12]. Indeed, it unveils the need for strong coupling for the optimal energy management of erasure processes. Furthermore, despite the result being derived in a specific setting, it reveals the general form of a universally valid finite-time correction to Landauer's bound with the emergence of *Planckian time*.

Remarkably, the results of Chapter 5 show how one can use the framework of geometric thermodynamics to unveil a novel type of collective effects that allow to drastically reduce the amount of energy that is dissipated when performing a task on a collection of systems simultaneously [13]. Collective effects are a well known and important phenomenon in physics, ranging from phase transition to quantum entanglement [14–18]. It is often the case that one can exploit these effects to improve the result or cost of a given task, leading to a notion of collective advantages: the outcome of a task is improved when performed globally on a collection of systems instead of each system individually. Indeed, our results show that if one wishes to perform multiple tasks on multiples systems, then it is possible to exploit classical correlations between these systems to drastically suppress the amount of energy that is dissipated into the environment. To put it simply, one manages to "share the losses" between the individual systems. With sufficient amount of control, this suppression is strong enough to obtain a vanishing dissipation per system in the thermodynamic limit. This is an astounding result, as it seems to go counter to the third law of thermodynamics, but on a technical level there seems to be no contradiction as the remaining finite-time dissipation is always strictly positive.

Finally, in Chapter 6 we focus on the thermodynamic optimization of mesoscopic systems. We show how to fully optimize two types of nano-scale thermal engines and fast operations on a system. The optimization of thermal engines and, more generally, operations at the nano-scale are questions that allows us to probe the fundamental limits of the trade-offs between relevant physical costs and desiderata [19–23]. In steady state heat engines, these trade-offs are captured by thermodynamic uncertainty relations [21, 24]. First, we study how one can fully optimize all the relevant thermodynamic aspects of the simplest possible thermal engine: a periodically driven quantum dot engine [25]. Indeed, with the use of analytical techniques and reinforcement learning we characterize the optimization trade-off of power, efficiency and power fluctuations of a quantum dot engine in all driving regimes. Second, we characterize and optimize the performance of an information engine at all driving speeds. Information engines stand in a class of their own, as they make use of measurements on the system instead of a cold reservoir. Furthermore, we confirm the feasibility of the optimal protocols we compute with an experimental implementation thanks to the collaboration of the group of prof. N. Ares. Last, but not least, we develop a general framework for the optimization of work and work fluctuations in rapidly driven systems [26]. Our results show that optimal fast protocols, in both open and closed system dynamics, consist of two instantaneous jumps in the control parameters – one at start and one at the end of the protocol. Interestingly, this is true whether we are aiming to optimize work or work fluctuations – or any trade-off of the two quantities, but it is seldom the case that the optimal "jump point" is the same for both objectives. We showcase this phenomenon by applying the framework to compute the optimal fast protocols across phase transitions of many-body quantum systems.

In Chapter 7 we conclude on the presented work and reflect on the future perspectives of research that were opened by this thesis.

## Chapter 2

# The Laws of Thermodynamics

The law that entropy always increases holds, I think, the supreme position among the laws of Nature. If someone points out to you that your pet theory of the universe is in disagreement with Maxwell's equations – then so much the worse for Maxwell's equations. If it is found to be contradicted by observation – well, these experimentalists do bungle things sometimes. But if your theory is found to be against the second law of thermodynamics I can give you no hope; there is nothing for it but to collapse in deepest humiliation.

— Sir Arthur Eddington, The Nature of the Physical World

### 2.1 Thermodynamic Operations and Work

One of the main objectives of Thermodynamics is to describe flows of energy in a physical process [27]. This question is so general that it can be applied to any field of physics, which makes thermodynamics a so-called "universal" theory. Before stating the laws of thermodynamics, we will define what is an "operation" in the thermodynamic sense. In a typical thermodynamic setting one is studying a system S with a set of parameters that can be controlled by an external agent. For example, if we consider the gas in a piston (cf. Fig. 2.1), an agent can control the volume of this gas by moving the piston rod. Another example – in the world of Quantum Mechanics – would be an electron in the magnetic field of an experiment.

We define a thermodynamic operation as the changing of one or more parameters of the system from an initial value to a final value – which could be the same as the initial value. It is worth noting that any physical process could be framed as a

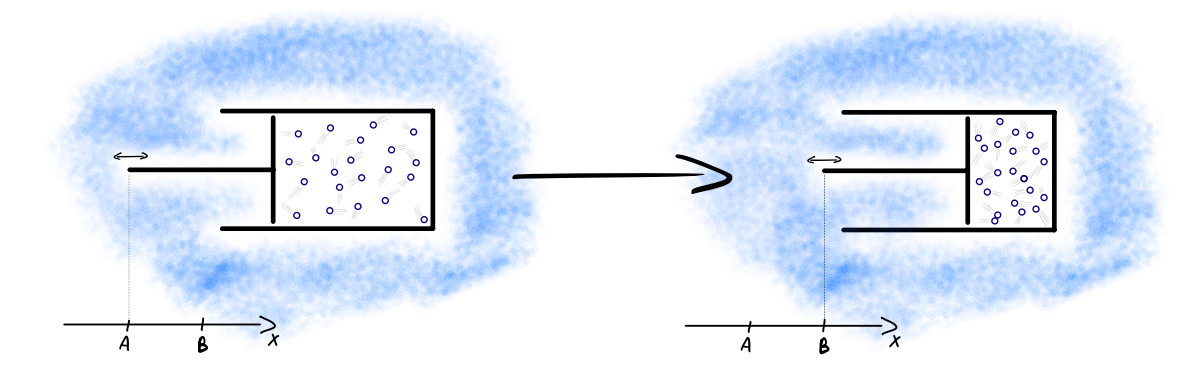


Figure 2.1: Example of a thermodynamic operation: compressing a piston. The studied system is a gas of N particles inside a piston. The whole system is in an environment that is depicted in blue. On the left we have the gas in its initial state with the piston in position A and on the right the gas after the piston has been compressed to position B, reducing the volume of the system.

thermodynamic operation. In Fig. 2.1 we give a typical textbook example of such a task: the compression of a gas in a piston. In mathematical terms, this corresponds to changing the Hamiltonian of the system S from its initial value  $\hat{H}_i$  to its final value  $\hat{H}_f$ . We will be calling *protocol* the function  $\hat{H}(t)$  that describes how this change is implemented. This leads naturally to the following definition:

**Definition 1** (Thermodynamic Work). The thermodynamic work W of an operation on a system S is the amount of energy that the agent has to spend in order to perform the aforementioned operation on the system S.

If we denote by  $\hat{\rho}_{tot}(t)$  and  $\hat{H}_{tot}(t)$  the state and Hamiltonian of the system and everything that it is interacting with – except the agent – we have a very natural definition for the expected value of work

$$\langle W \rangle = \text{Tr} \left[ \hat{\rho}_{tot}(\tau) \hat{H}_{tot}(\tau) - \hat{\rho}_{tot}(0) \hat{H}_{tot}(0) \right] ,$$
 (2.1)

where we denoted by  $\tau$  the amount of time it took to perform the operation. The study of work and how to minimize it is a central question in thermodynamics. Typically, one can expect the work cost to increase for decreasing values of  $\tau$  and to decrease for increasing values of  $\tau$ . In fact, one can show that the work cost is minimal when  $\tau$  goes to infinity (cf. Sec. 2.4). Since we will be treating stochastic systems throughout this thesis and will never explore single shot scenarios, we will only be speaking of the expected work cost  $\langle W \rangle$  instead of the work cost W. Therefore, to lighten the notation and text, we will drop the average symbol  $\langle \cdot \rangle$  for this quantity and will be writing "work cost" implying that the average has been taken.

#### 2.2 The First Law and the Definition of Heat

As in the example shown in Fig. 2.1, during a thermodynamic operation one can distinguish three parties that are involved: an agent, the system being described, and the environment. If one considers the energy flow that happens between these three parties during a thermodynamic operation then, by conservation of energy, when the agent provides  $\delta W$  of energy it is split between the system and the environment.

The First Law of Thermodynamics. During a thermodynamic operation, the following holds by conservation of energy

$$\delta W = dE + \delta Q , \qquad (2.2)$$

where  $\delta W$  is the amount of energy provided by the agent during an infinitesimal amount of time dt, dE is the energy gained by the system S and  $\delta Q$  is the energy gained by the environment.

Typically one identifies the environment as "whatever is not the system and is interacting with it". This usually coincides with something that cannot be controlled by the agent – or at least not as well as the system. Therefore the energy that is gained by the environment cannot be directly accessed anymore by the agent. Which leads us to another definition:

**Definition 2** (Heat). The heat

$$Q := W - \Delta E \tag{2.3}$$

of an operation is the amount of energy that the environment has gained when the agent performed a thermodynamic operation on a system S – which gained  $\Delta E$  of energy<sup>1</sup>.

It is interesting to note that by defining a different cut between what is being studied and what is the environment, one gets a different definition of heat. Which might make it seem arbitrary, but this a fundamental feature of thermodynamics

<sup>&</sup>lt;sup>1</sup>This partition of the energy is omitting any amount of energy that is stored in the interaction between system and environment. In all the scenarios we will study, the interaction energy at the start and end of the process will be the same, thus allowing us to write the energy balance as in Definition 2. This is still a lively topic in the community, see [28] for a summary.

that ties it to information-theory. By distinguishing between what can and cannot be acted upon by the agent, we are making an information-theoretic statement. And by applying conservation of energy to this statement we obtain the first law of thermodynamics. Therefore we can see that, at least partially, the first law of thermodynamics is an information-theoretic statement.

If we denote by  $\hat{\rho}(t)$  the state of the system S at a time t and its Hamiltonian by  $\hat{H}(t)$ , then its expected energy is given by  $E(t) = \text{Tr}\left[\hat{\rho}(t)\hat{H}(t)\right]$ . If we differentiate this expression in time we get

$$\frac{dE}{dt} = \text{Tr}\left[\hat{\rho}(t)\frac{d\hat{H}(t)}{dt}\right] + \text{Tr}\left[\frac{d\hat{\rho}(t)}{dt}\hat{H}(t)\right] . \tag{2.4}$$

By using the first law eq. (2.2) and the definition of work, we can identify that work corresponds to the term with the change in the Hamiltonian:  $\delta W = \text{Tr} \left[ \hat{\rho}(t) \hat{H}'(t) \right]$ , where we used ' to denote the time derivative to lighten the notation. One can recover this term by taking the time derivative of eq. (2.1), but it can be also understood as the term that the agent has control over. This leads to the two integral formulas for the work and heat of a process

$$W = \int_0^{\tau} dt \operatorname{Tr} \left[ \hat{\rho}(t) \frac{d\hat{H}(t)}{dt} \right] , \qquad (2.5)$$

$$Q = -\int_0^{\tau} dt \operatorname{Tr} \left[ \frac{d\hat{\rho}(t)}{dt} \hat{H}(t) \right] . \tag{2.6}$$

It is worth noting that these integral forms are not fully rigorous – despite being widely used – as they do not give the proper result in the case one introduces discontinuities at the start and end of the protocol. In particular, if we imagine a protocol where at t=0 there is a sudden change in the Hamiltonian – which we will call quench going forward – then the integral in eq. (2.5) will give an erroneous 1/2 factor to the term corresponding to the quench. However this can be easily "fixed" if we keep in mind that the true boundaries of the integrals in eq. (2.5) and eq. (2.6) are  $-\varepsilon$  and  $\tau + \varepsilon$  in the limit that  $\varepsilon$  tends to  $0^+$ .

### 2.3 Equilibrium and the Second Law

And on the pedestal these words appear:
"My name is Ozymandias, King of Kings:
Look on my works, ye Mighty, and despair!"
No thing beside remains. Round the decay
Of that colossal wreck, boundless and bare
The lone and level sands stretch far away.

— Percy Shelley, Ozymandias

As opposed to Maxwell's equations, the second law of thermodynamics is still today a source of lively arguments and discussion. The core physical phenomenon it addresses is the presence of irreversible phenomena in the macroscopic world – e.g. the mixing of liquids – despite the time-symmetry of the underlying physical laws. On the fundamental side, the second law has deep ties to the emergence of the arrow of time. While on a more practical aspect, together with the first law it is essential for the design of thermal engines, power plants, and the analysis of chemical reactions [29]. It was first stated by Clausius in 1865 as "Heat can never pass from a colder to a warmer body without some other change, connected therewith, occurring at the same time" [30]. It is important to note that this is a law of averages: it does not forbid the transfer of energy from a cold body to a warmer body in a single instance, but rather it states that the energy transfer is more likely in a direction than the other. The comparison of the probability of an energy transfer occurring in one direction or the other is a well studied subject in the context of fluctuation theorems [29].

The formulation of Clausius has been changed into many forms since he stated it, but today the most common statement of the second law of thermodynamics is in terms of *entropy production*.

The Second Law of Thermodynamics. The entropy production of a thermodynamic operation is non-negative

$$\Sigma \ge 0 \ . \tag{2.7}$$

Before defining entropy production, we will introduce a few concepts that build up to it. Clearly, the first of these concepts should be entropy. Entropy is an information-theoretic quantity that captures the lack of knowledge that an observer has on the system – in this context the thermodynamic agent is the observer. This abstract notion of "lack of knowledge" can be exemplified by Gibbs' definition of entropy:  $S = \ln \Omega$ , where  $\Omega$  is the number of (equally likely) configurations of the system that are compatible with the knowledge of the observer. With this definition we have a natural operational interpretation of the entropy of a system: it is the minimal amount of information (in number of bits) that we need to measure about the system to pin down the specific configuration of the system. For quantum systems we will be using a more general definition of entropy:

**Definition 3** (von Neumann Entropy). The von Neumann entropy of a system described by the state  $\hat{\rho}$  is given by

$$S(\hat{\rho}) := -\text{Tr}\left[\hat{\rho}\ln\hat{\rho}\right] . \tag{2.8}$$

It is worth noting how the von Neumann entropy reduces to the Gibbs definition of entropy when we have a uniform mixture between  $\Omega$  orthogonal states. Furthermore, this definition carries the same operational interpretation about "lack of information". In particular, it is minimal (equal to zero) if and only if the state is pure, and it is maximal if and only if the state is fully mixed.

The concept of entropy allows us to define a notion of "usefulness" of a state. To illustrate this, let us consider two scenarios of a gas with many particles. First suppose that we have no information on the state of the gas. This would imply that we describe the state of the gas with a completely mixed density matrix, which has maximal entropy. Because of our lack of information on the gas, there is no operation we can do to extract energy from it in a repeatable way. In the second scenario, suppose that thanks to some sophisticated measurement apparatus we acquired the information about the position and momentum of every particle in the gas. Therefore we can now describe the state of the gas with a pure state, which has zero entropy. Since we know the position and velocity of every particle in the gas, we can compute their future trajectories. And therefore, in principle, we could make a very contrived machine that extracts all of the kinetic energy from each gas particle and make use of all of the energy available. Since in both scenarios the energy of the system can be the same, but in one we can reliably extract all of it as opposed to the other, we naturally reach a notion of "useful energy", which is captured by the following definition.

**Definition 4** (Non-Equilibrium Free Energy). The non-equilibrium free energy  $F_{n.eq}(\hat{\rho})$  of a system  $\hat{\rho}$  with Hamiltonian  $\hat{H}$  is defined as

$$F_{n.eq}(\hat{\rho}) := \text{Tr}[\hat{\rho}\hat{H}] - k_B T S(\hat{\rho}) , \qquad (2.9)$$

where  $k_B$  is the Boltzmann constant and T is the temperature<sup>2</sup>.

With this definition, one can interpret the second law as a statement about how, over time, we have less and less free energy available in the system, until the entropy is maximized and the system is "useless". We then say that the system has reached equilibrium. For a given Hamiltonian and a given temperature there is a unique equilibrium state:

**Definition 5** (Gibbs state). For a system at temperature T with Hamiltonian  $\hat{H}$ , its equilibrium state is given by the *canonical ensemble*, also known as *Gibbs state* 

$$\hat{\pi} := \frac{e^{-\beta \hat{H}}}{\text{Tr}[e^{-\beta \hat{H}}]} , \qquad (2.10)$$

where  $\beta := 1/k_BT$  is the *inverse temperature*, and the normalization defines the partition function  $Z = \text{Tr}[e^{-\beta \hat{H}}]$ .

We can use this definition to rewrite the non-equilibrium free energy of a state  $\hat{\rho}$  in terms of the Gibbs state of the Hamiltonian

$$F_{n.eq}(\hat{\rho}) = F_{n.eq}(\hat{\pi}) + S(\hat{\rho}||\hat{\pi}) ,$$
 (2.11)

where  $S(\hat{\rho}||\hat{\pi}) := \text{Tr}[\hat{\rho}(\log \hat{\rho} - \log \hat{\pi})] \geq 0$  is the relative entropy. Since  $\text{Tr}[\hat{\rho}(\log \hat{\rho} - \log \hat{\pi})] = 0$  if and only if  $\hat{\rho} = \hat{\pi}$ , it is clear that Gibbs states minimize the free energy. And thus shows how Gibbs states correspond to the aforementioned notion of equilibrium state, which we will also refer to as thermal state. It is also worth noting that for a given expected energy and temperature, it also follows that Gibbs states maximize the entropy. In the jargon of resource theory, thermal states are also known as the only completely passive states [32]. This notion of equilibrium leads to a state-independent notion of free energy: the equilibrium free energy  $F_{eq} := F_{n.eq}(\hat{\pi}) = -k_B T \ln Z$ .

<sup>&</sup>lt;sup>2</sup>Here the temperature can be defined as  $k_B^{-1}\partial E/\partial S$ . However it is worth noting that often it coincides with the temperature of the environment with which the system is interacting. See [31] for a more detailed discussion.

At this point, one might be (very) tempted to take the change in von Neumann entropy of the state describing the system and environment as entropy production. However, von Neumann entropy is invariant under unitary transformations. Therefore the von Neumann entropy of a closed system remains constant when it evolves by the rules of quantum mechanics. Which means that we need to take a different approach to define entropy production.

The notion of "usefulness" given by the free energy is actually the key here: in a thermodynamic operation all the energy that can be recovered if we were to immediately revert the operation corresponds to changes in free energy. Therefore we can split the work of a thermodynamic operation as follows

$$W = \Delta F_{n.eq} + W_{diss} , \qquad (2.12)$$

where  $\Delta F_{n.eq} = F_{n.eq}(\hat{\rho}_S(\tau)) - F_{n.eq}(\hat{\rho}_S(0))$  is the difference in free energy of the system: the reversible component of work, and  $W_{diss}$  is the dissipated energy: the irreversible component of work – and is defined as the difference between work and free energy change. We also defined the reduced state  $\hat{\rho}_S := \text{Tr}_E[\hat{\rho}_{SE}]$ , that describes the state of the system S when one does not have knowledge of the total state of the system and environment together  $\hat{\rho}_{SE}$ . This leads us to a very natural definition of entropy production:  $\Sigma = \beta W_{diss}$ . With this definition one could already express the second law of thermodynamics as  $W \geq \Delta F_{n.eq}$ . Using eq. (2.12) with Definition 4 and Definition 2 we obtain a very common formulation of entropy production and the second law

$$\Sigma = \beta Q + \Delta S \ge 0 , \qquad (2.13)$$

where  $\Delta S = S(\hat{\rho}_S(\tau)) - S(\hat{\rho}_S(0))$  is the change of entropy of the system, and  $\beta$  is the inverse temperature of the environment. The term  $\beta Q$  corresponds to a flow of entropy from the system towards the environment. It is worth noting how the second law allows for a reduction in entropy of the system, as long as it is compensated with a sufficient flow of entropy into the environment (cf. Chapter 4). There are many situations in which it is not immediate to assign a unique temperature to the environment – e.g. an engine. However, one can always divide the environment into multiple uncorrelated parts  $E_1, ..., E_n$  and assign a temperature  $T_i$  to each of these parts [33]. In this case, one looses a clear definition of non-equilibrium free energy, because depending on the configuration of the system and environments there is not necessarily an equilibrium state towards which the state naturally evolves – e.g. non-equilibrium steady states [34]. Since the entropy is additive between independent

systems, each environment contributes  $\beta_i Q_i$  to the entropy production. Which allows us to generalize eq. (2.13) to

$$\Sigma = \sum_{i} \beta_{i} Q_{i} + \Delta S \ge 0 . \tag{2.14}$$

One often assumes that at the start of the process the environment – or each of its subdivisions – is at thermal equilibrium and uncorrelated to the system, which allows us to rewrite  $\Sigma$  in terms of information theoretic quantities

$$\Sigma = I_{\tau}(S:E) + S(\hat{\rho}_E(\tau)||\hat{\pi}_E) , \qquad (2.15)$$

where  $I_t(S:E) := S(\hat{\rho}_{SE}(t)||\hat{\rho}_S(t) \otimes \hat{\rho}_E(t))$  is the mutual information, which quantifies the amount of information that is stored in the correlations between system and environment, which is lost when one has lo longer access to either E or S. And the relative entropy  $S(\hat{\rho}_E||\hat{\pi}_E)$  quantifies how much the environment was "pushed away" from the equilibrium<sup>3</sup>. It is interesting to note how eq. (2.15) shows clearly this notion of the entropy production matching the concept of "lost information". Furthermore, since the quantities in eq. (2.15) are non-negative, the second law is mathematically proven for thermal environments.

Going back to processes where the system interacts with a single bath at temperature T, very often one also assumes that also the system is initialized in a thermal state. For these situations, usually the system is also left to thermalize after the operation is over at time  $\tau$ . And therefore the "useful energy" that is in the system at time  $\tau$  is also dissipated, which leads to the following definition of dissipation

$$k_B T \Sigma = W - \Delta F_{eq} . (2.16)$$

It is worth noting that  $W - \Delta F_{n.eq} = W - \Delta F_{eq} - k_B T S(\hat{\rho}_S(\tau)||\hat{\pi}_S(\tau)) \leq W - \Delta F_{eq}$ , where the difference is exactly entropy associated to the leftover free energy of the system at the end of protocol.

Finally, we will briefly cover a different approach to defining dissipation, which is purely information-theoretic. The main idea stems from finding a generalization of eq. (2.15). Starting from an initially uncorrelated system and environment, if

<sup>&</sup>lt;sup>3</sup>Strictly speaking the relative entropy is not a distance because it does not respect the triangular inequality. However it is non-negative, and equal to zero if and only if the two entries are equal.

14 2.4. The Third Law

one considers the amount of lost information during the thermodynamic process, then there are two contributions: the correlations generated between the system and environment, and the perturbation of the environment [35]. Which leads to the following definition

$$\Sigma = I_{\tau}(S:E) + S(\hat{\rho}_{E}(\tau)||\hat{\rho}_{E}(0)) , \qquad (2.17)$$

which coincides with eq. (2.15) when the environment – or its sub divisions – is assumed to start in a thermal state. However, the downside of this approach is that it is not equivalent to eq. (2.14) as these expressions do not coincide whenever the assumption of a thermal environment is not satisfied.

#### 2.4 The Third Law

The third law of thermodynamics has been formulated in many different forms over the years and the subject of intense discussions [36]. Unlike the second law, a fully general proof of the third law – or as general as the second law – is still lacking [37,38]. The first formulation, given by Nernst, is now known as the heat theorem. It states "At zero temperature, a finite size system has an entropy S, which is independent of any external parameters x, i.e.  $\lim_{T\to 0} S(T,x_1) - S(T,x_2) = 0$ ." [39]. However, in quantum mechanics it is clear that the zero-temperature entropy is equal to the logarithm of the ground state degeneracy. Therefore the validity of the heat theorem is dependent on the possibility of changing this degeneracy with the parameter x. Today, the third law is understood as Nernst's unattainability principle [39].

The Third Law of Thermodynamics. It is impossible to bring a system into its ground state without either *infinite time*, *infinite energy*, or *infinite complexity*.

This version of the third law – that includes complexity as a resource – is based on the most recent advances of the field [40]. However, one can find a mathematical formulation of it in [37] and [38]. In quantum mechanics the third law implies that it is impossible to prepare a pure state without one of the three aforementioned quantities going to infinity.

An interesting consequence of the third law is that the second law eq. (2.7) can only be saturated when the work, heat, complexity, or time diverge. In particular, when the time of the operation  $\tau$  goes to infinity, then the system is at all times in the instantaneous equilibrium state – typically given by  $\hat{\pi}(t)$ . Therefore the work

cost of the operation will be given exactly by the free energy change, which implies that the dissipation is exactly  $\Sigma=0$ . In this case we say that the operation is reversible. Conversely, for  $\tau<\infty$ , whenever we change the Hamiltonian the system will be pushed away from its equilibrium state. Which implies that there will be a non-zero dissipation  $\Sigma>0$ , and we say that the operation is irreversible.

# Chapter 3

## Mathematical Tools

Ludwig Boltzmann, who spent much of his life studying statistical mechanics, died in 1906 by his own hand. Paul Ehrenfest, carrying on the work, died similarly in 1933. Now it is our turn to study statistical mechanics.

— David Goodstein, States of Matter

### 3.1 Evolution of Quantum Systems

The evolution of a quantum system described by a state  $\hat{\rho}$  is given by a the dynamical equation

$$\frac{d}{dt}\hat{\rho}(t) = \mathcal{G}_t[\hat{\rho}(t)] , \qquad (3.1)$$

where  $\mathcal{G}_t$  is the time-dependent generator of the dynamics. The solution of this equation is given by

$$\hat{\rho}(t) = G(t,0)[\hat{\rho}(0)] \tag{3.2}$$

where  $G(t,t')[\cdot]$  is a completely positive trace preserving map known as the propagator of the dynamics from t' to t. It is defined as

$$G(t,t') := \overleftarrow{\mathcal{T}} \exp\left[\int_{t'}^{t} ds \ \mathcal{G}_s\right] ,$$
 (3.3)

where we introduced the *time ordering operator*  $\overleftarrow{\mathcal{T}}$ . The exponential operator is defined via its usual series; that, when expanded, yields the Dyson expansion

$$G(t,t') = 1 + \sum_{n=1}^{\infty} \int_{t'}^{t} dt_n \int_{t'}^{t_n} dt_{n-1} \dots \int_{t'}^{t_2} dt_1 \, \mathcal{G}_{t_n} \circ \mathcal{G}_{t_{n-1}} \circ \dots \circ \mathcal{G}_{t_1} , \qquad (3.4)$$

where  $\mathbb{I}$  denotes the identity super-operator, and  $\circ$  denotes the map composition.

When we consider an isolated quantum system – in the thermodynamic setting this is the case when we consider a system together with its environment – then its evolution is described by unitary dynamics:  $\mathcal{G}_t[\cdot] = \frac{-i}{\hbar}[\hat{H}(t), \cdot]$ . Therefore eq. (3.1) reduces to

$$\frac{d}{dt}\hat{\rho}(t) = \frac{-i}{\hbar} \left[ \hat{H}(t), \hat{\rho}(t) \right] . \tag{3.5}$$

The solution of this equation leads to the unitary evolution of the system

$$\hat{\rho}(t) = \hat{U}(t)\hat{\rho}(0)\hat{U}^{\dagger}(t) , \qquad (3.6)$$

where the unitary operator is given by

$$\hat{U}(t) = \overleftarrow{\mathcal{T}} \exp\left[-\frac{i}{\hbar} \int_0^t ds \ \hat{H}(s)\right] , \qquad (3.7)$$

which has a similar expansion as in eq. (3.4).

Taking the typical thermodynamic scenario, we are often only interested in describing the dynamics of the system without the environment. In this case the evolution of the system alone is naturally given by

$$\hat{\rho}_S(t) = \text{Tr}_E \left[ \hat{U}(t) \hat{\rho}_{SE}(0) \hat{U}^{\dagger}(t) \right] . \tag{3.8}$$

This problem is can still be very challenging to solve analytically, in particular when the traced out part is large, which is typically the case for the environment. However, one can usually make two approximations that greatly simplify eq. (3.8): first, that the environment is well described by a thermal state at the start of the evolution  $\hat{\rho}_{SE}(0) = \hat{\rho}_S(0) \otimes \hat{\pi}_B$ . Second, that the interaction between system and environment is weak and Markovian. It is worth noting that this second approximation is often made also in classical thermodynamics, where the interactions between system and environment are attributed to boundary effects. With these two approximations one can simplify the the time derivative of eq. (3.8) to the famed Lindblad master equation (c.f. [41] for a detailed derivation)

$$\frac{d}{dt}\hat{\rho}_S(t) = \mathcal{L}[\hat{\rho}_S(t)] , \qquad (3.9)$$

where  $\mathcal{L}$  is the *Lindbladian*. It is defined as

$$\mathcal{L}[\hat{\rho}_S(t)] := \frac{-i}{\hbar} \left[ \hat{H}_S(t), \hat{\rho}_S(t) \right] + \sum_i \gamma_i \left( \hat{L}_i \hat{\rho}_S(t) \hat{L}_i^{\dagger} - \frac{1}{2} \left\{ \hat{L}_i^{\dagger} \hat{L}_i, \hat{\rho}_S(t) \right\} \right) , \quad (3.10)$$

where  $\hat{H}_S(t)$  is the Hamiltonian of the system – without the parts acting on the environment. The  $\hat{L}_i$  are the *jump operators*, they describe the dissipative aspects of the dynamics and how the environment acts on the system. Finally, the  $\gamma_i \geq 0$  are the *damping rates* associated to the jump operators, they encode the strength of the effect of the corresponding jump operator. It is difficult to overstate the success and importance of this equation: it plays a crucial role in the field of quantum optics, quantum biology, quantum information and condensed matter.

### 3.2 Geometric Thermodynamics

#### 3.2.1 General Derivation of the Thermodynamic Metric

The framework of quantum thermodynamic geometry [9,42,43] allows us to minimize the entropy production  $\Sigma$  for protocols that are slow compared to their relaxation time-scale. We start by considering a system described by a state  $\hat{\rho}(t)$  with an externally driven Hamiltonian  $\hat{H}(t)$  that is undergoing the dynamics described by eq. (3.1) with the generator  $\mathcal{G}_{\lambda(t)}$ , where we made the dependence on the control parameters explicit. This description could be only about the system – thus in the setting of the Lindblad master equation, or about the system and environment – thus undergoing unitary dynamics. Since the Hamiltonian is a linear operator over the Hilbert space it can be decomposed in the following manner

$$\hat{H}(t) = \hat{H}_0 + \sum_{j=1}^n \lambda^j(t) \hat{X}_j , \qquad (3.11)$$

where  $\hat{H}_0$  contains the parts of the Hamiltonian that cannot be controlled,  $\{\lambda^j\}_{j=1}^n$  are externally controllable parameters and  $\{\hat{X}_j\}_{j=1}^n$  are the corresponding observables. These control parameters can be constrained, and we will denote by  $M \subseteq \mathbb{R}^n$  the manifold of the allowed values for these parameters. A thermodynamic protocol corresponds to a curve within the space M, as is illustrated in Fig. 3.1. In order to apply the framework of geometric thermodynamics, we need to satisfy three properties.

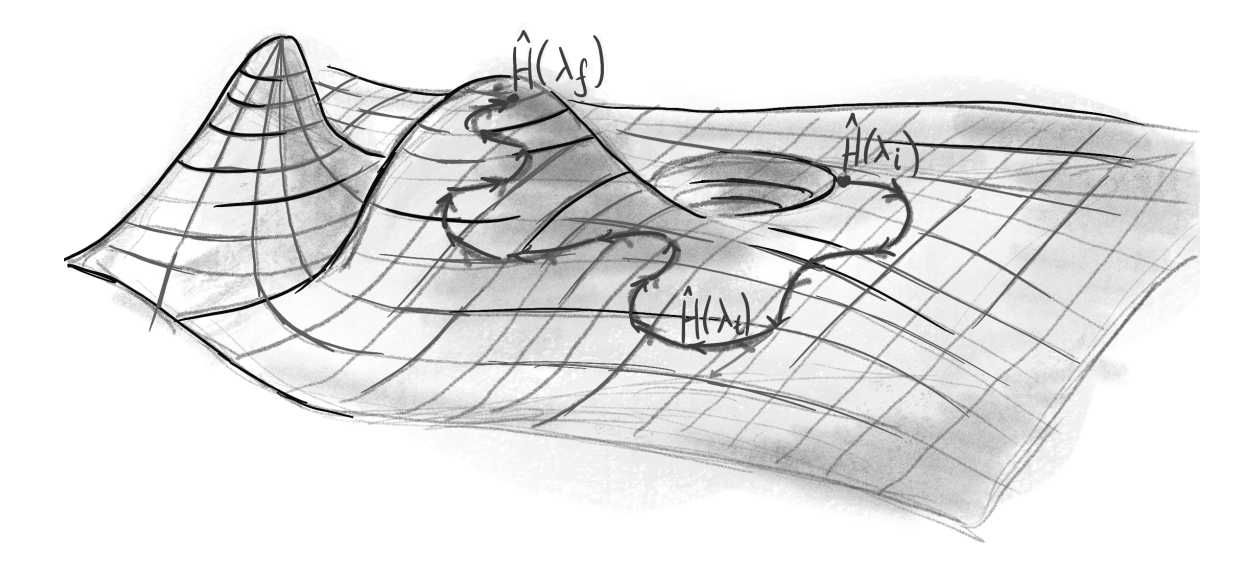


Figure 3.1: Curve of a protocol on the manifold of thermal states. [46]

Requirement 0: A Single Thermal Environment. We assume that the environment is initialized in a thermal state at a single well defined temperature T and that it is infinitely large. So that, by the second law, there is a well defined thermal equilibrium for the state  $\hat{\rho}$  if we were to freeze the control of the Hamiltonian. This is implies that  $\hat{\pi}_t$  is a fixed point of the dynamics:  $\mathcal{G}_{\lambda(t)}[\hat{\pi}_t] = 0$ .

For unitary dynamics this is automatically the case since the thermal state commutes with its corresponding Hamiltonian. While for the Lindblad master equation we need to require that the whole environment is already at thermal equilibrium.

Requirement 1: Thermalization of the Work Observables. In absence of driving, the expectation values of the observables  $\{\hat{X}_j\}$  thermalize. More precisely, if at time t we were to freeze the driving, then the propagator of the evolution becomes  $G_{\lambda(t)}^{fz}(s,r) = e^{(s-r)\mathcal{G}_{\lambda(t)}}$  for  $s \geq r \geq t$ . We then say that the expectation value of  $\hat{X}_j$  thermalizes if

$$\lim_{s \to \infty} \operatorname{Tr}[\hat{X}_j e^{s\mathcal{G}_{\lambda(t)}}[\hat{\rho}(t)]] = \operatorname{Tr}[\hat{\pi}(t)\hat{X}_j] . \tag{3.12}$$

This condition is typically satisfied by open quantum systems [44] and by non-integrable systems that satisfy the *eigenstate thermalization hypothesis* [45].

These two requirements are usually combined into one for the Lindblad master equation by simply stating that the state of the system converges to the thermal state in absence of driving. However, this is not the case for unitary dynamics, and thus we have to weaken this assumption into Requirements 0 and 1. Before stating the last requirement, let us consider the following decomposition of the state:

 $\hat{\rho}(t) = \hat{\pi}(t) + \Delta \hat{\rho}(t)$ , where  $\Delta \hat{\rho}(t)$  is defined as the difference between the thermal state and the state of the system. Inserting this decomposition into the dynamics eq. (3.1) we obtain

$$\left(\mathcal{G}_{\lambda(t)} - \frac{d}{dt}\right) [\Delta \hat{\rho}(t)] = \frac{d}{dt} \hat{\pi}(t) . \tag{3.13}$$

Since  $\mathcal{G}_{\lambda(t)}$  has a non-trivial kernel it is not invertible. However, we can solve this equation by introducing the concept of *Drazin inverse* [47]. In this case, it reduces to taking the inverse over the support of  $\mathcal{G}_{\lambda(t)}$ :

$$\mathcal{G}_{\lambda(t)}^{D} = (\mathcal{G}_{\lambda(t)}|_{\operatorname{supp}(\mathcal{G}_{\lambda(t)})})^{-1} \oplus \mathbf{0}_{\ker(\mathcal{G}_{\lambda(t)})} , \qquad (3.14)$$

where  $\oplus$  denotes the direct sum and  $\mathbf{0}_{\ker(\mathcal{G}_{\lambda(t)})}$  denotes the zero operator over the kernel of  $\mathcal{G}_{\lambda(t)}$ . It is useful to note that  $\mathcal{G}_{\lambda(t)}^D \mathcal{G}_{\lambda(t)} = \mathcal{G}_{\lambda(t)} \mathcal{G}_{\lambda(t)}^D$  and is equal to the projector over the support of  $\mathcal{G}_{\lambda(t)}$ :  $\mathcal{P}_{\operatorname{supp}(\mathcal{G}_{\lambda(t)})}$ . Therefore we can apply the Drazin inverse to both sides of eq. (3.13) to obtain

$$\left(\mathcal{P}_{\text{supp}(\mathcal{G}_{\lambda(t)})} - \mathcal{G}_{\lambda(t)}^{D} \frac{d}{dt}\right) [\Delta \hat{\rho}(t)] = \mathcal{G}_{\lambda(t)}^{D} \frac{d}{dt} [\hat{\pi}(t)] . \tag{3.15}$$

Since, by construction, the image and support of  $\mathcal{G}_{\lambda(t)}^D$  are the support of  $\mathcal{G}_{\lambda(t)}$ , we can write

$$\left(\mathbb{1} - \mathcal{G}_{\lambda(t)}^{D} \frac{d}{dt}\right) [\Delta \hat{\rho}_s(t)] = \mathcal{G}_{\lambda(t)}^{D} \frac{d}{dt} [\hat{\pi}(t)] , \qquad (3.16)$$

where we decomposed  $\Delta \hat{\rho}(t)$  into  $\Delta \hat{\rho}_s(t)$  its projection onto the support of  $\mathcal{G}_{\lambda(t)}$  and  $\Delta \hat{\rho}_k(t)$  its projection onto the kernel of  $\mathcal{G}_{\lambda(t)}$ . Finally, with  $(\mathbb{I} - X)^{-1} = \sum_{n=0}^{\infty} X^n$  we find

$$\hat{\rho}(t) = \Delta \hat{\rho}_k(t) + \sum_{n=0}^{\infty} \left( \mathcal{G}_{\lambda(t)}^D \frac{d}{dt} \right)^n [\hat{\pi}(t)] . \tag{3.17}$$

Each term in the sum is proportional to  $\|\dot{\lambda}(t)\|^n$ , therefore if  $\|\dot{\lambda}(t)\|$  is progressively going to 0 the only surviving term in the sum is  $\hat{\pi}(t)$ . Nonetheless the state will not necessarily thermal because of the term  $\Delta \hat{\rho}_k(t)$ . If we are in the case of a Lindblad master equation where the only fixed point of the evolution is  $\hat{\pi}(t)$ , then  $\delta \hat{\rho}(t) = 0$ . However, in the case of a full unitary description  $\Delta \hat{\rho}_k(t)$  cannot be vanishing because only the thermal state maps to the thermal state in a unitary evolution. In particular, if we were to freeze the evolution as described in Requirement 1, since  $\Delta \hat{\rho}_k(t)$  is a fixed point of the frozen evolution, we have

$$\lim_{s \to \infty} e^{s\mathcal{G}_t} [\hat{\rho}(t)] = \Delta \hat{\rho}_k(t) + \hat{\pi}(t) . \tag{3.18}$$

Combining this last equation with Requirement 1, we get

$$Tr[\Delta \hat{\rho}_k(t)\hat{X}_j] = 0. (3.19)$$

The limit where  $\|\dot{\lambda}(t)\|$  goes to zero corresponds to the quasi-static limit with the protocol time  $\tau$  going to infinity. But here we are interested in the case where  $\tau$  is finite and  $\|\dot{\lambda}(t)\|$  is sufficiently small to drop most of the terms in the sum of eq. (3.17). Which naturally leads us to the last requirement:

Requirement 2: Slow driving. The system is driven in such a way that its evolution is slow compared to the relaxation timescales of evolution of the expectation values of the observables  $\{\hat{X}_j\}$ . More precisely, if we denote by  $\tau_j^{eq}(t)$  the relaxation timescale of  $\text{Tr}[\hat{X}_j e^{s\mathcal{G}_{\lambda(t)}}[\hat{\rho}(t)]]$  as we let s increase. Then by defining  $\tau_{eq} := \max_j \sup_{0 \le t \le \tau} \tau_j^{eq}(t)$ , we are in the slow driving regime when  $\tau_{eq}/\tau \ll 1$ .

The expansion for a varying  $\tau$  should be understood as done for a fixed curve  $\{\lambda(t)\}\subset M$ , so that changing the value of  $\tau$  only changes the speed over which the path on the curve is covered. Which allows us to identify  $\|\dot{\lambda}\| = \mathcal{O}(\tau_{eq}/\tau)$ , we then get from eq. (3.17)

$$\hat{\rho}(t) = \Delta \hat{\rho}_k(t) + \hat{\pi}(t) - \beta \mathcal{G}_{\lambda(t)}^D[\mathbb{D}_{\hat{\pi}(t)}[\hat{H}'(t)]] + \mathcal{O}(\tau_{eq}^2/\tau^2) , \qquad (3.20)$$

where we used  $\frac{d}{dt}\hat{\pi}(t) = -\beta \mathbb{D}_{\hat{\pi}(t)}[\hat{H}'(t)]$ , with

$$\mathbb{D}_{\hat{\rho}}[\hat{A}] := \int_0^1 ds \ \hat{\rho}^s \left( \hat{A} - \text{Tr}[\hat{\rho}\hat{A}] \mathbb{1} \right) \hat{\rho}^{1-s} \ . \tag{3.21}$$

From eq. (2.5), eq. (3.19) and eq. (3.20) we can find the following expression for work

$$W = \Delta F_{eq} - \beta \int_0^{\tau} dt \operatorname{Tr} \left[ H'(t) \mathcal{G}_{\lambda(t)}^D [\mathbb{D}_{\hat{\pi}(t)}[\hat{H}'(t)]] \right] + \mathcal{O}(\tau_{eq}^2/\tau^2) , \qquad (3.22)$$

where we obtained  $\Delta F_{eq}$  from integrating  $\text{Tr}[\hat{\pi}(t)\hat{H}'(t)]$ . By using  $\hat{H}'(t) = \sum_j \dot{\lambda}^j(t)\hat{X}_j$ , we can now easily identify the leading order for the entropy production in the slow driving regime

$$\Sigma = \sum_{ij} \int_0^{\tau} dt \ \dot{\lambda}^i(t) \dot{\lambda}^j(t) g_{ij}(\lambda(t)) \ , \tag{3.23}$$

where we defined the symmetric tensor  $g(\lambda)$  as

$$g_{ij}(\lambda) := -\frac{\beta^2}{2} \operatorname{Tr} \left[ \hat{X}_i \mathcal{G}_{\lambda}^D[\mathbb{D}_{\hat{\pi}(\lambda)}[\hat{X}_j]] + \hat{X}_j \mathcal{G}_{\lambda}^D[\mathbb{D}_{\hat{\pi}(\lambda)}[\hat{X}_i]] \right] . \tag{3.24}$$

From the second law of thermodynamics we have  $\Sigma \geq 0$ . Therefore, since eq. (3.23) is valid for any choice of  $\lambda$  as long as  $\tau$  is large enough, then we necessarily have that the tensor g is positive definite – and because of the third law we know that it is strictly positive definite. Since it also depends smoothly on  $\lambda$  and is independent of the velocity  $\dot{\lambda}$ , we can notice that g has all the properties of a metric over M. In fact, it is known in the literature as the thermodynamic metric and defines the length of a curve  $\gamma:[0,\tau]\mapsto M$ 

$$L[\gamma] := \int_{\gamma} dt \sqrt{\dot{\gamma}^i(t)\dot{\gamma}^j(t)g_{ij}(\gamma(t))} , \qquad (3.25)$$

where we adopted the Einstein summation convention, which we will keep through the rest of this thesis.

#### 3.2.2 Minimally Dissipating Curves

We will now discuss how to use the metric eq. (3.24) to find minimally dissipating protocols from an initial configuration  $\hat{H}_i$  and initial state  $\hat{\rho}(0) = \hat{\pi}_i$  to a final configuration  $\hat{H}_f$ . The entropy production and length associated to a specific protocol  $\lambda : [0, \tau] \mapsto M$  are related via a Cauchy-Schwarz inequality:

$$\Sigma[\lambda] \ge \frac{1}{\tau} L[\lambda]^2 \,, \tag{3.26}$$

where we made explicit the dependence of  $\Sigma$  on  $\lambda$ . This inequality can always be saturated by making the integral of the entropy production  $\dot{\lambda}^i(t)\dot{\lambda}^j(t)g_{ij}(\lambda)$  constant, which can always be achieved by modulating the speed along the curve – and it does not affect its length. Therefore to minimize the dissipation  $W_{diss} = k_B T \Sigma$  we need to find the curve in the space  $C_{\lambda_i,\lambda_f}(M)$  of smooth paths connecting  $\hat{H}_i$  and  $\hat{H}_f$  that minimizes its length. This corresponds to a geodesic path on M, which satisfies the geodesic equation

$$\ddot{\lambda}^i + \Gamma^i_{jk} \dot{\lambda}^j \dot{\lambda}^k = 0 , \qquad (3.27)$$

where  $\Gamma^{i}_{jk}$  are the Christoffel symbols

$$\Gamma_{jk}^{i} = \frac{1}{2}g^{il}(\partial_{j}g_{kl} + \partial_{k}g_{lj} - \partial_{l}g_{jk}) , \qquad (3.28)$$

where  $g^{il}$  denotes the elements of the inverse of the metric and  $\partial_{\alpha} := \frac{\partial}{\partial \lambda^{\alpha}}$ . We can therefore define  $\mathcal{L}(\hat{H}_i, \hat{H}_f)$  as the length of the geodesic curve connecting  $\lambda_i$  and  $\lambda_f$ . Automatically  $\mathcal{L}$  satisfies all the properties of a distance function over

the space M, furthermore it gives us an expression for the minimal dissipation  $W_{diss}^* := \min_{\lambda \in \mathcal{C}_{\lambda_i,\lambda_f}(M)} W_{diss}[\lambda]$  and the minimal entropy production  $\Sigma^* = \beta W_{diss}^*$ 

$$W_{diss}^* = k_B T \Sigma^* = \frac{k_B T}{\tau} \mathcal{L}^2 + \mathcal{O}(\tau_{eq}^2/\tau^2) \ .$$
 (3.29)

It is interesting to note that the length of a curve in M is independent of  $\tau$ , and therefore all the dependency of the dissipation on the protocol time is in the prefactor  $1/\tau$ .

It is well known that optimal finite-time protocols feature jumps [48]. However, these jumps disappear near the reversible limit (cf. [49] and Fig. 4.1) and their contribution to the dissipated heat becomes either negligible or is disadvantageous. Let us first consider jumps at the start of the protocol  $\Delta \hat{H}_i = \hat{H}(0^+) - \hat{H}_i$ , the work cost of this jump is  $\text{Tr}[\hat{\pi}_i \Delta \hat{H}_i]$ , which yields a contribution to the dissipation that is independent of  $\tau$ . Therefore, however small is the work cost of the rest of the protocol, by eq. (3.29) there exists  $\tau^*$  such that for all  $\tau \geq \tau^*$  the geodesic will dissipate less than the protocol with a jump at the start. A similar argument can be applied to the end of the protocol. What this shows is that the jumps need to at most be of magnitude  $\mathcal{O}(\tau^{eq}/\tau)$ , which implies that they are vanishing in the slow driving limit, and most of the time we will be ignoring their contribution.

# Chapter 4

# Finite-Time Landauer Principle

Ahimè, non mai due volte configura il tempo in egual modo i grani! E scampo n'è: che, se accada, insieme alla natura la nostra fiaba brucerà in un lampo.

— Eugenio Montale, Vento e bandiere, Ossi di seppia

Any logical irreversible operation will incur a thermodynamic cost in the form of heat dissipated into the environment. On a fundamental level this is because logically irreversible operations lead to a loss of information, and in the words of Rolf Landauer "information is physical". Therefore a loss of information results in a loss of energy. Landauer's principle quantifies this relation between information processing and thermodynamics with the bound  $Q \geq k_B T \ln 2$  for the erasure of a single bit of information [4]. Here Q is the dissipated heat,  $k_B$  is the Boltzmann constant and T is the absolute temperature at which the process is taking place. In recent years, this principle has been intensively studied within the fields of stochastic and quantum thermodynamics [50,51], and has been approached in several experimental platforms [52–54].

The third law of thermodynamics (cf. Sec. 2.4) implies that Landauer's bound cannot be saturated with finite resources, namely time and energy [37,39]. In finite time, using tools from optimal transport theory [55] and thermodynamic geometry [43,56], optimal erasure protocols have been derived both for classical systems described by over-damped Langevin dynamics [57] and open quantum systems described by Lindblad master equations [10,58]. Such optimal protocols naturally lead to a finite-time correction to Landauer's bound in different physical set-ups, which has given rise to the term finite-time Landauer principle [59]. For a slowly driven

(quantum) two-level system weakly coupled to a thermal bath, the finite-time bound takes the simple form [9]

$$Q \ge k_B T \left( \ln 2 + \frac{\pi^2}{4\Gamma \tau} \right) + \mathcal{O}\left( \frac{1}{\Gamma^2 \tau^2} \right), \tag{4.1}$$

where  $\tau$  is the total time of the process and  $\Gamma$  is the thermalization rate. The finite-time correction is positive, in agreement with the second law of thermodynamics, and when  $\Gamma\tau \to \infty$  we recover the standard bound. We also note that the optimal protocol saturating the finite bound eq. (4.1) has been recently implemented in a semiconductor quantum dot [54]. More general versions of eq. (4.1) have also been recently developed for Markovian systems driven at any speed [10,11].

Despite this remarkable progress, previous works on the *finite-time Landauer* principle have focused in Markovian systems which, for quantum systems, can be guaranteed by a sufficiently weak interaction between system and bath. In the presence of strong coupling, we expect both new opportunities arising due to faster relaxation rates and non-Markovian dynamics [60], as well as challenges due to the presence of new sources of irreversibility [61]. In this chapter we will derive the first order to a tight finite-time correction of Landauer's principle for a single fermion that can interact strongly with a reservoir, as described by the resonant-level model [62]. The main result of this chapter can be summarized as follows.

Given a two-level system that can be strongly coupled to a thermal bath, we find that the finite-time version of Landauer's principle can be expressed as

$$Q \ge k_B T \left( \ln 2 + a \frac{\tau_{\text{Pl}}}{\tau} \right) + \mathcal{O} \left( \frac{1}{\Gamma^2 \tau^2} \right)$$
 (4.2)

where  $a \approx 2.57946$ ,  $\tau_{\rm Pl} = \hbar/k_BT$  is the so-called Planckian time [63], and  $\Gamma$  is the average thermalization rate (see details below). This expression generalizes eq. (4.1) to strong system-bath couplings, with the transition between the two being characterized in Fig. 4.2. The finite-time correction in eq. (4.2) is of quantum-mechanical nature and independent of the coupling strength, hence prevailing even for arbitrarily strong system-bath coupling (roughly speaking,  $\Gamma \to \infty$  in eq. (4.1)).

The appearance of the Planckian time  $\tau_{\rm Pl} = \hbar/k_BT$  in eq. (4.2) is particularly interesting. This timescale encodes two fundamental constants of nature: Boltzmann's constant  $k_B$  and Planck's constant  $\hbar$ . It arises in several contexts in many-body physics, including quantum transport and quantum chaos; see Ref. [63] for a

review. In analogy with the "Planck time" in quantum gravity, it is associated with the shortest timescale of thermalization [63,64]; that is, the shortest time needed to redistribute energy between particles and reach thermal equilibrium. This gives an insightful context to our main result eq. (4.2): a fundamental finite-time quantum correction must appear to Landauer's bound due to a minimal time required for thermalization. This also suggests that the form of eq. (4.2) has a broader range of applicability, with the dimensionless value a depending on the specific manybody thermalizing dynamics considered. In order to obtain eq. (4.2), we exploit the framework of thermodynamic geometry explained in Sec. 3.2.

### 4.1 Framework

We consider a driven system S that can be put in contact with a thermal bath B, so that the total time-dependent Hamiltonian reads:

$$\hat{H}(t) = \hat{H}_S(t) + \hat{H}_{int}(t) + \hat{H}_B.$$
 (4.3)

Here,  $\hat{H}_S(t)$ ,  $\hat{H}_{int}(t)$  are the externally controllable Hamiltonian of S and the SB coupling, whereas  $\hat{H}_B$  is the Hamiltonian of B. The state  $\hat{\rho}(t)$  of SB evolves according to eq. (3.6). From eq. (2.5), the work cost induced by driving  $\hat{H}(t)$ , with  $t \in [0, \tau]$ , reads:

$$W = \int_0^{\tau} dt \, \text{Tr}[\hat{\rho}(t)\hat{H}'(t)] = \text{Tr}[\hat{H}(\tau)\hat{\rho}(\tau) - \hat{H}(0)\hat{\rho}(0)]$$
 (4.4)

Focusing on protocols where  $\hat{H}_{\rm int}(0) = \hat{H}_{\rm int}(\tau) = 0$ , we can naturally identify from the first law of thermodynamics eq. (2.2)  $W = Q + \Delta E$ , with the change in energy of the system

$$\Delta E = \text{Tr}[\hat{H}_S(\tau)\hat{\rho}_S(\tau) - \hat{H}_S(0)\hat{\rho}_S(0)] \tag{4.5}$$

with  $\hat{\rho}_S(t) := \text{Tr}_B[\hat{\rho}(t)]$ , and the energy absorbed by the bath

$$Q = \text{Tr}[\hat{H}_B(\hat{\rho}_B(\tau) - \hat{\rho}_B(0))] \tag{4.6}$$

with  $\hat{\rho}_B(t) := \operatorname{Tr}_S[\hat{\rho}(t)].$ 

Assuming that the initial state of SB is a thermal state:  $\hat{\rho}(0) = \hat{\pi}(0) := \frac{e^{-\beta \hat{H}(0)}}{Z(0)}$ 

with  $Z(t) := \text{Tr}[e^{-\beta \hat{H}(t)}]$ , we can be re-express the work cost as:

$$W = \Delta F_{eq} + k_B T \Sigma , \qquad (4.7)$$

where  $\Delta F_{eq} = k_B T \ln[Z(0)/Z(\tau)]$  is the change of equilibrium free energy of SB, and the entropy production  $\Sigma$  can be expressed as  $\Sigma = S(\hat{\rho}(\tau)||\hat{\pi}(\tau))$  (cf. Sec. 2.3 for more detail). The entropy production  $\Sigma \geq 0$  accounts for the irreversible energetic contribution in finite-time processes, and depends on the particular driving path  $\hat{H}(t)$  linking  $\hat{H}(0)$  to  $\hat{H}(\tau)$ . Minimizing  $\Sigma$  over all finite-time processes leads to thermodynamic protocols that minimize the work W. Furthermore, in an erasure process,  $\Delta E = 0$  (see details below) therefore these protocols also minimize the dissipated heat Q.

### 4.2 The Resonant Level Model

We now focus on finite-time driving processes of a single fermionic mode coupled to a fermionic bath, which can e.g. describe a single-electron quantum dot. The total Hamiltonian reads:

$$\hat{H}(t) = \varepsilon(t)\hat{a}^{\dagger}\hat{a} + \sum_{k=1}^{n} \omega_k \hat{b}_k^{\dagger} \hat{b}_k + \kappa(t) \sum_{k=1}^{n} \lambda_k \hat{a}^{\dagger} \hat{b}_k + \lambda_k^* \hat{b}_k^{\dagger} \hat{a}. \tag{4.8}$$

where  $\hat{a}^{\dagger}$  is the creation operator of the two-level system and  $\hat{b}_{k}^{\dagger}$  is the creation operator of a bath mode with frequency  $\omega_{k}$ . These operators follow the canonical anti-commutation relations:  $\{\hat{a}^{\dagger},\hat{a}\}=1$ ,  $\{\hat{b}_{j}^{\dagger},\hat{b}_{k}\}=\delta_{jk}1$ ,  $\{\hat{b}_{j},\hat{b}_{k}\}=\{\hat{a},\hat{b}_{k}\}=\{\hat{a},\hat{b}_{k}\}=\{\hat{a},\hat{b}_{k}\}=\{\hat{a},\hat{a}\}=0$ .  $\kappa(t)$  modulates the interaction Hamiltonian and  $\lambda_{k}$  are the interaction weights which define the spectral density function of the bath  $\mathfrak{J}(\omega)=2\pi\sum_{k}|\lambda_{k}|^{2}\delta(\omega-\omega_{k})$ . Finally, the energy  $\varepsilon(t)$  is the difference between the energy gap of the two-level system and the chemical potential of the bath<sup>1</sup>. We are assuming optimal control over the functions  $\varepsilon(t)$  and g(t) so that we can fully optimize the protocol and reach the fundamental limit for this system. While this level of control is, in principle, ambitious experimentally in regards to the coupling, it has been achieved in quantum dots [65] where the tunneling rate (i.e. interaction strength) can be modified by several orders of magnitude. We take the continuum limit and

<sup>&</sup>lt;sup>1</sup>The chemical  $\nu$  potential of the bath is incorporated by subtracting  $\nu \hat{a}^{\dagger} \hat{a}$  to the system's Hamiltonian. Since here  $\hat{H}_S = \varepsilon a^{\dagger} \hat{a}$  (with  $\varepsilon$  the energy of the system), we can simply redefine  $\varepsilon$  to be the difference between the system's energy and the chemical potential and set  $\nu = 0$  without loss of generality.

assume that the spectral density of the bath is a Lorentzian

$$\mathfrak{J}(\omega) = \frac{\Lambda^2}{\Lambda^2 + \omega^2} \,\,\,(4.9)$$

where  $\Lambda > 0$  is a parameter characterizing its width. Exact and explicit solutions for the resonant-level model are known in the wide-band limit  $\Lambda \to \infty$  [62]. This limit is commonly used to describe quantum systems in contact with fermionic macroscopic baths, e.g. in quantum dots or single-molecule junctions (see [66] for an example). In essence, it neglects the structure of the density of states in the bath and, as a consequence, a main limitation is that it fails to describe the short-time dynamics [66]. Nevertheless, this problem does not affect this study since we are interested in large times. We should further note that the energy of the system-bath interaction is proportional to  $\Lambda$ , and therefore is divergent in this limit. We will therefore take  $\Lambda$  to be finite but much larger than any other energy scale of the system. For our analysis to be valid we simply require dynamics much slower than  $\Lambda^{-1}$  [62].

The dynamics are solved via a quantum Langevin approach [12, 67]. For an uncorrelated initial state  $\hat{\rho}(0) = \hat{\rho}_S(0) \otimes \hat{\pi}_B$ , we compute the expectation values that are relevant to the work cost: the probability of occupation of the excited level of the system  $p(t) = \langle \hat{a}^{\dagger} \hat{a} \rangle$  and the system-bath interaction energy  $v(t) = \sum_k \lambda_k \langle \hat{a}^{\dagger} \hat{b}_k \rangle + h.c.$ .

$$p(t) = |G(t,0)|^2 p(0) + \frac{1}{2\pi} \int_{-\infty}^{\infty} d\omega \ f_{\beta}(\omega) \left| \int_{0}^{t} ds \ \kappa(s) G(t,s) e^{i\frac{\omega}{\hbar}(t-s)} \right|^2, \tag{4.10}$$

$$v(t) = \frac{1}{\pi} \Im \int_{-\infty}^{\infty} d\omega \ f_{\beta}(\omega) \int_{0}^{t} ds \ \kappa(s) G(t, s) e^{i\frac{\omega}{\hbar}(t-s)}, \tag{4.11}$$

where  $f_{\beta}(\omega) = (1+e^{\beta\omega})^{-1}$  is the Fermi-Dirac distribution. We defined the propagator

$$G(t,s) = \exp\left[-\frac{1}{\hbar} \int_{s}^{t} dr \ \mu(r) + i\varepsilon(r)\right] , \qquad (4.12)$$

where we introduced  $\mu(t) := \frac{1}{2}\kappa(t)^2$  in order to have more concise equation in the rest of the chapter. We therefore obtain the expected thermodynamic work cost to be

$$W = \int_0^\tau dt \ \dot{\varepsilon}(t)p(t) + \dot{\mu}(t)v(t)/\kappa(t). \tag{4.13}$$

The framework of quantum thermodynamic geometry allows us to minimize the

dissipated work  $W_{diss} = W - \Delta F_{eq}$ , and therefore the dissipated heat Q for erasure, for protocols that are slow compared to their relaxation time-scale. In order to apply the framework presented in Sec. 3.2, we have to ensure that the requirements are satisfied. Since we are in unitary dynamics we already satisfy requirement 0. The proof that requirement 1 is satisfied is quite convoluted, which is why we left it for the end of the chapter in Sec. 4.6. While requirement 2 can be easily imposed by choose  $\tau$  appropriately. In particular, using that the thermalization rate of the system is  $\Gamma := \frac{2}{\hbar\tau} \int_0^{\tau} dt \, \mu(t)$  we can perform the slow driving expansion of eq. (4.10) and eq. (4.11) in orders of  $1/(\tau\Gamma)$ . We then obtain an expansion for W analogous to eq. (4.7) where the entropy production  $\Sigma$  is described by eq. (3.23) with  $\lambda(t) = (\varepsilon(t), \mu(t))$  and the thermodynamic metric

$$g(\lambda(t)) = \frac{\beta \hbar}{\pi} \int_{-\infty}^{\infty} d\omega \ f_{\beta}(\omega) m_{\omega}(\varepsilon(t) - \omega, \mu(t)) \ , \tag{4.14}$$

where

$$m_{\omega}(\varepsilon,\mu) := \frac{1}{(\mu^2 + \varepsilon^2)^3} \begin{pmatrix} 4\varepsilon\mu^2 & -\mu(\mu^2 - 3\varepsilon^2) \\ \mu(\mu^2 - 3\varepsilon^2) & 2\varepsilon(\varepsilon^2 - \mu^2) \end{pmatrix} . \tag{4.15}$$

This metric gives a geometrical description of slow thermodynamic protocols performed on the system. By solving the geodesic equations, we can find the geodesic length  $\mathcal{L}$  and hence the minimal entropy production.

## 4.3 Special Limits of the Metric

Before attempting to solve the geodesic equations for the case of erasure, we now study the high and low temperature limits, as well as the limit of weak coupling, to gain further analytical insights on the form of optimal protocols and the associated entropy production.

# 4.3.1 High Temperature Limit $(\beta \varepsilon, \beta \mu \ll 1)$

Since the terms of eq. (4.14) quickly decay at high frequencies, we can perform the high temperature expansion  $f_{\beta}(\omega) = \frac{1}{2} - \frac{1}{4}\beta\omega + \mathcal{O}(\beta^3\omega^3)$  directly in the metric. At leading order, we find:

$$g_{HT} = \frac{\beta^2 \hbar}{8\mu} \mathbb{1} . \tag{4.16}$$

This enables an analytical solution of the geodesic equations. Given the boundary conditions  $\{\varepsilon(0) = \mu(0) = \mu(\tau) = 0, \, \varepsilon(\tau) = \varepsilon_* > 0\}$ , which will later match those of

an erasure protocol<sup>2</sup>, we find the following geodesic path

$$\varepsilon(t) = \varepsilon_* \left( t/\tau - \frac{\sin(2\pi t/\tau)}{2\pi} \right) ,$$
 (4.17)

$$\mu(t) = \frac{\varepsilon_*}{\pi} \sin(\pi t/\tau)^2 \ . \tag{4.18}$$

In the regime  $\beta \varepsilon(t) \ll 1$ , we observe that minimising entropy production requires a maximal coupling strength  $\varepsilon(\tau)/\pi$ . The entropy production of the geodesic protocol is

$$k_B T \Sigma^* = \frac{\pi \hbar \beta \varepsilon_*}{2\tau} + \mathcal{O}(\beta^3 \varepsilon_*^3) , \qquad (4.19)$$

which linearly scales with the final energy  $\beta \varepsilon_*$ .

### 4.3.2 Zero Temperature Limit ( $\beta \varepsilon$ or $\beta \mu \to \infty$ )

In the limit of  $T = 0^3$  we have  $f_{\beta}(\omega) \to f_{\infty}(\omega) = \Theta(-\omega)$ , where  $\Theta$  is the Heaviside step function. Therefore the metric becomes

$$g_{T=0} = \frac{\beta \hbar}{\pi} \frac{1}{(\mu^2 + \varepsilon^2)^2} \begin{pmatrix} \mu^2 & -\varepsilon \mu \\ -\varepsilon \mu & \varepsilon^2 \end{pmatrix} , \qquad (4.20)$$

which coincides with the metric of an angle distance in the  $(\varepsilon, \mu)$  space – hence the metric is singular. If we re-parameterize  $(\varepsilon, \mu)$  as  $(r\cos\phi, r\sin\phi)$  we find  $k_BT\Sigma = \frac{1}{\pi} \int_0^{\tau} dt \, \dot{\phi}(t)^2$ . Therefore any protocol that keeps  $\dot{\phi}(t)$  constant is a geodesic, leading to the minimal entropy production:

$$k_B T \Sigma^* \bigg|_{T=0} = \frac{\hbar (\Delta \phi)^2}{\pi \tau}, \tag{4.21}$$

with  $\phi = \arctan(\mu/\varepsilon)$ . Note that there are multiple (infinitely many) geodesics for any pair of boundary points. This fact prevents us from continuing the expansion to further orders in temperature. Nevertheless, this limit provides analytical insights on optimal protocols with  $\beta\varepsilon$  or  $\beta\mu\gg 1$ . In particular, we note that there is no need for a diverging coupling even when  $\varepsilon(\tau)\to\infty$  as, once  $\mu$  has become large,

<sup>&</sup>lt;sup>2</sup>Usually, the initial condition for erasure would be  $\varepsilon(0) = \nu$  for  $\nu$  the chemical potential of the bath and  $\varepsilon$  the energy of the two-level system (so that the corresponding thermal state is the fully mixed state). But since here we defined  $\varepsilon$  to be the difference to the chemical potential we take  $\varepsilon(0) = 0$  without loss of generality.

<sup>&</sup>lt;sup>3</sup>The zero temperature limit is achieved whenever the energy gaps of the system are too large for thermal fluctuations to occur between the energy levels. Bringing either  $\beta\varepsilon$  or  $\beta\mu$  to infinity achieves this effect. It is the opposite in the infinite temperature limit, where the thermal fluctuations need to overcome any energy gap, therefore in that limit, both  $\beta\varepsilon$  and  $\beta\mu$  need to be brought to zero.

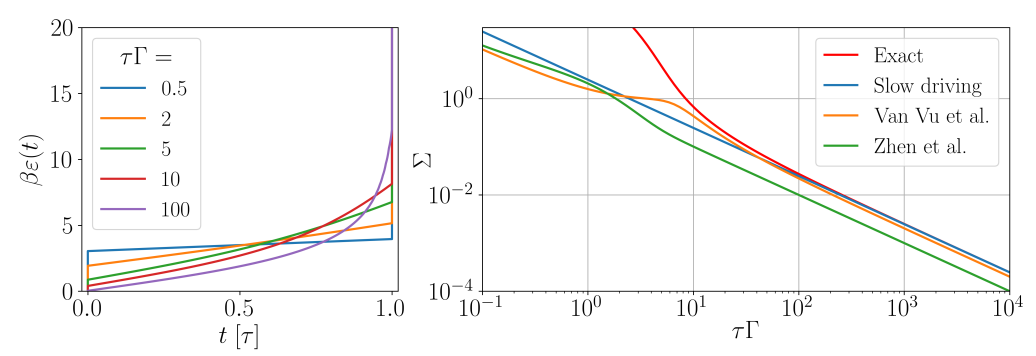


Figure 4.1: (left) Examples of optimal protocols computed from [49] for boundary conditions  $\varepsilon(0) = 0$  and  $\beta \varepsilon(\tau) = 20$  at different values of  $\tau$ . (right) Comparison of the entropy production of the optimal protocols from [49] with boundary conditions  $\varepsilon(0) = 0$  and  $\beta \varepsilon(\tau) = 100$  to the lower bounds given by eq. (4.1), Van Vu et al. [10] and Zhen et al. [11].

eq. (4.21) shows that it is optimal to reduce the coupling while increasing the energy. Furthermore, eq. (4.21) shows that at zero temperature, while the reversible cost of the operation goes to zero, the dissipation  $W_{diss}^* = k_B T \Sigma^*$  remains strictly positive. This result is complementary to the findings of Ref. [68] which demonstrate a finite-size correction to Landauer's bound that does not disappear in the zero-temperature regime.

## 4.3.3 Weak Coupling Limit

Lastly, we take take the weak coupling limit to compare to previous erasure results that are obtained via Lindbladian dynamics, which is a common assumption in previous works on optimal thermodynamic control in the quantum regime. In this limit the coupling is taken to be small and constant, therefore the metric becomes a scalar:

$$g_{weak}(\varepsilon) = \frac{\beta^2 \hbar}{\Gamma} f_{\beta}(\varepsilon) (1 - f_{\beta}(\varepsilon)) . \qquad (4.22)$$

Which matches the metric one obtains from the rate equation

$$\frac{dp(t)}{dt} = -\Gamma\left(p(t) - \frac{1}{1 + e^{\beta \varepsilon(t)}}\right) . \tag{4.23}$$

In this regime, protocols that minimize dissipated heat at arbitrary speed were found by [49]. Therefore we will compare the results one obtains in slow driving and the results of [10,11] to the exact minimization of [49].

We are interested in erasure processes, where  $\varepsilon(t)$  is driven from  $\varepsilon(0) = 0$  to

 $\varepsilon(\tau) = \varepsilon_*$  with  $\varepsilon_* \gg k_B T$  in a time  $\tau$ . Optimal finite-time protocols are those which minimize the work cost  $W = \int_0^\tau dt \ \dot{\varepsilon}(t) p(t)$ , and hence the heat dissipated to the environment  $Q = W - \Delta E$ . The results of [49] provide an exact solution to this problem, which is shown in Fig. 4.1. As is well-known in finite time stochastic thermodynamics [48], jumps appear in the optimal solution. However, as we approach the quasi-static limit where  $\tau\Gamma \gg 1$ , the jumps progressively disappear (cf. Fig. 4.1). In Sec. 3.2 we prove why the jumps should also disappear in the long times limit at strong coupling. The optimal driving solution in this limit has the simple analytical form

$$\varepsilon(t) = 2k_B T \ln \tan \left[ \frac{\pi}{4} (t/\tau + 1) \right] , \qquad (4.24)$$

leading to the work cost

$$W = k_B T \left( \ln 2 + \frac{\pi^2}{4\tau\Gamma} \right) , \qquad (4.25)$$

from where we can directly recover eq. (4.1) through the first law of thermodynamics (note that  $\Delta E = 0$ ). In Fig. 4.1 we notice that the exact solution of [49] agrees well with this analytical form in the slow driving limit. For completeness, we also show recent results of [10,11]. These results apply more generally to any Markovian master equation – here we apply them to the particular case of eq. (4.23), and one can see that they provide a bound to the exact numerical – and approximate analytical – solutions.

## 4.4 Optimized Erasure

We now focus on erasure outside any approximation, where we will optimize the driving over both the energy and coupling. In what follows, we focus on minimizing  $\Sigma$  in an erasure process, which imposes specific boundary conditions to the geodesic equations. We assume that we have no prior knowledge of the system, therefore its initial state is  $\rho_S(0) = 1/2$ . This translates in taking  $\varepsilon(0) = 0$  so that it coincides with the thermal state of  $\hat{H}(0)$ . For the qubit to be erased we want its final state to be  $\rho_S(\tau) \approx |0\rangle\langle 0|$  (i.e.  $p(\tau) \approx 0$ ). Since the driving is done slowly, p(t) is always close to its thermal expectation value. Therefore by choosing  $\beta \varepsilon(\tau) \to \infty$  we ensure  $p(\tau) \approx 0^4$ . For the coupling, the boundary conditions are  $\mu(0) = \mu(\tau) = 0$ , because

<sup>&</sup>lt;sup>4</sup>Strictly speaking, in order to ensure consistency with the slow driving limit,  $\beta \varepsilon(\tau)$  has to remain finite (so that the speed  $\dot{\lambda}$  remain finite). However, the final population  $p(\tau)$  is exponentially small with  $\beta \varepsilon(\tau)$ , leading to exponentially small corrections. Our results are valid up to such corrections,

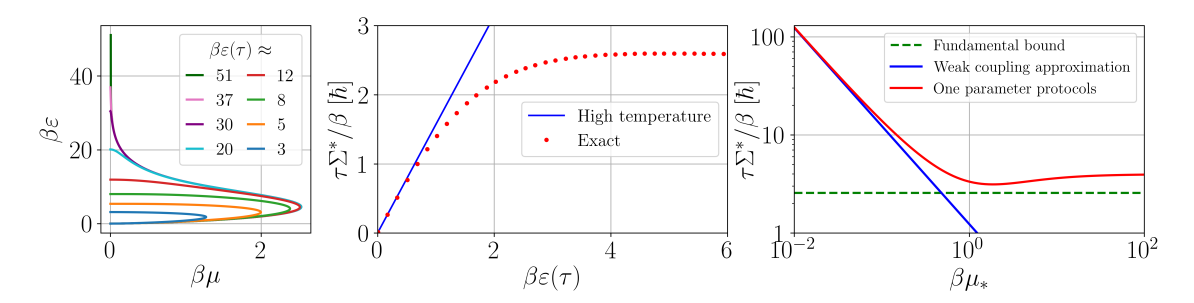


Figure 4.2: (left) A series of optimal protocols depicted in the  $(\mu, \varepsilon)$  space. They all start with zero energy and coupling and end with finite energy and zero coupling. In the limit of large  $\beta \varepsilon(\tau)$  they can be considered as erasure protocols. (middle) The entropy production of the optimal erasure protocol as a function of the final energy, compared to the high temperature regime cost eq. (4.19). (right) Comparison of the entropy production for a geodesic protocol in which one parameter is varied at a time (with  $\mu$  being increased until  $\mu^*$ ) and the weak coupling approximation eq. (4.1); the minimal possible entropy production,  $\tau \Sigma^*/\beta = 2.57946 \pm 1 \cdot 10^{-5}$  [ $\hbar$ ], obtained when both parameters are changed simultaneously is also shown.

we want to think of this as an "erasure machine" that the qubit is "brought to" at the start and "retrieved from" at the end. Given this family of protocols, we recognize from eq. (4.7) that  $W = Q = k_B T(\ln 2 + \Sigma)$ . After the qubit has been decoupled (i.e. at  $t > \tau$ ), we bring the Hamiltonian of the system back to its starting value ( $\varepsilon = 0$ ) to close the cycle. Since  $p(\tau) \approx 0$ , this step requires no work, and it can be done arbitrarily quickly.

The geodesic equations we obtain for this process are not solvable analytically. The integral of eq. (4.14) can be solved to give us an expression of the metric in terms of polygamma functions but it does not simplify the geodesic equations into an analytically solvable form. We therefore turn to numerical tools to obtain the optimal protocol and compute the dissipated work. However, in our case, we want to impose the aforementioned boundary conditions; this is known as a Boundary Value Problem (BVP), which is famously hard to solve numerically [69]. Though we can use the fact that the high temperature limit is accurate at the start of an erasure protocol, therefore the initial conditions of the optimal protocol for erasure will match the initial conditions of eq. (4.17) and eq. (4.18). This allows us to turn the BVP into an Initial Value Problem which is much simpler to solve.

In Fig. 4.2 we show optimal erasure protocols in the  $(\mu, \varepsilon)$  space for different final values of  $\beta \varepsilon$ . We can notice that the predictions of the high and low temperature limit are verified: at the start of the protocols the coupling is increased, but once we reach a certain value there is no more need to increase it, regardless of the final value

and for sufficiently large  $\tau$  to ensure the validity of the approximation.

of  $\beta\varepsilon$  we try to reach. Interestingly, the maximal value reached by  $\beta\mu$  is larger than 1. This shows that reaching the strong coupling regime is needed to achieve optimal erasure, which is one of the main insights of our work. In the same figure we also show the value of  $\tau\Sigma^*/\beta$  for the optimal protocol as a function of the final energy. We can see that for small values of  $\beta\varepsilon(\tau)$  the high temperature limit eq. (4.19) gives an accurate description of the work cost, but as we reach higher values it saturates to  $\tau\Sigma^*/\beta = 2.57946 \pm 1 \cdot 10^{-5}$  [ $\hbar$ ]. This provides a finite-time correction to Landauer's principle in this setup:

$$Q \ge k_B T \left( \ln 2 + a \frac{\tau_{\text{Pl}}}{\tau} \right) + \mathcal{O} \left( \frac{1}{\Gamma^2 \tau^2} \right). \tag{4.26}$$

with  $a \approx 2.57946$  and  $\tau_{\rm Pl} = \beta \hbar$ . This is one of the main results of this work and can be seen as a generalization of eq. (4.1). As opposed to the results of [11] and [10], eq. (4.26) is only valid for large protocol times; yet, it has the advantage of taking into account strong coupling effects (including any possible variation of the coupling strength), having a much simpler form for the correction (which is independent of any chosen relaxation timescale), and we provide an explicit protocol to achieve it. By turning around eq. (4.26) one can highlight a quantum speed limit for erasure of a qubit, furthermore this speed limit is of the order of the Planckian time  $\tau_{\rm Pl} = \hbar/k_B T$  which is conjectured to be the fastest relaxation timescale for thermalization [63]. In particular, one can see that eq. (4.26) bounds the speed of erasure by the order of  $\tau_{\rm Pl}$  regardless of how large is the coupling strength used in the protocol.

Interestingly, we now argue that the form of the correction eq. (4.26) is in fact general of any Landauer erasure protocol with control on S and the SB coupling. Indeed, first note that – in natural units – the minimal dissipation  $\Sigma^*$  is dimensionless and can only depend on  $\beta$  and the boundary conditions as we optimize over  $\mu$  and  $\varepsilon$ . In an erasure process, the boundary conditions read:  $\varepsilon(0) = 0$ ,  $\varepsilon(\tau) \to \infty$ , and  $\mu_i(0) = \mu_i(\tau) = 0$  where i runs over all the possible control parameters on SB. But this implies that  $\Sigma^*$  is independent of them and hence of  $\beta$ . Therefore  $W_{diss}^*$  will take the form of a constant, independent of any parameter of the system and bath, divided by  $\tau$ . This is a crucial difference from eq. (4.1).

This simple argument based on dimensional analysis thus shows that eq. (4.26) is rather general, with the value of a depending on the specific implementation (e.g. the ohmicity of the bath). It is important to highlight that the bound eq. (4.26) implies that, even when having access to arbitrary strong SB interactions (naively taking  $\Gamma \to \infty$  in eq. (4.1)), infinite time is still required for perfect erasure due to

the quantum-mechanical correction derived here.

Finally, we analyze a scenario where the coupling is kept constant while  $\varepsilon(t)$  is driven, which is motivated both by experimental set-ups and for a comparison with the weakly interacting case. Therefore, we restrict to *one-parameter protocols* consisting of the three following steps: 1. while keeping  $\varepsilon$  at 0 we turn on the coupling to some value  $\mu_*$ ; 2. while keeping the coupling fixed we bring  $\varepsilon$  from 0 to some value  $\varepsilon_* \gg k_B T$ ; 3. while keeping  $\varepsilon$  constant we turn off the coupling. Each step contributes positively to the entropy production, and their minimization leads to the following dissipation

$$\Sigma_{\text{one param}}^* = \frac{1}{\tau} \left( \int_0^{\mu_*} d\mu \ [g_{\mu\mu}(0,\mu)]^{1/2} + \int_0^{\infty} d\varepsilon \ [g_{\varepsilon\varepsilon}(\varepsilon,\mu_*)]^{1/2} \right)^2 \ . \tag{4.27}$$

In Fig. 4.2, we show  $\Sigma^*$  for different values of  $\mu_*$ , ranging from the weak to the superstrong coupling regime. It can be appreciated how eq. (4.1) breaks down, and also how such one-parameter protocols become close to the fundamental limit eq. (4.26) for  $\beta\mu_* > 1$ .

### 4.5 Conclusions and Outlook

Deriving finite-time corrections to the seminal Landauer bound is a challenging endeavor in stochastic and quantum thermodynamics. Previous works have focused on Markovian systems only, which in the quantum regime is obtained through the weak coupling limit ( $\beta\kappa^2 \to 0$ ). However, should a general finite-time correction exist, it will require the presence of strong coupling at some point during the process as the dissipation generated in finite time is proportional to  $\kappa^{-2}$  when  $\kappa$  is small<sup>5</sup>. Motivated by this observation, we have developed new insights into the form of optimal protocols for erasure beyond the weak coupling limit.

We have focused on a bit encoded in the occupation of a single fermionic mode, which can be strongly coupled to a reservoir. We have derived analytically the thermodynamic metric, which governs the dissipation rate in the slow driving regime, and showed that it takes a simple form in the high and low temperature limits. From the general form of the metric we obtained the optimal erasure protocol, which requires increasing the coupling strength to  $\kappa^2 \sim k_B T$ , which corresponds to a relaxation timescale of the order of the Planckian time  $\tau_{\rm Pl}$ . The corresponding

This can be seen by expanding the finite time dissipation around  $\kappa^2 = 0$  for long times:  $k_B T \Sigma \propto 1/\kappa^2 \tau$ , which follows by noticing that the relaxation time-scale is of the order of  $\kappa^{-2}$ .

dissipation yields a finite-time correction to Landauer's bound for this setup, which is substantially lower than similar results in the weak coupling regime. Furthermore, by using the obtained bound as a quantum speed limit, this result adds further evidence to the conjecture [63] that  $\tau_{\rm Pl}$  is fastest relaxation timescale many-body systems can achieve.

While our results were derived in a fermionic model, there are some general insights that follow from our work. First there is a fundamental quantum correction that prevails, see eq. (4.26), which can be compared with eq. (4.1) derived in the weak coupling regime. While the specific value of a in eq. (4.26) will depend on the specific setup, it will never approach 0 (even for diverging system-bath coupling) due to the inherent cost of changing the interaction strength. Furthermore, to obtain these results we adapted the framework of thermodynamic geometry to system-bath unitary dynamics in which the coupling can be arbitrarily large or small. Finally, as was argued before, our results make evident the need for strong coupling in a general finite-time correction to Landauer's principle.

This work opens exciting directions for the future. On the one hand, the level of experimental control required to implement such protocols is in principle possible in quantum dots, where the energy-level  $\varepsilon(t)$  and coupling  $\kappa(t)$  can be independently controlled, even by several orders of magnitude [65]. On the other hand, it would be interesting to characterize the dependence of a in the nature of the bath and the SB coupling – e.g. its spectral density, more generally to derive similar quantum-mechanical finite-time corrections that are independent of the specific implementation, and to gain further insights in the connection between Landauer erasure and the Planckian time.

### 4.6 Proof of Thermalization

In this section we will prove that, in absence of driving, p(t) and v(t) thermalize. We do so in two steps, we first simplify the expressions of eq. (4.10) and eq. (4.11) for  $\varepsilon(t) = \varepsilon$  and  $\kappa(t) = \kappa$  and compute the infinite time limit. Then we compute the thermal expectation value of the corresponding observables and prove that the obtained expressions are the same.

#### 4.6.1 Infinite Time Limit in Absence of Driving

By assuming that the driving parameters are kept constant the propagator becomes

$$G(t,s) = e^{-(t-s)(\frac{1}{2}\kappa^2 + i\varepsilon)} . \tag{4.28}$$

This allows us to compute the time integrals in eq. (4.10) and eq. (4.11):

$$p(t) = p(0)e^{-\kappa^2 t} + \frac{\kappa^2}{2\pi} \int_{-\infty}^{\infty} d\omega \ f_{\beta}(\omega) \frac{1 - 2e^{-\kappa^2 t/2} \cos([\omega - \varepsilon]t) + e^{-\kappa^2 t}}{\kappa^4 / 4 + (\omega - \varepsilon)^2} , \qquad (4.29)$$

$$v(t) = \frac{\kappa}{\pi} \int_{-\infty}^{\infty} d\omega \ f_{\beta}(\omega) \frac{(\omega - \varepsilon) \left[ 1 - e^{-\kappa^2 t/2} \cos([\omega - \varepsilon]t) \right] - \frac{1}{2} \kappa^2 e^{-\kappa^2 t/2} \sin([\omega - \varepsilon]t)}{\kappa^4 / 4 + (\omega - \varepsilon)^2} \ . \tag{4.30}$$

By taking the limit  $t \to \infty$ , we find

$$\lim_{t \to \infty} p(t) = \int_{-\infty}^{\infty} \frac{d\omega}{\pi} f_{\beta}(\omega) \frac{\kappa^2/2}{\kappa^4/4 + (\omega - \varepsilon)^2} , \qquad (4.31)$$

$$\lim_{t \to \infty} v(t) = \kappa \int_{-\infty}^{\infty} \frac{d\omega}{\pi} f_{\beta}(\omega) \frac{(\omega - \varepsilon)}{\kappa^4 / 4 + (\omega - \varepsilon)^2} . \tag{4.32}$$

Here we can notice that if we take the Laplace transform of the propagator we obtain

$$\tilde{G}(z) := \int_0^\infty dt \ G(t,0)e^{-zt} = \frac{1}{z + i\varepsilon + \kappa^2/2} \ ,$$
 (4.33)

which allows us to rewrite eq. (4.31) and eq. (4.32) as

$$\lim_{t \to \infty} p(t) = \int_{-\infty}^{\infty} \frac{d\omega}{\pi} f_{\beta}(\omega) \Re \left[ \tilde{G}(-i\omega) \right] , \qquad (4.34)$$

$$\lim_{t \to \infty} v(t) = \kappa \int_{-\infty}^{\infty} \frac{d\omega}{\pi} f_{\beta}(\omega) \Im \left[ \tilde{G}(-i\omega) \right] . \tag{4.35}$$

#### 4.6.2 Thermal Expectation Value

We now compute the expectation value of  $\hat{a}^{\dagger}\hat{a}$  and  $\hat{V} = \sum_{k=1}^{n} \lambda_k \hat{a}^{\dagger}\hat{b}_k + \lambda_k^* \hat{b}_k^{\dagger}\hat{a}$  when the state is a Gibbs state. Therefore we want to find  $p_{th} := \text{Tr}[\hat{\pi}\hat{a}^{\dagger}\hat{a}]$  and  $v_{th} := \text{Tr}[\hat{\pi}\hat{V}]$ . Using the fact that the total Hamiltonian is quadratic, we can diagonalize it to rewrite it in the following way

$$\hat{H} = \sum_{k} \varepsilon_k \hat{c}_k^{\dagger} \hat{c}_k , \qquad (4.36)$$

where  $\varepsilon_k$  are eigen-energies and  $\hat{c}_k$  are fermionic ladder operators that follow the CAR:  $\{\hat{c}_j^{\dagger}, \hat{c}_k\} = \delta_{jk} \mathbb{1}, \{\hat{c}_j, \hat{c}_k\} = 0$ . They are related to the original ones by

$$\hat{a} = \sum_{k} \langle 0|\hat{a}|k\rangle \,\hat{c}_k \;, \qquad \hat{b}_j = \sum_{k} \langle 0|\hat{b}_j|k\rangle \,\hat{c}_k \;, \tag{4.37}$$

where  $|k\rangle = \hat{c}_k^{\dagger} |0\rangle$  are 1-particle eigenstates of the Hamiltonian with eigenvalue  $\varepsilon_k$ . Inserting this relation in the expression for the thermal expectation of the probability of occupation we find

$$p_{th} = \frac{1}{Z} \sum_{jk} \langle j | \hat{a}^{\dagger} | 0 \rangle \langle 0 | \hat{a} | k \rangle \operatorname{Tr} \left[ e^{-\beta \hat{H}} \hat{c}_{j}^{\dagger} \hat{c}_{k} \right] = \sum_{k} \left| \langle k | \hat{a}^{\dagger} | 0 \rangle \right|^{2} f_{\beta}(\varepsilon_{k}) . \tag{4.38}$$

By its definition, we can write the propagator as follows

$$G(t,0) = \langle 0|\hat{a}_H(t)\hat{a}^{\dagger}|0\rangle = \sum_{k} e^{-i\varepsilon_k t} \langle 0|\hat{U}^{\dagger}(t)\hat{a}|k\rangle \langle k|\hat{a}^{\dagger}|0\rangle = \sum_{k} e^{-i\varepsilon_k t} \left|\langle k|\hat{a}^{\dagger}|0\rangle\right|^2 ,$$

$$(4.39)$$

where we used the fact that the vacuum state does not evolve  $\hat{U}(t)|0\rangle = |0\rangle$  and  $\hat{U}(t) = e^{-it\sum_k \varepsilon_k \hat{c}_k^{\dagger} \hat{c}_k}$ . By now defining  $\varphi(\omega) := \sum_k \left| \langle k|\hat{a}^{\dagger}|0\rangle \right|^2 \delta(\omega - \varepsilon_k)$ , we can identify

$$G(t,0) = \int_{-\infty}^{\infty} d\omega \ \varphi(\omega) e^{-i\omega t} \ , \quad p_{th} = \int_{-\infty}^{\infty} d\omega \ f_{\beta}(\omega) \varphi(\omega) \ . \tag{4.40}$$

Considering eq. (4.34) it is clear that if  $\varphi(\omega) = \frac{1}{\pi} \Re \left[ \tilde{G}(-i\omega) \right]$  then we have proven  $p_{th} = \lim_{t \to \infty} p(t)$ . Therefore we compute the Laplace transform of G(t,0) using eq. (4.40)

$$\tilde{G}(-i\omega) = \int_0^\infty dt \ G(t,0)e^{i\omega t} = \pi\varphi(\omega) + iP. \int_{-\infty}^\infty d\omega' \ \frac{\varphi(\omega')}{\omega - \omega'} \ , \tag{4.41}$$

where P denotes the Cauchy principal value. Since  $\varphi(\omega)$  is by definition a real function we can see that P.  $\int_{-\infty}^{\infty} d\omega' \, \frac{\varphi(\omega')}{\omega - \omega'}$  is a real number. Therefore we can conclude  $\varphi(\omega) = \frac{1}{\pi} \Re \left[ \tilde{G}(-i\omega) \right]$ . Which concludes the proof of the thermalization of p(t).

To prove the thermalization of v(t) we proceed in a similar fashion. We start by computing  $v_{th}$ 

$$v_{th} = \sum_{jk} f_{\beta}(\varepsilon_k) \left( \lambda_j \langle k | \hat{a}^{\dagger} | 0 \rangle \langle 0 | \hat{b}_j | k \rangle + \lambda_j^* \langle k | \hat{b}_j^{\dagger} | 0 \rangle \langle 0 | \hat{a} | k \rangle \right) . \tag{4.42}$$

To proceed we have to define the following cross-propagators

$$\lambda_{j}K_{j}(t) := \langle 0|\hat{a}_{H}(t)\hat{b}_{j}^{\dagger}|0\rangle = \sum_{k} e^{-i\varepsilon_{k}t} \langle k|\hat{b}_{j}^{\dagger}|0\rangle \langle 0|\hat{a}|k\rangle = \int_{-\infty}^{\infty} d\omega \ \psi_{j}(\omega)e^{-i\omega t} \ , \quad (4.43)$$

$$\lambda_{j}^{*}H_{j}(t) := \langle 0|\hat{b}_{j,H}(t)\hat{a}^{\dagger}|0\rangle = \sum_{k} e^{-i\varepsilon_{k}t} \langle k|\hat{a}^{\dagger}|0\rangle \langle 0|\hat{b}_{j}|k\rangle = \int_{-\infty}^{\infty} d\omega \ \psi_{j}^{*}(\omega)e^{-i\omega t} \ , \quad (4.44)$$

where we defined  $\psi_j(\omega) = \sum_k \langle k | \hat{b}_j^{\dagger} | 0 \rangle \langle 0 | \hat{a} | k \rangle \, \delta(\omega - \varepsilon_k)$ . By further defining  $\psi_0(\omega) := \sum_k \lambda_k^* \psi_k(\omega)$  and  $\psi(\omega) = \psi_0(\omega) + \psi_0^*(\omega)$  we can see that

$$K(t) := \sum_{j} |\lambda_{j}|^{2} \left( K_{j}(t) + H_{j}(t) \right) = \int_{-\infty}^{\infty} d\omega \ \psi(\omega) e^{-i\omega t} , \qquad (4.45)$$

$$v_{th} = \int_{-\infty}^{\infty} d\omega \ f_{\beta}(\omega)\psi(\omega) \ . \tag{4.46}$$

Therefore, similarly to the case of G(t,0), we have

$$\tilde{K}(-i\omega) = \pi\psi(\omega) + iP.\int_{-\infty}^{\infty} d\omega' \frac{\psi(\omega')}{\omega - \omega'}$$

and in particular  $\pi\psi(\omega) = \Re\left[\tilde{K}(-i\omega)\right]$  (since  $\psi(\omega)$  is real by definition). Hence, by eq. (4.35) and eq. (4.46), the last step to prove that v(t) thermalizes is to check that  $\Re\left[\tilde{K}(-i\omega)\right] = g\Im\left[\tilde{G}(-i\omega)\right]$ . To do so we start by computing the components of K(t): from the solution of the evolution of  $\hat{a}_H$  and  $\hat{b}_{j,H}$  (cf. [12] for more detail) we can find

$$K_j(t) = H_j(t) = -ig \frac{e^{-i\omega_j t} - G(t, 0)}{\frac{1}{2}g^2 + i(\varepsilon - \omega_j)}$$
 (4.47)

Since the time time dependence is contained in the exponentials, it is straightforward

to compute the Laplace transform

$$\tilde{K}_j(z) = \tilde{H}_j(z) = \frac{-ig}{z + i\omega_j} \tilde{G}(z) . \tag{4.48}$$

Therefore we find

$$\tilde{K}(-i\omega) = \frac{g}{\pi}\tilde{G}(-i\omega)P.\int_{-\infty}^{\infty} d\omega' \frac{1}{\omega - \omega'} = -ig\tilde{G}(-i\omega) , \qquad (4.49)$$

which allows us to conclude  $\psi(\omega)=g\Im\left[\tilde{G}(-i\omega)\right]$ . This concludes the proof of the thermalization of v(t).

# Chapter 5

# Collective Advantages

¡Hasta la victoria siempre!

— Ernesto Che Guevara

Collective effects play a central role in physics, ranging from phase transitions to quantum entanglement. Often, they can be exploited for a useful task, such as ultra-precise measurements [70], leading to the notion of a collective advantage<sup>1</sup>. In the growing fields of stochastic and quantum thermodynamics, such advantages have received notable attention: relevant examples are found in quantum batteries, where entangling operations have been proven to enable faster charging [14]; in many-body thermal engines, whose performance can be enhanced via phase transitions [15], many-body interactions [16], or superradiance [17]; and in quantum transport [18]. In this chapter, we uncover a new collective advantage in a crucial task in non-equilibrium thermodynamics: the minimization of dissipation in finite time. In general, the thermodynamic work W required to transform a system, in contact with an environment, in a finite time  $\tau$  can be split into two contributions (cf. Sec. 2.3)

$$W = \Delta F_{eq} + W_{diss} \tag{5.1}$$

a reversible contribution  $\Delta F_{eq}$ , the free energy change, and an irreversible positive contribution  $W_{diss}$ , the dissipated work. Whereas  $\Delta F_{eq}$  is extensive with the size N of the system, we will show here that  $W_{diss}$  can grow sub-linearly in N. This is proven in the regime of slow-but-finite-time processes and becomes possible by

<sup>&</sup>lt;sup>1</sup>The outcome of a task is improved when performed globally on a collection of systems compared than when realized on each system individually. There are multiple real life analogues of collective advantages in real life – unrelated to physics – such as collective action and bargaining or streamlined production (cf. Fig. 5.1).

5.1. Framework

exploiting many-body interactions suitably created along the process.

The advantage is dramatic: in principle, collective processes enable an N-fold reduction of  $W_{diss}$  when compared to local processes (see Fig. 5.2). While we will show that reaching this limit requires highly non-local or long-range interactions, a sub-linear growth of  $W_{diss}$  can be achieved with two-body interactions and realistic control. To obtain these results, we rely on the framework of thermodynamic geometry (cf. Sec. 3.2). Our results show that geodesic protocols generically explore highly interacting Hamiltonians, even if interactions are absent at the beginning and end of the process. As an application, we focus on finite-time information erasure (cf. Chapter 4) of N qubits. We show that collective processing can substantially re-



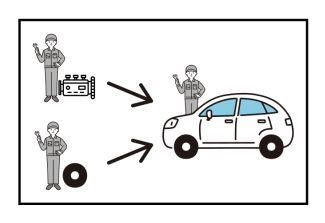


Figure 5.1: Analogue of collective advantages in the macroscopic world: the streamlining of production. Streamlined production lines (bottom) are much more efficient than a production line where each worker is creating the product independently (top). [71]

duce dissipation in this relevant task, leading to a faster convergence to Landauer's bound.

Overall, these results uncover a genuine collective advantage in stochastic and quantum thermodynamics, which is not linked to standard collective phenomena such as quantum entanglement, phase transitions, or collective system-baths couplings (e.g. superradiance).

### 5.1 Framework

Following the formalism introduced in Sec. 3.2, let us consider a system in a d-dimensional Hilbert space  $\mathbb{C}^d$  with an externally driven Hamiltonian  $\hat{h}(t)$ . It can be parameterized as  $\hat{h}(t) = \sum_{j=1}^{n} \lambda^{j}(t)\hat{x}_{j}$ ,  $\{\lambda^{j}\}$  are externally controllable parameters, and  $\{\hat{x}_{j}\}$  are the corresponding observables. Additionally, the system is in contact with an external thermal bath at inverse temperature  $\beta$ , so that the system is undergoing Lindblad dynamics eq. (3.9).

We focus on the task of driving  $\hat{h}(t)$  from an initial configuration  $\hat{h}(0) = \hat{h}_i$  to a final one  $\hat{h}(\tau) = \hat{h}_f$  in a time  $t \in [0, \tau]$ . External energy is needed to realize this

transformation, quantified by the (average) thermodynamic work:

$$W = \int_0^{\tau} dt \operatorname{Tr} \left[ \frac{d\hat{h}(t)}{dt} \hat{\rho}(t) \right] , \qquad (5.2)$$

where  $\hat{\rho}(t)$  is the state of the system. This expression can be split as in eq. (5.1), where  $\Delta F_{eq} = \beta^{-1} \ln Z(0)/Z(\tau)$ . The minimal dissipated work  $W_{diss}$  in a finite time  $\tau$  can then be found by optimizing the driving protocol  $\lambda : [0, \tau] \to M \subset \mathbb{R}^n$ . To address the non-trivial optimization we make some assumptions.

First, we assume that the driving  $\frac{d}{dt}\hat{h}(t)$  is slow compared to the relaxation rate. Then  $W_{diss}$  can be expressed as a quadratic form at leading order in  $\tau^{-1}$  (cf. Sec. 3.2):

$$W_{diss} = k_B T \int_0^{\tau} dt \ \dot{\lambda}^i(t) \dot{\lambda}^j(t) g_{ij}(\lambda(t)) + \mathcal{O}(\tau^{-2}) \ , \tag{5.3}$$

where  $g_{ij}(\lambda)$  is the so-called thermodynamic metric. By solving the geodesic equation that derive from the metric we can find the protocols that of minimal length  $\mathcal{L}$  by the metric and minimal dissipation  $W_{diss}^* = k_B T \mathcal{L}^2/\tau$ .

As a second simplification, we assume there is a single relaxation timescale  $\tau_{eq}^2$ , so that the metric becomes [9]:

$$g_{ij} = -\tau_{\rm eq} \beta \frac{\partial^2 F_{eq}(\lambda)}{\partial \lambda^i \partial \lambda^j} \ . \tag{5.4}$$

Note that  $g_{ij}$  then becomes the standard thermodynamic metric for macroscopic systems [72, 73], which can also describes step-processes [74]. In what follows, without loss of generality, we set  $\tau_{eq} = 1$ .

As a last simplification, we will assume that the initial and final Hamiltonian commute  $[\hat{h}_i, \hat{h}_f] = 0$ . This allows us to conclude that at all times  $[\frac{d}{dt}\hat{h}(t), \hat{h}(t)] = 0$ , as changes in the eigen-basis can only increase dissipation in the linear response regime [43].

Let us now consider a scenario in which we perform the driving on N copies of the system. We denote by  $\hat{H}(t) = \hat{H}_0(t) + \hat{H}_{\rm int}(t)$  the total Hamiltonian for all the copies, where  $\hat{H}_0(t) = \sum_{j=1}^N \hat{h}^{(j)}(t)$  and  $\hat{H}_{\rm int}(t)$  contains the interaction between the copies. We parameterize  $\hat{H}(t)$  similarly to  $\hat{h}(t)$ :  $\hat{H}(t) = \sum_{i=1}^n \gamma^i(t) \hat{X}_i$ , where the sum can have up to  $n = d^N$  terms. The problem at hand imposes the following boundary conditions on the protocol:  $\hat{H}_{\rm int}(0) = \hat{H}_{\rm int}(\tau) = 0$ ,  $\hat{h}^{(j)}(0) = \hat{h}_i$ , and  $\hat{h}^{(j)}(\tau) = \hat{h}_f \ \forall j$ .

<sup>&</sup>lt;sup>2</sup>We assume that all driven observables decay exponentially to equilibrium with the same timescale [43].

Furthermore, by the same reasoning as in the case for a single copy, we have that  $\left[\frac{d}{dt}\hat{H}(t),\hat{H}(t)\right]=0$  for the geodesic protocol.

## 5.2 Fundamental Limit of Collective Advantages

Let us first note that  $\Delta F_{eq}$  is extensive with N which directly follows from the boundary conditions. Instead,  $W_{diss}$  depends on the process and can exhibit a non-trivial behavior whenever  $\hat{H}_{int}(t) \neq 0$ . Indeed, we find that, in general, geodesic paths explore highly interacting Hamiltonians if the constraints allow for it.

To reach the fundamental limit of  $W_{diss}^*$  we can assume full control on  $\hat{H}(t)$ , so that the  $n=d^N$  different eigen-energies  $\{\gamma^i\}$  can be externally controlled at will – the corresponding  $\{\hat{X}_i\}$  are chosen to be the corresponding eigen-projectors. In this case, the distance function corresponding to the thermodynamic metric eq. (5.4) is known to be the quantum Hellinger angle:  $\mathcal{L}(\gamma, \gamma') = 2 \arccos \text{Tr} \left[\sqrt{\hat{\pi}(\gamma)} \sqrt{\hat{\pi}(\gamma')}\right]$  where  $\hat{\pi}(\gamma) = e^{-\beta \hat{H}(\gamma)}/Z(\gamma)$  is the thermal state (cf. [13]). Therefore the optimal dissipation of a protocol is

$$\beta W_{diss}^* = \frac{1}{\tau} \left( 2 \arccos \operatorname{Tr} \left[ \sqrt{\hat{\pi}(0)} \sqrt{\hat{\pi}(\tau)} \right] \right)^2 . \tag{5.5}$$

Since trivially  $\arccos(x) \leq \pi/2$  for x > 0, the minimal dissipation of a N-body system is bounded by a constant  $W_{diss}^* \leq \frac{1}{\tau}\pi^2$  independent of N. This is somehow astonishing, as we expect the dissipation generated when driving a many-body system to increase extensively with its size. The corresponding protocol that achieves this limit is given by

$$\beta \hat{H}(t) = -2\log\left[\sin\left[\frac{(\tau - t)\mathcal{L}^*}{2\tau}\right]\sqrt{\hat{\pi}(0)} + \sin\left[\frac{t\mathcal{L}^*}{2\tau}\right]\sqrt{\hat{\pi}(\tau)}\right],\tag{5.6}$$

where  $\mathcal{L}^* = \mathcal{L}(\hat{\pi}(0), \hat{\pi}(\tau))$ . Crucially, this protocol generally requires all possible interacting terms available in the Hamiltonian space, including highly non-local N-body interactions. One can easily prove this, by contradiction, for generic protocols using the non linearity of the logarithm. This is illustrated in what follows for the paradigmatic task of erasing N bits of information.

### 5.3 Collective Erasure

Let us consider N qubits, each with local Hamiltonian  $\hat{h}(t) = \varepsilon(t)\hat{\sigma}_z$ . We want to drive  $\varepsilon(t)$  from  $\varepsilon(0) = 0$  to  $\varepsilon(\tau) = E$  with  $E \gg k_B T$ , so that the state of each qubit evolves from a fully mixed state  $\hat{\pi}(0) = \frac{1}{2}\mathbb{1}$  to an (almost) pure state  $\hat{\pi}(\tau) \approx |0\rangle\langle 0|$  due to the action of the external bath. We have  $\Delta F_{eq} = Nk_B T \ln 2$ , corresponding to Landauer's bound.

Consider first the independent scenario, so that during the whole protocol  $\hat{H}_{\rm int}(t) = 0$ . For each qubit, the dissipation generated via an optimal driving can be computed from eq. (5.5) with the aforementioned boundary conditions, yielding  $\beta W_{diss}^* = \pi^2/4\tau$ . The total dissipation of N qubits then reads:

$$W_{diss}^{*,\text{local}} = \frac{\pi^2}{4\tau} N k_B T , \qquad (5.7)$$

which grows linearly with N. The corresponding optimal driving reads  $\beta \varepsilon(t) = \ln \tan[\pi(t+\tau)/4\tau]$ , which has been implemented experimentally in a single-energy driven dot [54].

If we now allow for full control of the Hamiltonian, we can again use eq. (5.5) to compute the minimal dissipation, but this time we use the global states  $\hat{\pi}(0) = \frac{1}{2^N} \mathbb{I}$  and  $\hat{\pi}(\tau) \approx |0\rangle\langle 0|^{\otimes N}$  instead of the local ones. This leads to:

$$W_{diss}^{*,\text{global}} = \frac{k_B T}{\tau} \left( 2 \arccos\left[\frac{1}{2^{N/2}}\right] \right)^2 = \frac{\pi^2}{\tau} k_B T + \mathcal{O}(e^{-N/2}) . \tag{5.8}$$

Therefore, an N-fold advantage can potentially be achieved by global processes, as illustrated in Fig. 5.2.

Let us now discuss the implications of this result for the reachability of Landauer's bound. From eq. (5.1) we have  $\Delta F_{eq} = Nk_BT \ln 2$  whereas  $W_{diss}$  can reach eq. (5.8) at leading order in  $\tau^{-1}$  (recall that our results are based on the slow driving assumption where the expansion eq. (5.3) is well justified). Hence, the work cost of erasure for each qubit can be written as:

$$W_{\text{qubit}}^* = k_B T \left( \ln 2 + \frac{\pi^2}{\tau N} \right) + \mathcal{O}\left(\tau^{-2}\right). \tag{5.9}$$

Hence, in the thermodynamic limit  $N \to \infty$ , we can approach Landauer's bound with an error that scales as  $\tau^{-2}$  instead of the standard  $\tau^{-1}$  (cf. Chapter 4). We note that a link between complexity, as in higher level k-body interactions and faster information erasure has been suggested in Ref. [40]. The optimal driving achieving

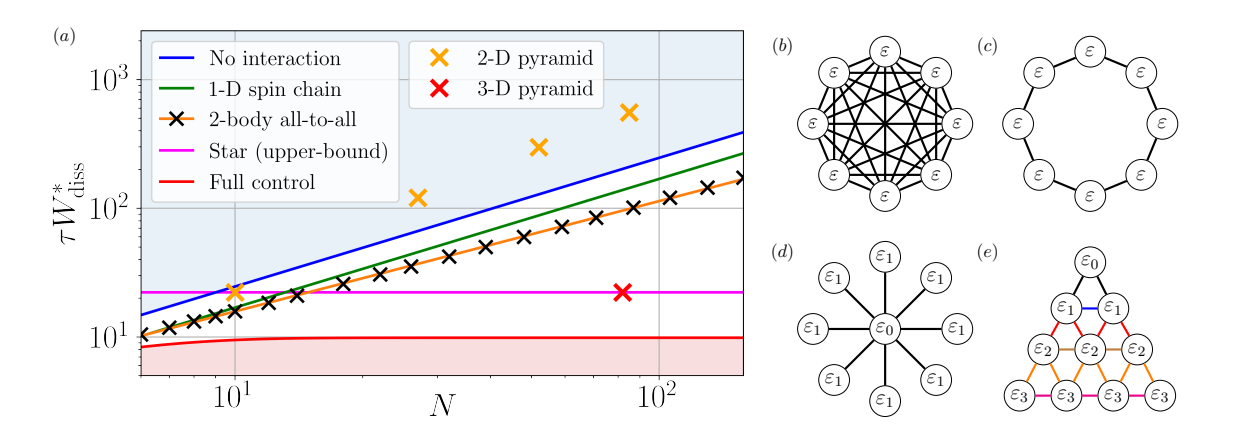


Figure 5.2: (a) Minimal dissipation for the erasure of N spins for different control designs analyzed in this chapter. These are compared with the dissipations that are achievable with no interactions (eq. (5.7), blue-shaded area), and with the dissipations that are not achievable regardless of the protocol (eq. (5.8), red-shaded area). We find  $\tau W_{diss}^{*,{\rm chain}} \approx 1.69N$ ,  $\tau W_{diss}^{*,{\rm all}} \approx 2.20N^{0.857}$ , while  $\tau W_{diss}^{*,{\rm Star}} \leq 9\pi^2/4$ . Single points are provided for 2-D and 3-D Pyramid models with few layers and an aperture of 8. (b-e) Depiction of the geometries of the interactions in eq. (5.12) (equal colors/labels correspond to equal values of the local fields). (b) all-to-all model with N=8, (c) 1-D spin chain with N=8, (d) the Star model with N=9, (e) 2-D Pyramid model with 4 layers and an aperture of 1.

the limit eq. (5.8) can be computed from eq. (5.6):

$$\beta \hat{H}(t) = \gamma(t) \sum_{j=1}^{N} (-1)^{j+1} \sum_{i_1 < i_2 < \dots < i_j}^{N} \hat{x}^{(i_1)} \hat{x}^{(i_2)} \dots \hat{x}^{(i_j)} , \qquad (5.10)$$

where  $\hat{x} = \hat{\sigma}_{+}\hat{\sigma}_{-}$  and the control function can be written as

$$\gamma(t) = 2\log\left[1 + 2^{N/2}\sin\left(\frac{\pi t}{2\tau}\right)\sin^{-1}\left(\frac{\pi(\tau - t)}{2\tau}\right)\right] . \tag{5.11}$$

It follows that highly non-local N-body interactions are required to saturate the bound eq. (5.8). More specifically, one needs to activate every possible (classical) interaction present in the system. This makes reaching the fundamental bound eq. (5.8) highly challenging in practice, and opens the question as to whether collective advantages beyond the local bound eq. (5.7) can be achieved via more realistic driven many-body systems featuring (local) few-body interactions. We address this relevant question in what follows.

## 5.4 Driven Many-Body Systems

In this section, we constrain the total system to only feature at most 2-body interactions, to seek collective advantages in a more realistic model. Specifically, we consider a spin system with Hamiltonian of the form

$$\hat{H}(t) = \sum_{i=1}^{N} \varepsilon_i(t)\hat{\sigma}_z^{(i)} + \frac{1}{2} \sum_{i,j=1}^{N} J_{ij}(t)\hat{\sigma}_z^{(i)}\hat{\sigma}_z^{(j)}$$
(5.12)

We thus examine different degrees of control, reflected in the topologies represented in Fig. 5.2: (i) an all-to-all spin model, (ii) a 1-D spin chain with nearest neighbor interaction (with periodic boundary conditions) (iii) a Star-shaped design, which we generalize to (iv) a multi-layer Pyramid scheme. In practice, the energies  $\varepsilon_i(t)$  could be tuned via an external magnetic field whereas the interaction strength  $J_{ij}(t)$  could be controlled by changing the distance between the spins, which are interacting via dipole-dipole coupling. Current quantum annealers have the capacity of tuning generic Hamiltonians of the form eq.  $(5.12)^3$ .

The all-to-all model corresponds to taking uniform magnetic fields and spin interactions, i.e.  $\varepsilon_i(t) \equiv \varepsilon(t)$  and  $J_{ij}(t) \equiv J(t)$  in eq. (5.12). We can compute the partition function as follows

$$Z_{\text{all}} = \sum_{k=0}^{N} \binom{N}{k} e^{-\beta E_k} , \qquad (5.13)$$

where  $E_k = \varepsilon(2k - N) + \frac{1}{2}J(2k - N)^2$ . The standard 1-D Ising model corresponds to uniform local terms  $\varepsilon$ , and  $J_{i,i+1} \equiv J$  for nearest neighbors and 0 elsewhere. The partition function can be found by making use of the transfer matrix method:

$$Z_{\text{chain}} = z_{+}^{N} + z_{-}^{N} ,$$
 (5.14)

where  $z_{\pm} = e^{-\beta J/2} \cosh \beta \varepsilon \pm \sqrt{e^{-\beta J} \sinh \beta \varepsilon + e^{\beta J}}$ . Thirdly, we consider a Star topology corresponding to a central spin  $\hat{\sigma}_z^{(1)}$  with local magnetic field  $\varepsilon_0(t)$  and uniform elsewhere  $\varepsilon_i(t) \equiv \varepsilon_1(t) \ \forall i > 1$ , and uniform "radial" interaction  $J_{1j}(t) = J_{j1}(t) \equiv J(t)$ , and 0 elsewhere. The partition function is easily computed as

$$Z_{\text{Star}} = e^{-\beta \varepsilon} (2\cosh\beta\lambda_{+})^{N-1} + e^{\beta \varepsilon} (2\cosh\beta\lambda_{-})^{N-1} , \qquad (5.15)$$

<sup>&</sup>lt;sup>3</sup>See for example D-Wave Systems.

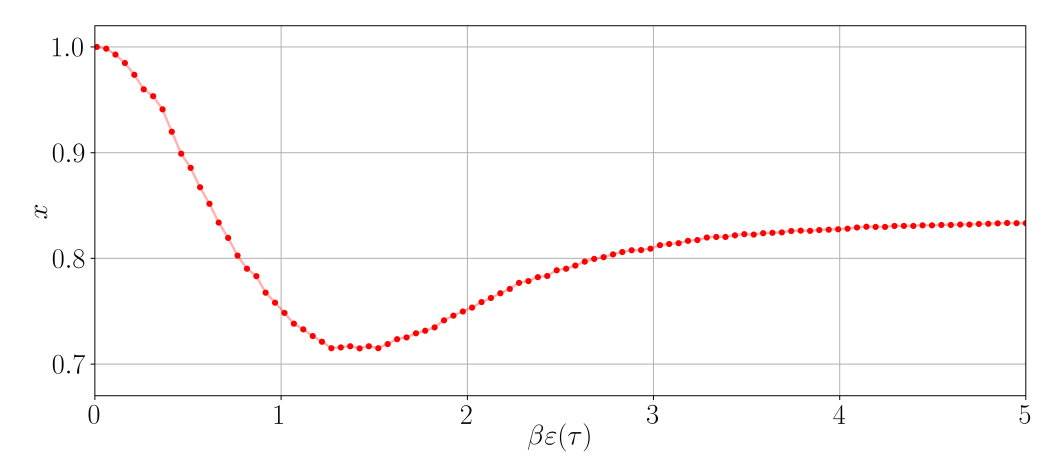


Figure 5.3: Dependence of the exponent x of the dissipation  $W_{diss}^{*,\text{all}} = \alpha N^x$  on the boundary condition  $\beta \varepsilon(\tau)$  (with  $\varepsilon(0) = 0$ ). The fit is achieved for numerical data up to N = 150.

where  $\lambda_{\pm} = \varepsilon_1 \pm J$ .

For the models above, given the partition function, we compute the metric according to eq. (5.4), from which we can obtain the geodesic equations. Their solution provides us with the minimal length for given boundary conditions, from which we find the minimal dissipation. We implemented this procedure numerically for the task of approximate erasure, we take  $\varepsilon(0) = J(0) = J(\tau) = 0$  and  $\varepsilon(\tau) = 5k_BT$  which corresponds to an erasure process with an error of  $4.5 \cdot 10^{-5}$ .

In Fig. 5.2 we present the resulting minimal dissipation for the different many-body models. The results are contrasted with the optimal non-interacting protocol eq. (5.7) and the fundamental bound obtained with full-control eq. (5.8) (i.e. arbitrarily complex interactions).

First, we observe that the nearest neighbor model displays a linear increase of the dissipation with N, but with a better pre-factor than the non-interacting case  $(W_{diss}^{*,\text{chain}}/W_{diss}^{*,\text{local}} \approx 0.686)$ . On the other hand, the all-to-all model displays a sub-linear dependence on N:  $W_{diss}^{*,\text{all}} = \alpha N^x$  with  $x \approx 6/7$ . Furthermore, the exponent x displays a non-trivial dependence on the specific boundary conditions, which can been seen in Fig. 5.3. Finally, quite remarkably, the Star model can achieve a finite value of the dissipation, independent of N. This feature is enabled by a 3-step protocol that suppresses specific terms in the otherwise-extensive  $\log Z_{\text{Star}}$ . Interestingly, the Star model was found to be optimal in the context of two-body probes used for thermometry [75].

The sub-linearity of the all-to-all's and Star-model's dissipation is remarkable as it allows for the same effect as in eq. (5.9): it is possible to reach Landauer's bound

Model	1D chain	All-to-All	Star	Pyramid
Asymptotic $W_{diss}$	$\mathcal{O}(N)$	$\mathcal{O}(N^x)$	$\mathcal{O}(1)$	$O(N^{2/D})$
Short-range	✓	X	Х	<b>✓</b>

Table 5.1: All models studied in this work are based on two-body interactions (cf. eq. (5.12)). The All-to-all and Star model feature long-range interactions that enable a sub-linear scaling of  $W_{diss}$ , i.e. a *collective advantage*. The Pyramid models can achieve such advantage in D=3 spatial dimensions using short-range interactions only.

in finite-time with an error that scales as  $\tau^{-2}$  instead of  $\tau^{-1}$  as one approaches the thermodynamic limit. However, both these models use long-range interactions between arbitrarily far spins as N grows, and their scaling properties might thus be seen as inconsequential. However, we can generalize the Star model to a multi-layer structure, i.e. a Pyramid model (cf. Fig. 5.2). By generalizing the Star protocol, it can be shown that (cf. Supp. Mat. of [13]) such model can achieve  $W_{diss}^{\rm Pyr} \propto \ell^2$ , where  $\ell$  is the number of layers of the pyramid. Given that  $N \propto \ell^D$  for pyramids in D spatial dimensions,  $W_{diss}^{\rm Pyr} \propto N^{2/D}$  follows asymptotically.

### 5.5 Conclusions and Discussion

In this chapter, we considered the task of minimizing dissipated work,  $W_{diss}$ , for an N-body system. We showed that, in contrast to  $\Delta F_{eq}$ ,  $W_{diss}$  can grow sublinearly with N by suitably creating interactions between the N systems along the process. This leads to a finite-time reduction of dissipation induced by collective processes and has a clear potential for improving various thermodynamic tasks ranging from quantum/stochastic engines [76,77] to the estimation of equilibrium free energy via non-equilibrium work measurements [78]; or, as is shown here, for the erasure of information in finite time. There are several observations to be made about these collective processes.

First, the derived collective processes are a genuine effect of finite-time thermodynamic protocols, which cannot be directly linked to other well-known collective phenomena such as entanglement, phase transitions, or superradiance. Indeed, (i) they do not require the presence of quantum correlations or coherence, but rather arise due to the interplay between interactions and dissipation to an external thermal environment; and (ii) they are process dependent – i.e. depend on the whole driving protocol  $\hat{H}(t)$  – unlike phase transitions which take place in a particular point in the parameter space.

Second, the results of this chapter suggest an interesting interplay between the complexity of the interactions and the associated reduction in dissipation, which is to be confronted with the results of Ref. [40]. In particular, we argued that reaching the maximal advantage requires highly non-local N-body interactions. Despite this, we showed that similar reductions (in scaling) can be achieved with only two-body long-range interactions via the Star model. A sub-linear growth of  $W_{diss}$  was found in the all-to-all model and, crucially, in the Pyramid model that only features short-range strong interactions. See Table 5.1 for a compact summary.

Third, being derived in the linear response regime, the dissipated work is directly related to the work fluctuations  $\sigma_W^2$  via the work fluctuation-dissipation relation  $\frac{\beta}{2}\sigma_W^2 = W_{diss}$ . This implies that the collective gains also lead to a reduction of work fluctuations, a desired property in stochastic thermodynamics.

Finally, it is important to stress that our results have been derived in the slow driving regime, i.e., for the leading order contribution of  $W_{diss}$  in  $\tau^{-1}$ . For a finite (large) time  $\tau$ , the next order contributions of  $\mathcal{O}(\tau^{-2})$  can become relevant when increasing N. An exciting future endeavor is to generalize such collective advantages for arbitrary non-equilibrium protocols. For this, it might be useful to exploit recent results on minimal dissipation and the Wasserstein distance [79] as well as new tools such as reinforcement learning [25] or fast-driving expansions [26] for finding optimal protocols.

Another future challenge is to understand how the collective advantages are modified beyond the simple model of thermalization used in eq. (5.4) and by adding constraints on the strength of the couplings in eq. (5.12). In particular, whether such advantages can still be found for more realistic thermalization models where the relaxation timescale(s) is modified in the presence of interactions, which can lead to a critical slowdown of relaxation.

# Chapter 6

# Thermodynamic Optimization

Give me a lever long enough and a fulcrum on which to place it, and I shall move the world.

— Archimedes

The study of how to optimize the energetic cost of a physical task goes back to the very origin of Thermodynamics with Carnot optimizing the efficiency of thermal steam engines [80]. This is a question that has a dual scope, on the one hand it can applied for very practical purposes such as optimizing car engines [27] or minimizing the overheating of the chips in super-computers [81], while on the other hand it can applied to probe the most fundamental aspects of the laws of thermodynamics – e.g. finding the fundamental limit between a finite-resource process and a reversible process [40].

Generally, optimizing a thermodynamic operation that brings the Hamiltonian of a system from  $\hat{H}_i$  to  $\hat{H}_f$  consists in finding the optimal time variation  $\hat{H}(t)$  that minimizes the energy dissipated into the environment. This optimization can be done with varying degrees of constraints to achieve more applied or more fundamental lower bounds on dissipation. These bounds can then also be used as speed limits [82] for performing the described operations, which is of particular interest for classical and quantum computers. However, it is always a very challenging problem as it requires functional optimization and boundary value problems to be solved [69] over solutions of the time-dependent Schrodinger (or Lindblad) equation. There are a variety of methods to tackle this problem – analytical as well as numerical – these range from optimal transport [83] and optimal control theory [49, 84, 85] to geometric methods (cf. Sec. 3.2 and [12]). Because of the fundamental difficulty of this problem, many open questions remain that range from direct applications to

more general and fundamental ones.

It is important to note that the minimal amount of work W can be negative, thus resulting in a gain of energy for the agent. Therefore, in the proper setting, one can find thermodynamic protocols such that work is extracted from an environment that is out of equilibrium (cf. Sec. 2.3). Typically an out-of-equilibrium-environment is modeled as a collection of thermal baths at different temperatures – often two of those. A thermal engine is a device that implements periodically a work extracting protocol, so that it can convert a flow of heat between two (or more) thermal baths into "useful energy" (e.g. kinetic energy).

A relatively simple example to showcase how an engine can exploit a difference in temperature between two thermals baths to extract work is a periodically driven quantum dot engine. Since the quantum dot has only two energy levels, we can choose the Hamiltonian so that the lower energy state has zero energy and the higher energy state has energy  $\varepsilon$ . Let us now consider the following process: we first let the dot thermalize with the colder bath, then we pay some energy to increase the energy gap  $\varepsilon$ . At this point, we let the dot thermalize with the warmer bath and then gain some energy by taking  $\varepsilon$  back to its initial value. The main thing to note, to see why one could gain energy in such a process, is that one only pays or gains energy when the excited state is occupied, as can be see from the integral form of work eq. (2.5). Since the probability of being in the excited state is lower when the dot is thermalized with the colder bath compared to when it's thermalized with the warmer bath, it is more likely to gain energy from this process than it is to pay energy. Therefore, on average, energy flows from the warmer bath to the cold bath and the agent.

The performance of an engine can be quantified in different ways. One very natural metric to do so is the average amount of energy extracted per unit time: power, which is defined as

$$\langle P \rangle := -\frac{W}{\tau} \ , \tag{6.1}$$

where here we denote by W the work cost of a cycle and by  $\tau$  the length of the cycle. However, when we consider that some of the energy from the warm bath ends up in the cold bath during a cycle, it can also be natural to consider how efficient the engine is

$$\eta := \frac{W}{Q_h} \,, \tag{6.2}$$

where  $Q_h$  denotes the energy gained by the hot bath – the sign choice of  $Q_h$  might be making this definition less intuitive, but it was made so to be consistent with the first law as it is formulated in eq. (2.2). The optimization of these quantities is a topic which has been a widely studied in the literature [86–88]. However it is seldom the case that they can be optimized simultaneously. Finally, the systems we will be dealing with are stochastic in nature. As opposed to engines at the macroscopic scale, one cannot expect to extract the same amount of work at each cycle, therefore we will be quantifying the constancy – or more precisely, the lack thereof – with the power fluctuations  $\langle \Delta P \rangle := \sigma_W^2/\tau$ , where  $\sigma_W^2$  is the variance of work [89]

$$\sigma_W^2 := 2 \Re \int_0^\tau dt \int_0^t dt' \operatorname{Tr} \left[ \hat{H}'(t) G(t, t') \left[ \Delta_{\hat{\rho}(t')} \hat{H}'(t') \hat{\rho}(t') \right] \right] , \qquad (6.3)$$

for  $\Delta_{\hat{\rho}}\hat{A} := \hat{A} - \text{Tr}[\hat{A}\hat{\rho}]$  and G the propagator of the evolution (cf. Sec. 3.1).

In this chapter, we will be looking at three examples of thermodynamic optimization: for a quantum dot engine [25], for an information engine (a.k.a. Szilard engine), and finally for fast thermodynamic operations [26].

## 6.1 Quantum Dot Heat Engine

Stochastic heat engines are devices that convert a heat flow into work at the nanoscale [90]. We can distinguish between two classes of such engines: steady-state heat engines (SSHE) perform work against external thermodynamic forces (e.g. a chemical potential difference) after reaching a non-equilibrium steady state [91], while periodically driven heat engines (PDHE) perform work against external driving fields through time-dependent cycles. Earlier works have started optimizing the power fluctuation of these engines [19,20]. However, a framework to fully optimize the performance of microscopic heat engines that accounts power, efficiency and power fluctuations is currently lacking. In fact, an ideal engine operates at high power, high efficiency, and low power fluctuations; however, such quantities usually cannot be optimized simultaneously, but one must seek trade-offs. In SSHEs, a rigorous manifestation of this trade-off is given by thermodynamic uncertainty relations [21, 24]. For "classical" stochastic SSHE (i.e. in the absence of quantum coherence) operating between two thermal baths at inverse temperatures  $\beta_{\rm C}$  (cold) and  $\beta_{\rm H}$  (hot), they read [21]:

$$\xi \equiv \frac{2}{\beta_{\rm C}} \frac{\langle P \rangle}{\langle \Delta P \rangle} \frac{\eta}{\eta_{\rm c} - \eta} \le 1, \tag{6.4}$$

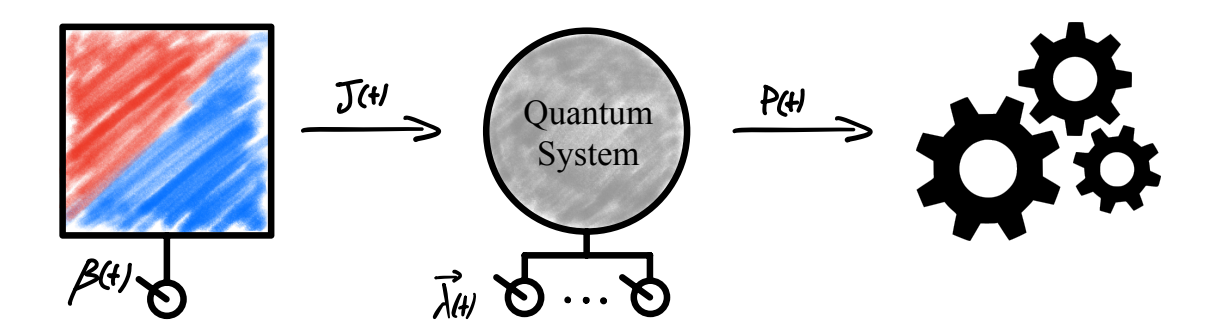


Figure 6.1: A quantum system (gray circle) is coupled to a thermal bath (left box) characterized by a controllable inverse temperature  $\beta(t)$ . The coupling produces a heat flux J(t). Control parameters  $\lambda(t)$  allow us to control the state of the system and the power P(t) extracted from the system.

where  $\eta_c \equiv 1 - \beta_H/\beta_C$  is the Carnot efficiency. Such thermodynamic uncertainty relations imply, for example, that high efficiency can only be attained at the expense of low power or high power fluctuations. The thermodynamic uncertainty relation inequality eq. (6.4) can be violated with quantum coherence [92] and in PDHEs [93]. This has motivated various generalized thermodynamic uncertainty relations [94], in particular for time-symmetric driving [95] and slowly driven stochastic engines [96]. Despite their importance, thermodynamic uncertainty relations provide an incomplete picture of the trade-off: while high values of  $\xi$  may appear more favorable, this does not give us any information on the individual objectives.

In this section, we present a framework to optimize any trade-off between power, efficiency, and power fluctuations in arbitrary PDHE described by Lindblad dynamics [97,98]. This allows us to find Pareto-optimal cycles, i.e. those cycles where no objective can be further improved without sacrificing another one. We then show how reinforcement learning (RL) can be used to fully optimize a quantum dot (QD) engine [99]. We characterize the Pareto front, i.e. the set of values  $\{\langle P \rangle, \langle \Delta P \rangle, \eta\}$  corresponding to Pareto-optimal cycles, and evaluate the thermodynamic uncertainty relation ratio  $\xi$  on such optimal cycles. Furthermore, we derive analytical results for the Pareto front and  $\xi$  in the fast and slow driving regimes, i.e. when the period of the cycle is respectively much shorter or much longer than the thermalization timescale of the system.

#### 6.1.1 Multi-Objective Optimization of Heat Engines

In this case we will study an engine featuring a single thermal bath with tunable inverse temperature  $\beta(t)$  between two extremal values  $\beta_{\rm H}$  and  $\beta_{\rm C}$ , which can be regarded as having a large selection of baths to choose from – thus allowing for further optimization. An illustration is presented in Fig. 6.1. The coupling between system and bath produces a heat flux J(t) from the bath to the quantum system, while the system itself is controlled by the parameters  $\vec{\lambda}(t)$  that allow exchanging work with the system. Therefore, in this framework, a thermodynamic cycle is described by periodic functions  $\beta(t)$  and  $\vec{\lambda}(t)$ . This framework includes standard PDHEs, in which the system is sequentially put in contact with two baths (by abruptly changing the values of  $\beta(t)$ ) and cases where  $\beta(t)$  varies smoothly in time. We assume that the dynamics of the system are described by a Markovian master equation (cf. Sec. 3.1), and we consider PDHEs in the asymptotic limit cycle – i.e. in the limit of infinite repetitions of the cycle. Because of this assumption, we can express that the time average  $\langle O \rangle$  of an arbitrary quantity O(t) as

$$\langle O \rangle = \frac{1}{\tau} \int_0^{\tau} dt \ O(t) \ , \tag{6.5}$$

where  $\tau$  is the period of the cycle. We can therefore compute the average power  $\langle P \rangle$ , power fluctuations  $\langle \Delta P \rangle$  and entropy production  $\langle \Sigma \rangle$  by averaging

$$P(t) = -\text{Tr}\left[\hat{\rho}(t)\hat{H}'(t)\right] , \qquad (6.6)$$

$$\Delta P(t) = \text{Tr}\left[\hat{s}(t)\hat{H}'(t)\right],\tag{6.7}$$

$$\Sigma(t) = -\beta(t) \operatorname{Tr} \left[ \hat{\rho}'(t) \hat{H}(t) \right] = -J(t) \beta(t) . \tag{6.8}$$

Here,  $\hat{\rho}(t)$  and  $\hat{H}(t)$  are respectively the reduced density matrix and the local Hamiltonian of the quantum system, while  $\hat{s}(t)$  is an auxiliary Hermitian operator satisfying  $\text{Tr}[\hat{s}(t)] = 0$  that we introduce to compute the power fluctuations. These satisfy

$$\frac{d\hat{\rho}(t)}{dt} = \mathcal{L}_{\vec{\lambda}(t),\beta(t)}[\hat{\rho}(t)],$$

$$\frac{d\hat{s}(t)}{dt} = \mathcal{L}_{\vec{\lambda}(t),\beta(t)}[\hat{s}(t)] + \{\hat{\rho}(t), \hat{H}'(t)\} - 2\text{Tr}[\hat{\rho}(t)\hat{H}'(t)]\hat{\rho}(t),$$
(6.9)

where  $\mathcal{L}_{\vec{\lambda}(t),\beta(t)}$  is the Lindbladian describing the evolution of the system and  $\{\cdot,\cdot\}$  is the anti-commutator. In the asymptotic limit cycle, it can be shown that both  $\hat{\rho}(t)$  and  $\hat{s}(t)$  are periodic with the same period as the control, and can thus be determined

by solving eq. (6.9) with periodic boundary conditions. While the expressions of  $\langle P \rangle$  and  $\langle \Sigma \rangle$  are standard in the limit cycle [100], the expression for  $\langle \Delta P \rangle$  in terms of  $\hat{s}(t)$  is less common. But we use it here as it is crucial to efficiently minimize the power fluctuations of the non-equilibrium engine using RL.

To identify Pareto-optimal cycles we introduce the dimensionless figure of merit

$$\langle F \rangle = a \frac{\langle P \rangle}{P_{\text{max}}} - b \frac{\langle \Delta P \rangle}{\Delta P(P_{\text{max}})} - c \frac{\langle \Sigma \rangle}{\Sigma(P_{\text{max}})},$$
 (6.10)

where  $a, b, c \geq 0$  are three scalar weights, satisfying a + b + c = 1, that determine how much we are interested in each of the three objectives, and  $P_{\text{max}}$ ,  $\Delta P(P_{\text{max}})$  and  $\Sigma(P_{\text{max}})$  are respectively the average power, fluctuations and entropy production of the cycle that maximizes the power. Notice that, given the relation between entropy production and efficiency, cycles that are Pareto-optimal for  $\{\langle P \rangle, \langle \Delta P \rangle, \eta \}$ , are also Pareto-optimal for  $\{\langle P \rangle, \langle \Delta P \rangle, \langle \Sigma \rangle\}$ . The positive sign in front of  $\langle P \rangle$  in eq. (6.10) ensures that we are maximizing the power, while the negative sign in front of  $\langle \Delta P \rangle$  and  $\langle \Sigma \rangle$  ensures that we are minimizing power fluctuations and the entropy production. Pareto-optimal trade-offs are then found maximizing  $\langle F \rangle$  for various choices of a, b and c.

### 6.1.2 Optimal Quantum Dot Heat Engine

In the following, we compute Pareto-optimal cycles in a minimal heat engine consisting of a two-level system coupled to a Fermionic bath with flat density of states. This represents a model of a single-level QD [86]. The Hamiltonian reads

$$\hat{H}(t) = \lambda(t) \frac{\varepsilon}{2} \hat{\sigma}_z, \tag{6.11}$$

where  $\lambda(t)$  is our single control parameter,  $\varepsilon$  is a fixed energy scale and  $\hat{\sigma}_z$  is the z-Pauli matrix. Denoting with  $|1\rangle$  the excited state of  $\hat{H}(t)$ , and defining  $p(t) := \langle 1|\hat{\rho}(t)|1\rangle$  as the probability of being in the excited state, the Lindblad equation eq. (6.9) becomes  $p'(t) = -\gamma(p(t) - f(\varepsilon\lambda(t)\beta(t)))$ , where  $\gamma^{-1}$  is the thermalization timescale arising from the coupling between system and bath, and  $f(x) = (1+e^x)^{-1}$  is the excited level population of the instantaneous Gibbs state.

We optimize  $\langle F \rangle$  of the QD heat engine using three different tools: RL, analytics in the fast-driving regime, and analytics in the slow-driving regime. The RL-based method allows us to numerically optimize  $\langle F \rangle$  without making any approximations on the dynamics, exploring all possible (time-discretized) time dependent controls

 $\beta(t)$  and  $\lambda(t)$  subject to the constraints  $\beta(t) \in [\beta_{\rm H}, \beta_{\rm C}]$  and  $\lambda(t) \in [\lambda_{\rm min}, \lambda_{\rm max}]$ , and identifying automatically also the optimal period  $\tau$ . The RL method, based on the soft actor-critic algorithm [101] and generalized from [102,103], additionally includes the crucial impact of power fluctuations, and identifies Pareto-optimal cycles. Machine learning methods have been employed for other quantum thermodynamic [104] and quantum control [105] tasks.

The fast-driving regime assumes that  $\tau \ll \gamma^{-1}$ . Interestingly, without any assumption on the driving speed, we show that any trade-off between power and entropy production (b = 0 in eq. (6.10)) in the QD engine is maximized by Otto cycles in the fast-driving regime, i.e. switching between two values of  $\beta(t)$  and  $\lambda(t)$  "as fast as possible" [106]. We thus expect such "fast-Otto cycles" to be nearly optimal in the high power regime.

The slow-driving regime corresponds to the opposite limit, i.e.  $\tau \gg \gamma^{-1}$ . Since entropy production and power fluctuations can be minimized by considering quasistatic cycles, we expect this regime to be nearly optimal in the high efficiency and low fluctuations regime, i.e. for low values of a in eq. (6.10). To make analytical progress in this regime, we maximize eq. (6.10) assuming a finite-time Carnot cycle. The obtained results naturally generalize previous considerations for low-dissipation engines [22,107,108] to account for the role of fluctuations. The main technical tool is the geometric concept of "thermodynamic length" [43,109] which yields the first order correction in  $(\gamma \tau)^{-1}$  from the quasi-static limit.

We now present the results. Each point in Fig. 6.2(a) corresponds to a separate optimization of  $\langle F \rangle$  with weights c and a displayed on the x-y axis. Since b=1-a-c, points lying on the sides of the triangle (highlighted in yellow) correspond to optimizing the trade-off between 2 objectives, whereas points inside the triangle take all 3 objectives into account. Denoting the figure of merit optimized with RL and with fast-Otto cycles with  $\langle F \rangle_{\rm RL}$  and  $\langle F \rangle_{\rm FAST}$ , in Fig. 6.2(a) we show blue (red) dots when  $\langle F \rangle_{\rm RL} > \langle F \rangle_{\rm FAST}$  ( $\langle F \rangle_{\rm RL} \leq \langle F \rangle_{\rm FAST}$ ), while Fig. 6.2(b) is a contour plot of  $\langle F \rangle_{\rm RL}$ . As expected, there are red dots when b=0 (along the hypotenuse), but it turns out that fast-Otto cycles are optimal also when c=0. However, as soon as all 3 weights are finite, the optimal cycles identified with RL change abruptly and outperform fast-Otto cycles. Furthermore, we notice that while  $\langle F \rangle_{\rm RL}$  is positive for all values of the weights,  $\langle F \rangle_{\rm FAST} = 0$  below the black curve shown in Fig. 6.2(b) for its analytic expression.

To visualize the changes in protocol space, in Fig. 6.2(c,d,e) we show the cycles identified with RL at the three different values of the weights highlighted by a black

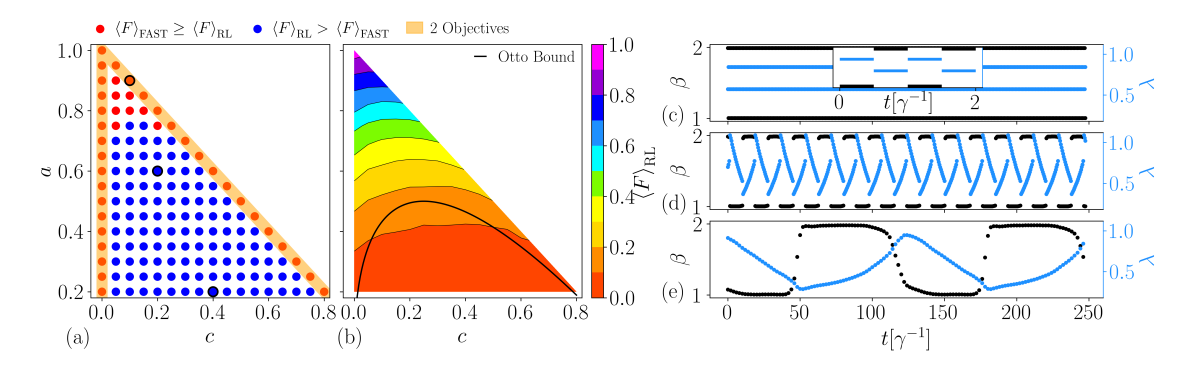


Figure 6.2: Optimization of  $\langle F \rangle$  at different values of a and c, with b=1-a-c, for a QD-based PDHE. Each dot in panel (a) displays, as a function of c and a, whether  $\langle F \rangle_{\rm RL} > \langle F \rangle_{\rm FAST}$  (blue dots) or not (red dots). Points with  $a \sim 0$  are not displayed since, in such a regime, optimal cycles become infinitely long (to minimize entropy production and fluctuations) and the RL method does not converge reliably. (b): contour plot of  $\langle F \rangle_{\rm RL}$ , as a function of c and a, using the data-points of (a). The black line represents the curve below which  $\langle F \rangle_{\rm FAST} = 0$ . (c,d,e): cycles, described by piece-wise constant values of  $\beta$  (black dots) and  $\lambda$  (blue dots) as a function of t, identified at the three values of a and c highlighted in black in panel (a) (respectively from top to bottom). The inset in panel (c) represents a zoom into the corresponding cycle, which is a fast-Otto cycle. Parameters:  $\beta_{\rm C}=2$ ,  $\beta_{\rm H}=1$ ,  $\lambda_{\rm min}=0.2$ ,  $\lambda_{\rm max}=1.1$  and  $\varepsilon=2.5$ .

circle in Fig. 6.2(a) (respectively from top to bottom). Since RL identifies piece-wise constant controls, the cycle is displayed as dots corresponding to the value of  $\beta(t)$ (black dots) and  $\lambda(t)$  (blue dots) at each small time-step. First, we notice that the inverse temperature abruptly switches between  $\beta_{\rm H}$  and  $\beta_{\rm C}$  for all values of the weights, so that in this engine no gain arises when smoothly varying the temperature. As expected, the cycle identified by RL in Fig. 6.2(c), corresponding to the black point on the hypotenuse in Fig. 6.2(a), is a fast-Otto cycle (a "zoom" in a short time interval is shown in the inset). However, moving down in weight space to the black dot at a = 0.6 and c = 0.2, we see that the corresponding cycle (Fig. 6.2(d)) now displays a finite period, with linear modulations of  $\lambda(t)$  at fixed temperatures, and a discontinuity of  $\lambda(t)$  when switching between  $\beta_{\rm H}$  and  $\beta_{\rm C}$ . The cycle in Fig. 6.2(e), corresponding to the lowest black dot at a = 0.2 and c = 0.4, displays an extremely long period  $\tau \approx 125\gamma^{-1}$ , which is far in the slow-driving regime. Optimal cycles, therefore, interpolate between the fast and the slow-driving regimes as we move in weight space (cf. Fig. 6.2(a)) from the sides to the lower and central region – i.e. switching from 2 to 3 objectives.

In Fig. 6.3 we display the Pareto-front, i.e. we plot the value of  $P/P_{\text{max}}$ ,  $\eta/\eta_c$ , and  $\Delta P/\Delta P(P_{\text{max}})$  found maximizing  $\langle F \rangle$  for various values of the weights. Fig. 6.3(a)

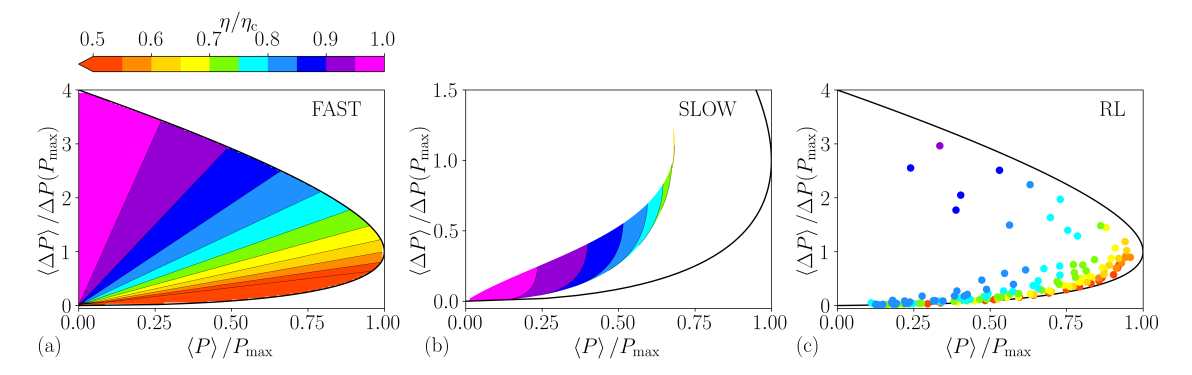


Figure 6.3: Pareto-front found optimizing  $\langle F \rangle$  with fast-Otto cycles in the limit of small temperature differences (panel (a)), optimizing  $\langle F \rangle$  in the slow-driving regime (panel (b)), and numerically using RL (panel (c)). The system parameters are as in Fig. 6.2. All panel display  $\langle \Delta P \rangle / \Delta P(P_{\text{max}})$  as a function of  $\langle P \rangle / P_{\text{max}}$  (x-axis) and of  $\eta/\eta_c$  (color). The black curve represents the outer border of the Pareto-front derived analytically.

is derived in the fast-driving regime assuming a small temperature difference, while Fig. 6.3(b) is derived in the slow-driving regime. The RL results, shown in Fig. 6.3(c), correspond to the points in Fig. 6.2(a). First, we notice that, by definition of the Pareto front, the "outer border" corresponds to points where we only maximize the trade-off between the two objectives  $\langle P \rangle$  and  $\langle \Delta P \rangle$ . Since these points are optimized by fast-Otto cycles, the black border of Fig. 6.3(a), also shown in Fig. 6.3(b,c), is exact. Moreover, in this setup, we can establish an exact mapping between the performance of a SSHE and of our PDHE operated with fast-Otto cycles. Since SSHE satisfy eq. (6.4), also fast-Otto cycles have  $\xi \leq 1$ . Furthermore, for small temperature differences,  $\xi = 1$ . This allows us to fully determine the internal part of the Pareto front in the fast-driving regime using the thermodynamic uncertainty relations, i.e.  $P/P_{\text{max}} = (\Delta P/\Delta P(P_{\text{max}}))(\eta_c - \eta)/\eta$ . Indeed, the linear contour lines in Fig. 6.3(a) stem from the linearity between P and  $\Delta P$ , the angular coefficient being determined by the efficiency.

Comparing Fig. 6.3(a,b), we see where the fast and slow-driving regimes are optimal. As expected, the slow-driving Pareto front cannot reach the black border, especially in the high-power area, where fast-Otto cycles are optimal. However, in the low power and low fluctuation regime, cycles in the slow-driving substantially outperform fast-Otto cycles by delivering a higher efficiency (pink and purple regions in Fig. 6.3(b)).

Interestingly, the RL points in Fig. 6.3(c) capture the best features of both regimes. RL can describe the high-power and low fluctuation regime displaying

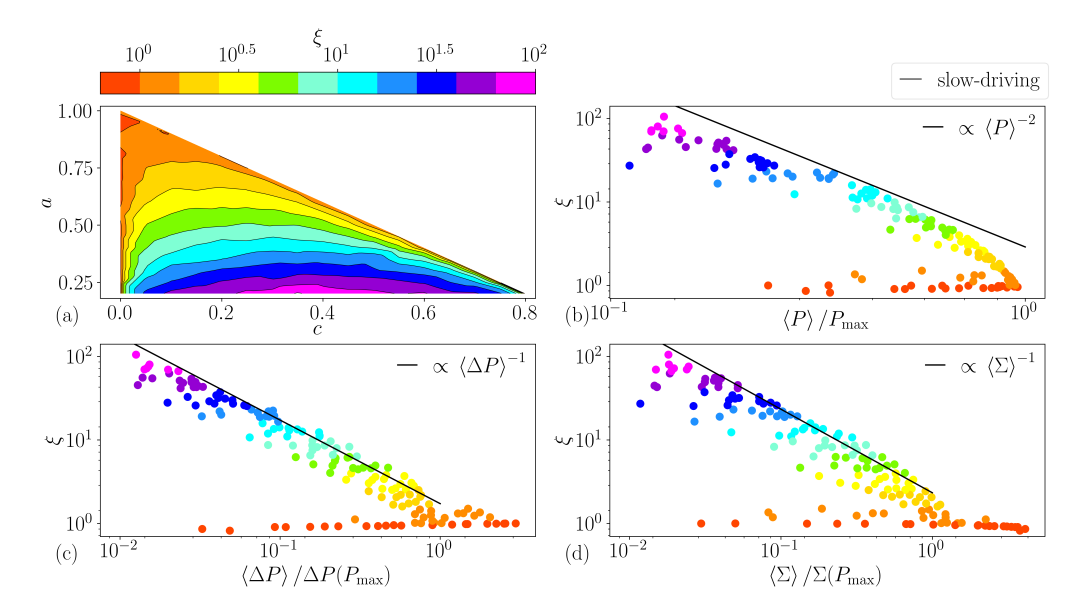


Figure 6.4: (a): contour plot of the SSHE thermodynamic uncertainty relationship ratio  $\xi$  as a function of c and a. (b,c,d): log-log plot of  $\xi$ , color mapped as in panel (a), as a function of  $\langle P \rangle / P_{\text{max}}$ ,  $\langle \Delta P \rangle / \Delta P (P_{\text{max}})$  and  $\langle \Sigma \rangle / \Sigma (P_{\text{max}})$ , respectively. Every point corresponds to the same RL optimization performed in Fig. 6.2. The black line is the behavior of  $\xi$  derived analytically in the slow-driving regime for small values of  $\langle P \rangle$ ,  $\langle \Delta P \rangle$  and  $\langle \Sigma \rangle$ .

both red and blue/green dots near the lower border. The red dots are fast-Otto cycles that are optimal exactly along the border but deliver a low efficiency. The blue/green dots instead are finite-time cycles that deliver a much higher efficiency by sacrificing a very small amount of power and fluctuations. This dramatic enhancement of the efficiency as we depart from the lower border is another signature of the abrupt change in optimal cycles.

## 6.1.3 Violation of Thermodynamic Uncertainty Relation

At last, we analyze the behavior of the thermodynamic uncertainty relation ratio  $\xi$  (cf. eq. (6.4)), which represents a relevant quantity combining the three objectives, computing it on Pareto-optimal cycles (recall that  $\xi \leq 1$  for classical stochastic SSHE but PDHE can violate this bound [93]). In Fig. 6.4(a) we show a contour plot of  $\xi$ , computed with RL, as a function of a and c. Because of the mapping between SSHE and fast-Otto cycles, we have  $\xi = 1$  along the sides of the triangle, where only 2 objectives are optimized. However, this mapping breaks down for finite-time cycles, allowing us to observe a strong increase of  $\xi$  in the green/purple region in Fig. 6.4(a). As shown in Fig. 6.2, this region corresponds to long cycles

operated in the slow-driving regime, where violations of thermodynamic uncertainty relations had already been reported. In Fig. 6.4(b,c,d) we show a log-log plot of  $\xi$  respectively as a function of  $P/P_{\text{max}}$ ,  $\Delta P/\Delta P(P_{\text{max}})$ , and  $\Sigma/\Sigma(P_{\text{max}})$  with the same color-map as in Fig. 6.4(a). We see that  $\xi$  diverges in the limit of low power, low fluctuations, and low entropy production as a power law. Indeed, using the slow-driving approximation, we analytically prove that  $\xi$  diverges as  $\langle P \rangle^{-2}$ ,  $\langle \Delta P \rangle^{-1}$ , and  $\langle \Sigma \rangle^{-1}$ . Such relations, plotted as black lines, nicely agree with our RL results.

## 6.2 Szilard Engine

As opposed to the typical heat engine, information engines function with a single thermal bath that is at equilibrium. Initially this might seem as if it would be violating a formulation of the second law of thermodynamics (cf. Sec. 2.3), but no such violation is occurring. Information engines function by making use of a measurement instead of a cold bath [110]. The fact that this is possible becomes less surprising once one considers that there is a tight thermodynamic link between perfect measurements and zero-temperature baths [40].

The reason why there is no violation of the second law is that information is physical and, as a consequence, its manipulation has a thermodynamic cost [111]. Likewise, information is a thermodynamic resource that can be exploited to generate work, e.g., by means of information engines – also known as *Szilard engines*. These deep links between information and thermodynamics go back to seminal ideas by Maxwell, Szilard and Landauer [4,112]. Their once thought-experiments can nowadays be realized in a variety of physical platforms driven by the development of the fields of stochastic and quantum thermodynamics [113,114]. Pioneering experimental works linking information and thermodynamics realized an information Szilard engine [115] and the erasure of information close to the Landauer limit [116] on single colloidal particle, which were followed by several demonstrations in Brownian colloidal particles [117] but also in quantum systems like single-electron quantum dots [118], ultra-cold atoms [119], NMR [120] and superconducting circuits [121].

The steps in the cycle of a Szilard quantum dot engine can be broken down as follows: 0) The effective energy gap starts at 0 and the system is always in contact with the bath. 1) Measure the occupation of the dot with the charge sensor. 2) If the outcome of the measurement at step 1 is that the dot in the state  $|0\rangle$ : quickly increase  $\varepsilon$  to a large value, if instead the outcome is  $|1\rangle$  quickly decrease  $\varepsilon$  to a large negative value. 3) Decrease the energy gap in some finite time  $\tau$  until it reaches 0.

The protocol is designed to use the information of the measurement so that we are always in a position of gaining energy during step 3. However, by Landauer's principle, at the measurement in step 1 there is an implicit cost of  $k_BT \ln 2$  that will be payed when the memory storing the result is erased.

Fully exploiting the thermodynamic content in information typically requires reversible, and hence infinitesimally slow, processes. This naturally raises the question of how information engines can be optimally driven in finite time and hence out-of-equilibrium conditions. This question has been extensively studied theoretically, including general optimization frameworks [22] as well as finite-time versions of the Landauer's principle [12]. At the experimental level, relevant progress has been achieved in the optimization of classical information engines based on optically trapped colloidal particles [122] whereas, for quantum systems, a recent work exploited the concept of thermodynamic length to perform optimal Landauer erasure in the slow driving limit [54].

The goal of this section is optimize – similarly to the previous section – and implement in a quantum dot experiment – collaborating with the group of Natalia Ares – a finite-time Szilard engine in the whole range of driving speeds: ranging from the slow (high efficiency, low power) to the fast (high power, low efficiency) driving regime. The optimal protocol is found from the theoretical results of [49], which interpolates between the two-jump protocols for fast driving [26] and the geodesic protocols of [9] at slow driving. We also characterize work fluctuations, which play a dominant role at these scales [29]. We observe that, whereas in the high efficiency regime work fluctuations disappear due to the fluctuation-dissipation regime, higher power comes inevitably with higher fluctuations.

## 6.2.1 Experiment

Here we discuss the experimental device, which was realized by the group of Prof. N. Ares. The device is is shown in Fig. 6.5(a). It consists of a quantum dot system in a strained Ge quantum well. An information bit is encoded in the occupancy of the right dot in the bottom array (QD1). This quantum dot QD1 is defined by applying voltages  $V_{G1}$  and  $V_{G3}$  that confine the electronic state. The discrete energy level E is controlled using the plunger gate voltage  $V_{G2}$ . The left dot in the array is positioned in Coulomb blockage which limits the tunneling of QD1 to the right reservoir. Another quantum dot in the top array, defined using gates  $V_{CS1-CS3}$ , serves as a probe for the occupancy n of QD1. The occupancy n is monitored by measuring the current  $I_{CS}$  through the charge sensor dot as shown in Fig. 6.5(b).

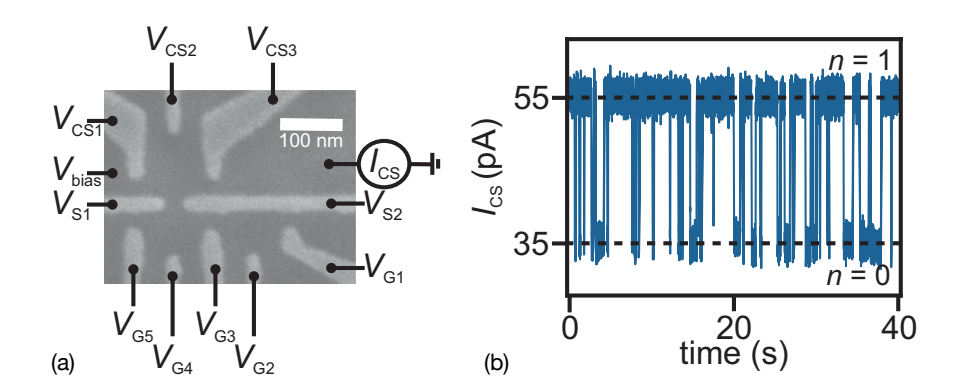


Figure 6.5: (a) The experimental device: a quantum dot system in a strained Ge quantum well. (b) Monitoring of the occupancy of the dot via the current  $I_{CS}$ .

The experiment is performed in a regime where  $n \in 0, 1$  i.e, when QD1 has an extra particle or not. The tunneling in and out rates are characterized by  $\gamma_{\rm in} = \Gamma_{\rm in} f(\varepsilon)$  and  $\gamma_{\rm out} = \Gamma_{\rm out} (1 - f(E))$ , where  $\Gamma_{\rm in} = 3.5$  Hz and  $\Gamma_{\rm out} = 7$  Hz. We note that  $\Gamma_{\rm out} \approx 2\Gamma_{\rm in}$  indicating the spin degeneracy of the system.

In this section, we operate this device as a Szilard engine, the details of which are described in the next section. From an operational perspective this requires us to let the quantum dot system thermalize with the reservoir while keeping its energy at  $E_0 = 2k_{\rm B}T$  which corresponds to a 50% - 50% occupation, where T is the electron temperature. Then the charge sensor measures the instantaneous charge state, and the gate voltage  $V_{\rm G2}$  is modified to realize the optimal protocol.

## 6.2.2 Optimization of a Szilard Engine

In this section we will present how the setup can be used as a Szilard engine and then proceed to optimize it. The two-level system can be effectively described by the Hamiltonian

$$\hat{H}(t) = \frac{1}{2}\varepsilon(t)\hat{\sigma}_z , \qquad (6.12)$$

where  $\varepsilon(t)$  is the effective gap between the energy levels, we define it so that it is 0 when the occupation probability is 0.5, therefore we have the relation  $\varepsilon = E + E_0$ . This energy gap can be be externally controlled by the gate voltage  $V_{G2}$ . By denoting with  $|1\rangle$  the excited state of  $\hat{H}(t)$ ,  $p(t) := \langle 1|\hat{\rho}(t)|1\rangle$  is the probability of being in the excited state. The Markovian dynamical equation becomes

$$\dot{p}(t) = \gamma(\omega(t) - p(t)) , \qquad (6.13)$$

where  $\omega(t) = (1 + e^{\beta \varepsilon(t)})^{-1}$  is the excited level population of the instantaneous Gibbs state,  $\gamma^{-1}$  is the thermalization timescale due to the interaction between system and bath, and  $\beta = (k_B T)^{-1}$  is the inverse temperature of the bath. Eq. (6.13) can be solved to find

$$p(t) = p(0)e^{-\gamma t} + \gamma \int_0^t ds \ \omega(s)e^{-\gamma(t-s)}$$
 (6.14)

Ref. [49] shows that for the system at hand the exact dynamics are simple enough to obtain a general analytical solution for  $\varepsilon(t)$  and p(t) that minimizes the work cost. Here we will focus on finding the optimal protocol  $\varepsilon_0(t)$  in the case we measure  $|0\rangle$  in step 1. By spin-flip symmetry, the optimal protocol  $\varepsilon_1(t)$  in the case where we measure  $|1\rangle$  is simply given by  $\varepsilon_1(t) = -\varepsilon_0(t)$ . Since we have to perform cycles, the symmetry of the problem imposes the boundary conditions  $\varepsilon(0) = \varepsilon(\tau) = 0$ . From ref. [49] optimal protocols satisfy

$$p(t) = \frac{1 - \sqrt{K}e^{\beta \varepsilon(t)/2}}{1 + e^{\beta \varepsilon(t)}}, \quad 0 < t < \tau , \qquad (6.15)$$

where K is an integration constant determined by the boundary conditions. For a given value of K, one can find  $p(t) = F_K^{-1}(t)$ , where  $F_K(p)$  is a transcendental function. By inserting eq. (6.15) into eq. (2.5) we can express the work cost of optimal protocols as a function of their boundary conditions on p

$$\min_{\varepsilon(t)} \beta W[\varepsilon(t)] = G(p(0)) - G(p(\tau)) , \qquad (6.16)$$

where G(p) is also a transcendental function that can be found in ref. [49].

The measurement at step 1 sets the boundary condition p(0) = 0. Since at the start of the next cycle another measurement will be performed, we do not need to impose a boundary condition at  $p(\tau)$ . Therefore by replacing  $p(\tau)$  with  $F_K^{-1}(\tau)$  in eq. (6.16) and minimizing with respect to K we can find the optimal integration constant  $\kappa_{\tau}$  (for a given protocol time  $\tau$ ) which defines the optimal protocol:

$$\beta \varepsilon_0(t) = 2 \ln \left[ \frac{\sqrt{\kappa_\tau + 4F_{\kappa_\tau}^{-1}(t)(1 - F_{\kappa_\tau}^{-1}(t))} - \sqrt{\kappa_\tau}}{2F_{\kappa_\tau}^{-1}(t)} \right]. \tag{6.17}$$

Since the optimal integration constant is defined by

$$\kappa_{\tau} := \arg\max_{K} G(F_K^{-1}(\tau)) , \qquad (6.18)$$

we turned the functional minimization problem in eq. (6.16) into a regular minimiza-

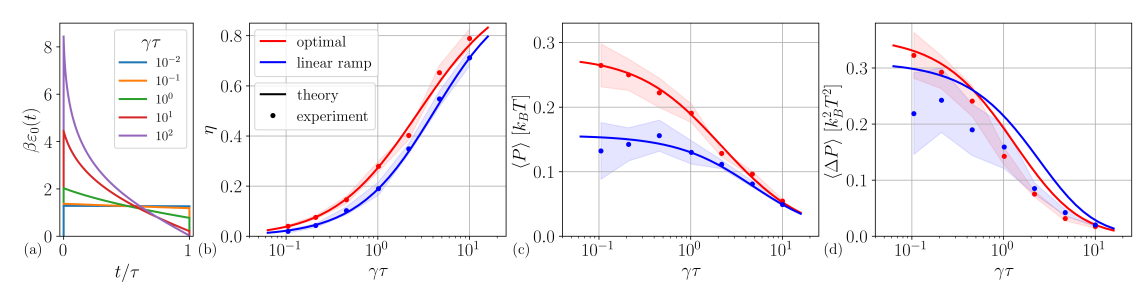


Figure 6.6: (a) Optimal protocol for different values of  $\gamma \tau$ . (b,c,d) Comparison of predicted and measured efficiency  $\eta = -\beta W/\ln 2$  (b), power  $\langle P \rangle = -W/\tau$  (c), and power fluctuations  $\langle \Delta P \rangle = \text{Var}(P)$  (d) for implementations of the optimal protocol eq. (6.17) (red) and a linear ramp  $\varepsilon(t) = 5k_BT(\tau - t)/\tau$  (blue) at different values of  $\gamma \tau$  that range from the fast-driving regime to the slow-driving regime. The experimental data is represented with points and the shaded area corresponds to the statistical error of the measurement.

tion problem, which is much simpler to handle numerically. It is worth noting that the optimal protocol features jumps at the start and the end of the protocol, as it can be noted from eq. (6.17) that  $\varepsilon(t) > 0$  for  $0 < t < \tau$ . In Fig. 6.6(a) we showcase these optimal protocols for a range of values of  $\gamma \tau$  from the slow-driving regime to the fast-driving regime.

#### 6.2.3 Results and Discussion

For the engine cycle to be truly closed, the information obtained from the measurement at step 1 will have to erased. Thus dissipating  $k_BT \ln 2$  of heat into the environment because of Landauer's principle (cf. Chapter 4). This gives us a simple formula for the efficiency of this engine

$$\eta = \frac{-W}{k_B T \ln 2} \ . \tag{6.19}$$

The efficiency of the information engine reaches its maximum  $\eta_C = 1$  in the static limit, which corresponds to the Carnot efficiency one obtains when setting the temperature of the cold bath to zero. This is simply one of many examples of the link between perfect measurements and zero temperature baths [40].

It is interesting to note that this expression for efficiency implies that, for a given cycle length  $\tau$ , the optimization of power and efficiency coincide. Therefore here it is sufficient to maximize the work gained to optimize both the power and efficiency. In Fig. 6.6(b,c) we show as red solid lines the maximal efficiency and maximum power that can be achieved for a given value of  $\gamma\tau$ . We also compare the obtained results to the power and efficiency of a "naive protocol": a linear ramp from

 $\pm 5k_BT$  to 0 over the whole period  $\tau$  – the + sign corresponds to measuring  $|0\rangle$  and – to measuring  $|1\rangle$ . We can se that the difference is not very significant in terms of efficiency. However, for power the optimal protocol has significant gains in the fast driving regime. In Fig. 6.6(d) we computed the power fluctuations  $\langle \Delta P \rangle = \text{Var}(P)$  (cf. eq. (6.3)) for the optimal and naive protocols. Interestingly, we can see that in the fast driving regime the naive protocol has slightly better fluctuations than the optimal protocol.

For a series of values of  $\gamma\tau$  between  $10^{-1}$  and  $10^{1}$  we implemented optimal protocols and linear ramps while measuring the dot's occupation. We can then use the dot occupation data to compute the work cost of a single round of the experiment, with multiple repetitions (in the thousands for the faster protocols and at least 200 for the slower ones) we can compute the corresponding statistical cumulants. The resulting values are shown in Fig. 6.6(b-d) as dots, and the shaded area corresponds to the statistical error. We can see that the experiment is in total agreement with the predicted values in for the power and efficiency. However for the fluctuations it seems that the measured values are generally lower than the predicted values (more than  $1\sigma$  away for most values). This bias could be explained with the fact that the calibration of the experiment drifts over time. But overall, the agreement between theory and experiment for the extracted work shows the feasibility of these optimal protocols in information engines.

## 6.3 Fast Operations

For the last section of this chapter we move away from heat engines and look at the optimization of operations in the fast driving regime. In particular, we will look at the problem of minimizing the dissipated work and minimizing the work fluctuations. However, typically it is not possible to minimize the dissipation and fluctuations simultaneously and a compromise must be chosen. Current research aims to understand the interplay and unavoidable trade-offs between dissipation and fluctuations in classical-stochastic and quantum thermodynamic systems [21, 23], and it remains an ongoing problem of how best to balance these two competing figures of merit in different scenarios.

With regard to dissipation, or equivalently the average excess work done to drive a system out of equilibrium, optimal processes are well characterized in slowly driven or linear response regimes where methods from thermodynamic geometry can be employed [43]. For classical stochastic systems operating in these close-to-equilibrium regimes the work fluctuation-dissipation relation holds [5], implying that paths of minimal dissipation simultaneously minimize the resulting work fluctuations. While this is not always satisfied by non-classical systems due to the impact of quantum coherence [89], an alternative geometric approach has been recently developed that can determine minimum fluctuation protocols for slowly driven quantum systems [123]. On the other hand, it is desirable to understand how to optimize systems beyond linear response driving and where shorter operation times are needed. The goal of this section is to establish a general optimization principle for minimizing both the average excess work and its fluctuations in rapidly driven small systems.

The study of driven Brownian particles first hinted at a key feature of minimumdissipation protocols for fast driving; such protocols contain discontinuous jumps in the system control parameters or degrees of freedom [48]. This has been further evidenced in a range of other systems through either analytic or numerical treatments of finite-time thermodynamic optimization problems [49, 57, 83, 84]. More recently the optimality of these control parameter quenches has been proven in general with regard to maximizing the power and efficiency of microscopic heat engines with fast operation cycles [85, 106], and furthermore proven optimal for minimizing the average excess work done on classical stochastic systems rapidly driven from equilibrium [124]. In contrast to dissipation, little is known about how to minimize work fluctuations under rapid driving, nor is it known how these protocols compare to those with minimal dissipation. In this section we show that protocols with minimal fluctuations also consist of instantaneous jumps in the systems control parameters. Our result applies in full generality to any quantum or classical system whose generator is independent of the control parameter velocities. While sharing the same general design principle as minimal-dissipation protocols, these control variables typically need to jump to a distinct point in the parameter space, meaning that average excess work and work fluctuations cannot be simultaneously optimized. Furthermore, and as we will illustrate, one practical advantage of this approach is that it enables us to optimize driving protocols for complex many-body systems where exact results are lacking.

In Sec. 6.3.1 we start by deriving general expressions for the average excess work and its variance for rapidly driven quantum systems. Then in Sec. 6.3.2 we present the general Euler-Lagrange equations for finding optimal protocols in this fast driving regime and show that all solutions consist of discrete jumps in the control parameter space. We then explore different scenarios where this optimization scheme can be implemented; Sec. 6.3.3 focuses on closed quantum systems, whereas Sec. 6.3.4

concerns open quantum systems including erasure of a quantum dot and driving a classical and quantum Ising spin chain.

#### 6.3.1 Excess Work and Fluctuations

We will begin with a rather general treatment of a finite-dimensional quantum system subject to rapid time-dependent driving, which may be isolated or in contact with an environment. Following the notation presented in Sec. 3.2 we decompose the Hamiltonian as follows

$$\hat{H}(\lambda) = \hat{H}_0 + \lambda^j \hat{X}_j, \qquad t \in [0, \tau], \tag{6.20}$$

where  $\hat{H}_0$  denotes a fixed Hamiltonian in the absence of driving,  $\{\lambda^j\}_{j=1}^n$  are externally controllable parameters and  $\{\hat{X}_j\}_{j=1}^n$  are the corresponding observables. For now we can assume the evolution is given by a Markovian generator of the form

$$\frac{d\hat{\rho}(t)}{dt} = \mathcal{G}_{\vec{\lambda}_t}[\hat{\rho}(t)]; \quad \hat{\rho}(0) = \hat{\pi}(\lambda_i).$$
 (6.21)

with a thermal initial condition. The most notable part of this assumption is that the generator is independent of the velocity  $d\lambda(t)/dt$ , and depends only on the local values of  $\lambda(t)$ . This is readily satisfied by isolated quantum systems evolving unitarily, adiabatically driven open quantum systems [125] and Markovian dynamics for classical/quasi-classical systems driven by scalar potentials. On the other hand, open quantum systems driven non-adiabatically may not meet this requirement [126]. We also stress that while our system is initially thermal, we place no restriction on the final state after the protocol has been applied.

As a quantifier for the degree of irreversibility associated with the process, the average *excess* – or dissipated, cf. Sec. 2.3 – work done on the system is given by

$$W_{\rm ex} = W - \Delta F,\tag{6.22}$$

where  $\Delta F$  is the change in equilibrium free energy. The excess work disappears  $W_{\rm ex} \to 0$  in quasi-static processes where the system is always in thermal equilibrium, which also implies absence of work fluctuations due to the work fluctuation-dissipation relation  $\beta \sigma_W^2/2 = W_{\rm ex}$  holding valid in this limit [5]. For non-equilibrium processes, both  $W_{\rm ex}$  and  $\sigma_W$  will become relevant, and we expect their magnitudes to increase with the speed of the process (i.e. as  $\tau$  decreases). Our goal is then to

investigate which protocols give the smallest values of average dissipation  $W_{\rm ex}$  and work fluctuations  $\sigma_W$  respectively. In general, computing and optimizing the work moments relies on knowing an exact solution to the dynamics eq. (6.21). While this is not generally tractable, we will demonstrate that this control problem becomes considerably simpler in fast driving regimes (i.e. when the overall time  $\tau$  taken to go from  $\lambda_i$  to  $\lambda_f$  is small relative to the characteristic timescales of the system).

We first quantify precisely what we mean by a fast protocol by defining a characteristic timescale  $\tau_c$  for the generator given by [106]

$$\tau_c^{-1} = \max_{0 \le t \le \tau} ||\mathcal{G}_{\lambda(t)}||, \tag{6.23}$$

where we introduce a norm

$$||\mathcal{G}_{\lambda}|| = \max_{\text{Tr}[O] < \infty} \frac{||\mathcal{G}_{\lambda}[O]||_1}{||O||_1}$$

$$(6.24)$$

and  $||A||_1 = \text{Tr}\left[\sqrt{A^{\dagger}A}\right]$ . For a finite-dimensional unitary generator, this parameter is bounded by the operator norm of the Hamiltonian, while for systems undergoing non-unitary dynamics with a unique fixed point then  $\tau_c$  bounds the shortest relaxation timescale associated with the system. Overall, this gives us a definition of the fast driving regime which assumes that the total duration is short enough such that  $\tau \ll \tau_c$ . To see how this approximation impacts the work moments, let us start by seeing how it impacts the evolution. We can expand the solution to eq. (6.21) as a Dyson series:

$$\hat{\rho}(t) = \hat{\pi}(\lambda_i) + \sum_{n=1}^{\infty} \int_0^t dt_n \int_0^{t_n} dt_{n-1} ... \int_0^{t_2} dt_1 \, \mathcal{G}_{\lambda(t_n)} \mathcal{G}_{\lambda(t_{n-1})} ... \mathcal{G}_{\lambda(t_1)} [\hat{\pi}(\lambda_i)] . \quad (6.25)$$

If one makes the integral parameters dimensionless by extracting  $\tau$ , with eq. (6.23) one can see that the *n*-th term of the sum is of order  $\mathcal{O}(\tau^n/\tau_c^n)$ . Therefore we define

$$\hat{\sigma}(t) = \hat{\pi}(\lambda_i) + \int_0^t dt' \ \mathcal{G}_{\lambda(t')}[\hat{\pi}(\lambda_i)] \ , \tag{6.26}$$

by construction  $||\hat{\rho}(t) - \hat{\sigma}(t)||_1 \leq \mathcal{O}(\tau^2/\tau_c^2)$ . Therefore we can approximate the state with  $\hat{\sigma}(t)$  so long as  $\tau \ll \tau_c$ . We can use this approximation to compute the excess work

$$W_{\rm ex} = k_B T S(\hat{\pi}(\lambda_i) || \hat{\pi}(\lambda_f)) + \int_0^{\tau} dt \, \frac{d\lambda^j(t)}{dt} \int_0^t dt' \, R_j(\lambda(t')) + \mathcal{O}\left(\tau^2/\tau_c^2\right) . \quad (6.27)$$

Where we use the relative entropy

$$S(\hat{\rho}_1||\hat{\rho}_2) = \text{Tr}[\hat{\rho}_1 \log \hat{\rho}_1] - \text{Tr}[\hat{\rho}_1 \log \hat{\rho}_2] , \qquad (6.28)$$

and defined the quantum initial force relaxation rate (IFRR):

$$R_j(\lambda) := \left\langle \mathcal{G}_{\lambda}^{\dagger}[\hat{X}_j] \right\rangle_{\lambda_i} \tag{6.29}$$

where  $\langle \hat{X}_j \rangle_{\lambda_i} = \text{Tr}[\hat{X}_j \hat{\pi}(\lambda_i)]$  is the expectation value with respect to the initial equilibrium state. We can then do an integration by parts on eq. (6.27) to obtain

$$W_{\rm ex} = k_B T S(\hat{\pi}(\lambda_i) || \hat{\pi}(\lambda_f)) + \int_0^{\tau} dt \left[ \lambda_f - \lambda(t) \right]^j R_j(\lambda(t)) + \mathcal{O}\left(\tau^2/\tau_c^2\right) . \tag{6.30}$$

The first term represents the excess work from a perfect Hamiltonian quench [74], while the second term gives the leading order correction for a protocol at finite speed. This expansion agrees with the results of [124] for classical Focker-Planck dynamics, now generalized to a fully quantum regime.

By applying the same procedure to work fluctuations eq. (6.3) we obtain

$$\sigma_W^2 = k_B^2 T^2 V(\hat{\pi}(\lambda_i) || \hat{\pi}(\lambda_f)) + \int_0^{\tau} dt \left[\lambda_f - \lambda(t)\right]^j \mathbf{G}_{jk}(\lambda(t)) \left[\lambda_f - \lambda(t)\right]^k + \int_0^{\tau} dt \left[\lambda_f - \lambda(t)\right]^j \mathbf{B}_{jk}(\lambda(t)) \left[\lambda(t) - \lambda_i\right]^k + \mathcal{O}(\tau^2/\tau_c^2) . \quad (6.31)$$

Where the first term is the relative entropy variance [127]:

$$V(\hat{\rho}_1||\hat{\rho}_2) = \text{Tr}[\hat{\rho}_1(\log \hat{\rho}_1 - \log \hat{\rho}_2)^2] - S^2(\hat{\rho}_1||\hat{\rho}_2) , \qquad (6.32)$$

 $\mathbf{G}(\lambda)$  is the initial force correlation matrix, with elements

$$\mathbf{G}_{jk}(\lambda) := \frac{1}{2} \langle \mathcal{G}_{\lambda}^{\dagger} [\{ \Delta \hat{X}_{j}, \Delta \hat{X}_{k} \}] \rangle_{\lambda_{i}} , \qquad (6.33)$$

where  $\{\hat{X}, \hat{Y}\} = \hat{X}\hat{Y} + \hat{Y}\hat{X}$  is the anti-commutator and we define shifted force observables as  $\Delta \hat{X}_j := \hat{X}_j - \left\langle \hat{X}_j \right\rangle_{\lambda_i}$ . Finally,  $\mathbf{B}(\lambda)$  is another correlation function given by

$$\mathbf{B}_{jk}(\lambda) := \left\langle \left\{ \mathcal{G}_{\lambda}^{\dagger} [\Delta \hat{X}_j], \Delta \hat{X}_k \right\} \right\rangle_{\lambda}. \tag{6.34}$$

As we saw with the average excess work, the first term here is what one would

expect for work fluctuations via an instantaneous quench [74], while the two integral terms are the leading order correction for a finite speed protocol. The expressions eq. (6.30) and eq. (6.31) are the first main result of this section, and will now form the basis for finding optimal protocols in the fast driving regime.

### 6.3.2 Optimality of Instantaneous Jump Protocols

Our aim is now to determine control protocols that minimize the dissipated work and the work fluctuations. Since the zero-th order terms in the expansions of the previous section depend only on the boundary conditions of the protocol, it is useful to define the *short-term power savings* [124]

$$P_{\text{save}} := \tau^{-1} \left[ k_B T S(\hat{\pi}(\lambda_i) || \hat{\pi}(\lambda_f)) - W_{\text{ex}} \right] , \qquad (6.35)$$

which quantifies any additional reduction to the rate of work done provided by the finite-time protocol beyond that of an instantaneous quench. In a similar fashion we also introduce the *short-term constancy savings*,

$$C_{\text{save}} := \tau^{-1} \left[ k_B^2 T^2 V \left( \hat{\pi}(\lambda_i) || \hat{\pi}(\lambda_f) \right) - \sigma_W^2 \right] , \qquad (6.36)$$

This measures the reductions to the rate of work fluctuations in a short-time protocol. These are now the two objectives to maximize in our control problem. Using our short-time approximations to both the average excess work eq. (6.30) and work fluctuations eq. (6.31), a general optimization principle becomes immediately apparent for this regime. Since the integrands appearing in eq. (6.30) and eq. (6.31) are each independent of the control velocity  $d\lambda/dt$ , we can infer that optimal protocols will consist of an instantaneous jump from  $\lambda_i$  to a point in the parameter space, remaining there for the total duration  $\tau$  and concluding with another instantaneous jump to the final boundary point  $\lambda_f$ . We will denote the control values that maximize  $P_{\text{save}}$  and  $C_{\text{save}}$  respectively by  $\xi$  and  $\Lambda$ , which are determined by the solutions to the following distinct Euler-Lagrange equations:

$$R_{j}(\xi) = \frac{\partial}{\partial \lambda^{j}} \left( \left[ \lambda_{f} - \vec{\xi} \right]^{k} R_{k}(\lambda) \right) \Big|_{\lambda = \xi}$$
(6.37)

and

$$\frac{\partial}{\partial \lambda^{j}} \left( \left[ \lambda_{f} - \lambda \right]^{k} \mathbf{G}_{kl}(\lambda) \left[ \lambda_{f} - \lambda \right]^{l} \right) \bigg|_{\lambda = \Lambda} = \frac{\partial}{\partial \lambda^{j}} \left( \left[ \lambda - \lambda_{f} \right]^{k} \mathbf{B}_{kl}(\lambda) \left[ \lambda - \lambda_{i} \right]^{l} \right) \bigg|_{\lambda = \Lambda}.$$
(6.38)

The maximal short-term power savings are then given by

$$P_{\text{save}} \le P_{\text{save}}^* := \left[\xi - \lambda_f\right]^j R_j(\xi) , \qquad (6.39)$$

which is saturated via the jump protocol  $\lambda(t) = \lambda_i + [\xi - \lambda_i]\theta(t) + [\lambda_f - \xi]\theta(t - \tau)$ , where  $\theta(t)$  denotes the Heaviside step function. The optimality of such processes was proven in [124] for classical systems. We have here shown that the same result applies to quantum mechanical systems, provided that the dynamical generator eq. (6.21) remains independent of  $d\lambda/dt$ . As a more significant result, we can now see that the same is true for fluctuations, albeit with a different choice of point in the parameter space. The maximum short-term constancy savings are given by

$$C_{\text{save}} \le C_{\text{save}}^* := \left[\Lambda - \lambda_f\right]^j \left(\mathbf{G}_{jk}(\Lambda) \left[\lambda_f - \Lambda\right]^l + \mathbf{B}_{jk}(\Lambda) \left[\Lambda - \lambda_i\right]^k\right). \tag{6.40}$$

which is saturated by jumping to  $\Lambda$  instead:  $\lambda(t) = \lambda_i + [\Lambda - \lambda_i]\theta(t) + [\lambda_f - \Lambda]\theta(t - \tau)$ . In general the values of  $\xi$  and  $\Lambda$  will not typically coincide, implying a trade-off between minimized excess work versus minimal fluctuations. This can remain the case even in quasi-classical regimes where only changes to the energy levels of the system are allowed. This should be contrasted with slow driving or linear response regimes, which allow for simultaneous optimization of the average and variance due to the validity of the fluctuation dissipation relation in the absence of quantum friction [89, 128]. However, depending on the particular Hamiltonian parameters and dynamics it is still possible to find situations where  $\xi = \Lambda$  and simultaneous optimization is possible, as we will highlight in subsequent sections.

Before we proceed it is important to highlight some consistency requirements needed to implement a jump protocol. As we are restricted to operating in fast driving regimes, this places restrictions on the set of points one can jump to in order to ensure that the Taylor expansions remain valid. We can compute the exact excess work and fluctuations induced by the jump protocols and compare that to the truncated expressions eq. (6.30) and eq. (6.31). We find that the error of the dissipation expansion is bounded by  $\Delta h(\xi)\mathcal{O}(\tau^2/\tau_c^2)$ , while for the fluctuations

expansions it is bounded by  $\Delta h(\Lambda)^2 \mathcal{O}(\tau^2/\tau_c^2)$ . Where we defined

$$\Delta h(\lambda) := 2 \max \left\{ ||\hat{H}(\lambda) - \hat{H}(\lambda_i)||_1, ||\hat{H}(\lambda_f) - \hat{H}(\vec{\xi})||_1 \right\}. \tag{6.41}$$

This tells us that one cannot jump arbitrarily far from the boundary points  $\lambda_i$ ,  $\lambda_f$  as this would lead to a large  $\Delta h$  and hence invalidate the fast driving approximation. Therefore any freedom in setting the magnitude of  $\xi$  and  $\Lambda$  must take these bounds into account, discounting arbitrarily large values of both  $P_{\text{save}}^*$  and  $C_{\text{save}}^*$ . In the remainder of this chapter we will demonstrate the utility of these jump protocols in a range of different types of system.

### 6.3.3 Closed Quantum Systems

As a starting point we consider an isolated quantum system whose dynamics are given by the time-dependent Liouville-von Neumann equation:

$$\mathcal{G}_{\lambda}[\hat{\rho}] = -\frac{i}{\hbar} [\hat{H}(\lambda), \hat{\rho}] . \tag{6.42}$$

The work statistics of quenched isolated systems are well studied, particularly in the context of many-body quantum systems [129]. Our formalism can now be used to calculate the leading short-time corrections to the excess work and fluctuations arising when the (instantaneous) quenches are replaced by fast Hamiltonian ramps, and then subsequently minimize them using the appropriate jump protocols outlined in the previous section. For closed, finite dimensional systems it is clear that the characteristic time scale is  $\tau_c \sim \hbar/E_{\rm max}(\lambda)$ , where  $E_{\rm max}(\lambda)$  denotes the maximum energy eigenvalue of  $\hat{H}(\lambda)$ . The relevant initial force relaxation rate and correlation functions are found to be

$$R_k(\lambda) = -\frac{i}{\hbar} \langle \left[ \hat{X}_k, \hat{H}(\lambda) \right] \rangle_{\lambda_i} , \qquad (6.43)$$

$$\left[\mathbf{G}(\lambda)\right]_{jk} = -\frac{i}{2\hbar} \left\langle \left[\left\{\Delta \hat{X}_j, \Delta \hat{X}_k\right\}, \hat{H}(\lambda)\right]\right\rangle_{\lambda_i}, \tag{6.44}$$

$$\left[\mathbf{B}(\lambda)\right]_{jk} = -\frac{i}{\hbar} \left\langle \left\{ \left[\Delta \hat{X}_j, \hat{H}(\lambda)\right], \Delta \hat{X}_k \right\} \right\rangle_{\lambda_i} . \tag{6.45}$$

The short-time power savings are then

$$P_{\text{save}} := \frac{i}{\tau \hbar} \int_0^{\tau} dt \, \left\langle \left[ \hat{H}(\lambda_f), \hat{H}(\lambda(t)) \right] \right\rangle_{\lambda_i} \tag{6.46}$$

while the constancy savings are

$$C_{\text{save}} := \frac{i}{\tau \hbar} \int_0^{\tau} dt \left( \left\langle \left[ \hat{H}(\lambda_f)^2, \hat{H}(\lambda(t)) \right] \right\rangle_{\lambda_i} - \left\langle \left\{ \hat{H}(\lambda_i), \left[ \hat{H}(\lambda_f), \hat{H}(\lambda(t)) \right] \right\} \right\rangle_{\lambda_i} - 2 \left\langle \hat{H}(\lambda_f) - \hat{H}(\lambda_i) \right\rangle_{\lambda_i} \left\langle \left[ \hat{H}(\lambda_f), \hat{H}(\lambda(t)) \right] \right\rangle_{\lambda_i} \right). \quad (6.47)$$

We can already see from eq. (6.46) and eq. (6.47) that if  $\hat{H}(\lambda_f)$  and  $\hat{H}(\lambda_i)$  commute, or  $\lambda(t)$  is chosen such that  $\hat{H}(\lambda(t))$  commutes with either  $\hat{H}(\lambda_f)$  or  $\hat{H}(\lambda_i)$ , then the integrand is exactly 0 - which directly follows using the cyclic property of the trace. Therefore, if  $\lambda(t)$  is a linear combination of  $\lambda_i$  and  $\lambda_f$ , the first order correction vanishes. An immediate consequence is that a naive protocol that linearly interpolates between the initial and final Hamiltonian in a closed system is equivalent to a

quench up to first order in driving speed.

We now choose a jump protocol to maximize either variable. We can notice that both  $P_{\text{save}}$  and  $C_{\text{save}}$  are linear in the control variables. Therefore the respective gradients are independent of  $\lambda$ . Which implies that the optimal points  $\xi$  and  $\Lambda$  are vectors pointing in the direction of the respective gradients, with the norm chosen as large as possible. However, as argued in the previous section, the larger this norm is chosen, the larger the error of the approximation is. In particular, setting  $\|\xi\| \gg \|\lambda_i\|, \|\lambda_f\|$  gives  $\|\xi\| \propto \Delta h(\xi)$  while  $\tau_c \propto 1/\|\xi\|$ . This implies that the error on the expansion of  $P_{\text{save}}$  scales as  $\mathcal{O}(\|\xi\|^3\tau^2)$ , which clearly limits how large the norm can be chosen relative to the duration of the protocol. A similar argument applies to the constancy savings and norm of the optimal point  $\Lambda$ .

We can make some further inferences about the relation between the different jumps  $\xi$  and  $\Lambda$ . We can show that

$$(\lambda_i)^j \frac{\partial}{\partial \lambda^j} P_{\text{save}} = (\lambda_i)^j \frac{\partial}{\partial \lambda^j} C_{\text{save}} = (\lambda_f)^j \frac{\partial}{\partial \lambda^j} P_{\text{save}} = (\lambda_f)^j \frac{\partial}{\partial \lambda^j} C_{\text{save}} = 0 , \qquad (6.48)$$

which means that both gradients are orthogonal to  $\lambda_i$  and  $\lambda_f$ . As was said before, this implies that if the protocol consists of a linear combination of  $\hat{H}_i$  and  $\hat{H}_f$  then the correction will be zero. But if the Hamiltonian has  $d \leq 2$  controllable parameters, it is impossible for  $\lambda(t)$  to be linearly independent from  $\lambda_i$  and  $\lambda_f$ . Therefore, regardless of the type of driving, with  $d \leq 2$  controllable parameters the correction is always zero.

It is interesting to consider what happens when we can control exactly three parameters, d=3. Eq. (6.48) constrains the gradients of  $P_{\text{save}}$  and  $C_{\text{save}}$  to be parallel, which implies

$$dP_{\text{save}} = \pm \frac{||\nabla_{\lambda} P_{\text{save}}||}{||\nabla_{\lambda} C_{\text{save}}||} dC_{\text{save}} , \qquad (6.49)$$

where the sign is positive if the gradients are oriented in the same direction and negative otherwise. If the sign is positive, we can optimize fluctuations and excess work simultaneously with  $\xi = \Lambda$ ; if the sign is negative, we have a direct trade-off between savings in power and constancy.

#### Driven Qubit

As an illustrative example, we can compute and optimize the excess work and work fluctuations of a qubit that is undergoing controlled unitary evolution. The most

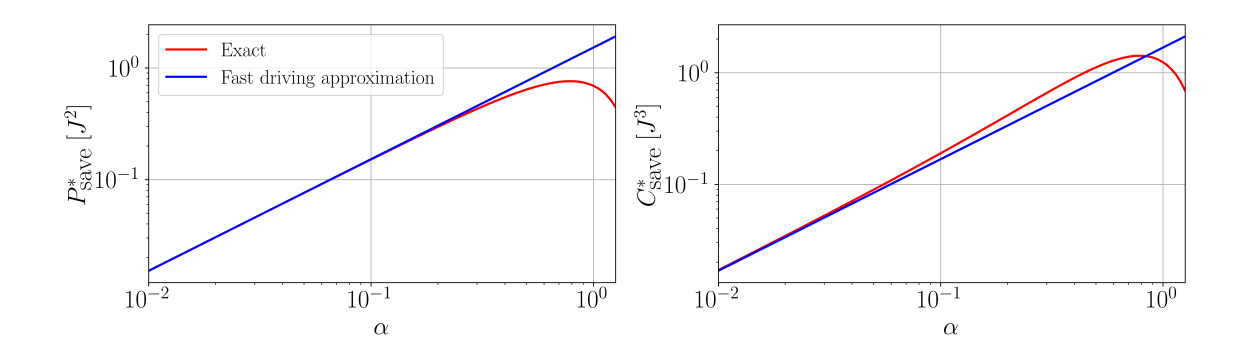


Figure 6.7: Comparison of  $P_{\text{save}}^*$  and  $C_{\text{save}}^*$  (in units of  $J^2$  and  $J^3$  respectively) in the exact case and fast driving approximation as a function of  $\alpha$  for a jump protocol with  $H_i = J\sigma^x$ ,  $H_f = J\sigma^z$  and  $J\tau = \beta J = 1$ .

general Hamiltonian for a qubit is

$$\hat{H}(\lambda) = J\vec{\lambda} \cdot \vec{\sigma} , \qquad (6.50)$$

where  $\vec{\sigma} = (\hat{\sigma}_x, \hat{\sigma}_y, \hat{\sigma}_z)$  is the Pauli vector, J is an energy scale and  $\vec{\lambda} = (\lambda^x, \lambda^y, \lambda^z)$  are dimensionless parameters that characterize the Hamiltonian. We find that the power and constancy savings can be optimized simultaneously with  $\vec{\xi} = \vec{\Lambda} = \alpha \vec{\lambda}_i \wedge \vec{\lambda}_f$ , where  $\alpha > 0$  controls the norm of the resulting Hamiltonian. We find the optimal values

$$P_{\text{save}}^* = 2\alpha J^2 \sin^2 \phi \|\lambda_i\| \|\lambda_f\|^2 \tanh(\beta J \|\lambda_i\|) , \qquad (6.51)$$

$$C_{\text{save}}^* = 4\alpha J^3 \sin^2 \phi \|\lambda_i\|^2 \|\lambda_f\|^2 \left[ 1 - \tanh(\beta J \|\lambda_i\|)^2 \left( 1 - \frac{\|\lambda_f\|}{\|\lambda_i\|} \cos \phi \right) \right] , \quad (6.52)$$

where  $\phi$  is the angle between  $\lambda_i$  and  $\lambda_f$ . The magnitude of  $\alpha$  has to be chosen in such a way that that the error of the approximation remains small. A sufficient condition is then given by choosing  $\alpha \ll (J\tau|\sin\phi|\|\lambda_i\|\|\lambda_f\|)^{-1}$ . This is illustrated in Fig. 6.7, in which we compare the results of eq. (6.51) and eq. (6.52) to the exact calculation of  $P_{\text{save}}$  and  $C_{\text{save}}$  for jump protocols in a qubit. The boundary conditions were set to  $\hat{H}_i = J\hat{\sigma}_x$ ,  $\hat{H}_f = J\hat{\sigma}_z$  and the relevant constants are set to  $\tau J = \beta J = 1$ . Then the condition for the validity of the approximation becomes  $\alpha \ll 1$ , indeed we can see from the figure that as  $\alpha$  approaches  $\mathcal{O}(1)$  the approximation breaks down.

It is important to stress that for higher dimensional closed systems, simultaneous optimization of  $P_{\text{save}}$  and  $C_{\text{save}}$  cannot always be guaranteed despite what we observe in the case of a qubit.

### 6.3.4 Open Quantum Systems

We now move to open quantum systems. Our framework can be applied to any Markovian Lindblad equation of the form eq. (6.21), in which the generator  $\mathcal{G}_{\lambda(t)}$  is independent of the velocity  $d\lambda(t)/dt$ . Here we illustrate it for the simple evolution:

$$\mathcal{G}_{\lambda}[\cdot] = \frac{\hat{\pi}(\lambda) \text{Tr}[\cdot] - (\cdot)}{\tau^{eq}} , \qquad (6.53)$$

which describes a decay of the state  $\hat{\rho}$  into the instantaneous Gibbs state  $\hat{\pi}(\lambda)$  with a timescale  $\tau^{eq}$ . This dissipative evolution naturally arises in collisional models [130] and also describes some systems weakly interacting with a reservoir with a sufficiently flat spectral density [49]. For this type of dynamics we find some more illuminating expressions for the various terms appearing in the leading corrections to the excess work and variance. Firstly, the initial force relaxation rate becomes

$$R_j(\lambda) := \frac{\langle \hat{X}_j \rangle_{\lambda} - \langle \hat{X}_j \rangle_{\lambda_i}}{\tau^{eq}} . \tag{6.54}$$

This demonstrates that  $R_j(\lambda)$  quantifies the average rate at which each expectation  $\langle \hat{X}_j \rangle$  changes from its initial value relative to the characteristic timescale  $\tau^{eq}$ . Furthermore, the correlation functions become

$$\left[\mathbf{G}(\lambda)\right]_{jk} = \frac{\mathcal{F}_{jk}(\lambda) - \mathcal{F}_{jk}(\lambda_i)}{\tau^{eq}} + \left(\langle \hat{X}_j \rangle_{\lambda} R_k(\lambda) + \langle \hat{X}_k \rangle_{\lambda} R_j(\lambda)\right). \tag{6.55}$$

and

$$\left[\mathbf{B}(\lambda)\right]_{jk} = -\frac{2}{\tau^{eq}} \mathcal{F}_{jk}(\lambda) , \qquad (6.56)$$

where  $\mathcal{F}_{jk}(\lambda)$  is the symmetric covariance defined as

$$\mathcal{F}_{jk}(\lambda) := \frac{1}{2} \langle \{\hat{X}_j, \hat{X}_k\} \rangle_{\lambda} - \langle \hat{X}_j \rangle_{\lambda} \langle \hat{X}_k \rangle_{\lambda} . \tag{6.57}$$

This function defines a metric tensor on the manifold of control parameters, and was first introduced in [131] as a means of quantifying the geometric structure of thermal states. In quasi-classical regimes where  $[\hat{X}_j, \hat{X}_k] = 0$ , this metric becomes proportional to the well-known thermodynamic metric, also known as the Fisher information matrix of the thermal state.

We will now illustrate these results with the optimization of three different systems: a driven quantum dot, and two Ising spin chains.

#### Fast Erasure of a Single Bit

A driven quantum dot interacting weakly with an environment is a paradigmatic example of a system that can be described by the simple dynamics eq. (6.53) [49]. In that case the Hamiltonian is given by  $\hat{H}(\varepsilon) = \frac{1}{2}\varepsilon\hat{\sigma}_z$  with a single control variable  $\lambda(t) = \varepsilon(t)$  given by the energy gap of the two-level system. The optimal finite-time thermodynamics of such systems has been well studied with regard to minimizing average dissipation in Landauer erasure, including a recent experimental implementation in a driven single dot [54]. In the present context, we apply our results to a rapid bit-erasure process. The boundary conditions for erasure are then  $\varepsilon_i = 0$  and  $\beta\varepsilon_f \gg 1$ , which leads to the following expressions for the power and constancy savings

$$P_{\text{save}} = \frac{k_B T}{\tau^{eq}} \int_0^1 ds \, \left(\beta \varepsilon_f - \beta \varepsilon(s)\right) \left(\frac{1}{2} - \frac{1}{1 + e^{\beta \varepsilon(s)}}\right) \,, \tag{6.58}$$

$$C_{\text{save}} = \frac{k_B^2 T^2}{2\tau^{eq}} \int_0^1 ds \ \beta \varepsilon(s) (\beta \varepsilon_f - \beta \varepsilon(s)) \ . \tag{6.59}$$

We now seek to find the optimal energy gaps to jump to in order to maximize either  $P_{\text{save}}$  or  $C_{\text{save}}$ . It will become clear in this case that the power and constancy savings cannot be simultaneously maximized, and so the distinct gaps are denoted by  $\xi$  and  $\Lambda$  respectively. Maximizing  $P_{\text{save}}$  amounts to solving the following transcendental equation  $\frac{1}{2} - \frac{1}{1+e^{\beta\xi}} = \frac{(\beta\varepsilon_f - \beta\xi)e^{\beta\xi}}{(1+e^{\beta\xi})^2}$ . In the limit of  $\beta\varepsilon_f \gg 1$  we can solve it analytically up to terms  $\mathcal{O}(\beta^{-1}\varepsilon_f^{-1}\ln\beta\varepsilon_f)$  and find the optimal jump  $\varepsilon \to \xi = \beta^{-1}\ln 2\beta\varepsilon_f$ . Maximum power savings are thus

$$P_{\text{save}}^* \simeq \frac{\varepsilon_f}{2\tau^{eq}} \ . \tag{6.60}$$

For this power-optimized jump let us denote the resulting sub-optimal constancy savings by  $C_{\text{save}}^{\xi}$ :

$$C_{\text{save}}^{\xi} = \frac{\varepsilon_f^2}{\tau^{eq}} \frac{\ln 2\beta \varepsilon_f}{2\beta \varepsilon_f} \ . \tag{6.61}$$

On the other hand, to maximize the constancy savings we need to choose a jump to  $\varepsilon \to \Lambda = \varepsilon_f/2$  instead. This yields

$$C_{\text{save}}^* = \frac{\varepsilon_f^2}{8\tau^{eq}} , \qquad P_{\text{save}}^{\Lambda} = \frac{\varepsilon_f}{4\tau^{eq}} .$$
 (6.62)

where the sub-optimal savings in power are denoted  $P_{\text{save}}^{\Lambda}$ . Clearly there exists a significant trade-off between these two choices of optimal protocol, with power-optimized jumps causing no improvement to the constancy while constancy-optimized jumps reducing the potential power savings by a factor of 1/2. Further comparison can be made with that of a naive linear driving  $\varepsilon(t) = \varepsilon_f t/\tau$ , which results in savings given by

$$P_{\text{naive}} \simeq \frac{\varepsilon_f}{4\tau^{eq}} , \qquad C_{\text{naive}} = \frac{\varepsilon_f^2}{12\tau^{eq}} , \qquad (6.63)$$

where we again drop terms of order  $\mathcal{O}(\beta^{-1}\varepsilon_f^{-1}\ln\beta\varepsilon_f)$ . Therefore we can see that choosing an optimal jump for the excess work leads to an improvement factor of 1/2, and choosing the optimal jump for the fluctuations gives an improvement factor of 3/2, each indicating significant improvements over a naive protocol. However, two unexpected observations here are that naive protocols are able to achieve larger savings in constancy than that of the power optimized protocol, and also achieve the same level of power savings to the constancy-optimized protocol. This emphasizes that improvements to one objective do not necessarily translate into improvements of the other.

#### Dissipative Classical Ising Chain

The strength of our approach is that it enables to deal with more complex systems, where exact solutions for minimizing dissipation and/or fluctuations are lacking – in contrast to the previous example. This is illustrated now for an Ising chain weakly coupled to a bath with dynamics eq. (6.53). We note that optimal driving protocols for classical spin chains have been devised in the slow driving regime, and now we complement such results by studying the opposite fast-driving regime. We first consider a classical spin chain,

$$\hat{H}(\varepsilon) = J \sum_{i=1}^{n} \left( \varepsilon \hat{\sigma}_z^{(i)} - \hat{\sigma}_z^{(i)} \hat{\sigma}_z^{(i+1)} \right) , \qquad (6.64)$$

where J is the energy scale and  $\varepsilon$  is a dimensionless parameter which can be interpreted as the strength of an external magnetic field. By assuming periodic boundary conditions, we can compute the partition function in the thermodynamic limit  $n \to \infty$ :

$$\lim_{n \to \infty} \frac{1}{n} \ln Z = \beta J + \ln \left[ \cosh(\beta J \varepsilon) + \sqrt{\sinh(\beta J \varepsilon)^2 + e^{-4\beta J}} \right] . \tag{6.65}$$

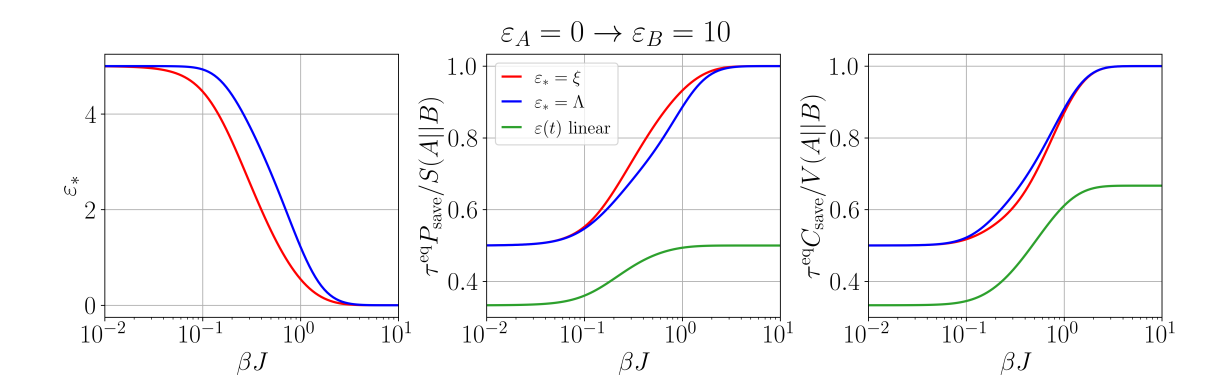


Figure 6.8: (left) Optimal value of  $\varepsilon_*$  for a protocol going from  $\varepsilon_i = 0$  to  $\varepsilon_f = 10$ . (center and right) Relative power and constancy savings in three protocols going from  $\varepsilon_i = 0$  to  $\varepsilon_f = 10$ . We compare protocols that optimize excess work and fluctuations to a protocol that varies linearly the value of  $\varepsilon$ .

The relevant force here is then the total  $\hat{X} = J \sum_{i} \hat{\sigma}_{z}^{(i)}$ . We now identify the following the relations

$$-\frac{1}{\beta} \frac{\partial}{\partial \varepsilon} \log Z = \text{Tr} \Big[ \hat{X} \hat{\pi}(\varepsilon) \Big] , \qquad (6.66)$$

$$\frac{1}{\beta^2} \frac{\partial^2}{\partial \varepsilon^2} \log Z = \text{Tr} \left[ \hat{X}^2 \hat{\pi}(\varepsilon) \right] - \text{Tr} \left[ \hat{X} \hat{\pi}(\varepsilon) \right]^2 . \tag{6.67}$$

These allow us to compute the first order corrections to the excess work and the fluctuations per site of the protocol in the thermodynamic limit from eq. (6.30) and eq. (6.31). We find

$$\tau^{eq}R(\varepsilon) = \frac{\sinh(\beta J \varepsilon_i)}{\sqrt{\sinh(\beta J \varepsilon_i)^2 + e^{-4\beta J}}} - \frac{\sinh(\beta J \varepsilon)}{\sqrt{\sinh(\beta J \varepsilon)^2 + e^{-4\beta J}}}, \qquad (6.68)$$

$$\tau^{eq}G(\varepsilon) = e^{-4\beta J} \left. \frac{\cosh(\beta J x)}{(\sinh(\beta J x)^2 + e^{-4\beta J})^{3/2}} \right|_{x=\varepsilon_i}^{x=\varepsilon} + (\tau^{eq} R(\varepsilon))^2, \tag{6.69}$$

$$\tau^{eq}B(\varepsilon) = -2e^{-4\beta J} \frac{\cosh(\beta J \varepsilon_i)}{(\sinh(\beta J \varepsilon_i)^2 + e^{-4\beta J})^{3/2}}.$$
 (6.70)

It is now a case of substituting these into the two different Euler-Lagrange equations eq. (6.37) and eq. (6.38) to determine the optimal points  $\xi$  and  $\Lambda$  needed in each jump protocol, with solutions found numerically for a process that brings  $\varepsilon$  from  $\varepsilon_i = 0$  to  $\varepsilon_f = 10$  – i.e. turning on the magnetic field. In Fig. 6.8 (left) we display the optimal field strength  $\varepsilon_* = \{\xi, \Lambda\}$  that maximizes either the power or constancy savings. We can notice that in the limits of high and low temperatures they coincide, while we cannot maximize them simultaneously in between these regimes. In Fig. 6.8

(center) we plot the power savings  $P_{\text{save}}^*$  relative to the zero-th order contribution  $k_B TS(\pi(\lambda_i)||\pi(\lambda_f))/\tau_c$ , while Fig. 6.8 (right) displays the constancy savings  $C_{\text{save}}^*$  in units of  $k_B^2 T^2 V(\pi(\lambda_i)||\pi(\lambda_f))/\tau_c$ . Both plots show the relative savings depending on whether we choose to optimize the power or constancy, and this is also compared to the savings achieved by taking a naive linear driving  $\varepsilon(t) = \varepsilon_i (1-t/\tau) + \varepsilon_f t/\tau$ . In this case we can see that there is only a modest difference between the  $\varepsilon_i \to \xi \to \varepsilon_f$  and  $\varepsilon_i \to \Lambda \to \varepsilon_f$  jump protocols, and they each perform considerably better than the naive approach, contrasting with what we observed for the driven quantum dot. This highlights the importance of optimal control in many-body open quantum systems. It is also interesting to note that in the low temperature regime the best protocol becomes to simply do a quench directly to  $\varepsilon_f$  for both power and fluctuations.

#### Ising Chain in Transverse Field

We will conclude with a final example covering the remaining scenario of an open quantum system where the control is such that the Hamiltonian may not commute at different times, so that  $[\hat{H}(\lambda(t)), \hat{H}(\lambda(t'))] \neq 0$ . This non-commutativity implies the presence of quantum friction, which is a distinctly non-classical contribution to the work done to drive the system that arises from allowing transitions between energy eigenstates. For this purpose we will consider a dissipative Ising chain with simple dynamics eq. (6.53), though this time we apply a transverse field along the x-axis that can be controlled in time. We note that optimal driving protocols for this model have been considered in the slow driving regime [74], and the results presented here in the fast driving regime are hence complementary. In particular, we will focus on performing drivings close to a quantum phase transition, which has also been considered in previous works [129].

The Hamiltonian of the system is

$$\hat{H}(g) = -J \sum_{i=1}^{n} \left( \hat{\sigma}_{z}^{(i)} \hat{\sigma}_{z}^{(i+1)} + g \hat{\sigma}_{x}^{(i)} \right) , \qquad (6.71)$$

where J is the energy scale and g is a dimensionless parameter which can be interpreted as an external (transverse) magnetic field. Clearly such a model will generate quantum friction as we vary the strength g in time. Assuming again periodic boundary conditions, we can compute the spectrum of the system with a Jordan-Wigner transformation [132]. Then by taking the thermodynamic limit the partition func-

tion is given by

$$\lim_{n \to \infty} \frac{1}{n} \log Z = \int_0^{2\pi} dk \, \log \left[ 2 \cosh \frac{\beta \epsilon_k}{2} \right] , \qquad (6.72)$$

where  $\epsilon_k$  is the eigen-energy corresponding to the momentum k

$$\epsilon_k = 2J\sqrt{1 + g^2 - 2g\cos k} \ . \tag{6.73}$$

At zero temperature and g=1 this system presents a phase transition from an ordered ferromagnetic phase to a quantum paramagnetic phase. We will focus on studying protocols that take the system across this point by changing g at finite temperature. The relevant force this time is  $\hat{X} = -J \sum_i \hat{\sigma}_x^{(i)}$ , and we can use the relations

$$-\frac{1}{\beta}\frac{\partial}{\partial g}\log Z = \text{Tr}\Big[\hat{X}\hat{\pi}(g)\Big] , \qquad (6.74)$$

$$\frac{1}{\beta^2} \frac{\partial^2}{\partial g^2} \log Z = \text{Tr} \left[ \hat{X}^2 \hat{\pi}(g) \right] - \text{Tr} \left[ \hat{X} \hat{\pi}(g) \right]^2. \tag{6.75}$$

The first order corrections to the excess work and the fluctuations per site of the protocol are now computed within the thermodynamic limit, giving us

$$\tau^{eq} R(g_*) = -\frac{1}{2} \int_0^{2\pi} dk \, \dot{\epsilon}_k \tanh \frac{\beta \epsilon_k}{2} \bigg|_{q=q_*}^{g=g_*} , \qquad (6.76)$$

$$\tau^{eq}G(g_*) = \frac{J}{2} \int_0^{2\pi} dk \ \ddot{\epsilon}_k \tanh \frac{\beta \epsilon_k}{2} + \frac{\dot{\epsilon}_k^2}{2J} \cosh^{-2} \frac{\beta \epsilon_k}{2} \Big|_{g=g_*}^{g=g_*} + (\tau^{eq}R(g_*))^2, \tag{6.77}$$

$$\tau^{eq}B(g_*) = -J \int_0^{2\pi} dk \ \ddot{\epsilon}_k \tanh \frac{\beta \epsilon_k}{2} + \frac{\dot{\epsilon}_k^2}{2J} \cosh^{-2} \frac{\beta \epsilon_k}{2} \bigg|_{q=q_*} , \qquad (6.78)$$

where  $\dot{\epsilon}_k = \frac{d\epsilon_k}{dg}$ . Substituting into the Euler-Lagrange equations eq. (6.37) and eq. (6.38) and solving numerically, we can determine the instantaneous jumps  $g_i \to \xi \to g_f$  and  $g_i \to \Lambda \to g_f$  for maximizing the respective power and constancy savings. We set our boundary conditions to be  $g_i = 0$  and  $g_f = 3$  so that we turn on the transverse magnetic field and cross the phase transition point at g = 1. Similarly to the classical case, we also compare these optimal protocols to a "naive" protocol in which the parameter is varied linearly in time,  $g(t) = g_i(1 - t/\tau) + g_f t/\tau$ .

In Fig. 6.9 (left) we display the optimal fields strength of  $g_* = \{\xi, \Lambda\}$ , which noticeably coincide in the limit of high temperatures like we saw with the classical Ising chain. On the other hand at low temperatures they no longer coincide, indicating a distinctly non-classical feature of this example and demonstrating that simultaneous

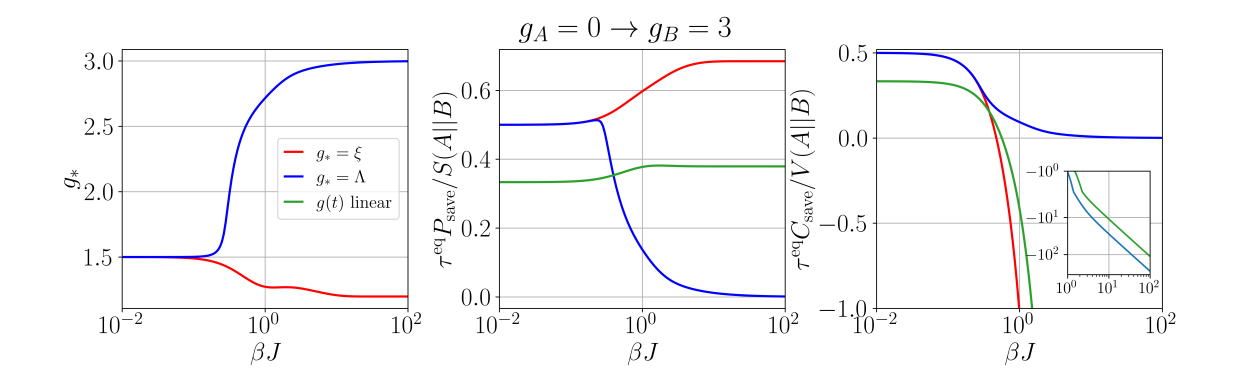


Figure 6.9: (left) Optimal value of  $g_* = \{\xi, \Lambda\}$  for a protocol going from  $g_i = 0$  to  $g_f = 3$ . (center) Relative power savings in three protocols going from  $g_i = 0$  to  $g_f = 3$  and (right) relative constancy savings for the same three protocols. In each figure we compare these optimal protocols to one that varies linearly the value of g.

optimization is no longer possible. In Fig. 6.9 we compare these two choices of protocol to linear driving and plot the resulting power savings (center) and constancy savings (right). Since temperature is finite, the phase transition is washed out but we can still observe a signature in the power and constancy savings occurring at lower temperatures, where we see that the two quantities move significantly further apart. One dramatic feature is the fact that optimizing the power savings results in the constancy savings becoming significantly negative at lower temperatures beyond the phase transition, indicating a large growth in overall work fluctuations above that of an infinitely fast quench. On the other hand, if we choose to maximize the constancy savings we see that this drops to zero alongside the power savings at low temperatures. This indicates that the system is highly sensitive to the choice of protocol when driven close to a quantum phase transition.

## 6.4 Conclusions

In this chapter we studied three examples of thermodynamic optimization. First, we introduced a general framework, described by eqs. (6.6-6.9), to identify Pareto-optimal cycles between power, efficiency, and power fluctuations in quantum or classical stochastic heat engines. As opposed to previous works, we account for the crucial impact of power fluctuations, which modify non-trivially the optimal driving solution. We then employed RL to optimize a quantum dot-based heat engine solving its exact finite-time and out-of-equilibrium dynamics. We observed an abrupt change in Pareto-optimal cycles when switching from the optimization of 2 objectives, where Otto cycles in the fast-driving regime are optimal, to 3 objectives,

86 6.4. Conclusions

where the optimal cycles have a finite period. This feature, which shares analogies with the phase transition in protocol space observed in Ref. [133], corresponds to a large enhancement of one of the objectives while only slightly decreasing the other ones. Furthermore, we find an exact mapping between Otto cycles in the fast-driving regime and SSHEs, implying that a violation of the thermodynamic uncertainty relation ratio  $\xi$  in eq. (6.4) requires the optimization of all 3 objectives. We then find that  $\xi$  becomes arbitrarily large in the slow-driving regime. Cycles found with RL display the best features analytically identified in the fast and slow driving regimes.

Secondly, we optimized and implemented an information engine, which represents a special class on its own among thermal engines that explicitly demonstrates the intricate connection between information and thermodynamics. We successfully implemented an optimized finite-time Szilard engine within a quantum dot system. The experimental setup consisted of a quantum dot system strained in a Germanium quantum well, where the occupancy of the dot can be manipulated and monitored. The optimization is based on maximizing the extracted energy for a given, arbitrary, cycle length. For the given system, it allows for the simultaneous optimization of power and efficiency. These optimal protocols showed significant improvements over a naive linear ramp protocol at all driving speeds, in particular in the fast driving regime. Additionally, we examined the work fluctuations generated by these optimal protocols, and observed that higher power inevitably comes with higher fluctuations. The experimental results corroborated the theoretical predictions, showing a high degree in precision of the (indirect) measurement of extracted work. The study described in this section showcased the successful optimization and implementation of a paradigmatic example of a quantum heat engine.

Finally, we have derived approximations for the average excess work done eq. (6.30) to rapidly drive a small system out of equilibrium along with the resulting work fluctuations eq. (6.31). This has been derived under the assumption that (i) the dynamics can be described by a Markovian generator that is independent of the velocities in the time-dependent control parameters, and (ii) the duration of the process is short relative to the characteristic timescale of the dynamics,  $\tau_c \gg \tau$ . Under these approximations we were able to prove that rapid processes that minimize either the average excess work, or work fluctuations, under fixed boundary conditions consist of two instantaneous jumps in the system control parameters, generalizing the results obtained for the fast driving regime in the first section of the chapter. Also bringing a contrast with the smooth geodesic paths that are optimal on slow driving and lin-

ear response regimes [89, 134]. Protocols that minimize the excess work cost, jump from the initial configuration to a point determined from the Euler-Lagrange equation eq. (6.37), stay there for the duration  $\tau$  then jump to the final boundary value. Protocols that minimize the work fluctuations follow the same pattern, but jump to an alternative point satisfying a different Euler-Lagrange equation eq. (6.38). We have seen that in general, these points do not coincide which indicates a trade-off between the optimal values of the average and variance. These results extend the work of [124] to show that jump protocols continue to be optimal when one also cares about keeping fluctuations minimal, while also extending this approach to the full quantum regime. In particular, it is worth emphasizing that, beyond the standard scenario of a driven system in contact with a Markovian environment, our approach also applies to closed quantum driven systems where the form of minimally dissipative driving processes remain less explored [135]. Due to its generality, our optimization scheme can be used to improve the control of complicated chemical, biological and quantum many-body systems whenever short operation times are desired. This has been illustrated by minimizing both excess work and fluctuations for a classical and quantum spin chain where an external magnetic field is rapidly changed in time. When driving the system close to a quantum phase transition, we found that optimizing over driving protocols leads to substantial gains (see Fig. 6.9). A number of improvements and generalizations to our approach are warranted. For open quantum systems, it is important to note that protocols with non-commuting Hamiltonians may not adequately be described by adiabatic Lindblad equations such as eq. (6.53) when operating in the fast driving regime [85]. Interestingly, since non-adiabatic corrections can potentially lead to a dependence on the control velocities [126], this would imply that instantaneous jumps are not necessarily optimal in these cases.

88 6.4. Conclusions

# Chapter 7

## Conclusion and Outlook

We always have, as we imagine, ideas that a certain thing is true, but we don't know what it means for something to be true. You may say, "I know what it means for it to be true that the atom is in the box; it's in the box." But we have found that it isn't in the box. And what you may say is, "I know what you mean by 'is in the box'. It means that if you put a detector there it'll click." No, that isn't what it means either.

— Richard Feynman, The Character of Physical Law

In this thesis we have covered a set of topics that shed light on the fundamental limits of the irreversibility of thermodynamic protocols. The general theme that links these results is the minimization of dissipation for finite-time operations. This is a fundamentally difficult question in thermodynamics – whether quantum or classical – because it requires to perform functional optimization over the solution of the dynamics of the system and environment – which is often not solvable. Through this question we were able to probe one of the most fundamental aspects of thermodynamics: how close one can get to reversible protocols with finite resources? Furthermore, thanks to the universality of the question of minimizing work, we were also able to address some more "applied" optimization problems for mesoscopic systems.

We started by presenting a self-contained review on the laws of thermodynamics in Chapter 2. We then presented the mathematical formalism that is used in the rest of the thesis. In particular, in Sec. 3.2 we generalized the results of [9] to obtain a derivation of the thermodynamic geometry technique that applies to all types of dynamics – i.e. for both open and closed quantum systems; thus giving a formal setting for the work minimization of thermodynamic protocols in the slow-driving

regime, which has been used multiple times in the rest of the thesis.

In Chapter 4 we applied this extended formalism to obtain a finite-time correction to Landauer's bound on the dissipated energy required to erase information. While previous works obtaining a finite-time correction to the bound already existed, these were limited to the Markovian regime [9–11]. The main result of the chapter eq. (4.2) is valid beyond such approximations. Indeed, it unveils the need for strong coupling for the optimal energy management of erasure processes. Furthermore, despite the result being derived in a specific setting, it reveals the general form of a universally valid finite-time correction to Landauer's bound with the emergence of *Planckian time*.

Remarkably, the results of Chapter 5 show how one can use the framework of geometric thermodynamics to unveil a novel type of collective effects that allow to drastically reduce the amount of energy that is dissipated when performing a task on a collection of systems simultaneously. Collective effects are a well known and important phenomenon in physics, ranging from phase transition to quantum entanglement [14-18]. It is often the case that one can exploit these effects to improve the result or cost of a given task, leading to a notion of collective advantages: the outcome of a task is improved when performed globally on a collection of systems instead of each system individually. Indeed, our results show that if one wishes to perform multiple tasks on multiples systems, then it is possible to exploit classical correlations between these systems to drastically suppress the amount of energy that is dissipated into the environment. To put it simply, one manages to "share the losses" between the individual systems. With sufficient amount of control, this suppression is strong enough to obtain a vanishing dissipation per system in the thermodynamic limit. This is an astounding result, as it seems to go counter to the third law of thermodynamics, but on a technical level there seems to be no contradiction as the remaining finite-time dissipation is always strictly positive.

Finally, in Chapter 6 we focused on the thermodynamic optimization of mesoscopic systems. We showed how to fully optimize two types of nano-scale thermal engines and fast operations on a system. The optimization of thermal engines and, more generally, operations at the nano-scale are questions that allows us to probe the fundamental limits of the trade-offs between relevant physical costs and desiderata [19–23]. In steady state heat engines, these trade-offs are captured by thermodynamic uncertainty relations [21,24]. First, we studied how one can fully optimize all the relevant thermodynamic aspects of the simplest possible thermal engine: a periodically driven quantum dot engine. Indeed, with the use of analytical techniques

and reinforcement learning we were able to characterize the optimization trade-off of power, efficiency and power fluctuations of a quantum dot engine in all driving regimes. Second, we characterized and optimized the performance of an information engine at all driving speeds. Information engines stand in a class of their own, as they make use of measurements on the system instead of a cold reservoir. Furthermore, we confirmed the feasibility of the optimal protocols we computed, with an experimental implementation thanks to the collaboration of the group of prof. N. Ares. Last, but not least, we developed a general framework for the optimization of work and work fluctuations in rapidly driven systems. Our results showed that optimal fast protocols, in both open and closed system dynamics, consist of two instantaneous jumps in the control parameters – one at start and one at the end of the protocol. Interestingly, this is true whether we are aiming to optimize work or work fluctuations – or any trade-off of the two quantities, but it is seldom the case that the optimal "jump point" is the same for both objectives. We showcased this phenomenon by applying the framework to compute the optimal fast protocols across phase transitions of many-body quantum systems.

A substantial portion of the presented results relies on the framework of geometric thermodynamics. Therefore, it is very natural to ask how could one could generalize these results beyond the slow-driving regime – particularly in the case of the finite-time correction to Landauer's principle. However, beyond purely technical extensions of the results, these works shed light on further questions regarding the fundamental limit of irreversible operations. First, whether one can characterize the dependence of the term a – in the main result of the chapter on Landauer's principle eq. (4.2) – on the type of interaction with the environment, or even a general non-trivial lower bound to it. Furthermore, the appearance of Planckian time – which is conjectured to be the fastest relaxation time scale possible in many-body systems – in the bound seems to suggest that it also has a role in limiting the speed of information processing and metrology.

Second, the results of Chapter 5 show that it is possible to exploit correlations between multiple systems to exploit collective effects to drastically reduce energy dissipated in a thermodynamic operation. However, this is heavily dependent on the relaxation dynamics of the system. Therefore, it is left as a future challenge to characterize how these collective advantages could arise from a microscopic model of interaction with the thermal bath. This is a crucial step to eventually prove experimentally the presence of such collective advantages, which could be used one

day to limit the overheating of chips in super-computers [81]. Furthermore, it is still unclear if these collective advantages are fully consistent with the third law of thermodynamics. Therefore it possible that these results help shed light on the thermodynamic consistency of master equations [136, 137]. For example, if these collective advantages cannot be derived from a microscopic model, they could be taken as a witness of thermodynamic inconsistency of some master equations. Thus opening another avenue on the question of which constraints one needs to impose on a master equation to ensure its thermodynamic consistency. Conversely, it is also possible that inconsistencies do not arise, which could be because of a divergence in the *complexity* of the protocols that realize these collective advantages – whose role in the third law of thermodynamics has recently been receiving increased attention [40].

# **Bibliography**

- [1] A. Einstein, Über einen die Erzeugung und Verwandlung des Lichtes betreffenden heuristischen Gesichtspunkt, Annalen der Physik **322**(6), 132–148 (Jan. 1905).
- [2] J. Von Neumann, Mathematical foundations of quantum mechanics, Princeton University Press, Princeton, NJ, Feb. 1932.
- [3] J. von Neumann, Proof of the ergodic theorem and the H-theorem in quantum mechanics: Translation of: Beweis des Ergodensatzes und des H-Theorems in der neuen Mechanik, The European Physical Journal H 35(2), 201–237 (Sept. 2010).
- [4] R. Landauer, Irreversibility and heat generation in the computing process, IBM Journal of Research and Development 5(3), 183–191 (1961).
- [5] C. Jarzynski, Nonequilibrium equality for free energy differences, Phys. Rev. Lett. 78(14), 2690 (1997).
- [6] G. E. Crooks, Entropy production fluctuation theorem and the nonequilibrium work relation for free energy differences, Phys. Rev. E 60, 2721–2726 (Sep 1999).
- [7] J. Roßnagel, S. T. Dawkins, K. N. Tolazzi, O. Abah, E. Lutz, F. Schmidt-Kaler, and K. Singer, *A single-atom heat engine*, Science **352**(6283), 325–329 (Apr. 2016).
- [8] M. Rademacher, M. Konopik, M. Debiossac, D. Grass, E. Lutz, and N. Kiesel, Nonequilibrium Control of Thermal and Mechanical Changes in a Levitated System, Physical Review Letters 128(7) (Feb. 2022).
- [9] M. Scandi and M. Perarnau-Llobet, *Thermodynamic Length in Open Quantum Systems*, Quantum **3**, 197 (Oct. 2019).
- [10] T. Van Vu and K. Saito, Finite-Time Quantum Landauer Principle and Quantum Coherence, Phys. Rev. Lett. 128, 010602 (Jan 2022).
- [11] Y.-Z. Zhen, D. Egloff, K. Modi, and O. Dahlsten, *Universal Bound on Energy Cost of Bit Reset in Finite Time*, Physical Review Letters **127**(19) (Nov. 2021).
- [12] A. Rolandi and M. Perarnau-Llobet, Finite-time Landauer principle beyond weak coupling, Quantum 7, 1161 (Nov. 2023).
- [13] A. Rolandi, P. Abiuso, and M. Perarnau-Llobet, *Collective Advantages in Finite-Time Ther-modynamics*, Physical Review Letters **131**(21) (Nov. 2023).
- [14] F. Campaioli, F. A. Pollock, and S. Vinjanampathy, Quantum Batteries, in *Fundamental Theories of Physics*, pages 207–225, Springer International Publishing, 2018.

94 Bibliography

[15] H. Vroylandt, M. Esposito, and G. Verley, Collective effects enhancing power and efficiency, EPL (Europhysics Letters) 120(3), 30009 (Nov. 2017).

- [16] L. d. S. Souza, G. Manzano, R. Fazio, and F. Iemini, Collective effects on the performance and stability of quantum heat engines, Phys. Rev. E 106, 014143 (Jul 2022).
- [17] W. Niedenzu and G. Kurizki, Cooperative many-body enhancement of quantum thermal machine power, New Journal of Physics 20(11), 113038 (nov 2018).
- [18] C. Chiaracane, M. T. Mitchison, A. Purkayastha, G. Haack, and J. Goold, *Quasiperiodic quantum heat engines with a mobility edge*, Physical Review Research **2**(1) (Jan. 2020).
- [19] V. Holubec, An exactly solvable model of a stochastic heat engine: optimization of power, power fluctuations and efficiency, Journal of Statistical Mechanics: Theory and Experiment 2014(5), P05022 (May 2014).
- [20] M. Mehboudi and H. J. D. Miller, Thermodynamic length and work optimization for Gaussian quantum states, Phys. Rev. A 105, 062434 (Jun 2022).
- [21] P. Pietzonka and U. Seifert, Universal Trade-Off between Power, Efficiency, and Constancy in Steady-State Heat Engines, Physical Review Letters 120(19) (May 2018).
- [22] P. Abiuso and M. Perarnau-Llobet, Optimal Cycles for Low-Dissipation Heat Engines, Phys. Rev. Lett. 124, 110606 (Mar 2020).
- [23] H. J. D. Miller and M. Perarnau Llobet, Finite-time bounds on the probabilistic violation of the second law of thermodynamics, SciPost Physics 14(4) (Apr. 2023).
- [24] A. C. Barato and U. Seifert, Thermodynamic Uncertainty Relation for Biomolecular Processes, Physical Review Letters 114(15) (Apr. 2015).
- [25] P. A. Erdman, A. Rolandi, P. Abiuso, M. Perarnau-Llobet, and F. Noé, Pareto-optimal cycles for power, efficiency and fluctuations of quantum heat engines using reinforcement learning, Phys. Rev. Res. 5, L022017 (Apr 2023).
- [26] A. Rolandi, M. Perarnau Llobet, and H. J. D. Miller, *Optimal control of dissipation and work fluctuations for rapidly driven systems*, New Journal of Physics (2023).
- [27] E. Fermi, *Thermodynamics*, Dover Publications, 1956.
- [28] R. Dann and R. Kosloff, Unification of the first law of quantum thermodynamics, New Journal of Physics 25(4), 043019 (Apr. 2023).
- [29] C. Jarzynski, Equalities and Inequalities: Irreversibility and the Second Law of Thermodynamics at the Nanoscale, Annual Review of Condensed Matter Physics 2(1), 329–351 (Mar. 2011).
- [30] R. Clausius, Ueber verschiedene für die Anwendung bequeme Formen der Hauptgleichungen der mechanischen Wärmetheorie, Annalen der Physik **201**(7), 353–400 (1865).
- [31] P. Strasberg and A. Winter, First and Second Law of Quantum Thermodynamics: A Consistent Derivation Based on a Microscopic Definition of Entropy, PRX Quantum 2(3) (Aug. 2021).

[32] M. Perarnau-Llobet, K. V. Hovhannisyan, M. Huber, P. Skrzypczyk, J. Tura, and A. Acín, Most energetic passive states, Physical Review E 92(4) (Oct. 2015).

- [33] N. Brunner, N. Linden, S. Popescu, and P. Skrzypczyk, Virtual qubits, virtual temperatures, and the foundations of thermodynamics, Phys. Rev. E 85, 051117 (May 2012).
- [34] P. R. Zulkowski, D. A. Sivak, and M. R. DeWeese, Optimal control of transitions between nonequilibrium steady states, PloS one 8(12), e82754 (2013).
- [35] G. T. Landi and M. Paternostro, Irreversible entropy production: From classical to quantum, Rev. Mod. Phys. 93, 035008 (Sep 2021).
- [36] A. Kox, Confusion and clarification: Albert Einstein and Walther Nernst's Heat Theorem, 1911–1916, Studies in History and Philosophy of Science Part B: Studies in History and Philosophy of Modern Physics 37(1), 101–114 (Mar. 2006).
- [37] L. Masanes and J. Oppenheim, A general derivation and quantification of the third law of thermodynamics, Nature Communications 8(1) (Mar. 2017).
- [38] H. Wilming and R. Gallego, *Third Law of Thermodynamics as a Single Inequality*, Physical Review X **7**(4) (Nov. 2017).
- [39] W. Nernst, Ueber die Berechnung chemischer Gleichgewichte aus thermischen Messungen, Nachrichten von der Gesellschaft der Wissenschaften zu Göttingen, Mathematisch-Physikalische Klasse 1906, 1–40 (1906).
- [40] P. Taranto, F. Bakhshinezhad, A. Bluhm, R. Silva, N. Friis, M. P. Lock, G. Vitagliano, F. C. Binder, T. Debarba, E. Schwarzhans, F. Clivaz, and M. Huber, Landauer Versus Nernst: What is the True Cost of Cooling a Quantum System?, PRX Quantum 4(1) (Mar. 2023).
- [41] D. Manzano, A short introduction to the Lindblad master equation, AIP Advances 10(2) (Feb. 2020).
- [42] P. Salamon and R. S. Berry, Thermodynamic length and dissipated availability, Phys. Rev. Lett. 51, 1127–1130 (Sep 1983).
- [43] P. Abiuso, H. J. D. Miller, M. Perarnau-Llobet, and M. Scandi, Geometric Optimisation of Quantum Thermodynamic Processes, Entropy 22(10), 1076 (Sept. 2020).
- [44] J. D. Cresser and J. Anders, Weak and Ultrastrong Coupling Limits of the Quantum Mean Force Gibbs State, Phys. Rev. Lett. 127, 250601 (Dec 2021).
- [45] J. Eisert, M. Friesdorf, and C. Gogolin, Quantum many-body systems out of equilibrium, Nature Physics 11(2), 124–130 (Feb. 2015).
- [46] J. Xuereb, Illustration of the geometric thermodynamics manifold, Aug. 2024.
- [47] T. L. Boullion and P. L. Odell, Generalized inverse matrices, Wiley-Interscience, July 1971.
- [48] T. Schmiedl and U. Seifert, Optimal Finite-Time Processes In Stochastic Thermodynamics, Phys. Rev. Lett. 98, 108301 (Mar 2007).
- [49] M. Esposito, R. Kawai, K. Lindenberg, and C. V. den Broeck, *Finite-time thermodynamics* for a single-level quantum dot, EPL (Europhysics Letters) **89**(2), 20003 (Jan. 2010).

[50] T. Sagawa and M. Ueda, Minimal Energy Cost for Thermodynamic Information Processing: Measurement and Information Erasure, Phys. Rev. Lett. 102, 250602 (Jun 2009).

- [51] M. Esposito and C. V. den Broeck, Second law and Landauer principle far from equilibrium, EPL (Europhysics Letters) 95(4), 40004 (Aug. 2011).
- [52] A. Bérut, A. Arakelyan, A. Petrosyan, S. Ciliberto, R. Dillenschneider, and E. Lutz, Experimental verification of Landauer's principle linking information and thermodynamics, Nature 483(7388), 187–189 (2012).
- [53] M. A. Ciampini, T. Wenzl, M. Konopik, G. Thalhammer, M. Aspelmeyer, E. Lutz, and N. Kiesel, Experimental nonequilibrium memory erasure beyond Landauer's bound, 2021, https://arxiv.org/abs/2107.04429.
- [54] M. Scandi, D. Barker, S. Lehmann, K. A. Dick, V. F. Maisi, and M. Perarnau-Llobet, Minimally Dissipative Information Erasure in a Quantum Dot via Thermodynamic Length, Phys. Rev. Lett. 129, 270601 (Dec 2022).
- [55] T. Van Vu and K. Saito, Thermodynamic Unification of Optimal Transport: Thermodynamic Uncertainty Relation, Minimum Dissipation, and Thermodynamic Speed Limits, Phys. Rev. X 13, 011013 (Feb 2023).
- [56] T. Van Vu and Y. Hasegawa, Geometrical Bounds of the Irreversibility in Markovian Systems, Phys. Rev. Lett. 126, 010601 (Jan 2021).
- [57] P. R. Zulkowski and M. R. DeWeese, Optimal finite-time erasure of a classical bit, Phys. Rev. E 89, 052140 (May 2014).
- [58] Y.-Z. Zhen, D. Egloff, K. Modi, and O. Dahlsten, *Inverse linear versus exponential scaling of work penalty in finite-time bit reset*, Phys. Rev. E **105**, 044147 (Apr 2022).
- [59] K. Proesmans, J. Ehrich, and J. Bechhoefer, Finite-Time Landauer Principle, Phys. Rev. Lett. 125, 100602 (Sep 2020).
- [60] A. Rivas, Strong Coupling Thermodynamics of Open Quantum Systems, Phys. Rev. Lett. 124, 160601 (Apr 2020).
- [61] M. Perarnau-Llobet, H. Wilming, A. Riera, R. Gallego, and J. Eisert, Strong Coupling Corrections in Quantum Thermodynamics, Physical Review Letters 120(12) (Mar. 2018).
- [62] G. Schaller, Open quantum systems far from equilibrium, volume 881, Springer, 2014.
- [63] S. A. Hartnoll and A. P. Mackenzie, Colloquium: Planckian dissipation in metals, Rev. Mod. Phys. 94, 041002 (Nov 2022).
- [64] S. Sachdev, Quantum Phase Transitions, Cambridge University Press, 2 edition, 2011.
- [65] S. Rochette, M. Rudolph, A.-M. Roy, M. J. Curry, G. A. T. Eyck, R. P. Manginell, J. R. Wendt, T. Pluym, S. M. Carr, D. R. Ward, M. P. Lilly, M. S. Carroll, and M. Pioro-Ladrière, Quantum dots with split enhancement gate tunnel barrier control, Applied Physics Letters 114(8), 083101 (Feb. 2019).
- [66] F. Covito, F. G. Eich, R. Tuovinen, M. A. Sentef, and A. Rubio, Transient Charge and Energy Flow in the Wide-Band Limit, Journal of Chemical Theory and Computation 14(5), 2495–2504 (Apr. 2018).

[67] L. P. Bettmann, M. J. Kewming, G. T. Landi, J. Goold, and M. T. Mitchison, Quantum stochastic thermodynamics in the mesoscopic-leads formulation, 2024, https://arxiv.org/ abs/2404.06426.

- [68] A. M. Timpanaro, J. P. Santos, and G. T. Landi, Landauer's Principle at Zero Temperature, Phys. Rev. Lett. 124, 240601 (Jun 2020).
- [69] L. Fox and D. F. Mayers, Numerical Solution of Ordinary Differential Equations, Springer Netherlands, 1987.
- [70] V. Giovannetti, S. Lloyd, and L. Maccone, Quantum Metrology, Phys. Rev. Lett. 96, 010401 (Jan 2006).
- [71] M. A. Pereira, Illustration individual and steamlined production, Jan. 2024.
- [72] P. Salamon, J. D. Nulton, and R. S. Berry, Length in statistical thermodynamics, The Journal of Chemical Physics 82(5), 2433–2436 (Mar. 1985).
- [73] G. E. Crooks, *Measuring Thermodynamic Length*, Physical Review Letters **99**(10) (Sept. 2007).
- [74] M. Scandi, H. J. D. Miller, J. Anders, and M. Perarnau-Llobet, *Quantum work statistics close to equilibrium*, Phys. Rev. Research 2, 023377 (Jun 2020).
- [75] P. Abiuso, P. Andrea Erdman, M. Ronen, F. Noé, G. Haack, and M. Perarnau-Llobet, Optimal thermometers with spin networks, Quantum Science and Technology 9(3), 035008 (Apr. 2024).
- [76] U. Seifert, Stochastic thermodynamics, fluctuation theorems and molecular machines, Reports on Progress in Physics **75**(12), 126001 (Nov. 2012).
- [77] N. M. Myers, O. Abah, and S. Deffner, Quantum thermodynamic devices: From theoretical proposals to experimental reality, AVS Quantum Science 4(2) (Apr. 2022).
- [78] S. Blaber and D. A. Sivak, Skewed thermodynamic geometry and optimal free energy estimation, The Journal of Chemical Physics 153(24), 244119 (Dec. 2020).
- [79] A. Dechant and Y. Sakurai, Thermodynamic interpretation of Wasserstein distance, 2019, https://arxiv.org/abs/1912.08405.
- [80] S. Carnot, Réflexions sur la puissance motrice du feu et sur les machines propres à développer cette puissance, Annales scientifiques de l'École normale supérieure 1, 393–457 (1824).
- [81] P. L. McMahon, *The physics of optical computing*, Nature Reviews Physics **5**(12), 717–734 (Oct. 2023).
- [82] A. Das, A. Bera, S. Chakraborty, and D. Chruściński, *Thermodynamics and the quantum speed limit in the non-Markovian regime*, Physical Review A **104**(4) (Oct. 2021).
- [83] E. Aurell, C. Mejía-Monasterio, and P. Muratore-Ginanneschi, Optimal Protocols and Optimal Transport in Stochastic Thermodynamics, Phys. Rev. Lett. 106, 250601 (Jun 2011).
- [84] V. Cavina, A. Mari, A. Carlini, and V. Giovannetti, *Optimal thermodynamic control in open quantum systems*, Physical Review A **98**(1) (July 2018).

[85] P. A. Erdman, V. Cavina, R. Fazio, F. Taddei, and V. Giovannetti, Maximum power and corresponding efficiency for two-level heat engines and refrigerators: optimality of fast cycles, New Journal of Physics 21(10), 103049 (Oct. 2019).

- [86] E. Geva and R. Kosloff, A quantum-mechanical heat engine operating in finite time. A model consisting of spin-1/2 systems as the working fluid, The Journal of Chemical Physics 96(4), 3054–3067 (Feb. 1992).
- [87] T. Feldmann and R. Kosloff, Performance of discrete heat engines and heat pumps in finite time, Physical Review E **61**(5), 4774–4790 (May 2000).
- [88] Z. Ye, F. Cerisola, P. Abiuso, J. Anders, M. Perarnau-Llobet, and V. Holubec, *Optimal finite-time heat engines under constrained control*, Physical Review Research 4(4) (Nov. 2022).
- [89] H. J. D. Miller, M. Scandi, J. Anders, and M. Perarnau-Llobet, Work Fluctuations in Slow Processes: Quantum Signatures and Optimal Control, Phys. Rev. Lett. 123, 230603 (Dec 2019).
- [90] F. Giazotto, T. T. Heikkilä, A. Luukanen, A. M. Savin, and J. P. Pekola, Opportunities for mesoscopics in thermometry and refrigeration: Physics and applications, Reviews of Modern Physics 78(1), 217–274 (Mar. 2006).
- [91] G. Benenti, G. Casati, K. Saito, and R. S. Whitney, Fundamental aspects of steady-state conversion of heat to work at the nanoscale, Physics Reports 694, 1–124 (June 2017).
- [92] B. K. Agarwalla and D. Segal, Assessing the validity of the thermodynamic uncertainty relation in quantum systems, Phys. Rev. B 98, 155438 (Oct 2018).
- [93] A. C. Barato and U. Seifert, Cost and Precision of Brownian Clocks, Physical Review X 6(4) (Dec. 2016).
- [94] T. Koyuk, U. Seifert, and P. Pietzonka, A generalization of the thermodynamic uncertainty relation to periodically driven systems, Journal of Physics A: Mathematical and Theoretical 52(2), 02LT02 (Dec. 2018).
- [95] K. Proesmans and C. Van den Broeck, Discrete-time thermodynamic uncertainty relation, EPL (Europhysics Letters) 119(2), 20001 (July 2017).
- [96] H. J. D. Miller, M. H. Mohammady, M. Perarnau-Llobet, and G. Guarnieri, Joint statistics of work and entropy production along quantum trajectories, Physical Review E 103(5) (May 2021).
- [97] G. Lindblad, On the generators of quantum dynamical semigroups, Communications in Mathematical Physics 48(2), 119–130 (June 1976).
- [98] H.-P. Breuer and F. Petruccione, *The Theory of Open Quantum Systems*, Oxford University PressOxford, Jan. 2007.
- [99] B. Sothmann, R. Sánchez, and A. N. Jordan, *Thermoelectric energy harvesting with quantum dots*, Nanotechnology **26**(3), 032001 (Dec. 2014).
- [100] R. Alicki, The quantum open system as a model of the heat engine, Journal of Physics A: Mathematical and General 12(5), L103–L107 (May 1979).

[101] T. Haarnoja, A. Zhou, P. Abbeel, and S. Levine, Soft Actor-Critic: Off-Policy Maximum Entropy Deep Reinforcement Learning with a Stochastic Actor, in *Proceedings of the 35th International Conference on Machine Learning*, edited by J. Dy and A. Krause, volume 80 of *Proceedings of Machine Learning Research*, pages 1861–1870, PMLR, 10–15 Jul 2018.

- [102] P. A. Erdman and F. Noé, *Identifying optimal cycles in quantum thermal machines with reinforcement-learning*, npj Quantum Information 8(1) (Jan. 2022).
- [103] P. A. Erdman and F. Noé, Model-free optimization of power/efficiency tradeoffs in quantum thermal machines using reinforcement learning, PNAS Nexus 2(8) (Aug. 2023).
- [104] S. Sgroi, G. M. Palma, and M. Paternostro, Reinforcement Learning Approach to Nonequilibrium Quantum Thermodynamics, Physical Review Letters 126(2) (Jan. 2021).
- [105] M. Bukov, A. G. Day, D. Sels, P. Weinberg, A. Polkovnikov, and P. Mehta, *Reinforcement Learning in Different Phases of Quantum Control*, Physical Review X 8(3) (Sept. 2018).
- [106] V. Cavina, P. A. Erdman, P. Abiuso, L. Tolomeo, and V. Giovannetti, *Maximum-power heat engines and refrigerators in the fast-driving regime*, Physical Review A **104**(3) (Sept. 2021).
- [107] M. Esposito, R. Kawai, K. Lindenberg, and C. Van den Broeck, *Efficiency at Maximum Power of Low-Dissipation Carnot Engines*, Physical Review Letters **105**(15) (Oct. 2010).
- [108] V. Holubec and A. Ryabov, Maximum efficiency of low-dissipation heat engines at arbitrary power, Journal of Statistical Mechanics: Theory and Experiment 2016(7), 073204 (July 2016).
- [109] P. Salamon and R. S. Berry, *Thermodynamic Length and Dissipated Availability*, Physical Review Letters **51**(13), 1127–1130 (Sept. 1983).
- [110] L. P. Bettmann, M. J. Kewming, and J. Goold, Thermodynamics of a continuously monitored double-quantum-dot heat engine in the repeated interactions framework, Physical Review E 107(4) (Apr. 2023).
- [111] R. Landauer, Information is Physical, Physics Today 44(5), 23–29 (May 1991).
- [112] L. Szilard, On the decrease of entropy in a thermodynamic system by the intervention of intelligent beings, Behavioral Science 9(4), 301–310 (1964).
- [113] S. Ciliberto, Experiments in Stochastic Thermodynamics: Short History and Perspectives, Phys. Rev. X 7, 021051 (Jun 2017).
- [114] N. M. Myers, O. Abah, and S. Deffner, Quantum thermodynamic devices: From theoretical proposals to experimental reality, AVS Quantum Science 4(2) (Apr. 2022).
- [115] S. Toyabe, T. Sagawa, M. Ueda, E. Muneyuki, and M. Sano, Experimental demonstration of information-to-energy conversion and validation of the generalized Jarzynski equality, Nature Physics 6(12), 988–992 (Nov. 2010).
- [116] A. Bérut, A. Arakelyan, A. Petrosyan, S. Ciliberto, R. Dillenschneider, and E. Lutz, Experimental verification of Landauer's principle linking information and thermodynamics, Nature 483(7388), 187–189 (Mar. 2012).

[117] G. Paneru, D. Y. Lee, T. Tlusty, and H. K. Pak, Lossless Brownian Information Engine, Phys. Rev. Lett. **120**, 020601 (Jan 2018).

- [118] J. V. Koski, V. F. Maisi, J. P. Pekola, and D. V. Averin, Experimental realization of a Szilard engine with a single electron, PNAS 111(38), 13786–13789 (Sept. 2014).
- [119] A. Kumar, T.-Y. Wu, F. Giraldo, and D. S. Weiss, Sorting ultracold atoms in a threedimensional optical lattice in a realization of Maxwell's demon, Nature 561(7721), 83–87 (Sept. 2018).
- [120] P. A. Camati, J. P. Peterson, T. B. Batalhão, K. Micadei, A. M. Souza, R. S. Sarthour, I. S. Oliveira, and R. M. Serra, Experimental Rectification of Entropy Production by Maxwell's Demon in a Quantum System, Physical Review Letters 117(24) (Dec. 2016).
- [121] N. Cottet, S. Jezouin, L. Bretheau, P. Campagne-Ibarcq, Q. Ficheux, J. Anders, A. Auffèves, R. Azouit, P. Rouchon, and B. Huard, Observing a quantum Maxwell demon at work, Proceedings of the National Academy of Sciences 114(29), 7561–7564 (July 2017).
- [122] G. Paneru, D. Y. Lee, J.-M. Park, J. T. Park, J. D. Noh, and H. K. Pak, Optimal tuning of a Brownian information engine operating in a nonequilibrium steady state, Phys. Rev. E 98, 052119 (Nov 2018).
- [123] H. J. Miller, G. Guarnieri, M. T. Mitchison, and J. Goold, Quantum Fluctuations Hinder Finite-Time Information Erasure near the Landauer Limit, Physical Review Letters 125(16) (Oct. 2020).
- [124] S. Blaber, M. D. Louwerse, and D. A. Sivak, Steps minimize dissipation in rapidly driven stochastic systems, Phys. Rev. E **104**, L022101 (Aug 2021).
- [125] T. Albash, S. Boixo, D. A. Lidar, and P. Zanardi, Quantum adiabatic Markovian master equations, New Journal of Physics 14(12), 123016 (Dec. 2012).
- [126] R. Dann, A. Levy, and R. Kosloff, *Time-dependent Markovian quantum master equation*, Physical Review A **98**(5) (Nov. 2018).
- [127] G. Guarnieri, N. H. Ng, K. Modi, J. Eisert, M. Paternostro, and J. Goold, *Quantum work statistics and resource theories: Bridging the gap through Rényi divergences*, Phys. Rev. E **99**(5), 050101 (2019).
- [128] T. Speck and U. Seifert, Distribution of work in isothermal non-equilibrium processes, Phys. Rev. E **70**, 066112 (2004).
- [129] L. Fusco, S. Pigeon, T. J. G. Apollaro, A. Xuereb, L. Mazzola, M. Campisi, A. Ferraro, M. Paternostro, and G. D. Chiara, Assessing the Nonequilibrium Thermodynamics in a Quenched Quantum Many-Body System via Single Projective Measurements, Phys. Rev. X 031029, 1–18 (2014).
- [130] E. Bäumer, M. Perarnau-Llobet, P. Kammerlander, H. Wilming, and R. Renner, *Imperfect Thermalizations Allow for Optimal Thermodynamic Processes*, Quantum **3**, 153 (June 2019).
- [131] H. Janyszek, On the geometrical structure of the generalized quantum Gibbs states, Reports on Mathematical Physics 24(1), 11–19 (Aug. 1986).

- [132] S. Sachdev, Quantum Phase Transitions, Cambridge University Press, Apr. 2011.
- [133] A. P. Solon and J. M. Horowitz, *Phase Transition in Protocols Minimizing Work Fluctua*tions, Physical Review Letters **120**(18) (May 2018).
- [134] D. A. Sivak and G. E. Crooks, Thermodynamic metrics and optimal paths, Phys. Rev. L 108(19), 190602 (2012) (2012).
- [135] S. Deffner and M. V. S. Bonança, Thermodynamic control —An old paradigm with new applications, EPL (Europhysics Letters) 131(2), 20001 (Aug. 2020).
- [136] P. P. Potts, A. A. S. Kalaee, and A. Wacker, A thermodynamically consistent Markovian master equation beyond the secular approximation, New Journal of Physics **23**(12), 123013 (dec 2021).
- [137] A. Soret, V. Cavina, and M. Esposito, *Thermodynamic consistency of quantum master equations*, Phys. Rev. A **106**, 062209 (Dec 2022).

# Finite-time Landauer principle beyond weak coupling

Alberto Rolandi and Martí Perarnau-Llobet

Département de Physique Appliquée, Université de Genève, 1211 Genève, Switzerland

Landauer's principle gives a fundamental limit to the thermodynamic cost of erasing information. Its saturation requires a reversible isothermal process, and hence infinite time. We develop a finite-time version of Landauer's principle for a bit encoded in the occupation of a single fermionic mode, which can be strongly coupled to By solving the exact nona reservoir. equilibrium dynamics, we optimize erasure processes (taking both the fermion's energy and system-bath coupling as control parameters) in the slow driving regime through a geometric approach to thermodynamics. We find analytic expressions for the thermodynamic metric and geodesic equations, which can be solved numerically. Their solution yields optimal processes that allow us to characterize a finitetime correction to Landauer's bound, fully taking into account strong coupling effects. Our result suggests the emergence of the Planckian time,  $\tau_{\rm Pl} = \hbar/k_BT$ , as the shortest timescale for information erasure.

### 1 Introduction

Any logical irreversible operation that will incur a thermodynamic cost in the form of heat dissipated into the environment. Landauer's principle quantifies this relation between information processing and thermodynamics with the bound  $Q \geq k_B T \ln 2$  for the erasure of a single bit of information [1]. Here Q is the dissipated heat,  $k_B$  is the Boltzmann constant and T is the absolute temperature at which the process is taking place. In recent years, this principle has been intensively studied within the fields of stochastic and quantum thermodynamics [2–17], and has been approached in several experimental platforms [18–29].

Alberto Rolandi: alberto.rolandi@unige.ch

Martí Perarnau-Llobet: marti.perarnaullobet@unige.ch

The unattainability principle suggests that Landauer's bound cannot be saturated with finite resources, namely time and energy [30–32]. In finite time, using tools from optimal transport theory [33–35] and thermodynamic geometry [36–43], optimal erasure protocols have been derived both for classical systems described by overdamped Langevin dynamics [44–48] and open quantum systems described by Lindblad master equations [35, 49–54]. Such optimal protocols naturally lead to a finite-time correction to Landauer's bound in different physical set-ups, which has given rise to the term finite-time Landauer principle [45, 48, 52]. For a slowly driven (quantum) two-level system weakly coupled to a thermal bath, the finite-time bound takes the simple form (see App. B.2 and Refs. [50, 54])

$$Q \ge k_B T \left( \ln 2 + \frac{\pi^2}{4\Gamma \tau} \right) + \mathcal{O}\left( \frac{1}{\Gamma^2 \tau^2} \right),$$
 (1)

where  $\tau$  is the total time of the process and  $\Gamma$  is the thermalization rate. The finite-time correction is positive, in agreement with the second law of thermodynamics, and when  $\Gamma\tau\to\infty$  we recover the standard bound. We also note that the optimal protocol saturating the finite bound eq. (1) has been recently implemented in a semiconductor quantum dot [29]. More general versions of eq. (1) have also been recently developed for Markovian systems driven at any speed [35, 51, 52].

Despite this remarkable progress, previous works on the *finite-time Landauer principle* have focused in Markovian systems which, for quantum systems, can be guaranteed by a sufficiently weak interaction between system and bath. In the presence of strong coupling [55–59], we expect both new opportunities arising due to faster relaxation rates and non-Markovian dynamics [60–67], as well as challenges due to the presence of new sources of irreversibility [68–75]. The goal of this work is to take a first step into this exciting regime by deriving the first order to a tight

finite-time correction of Landauer's principle for a single fermion that can interact *strongly* with a reservoir, as described by the resonant-level model [76–83]. Our main result is summarised in what follows:

#### Main result

Given a two-level system that can be strongly coupled to a thermal bath, we find that the finite-time version of Landauer's principle can be expressed as

$$Q \ge k_B T \left( \ln 2 + a \frac{\tau_{\text{Pl}}}{\tau} \right) + \mathcal{O} \left( \frac{1}{\Gamma^2 \tau^2} \right)$$
(2)

where  $a \approx 2.57946$ ,  $\tau_{\rm Pl} = \hbar/k_BT$  is the so-called Planckian time [84], and  $\Gamma$  is the average thermalization rate (see details below). This extends eq. (1) to strong system-bath couplings, with the transition between the two being characterized in Fig. 2. The finite-time correction in eq. (2) is of quantum-mechanical nature and independent of the coupling strength, hence prevailing even for arbitrarily strong system-bath coupling (roughly speaking,  $\Gamma \to \infty$  in eq. (1)).

The appearance of the Planckian time  $\tau_{\rm Pl}$  =  $\hbar/k_BT$  in eq. (2) is particularly interesting. This timescale encodes two fundamental constants in nature: Boltzmann's constant  $k_B$  and Planck's constant  $\hbar$ . It arises in several contexts in manybody physics, including quantum transport and quantum chaos; see Ref. [84] for a review. In analogy with the "Planck time" in quantum gravity, it is associated with the shortest timescale of thermalization [84–87]; that is, the shortest time needed to redistribute energy between particles and reach thermal equilibrium. This gives an insightful context to our main result eq. (2): a fundamental finite-time quantum correction must appear to Landauer's bound due to a minimal time required for thermalization. This also suggests that the form of eq. (2) has a broader range of applicability, with the value a depending on the specific many-body thermalizing dynamics considered.

In order to obtain eq. (2), we exploit the framework of thermodynamic geometry [36–42], which has proven successful to devise minimally dissi-

pative processes both in classical [40, 88–94] and quantum systems [12, 50, 95–99].

### 2 Framework

We consider a driven system S that can be put in contact with a thermal bath B, so that the total time-dependent Hamiltonian reads:

$$H(t) = H_S(t) + H_{\text{int}}(t) + H_B.$$
 (3)

Here,  $H_S(t)$ ,  $H_{\rm int}(t)$  are the externally controllable Hamiltonian of S and SB coupling, respectively, whereas  $H_B$  is the Hamiltonian of B. The state  $\rho(t)$  of SB evolves as  $\rho(t) = U(t)\rho(0)U^{\dagger}(t)$  with  $U(t) = \mathcal{T} \exp(-\frac{i}{\hbar} \int_0^t ds \ H(s))$ . The work cost induced by driving H(t), with  $t \in [0, \tau]$ , reads:

$$W = \int_0^{\tau} ds \operatorname{Tr}[\rho(s)\dot{H}(s)] = \operatorname{Tr}[H(\tau)\rho(\tau) - H(0)\rho(0)]$$
(4)

Focusing on protocols where  $H_{\rm int}(0) = H_{\rm int}(\tau) = 0$ , we can naturally identify from the first law of thermodynamics  $W = Q + \Delta E_S$  with  $\Delta E_S = \text{Tr}[H_S(\tau)\rho(\tau) - H_S(0)\rho(0)]$ , the dissipated heat

$$Q = \text{Tr}[H_B(\rho(\tau) - \rho(0))] \tag{5}$$

as the total energy absorbed by the bath [3].

Assuming that the initial state of SB is a thermal state:  $\rho(0) = e^{-\beta H(0)}/\mathcal{Z}(0)$  with  $\mathcal{Z}(t) \equiv \text{Tr}[e^{-\beta H(t)}]$ , eq. (4) can be re-expressed as [100]:

$$W = \Delta F + k_B T \Sigma , \qquad (6)$$

where  $\Delta F = k_B T \ln[\mathcal{Z}(0)/\mathcal{Z}(\tau)]$  is the change of equilibrium free energy of SB, and the entropy production  $\Sigma$  can be expressed as:  $\Sigma = S\left(\rho(\tau)||\frac{e^{-\beta H(\tau)}}{\mathcal{Z}(\tau)}\right)$ . The entropy production  $\Sigma \geq 0$  accounts for the irreversible energetic contribution in finite-time processes, and depends on the particular driving path H(t) linking H(0) to  $H(\tau)$ . Minimising  $\Sigma$  over all finite-time processes leads to thermodynamic protocols that minimize the work W. Furthermore, in an erasure process,  $\Delta E_S = 0$  (see details below) therefore these protocols also minimize the dissipated heat Q.

# 3 Thermodynamic geometry

The framework of quantum thermodynamic geometry [42] allows us to minimize the entropy

production  $\Sigma$ , and therefore the dissipated heat Q for erasure, for protocols that are slow compared to their relaxation time-scale.

# 3.1 Strongly coupled systems

Let us expand the Hamiltonian H(t) in eq. (3) as  $H(t) = \sum_{j} \lambda_{j}(t) X_{j}$  where  $\{\lambda_{j}(t)\}$  are the externally controllable parameters and  $\{X_{j}\}$  are the corresponding observables. In order to apply the geometric approach, we need to impose more structure on the possible evolutions U(t) generated by eq. (3). We require two basic ingredients: **Requirement 1: Thermalization.** In absence of driving, the conjugated observables  $X_{j}$  thermalize. More precisely, for a frozen Hamiltonian H(t), we have

$$\lim_{s \to \infty} \text{Tr}[\tilde{U}_t(s)\rho(0)\tilde{U}_t^{\dagger}(s)X_j] = \langle X_j(t) \rangle_{\text{eq}}, \quad (7)$$

where  $\tilde{U}_t(s) \equiv e^{-iH(t)s}$ ,  $\langle X_j(t) \rangle_{eq} = \text{Tr}[\omega_{\beta}(t)X_j]$ ,  $\omega_{\beta}(t) = e^{-\beta H(t)}/\mathcal{Z}(t)$ , and  $\beta$  is implicitly defined by the initial energy of the total system. In the context considered here, namely purely unitary dynamics of SB, this condition is satisfied both by non-integrable systems satisfying the ETH hypothesis [101, 102] and also for integrable systems typically appearing in open quantum systems [103–106].

Requirement 2: Slow driving, so that the system remains close to the instantaneous equilibrium state while being driven. This enables us to keep only leading terms when making a linear-response expansion in the driving speed [107], which can be expressed as:

$$\langle X_j(t)\rangle = \langle X_j(t)\rangle_{\text{eq}} + \sum_i m_{ij}\dot{\lambda}_i(t) + \dots$$
 (8)

The coefficients  $m_{ij}$ , which depend on the point  $\{\lambda_i(t)\}$ , can in principle be derived from the exact equations of motion. We should note that it is well known that optimal finite-time protocols feature jumps [108]. However, these jumps disappear near the reversible limit (see App. E and [109]) and their contribution to the dissipated heat becomes negligible. Therefore this requirement becomes a natural assumption in the context of finding a first order correction to Landauer's bound.

Combining the expansion of eq. (8) with eq. (4) and eq. (6), we obtain the standard expression for

entropy production at leading order in the inverse of the driving speed [37, 40, 42]:

$$k_B T \Sigma = \sum_{ij} \int_0^\tau dt \ \dot{\lambda}_i(t) m_{ij}(t) \dot{\lambda}_j(t) \qquad (9)$$

where, in contrast to previous works, the metric  $m_{ij}$  depends on the unitary dynamics of SB (this will later be solved for a specific model). Because of the second law of thermodynamics, it follows that  $m_{ij}$  can be expressed as a metric, i.e., a symmetric, positive-definite  $m \geq 0$  operator that depends smoothly on the point  $\{\lambda_i(t)\}$ . We can associate a length to a protocol by defining  $L = \int_0^{\tau} dt \sqrt{\sum_{ij} \dot{\lambda}_i(t) m_{ij}(t) \dot{\lambda}_j(t)}$ . It is related to the entropy production via a Cauchy-Schwarz inequality [37, 40, 42]:

$$k_B T \Sigma \ge \frac{1}{\tau} L^2 \,, \tag{10}$$

where equality is satisfied protocols with constant entropy production  $\sum_{ij} \dot{\lambda}_i(t) m_{ij}(t) \dot{\lambda}_j(t)$ . Furthermore, to minimize the entropy production of any (slow) protocol we have to find the shortest path between the desired initial and final value of the Hamiltonian's parameters. This corresponds to a geodesic path, with length  $\mathcal{L}$ , which naturally defines a minimal entropy production

$$k_B T \Sigma_{min} = \frac{1}{\tau} \mathcal{L}^2 \ . \tag{11}$$

We can find  $\Sigma_{min}$  by solving the geodesic equation that is derived from the metric and computing its length [37, 40, 42].

#### 3.2 Resonant-level model

Having explained the general ideas behind our work, we now focus on finite-time driving processes of a single fermionic mode coupled to a fermionic bath, which can e.g. describe a single-electron quantum dot. The total Hamiltonian reads:

$$H(t) = \varepsilon(t)\hat{a}^{\dagger}\hat{a} + \sum_{k=1}^{n} \omega_k \hat{b}_k^{\dagger} \hat{b}_k + g(t) \sum_{k=1}^{n} \lambda_k \hat{a}^{\dagger} \hat{b}_k + \lambda_k^* \hat{b}_k^{\dagger} \hat{a}.$$
(12)

where  $\hat{a}^{\dagger}$  is the creation operator of the two-level system and  $\hat{b}_{k}^{\dagger}$  is the creation operator of a bath mode with frequency  $\omega_{k}$ , following the canonical anti-commutation relations:  $\{\hat{a}^{\dagger}, \hat{a}\} = 1$ ,

 $\{\hat{b}_{j}^{\dagger},\hat{b}_{k}\} = \delta_{jk}\mathbb{1}, \ \{\hat{b}_{j},\hat{b}_{k}\} = \{\hat{a},\hat{b}_{k}\} = \{\hat{a}^{\dagger},\hat{b}_{k}\} = \{\hat{a}^$  $\{\hat{a}, \hat{a}\} = 0$ ; and finally  $\lambda_k$  are the interaction weights which define the spectral density function of the bath  $\mathfrak{J}(\omega) = 2\pi \sum_{k} |\lambda_{k}|^{2} \delta(\omega - \omega_{k})$ . The energy  $\varepsilon$  is the difference between the energy of the two-level system and the chemical potential of the bath<sup>1</sup>. We are assuming optimal control over the functions  $\varepsilon(t)$  and g(t) so that we can fully optimize the protocol and reach the fundamental limit for this system. While this level of control is, in principle, ambitious experimentally in regards to the coupling, it has been achieved in quantum dots [110] where the tunneling rate (i.e. interaction strength) can be modified by several orders of magnitude. We take the continuum limit and assume that the spectral density of the bath is a Lorentzian

$$\mathfrak{J}(\omega) = \frac{\Lambda^2}{\Lambda^2 + \omega^2} \;, \tag{13}$$

where  $\Lambda > 0$  is a parameter characterizing its Exact and explicit solutions for the resonant-level model are known in the wide-band limit  $\Lambda \to \infty$  [76–82]. This limit is commonly used to describe quantum systems in contact with fermionic macroscopic baths, e.g. in quantum dots or single-molecule junctions [111, 112]. In essence, it neglects the structure of the density of states in the bath and, as a consequence, a main limitation is that it fails to describe the shorttime dynamics [112]. Nevertheless, this problem does not affect this study since we are interested in large times. We should further note that the energy of the system-bath interaction is proportional to  $\Lambda$ , and therefore is divergent in this limit. We will therefore take  $\Lambda$  to be finite but much larger than any other energy scale of the system. For our analysis to be valid we simply require dynamics much slower than  $\Lambda^{-1}$  [76].

The dynamics are solved via a quantum Langevin approach, which is detailed in App. A (see also [62, 83]). Taking the initial state to have no correlations between S and B ( $\rho(0) = \rho_S(0) \otimes \rho_B(0)$ ) and the bath to be in a thermal state; we find the probability of occupation of the excited

<sup>1</sup>The chemical  $\nu$  potential of the bath is incorporated by subtracting  $\nu \hat{a}^{\dagger} \hat{a}$  to the system's Hamiltonian. Since here  $H_S = \varepsilon a^{\dagger} \hat{a}$  (with  $\varepsilon$  the energy of the system), we can simply redefine  $\varepsilon$  to be the difference between the system's energy and the chemical potential and set  $\nu = 0$  without loss of generality.

level of the system  $p(t) = \langle \hat{a}^{\dagger} \hat{a} \rangle$  and the systembath interaction energy  $v(t) = \sum_{k} \lambda_{k} \langle \hat{a}^{\dagger} \hat{b}_{k} \rangle + h.c.$ ,

$$p(t) = |G(t,0)|^2 p(0)$$

$$+ \frac{1}{2\pi} \int_{-\infty}^{\infty} d\omega \ f_{\beta}(\omega) \left| \int_{0}^{t} ds \ g(s) G(t,s) e^{i\frac{\omega}{\hbar}(t-s)} \right|^2,$$

$$v(t) = \frac{1}{\pi} \Im \int_{-\infty}^{\infty} d\omega \ f_{\beta}(\omega) \int_{0}^{t} ds \ g(s) G(t,s) e^{i\frac{\omega}{\hbar}(t-s)},$$

$$(15)$$

where  $f_{\beta}(\omega) = (1 + e^{\beta \omega})^{-1}$  is the Fermi-Dirac distribution and we defined the propagator

$$G(t,s) = \exp\left[-\frac{1}{\hbar} \int_{s}^{t} dr \ \mu(r) + i\varepsilon(r)\right] ,$$
 (16)

with  $\mu(t) := \frac{1}{2}g(t)^2$ . From these expressions we can exactly compute the thermodynamic work eq. (4), which reads:

$$W = \int_0^{\tau} dt \ \dot{\varepsilon}(t) p(t) + \dot{\mu}(t) v(t) / g(t). \tag{17}$$

From the exact solutions for p(t) and v(t), in App. A we show that **Requirement 1** is satisfied, and hence  $W = \Delta F$  in the quasistatic limit. For slow but finite-time processes, we perform a slow driving expansion of eq. (14) and eq. (15) (details in App. B) using that the thermalization rate of the system is  $\Gamma := \frac{2}{\hbar \tau} \int_0^{\tau} dt \, \mu(t)$ , so that the expansion can be performed in orders of  $1/(\tau\Gamma)$ . We then obtain an expansion for W analogous to eq. (6) where the entropy production  $\Sigma$  is described by eq. (9) with  $\vec{\lambda}(t) = (\varepsilon(t), \mu(t))$  and the thermodynamic metric

$$m(t) = \frac{\hbar}{\pi} \int_{-\infty}^{\infty} d\omega \, f_{\beta}(\omega) m_{\omega}(\varepsilon(t) - \omega, \mu(t)) \,, (18)$$

where

$$m_{\omega}(\varepsilon,\mu) = \frac{1}{(\mu^2 + \varepsilon^2)^3} \begin{pmatrix} 4\varepsilon\mu^2 & -\mu(\mu^2 - 3\varepsilon^2) \\ \mu(\mu^2 - 3\varepsilon^2) & 2\varepsilon(\varepsilon^2 - \mu^2) \end{pmatrix} .$$
(19)

This metric gives a geometrical description of slow thermodynamic protocols performed on the system. By solving the geodesic equations [113], we can find the geodesic length  $\mathcal{L}$  and hence the minimal entropy production eq. (11).

# 4 Special limits of the metric

Before attempting to solve the geodesic equations for the case of erasure, we now study the high

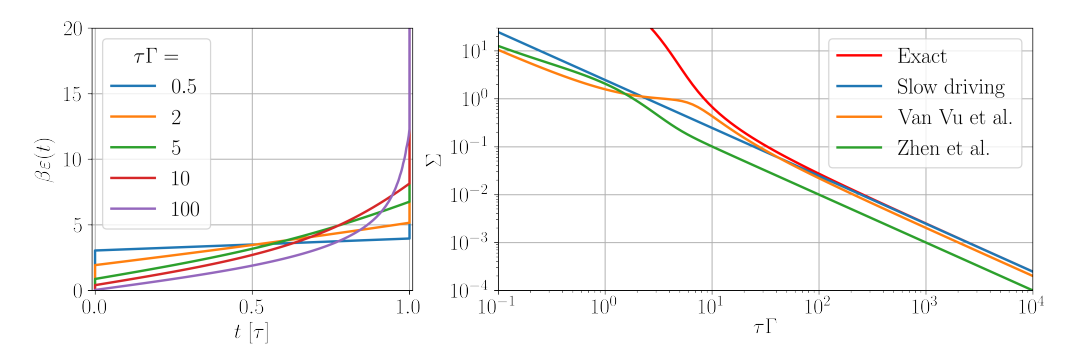


Figure 1: (left) Examples of optimal protocols computed from [109] for boundary conditions  $\varepsilon(0)=0$  and  $\beta\varepsilon(\tau)=20$  at different values of  $\tau$ . (right) Comparison of the entropy production of the optimal protocols from [109] with boundary conditions  $\varepsilon(0)=0$  and  $\beta\varepsilon(\tau)=100$  to the lower bounds given by eq. (1), Van Vu et al. [52] and Zhen et al. [51].

and low temperature limits, as well as the limit of weak coupling, to gain further analytical insights on the form of optimal protocols and the associated entropy production.

## 4.1 High temperature limit ( $\beta \varepsilon, \beta \mu \ll 1$ )

Since the terms of eq. (18) quickly decay at high frequencies we can perform the high temperature expansion  $f_{\beta}(\omega) = \frac{1}{2} - \frac{1}{4}\beta\omega + \mathcal{O}(\beta^3\omega^3)$  directly in the metric. At leading order, we find:

$$m_{HT} = \frac{\hbar \beta}{8\mu} \mathbb{1} \ . \tag{20}$$

This enables an analytical solution of the geodesic equations. Given the boundary conditions  $\{\varepsilon(0) = \mu(0) = \mu(\tau) = 0, \, \varepsilon(\tau) = \varepsilon_* > 0\}$ , which will later match those of an erasure protocol<sup>2</sup>, we find the following geodesic path (cf. App. C)

$$\varepsilon(t) = \varepsilon_* \left( t/\tau - \frac{\sin(2\pi t/\tau)}{2\pi} \right) , \qquad (21)$$

$$\mu(t) = \frac{\varepsilon_*}{\pi} \sin(\pi t/\tau)^2 . \tag{22}$$

In the regime  $\beta \varepsilon(t) \ll 1$ , we observe that minimising entropy production requires a maximal coupling strength  $\varepsilon(\tau)/\pi$ . The entropy production of the geodesic protocol is

$$k_B T \Sigma_{min} = \frac{\pi \hbar \beta \varepsilon_*}{2\tau} + \mathcal{O}(\beta^3 \varepsilon_*^3) , \qquad (23)$$

which linearly scales with the final energy  $\beta \varepsilon_*$ .

 $^2$ Usually, the initial condition for erasure would be  $\varepsilon(0) = \nu$  for  $\nu$  the chemical potential of the bath and  $\varepsilon$  the energy of the two-level system (so that the corresponding thermal state is the fully mixed state). But since here we defined  $\varepsilon$  to be the difference to the chemical potential we take  $\varepsilon(0) = 0$  without loss of generality.

# 4.2 Zero temperature limit ( $\beta \varepsilon$ or $\beta \mu \to \infty$ )

In the limit of  $T = 0^{\beta}$  we have  $f_{\beta}(\omega) \to f_{\infty}(\omega) = \Theta(-\omega)$ , where  $\Theta$  is the Heaviside step function. Therefore the metric becomes (cf. App. D)

$$m_{T=0} = \frac{\hbar}{\pi} \frac{1}{(\mu^2 + \varepsilon^2)^2} \begin{pmatrix} \mu^2 & -\varepsilon\mu \\ -\varepsilon\mu & \varepsilon^2 \end{pmatrix} , \quad (24)$$

which coincides with the metric of an angle distance in the  $(\varepsilon, \mu)$  space -hence the metric is singular. If we re-parameterize  $(\varepsilon, \mu)$  as  $(r\cos\phi, r\sin\phi)$  we find  $k_BT\Sigma = \frac{1}{\pi} \int_0^{\tau} dt \, \dot{\phi}(t)^2$ . Therefore any protocol that keeps  $\phi(t)$  constant is a geodesic, leading to the minimal entropy production:

$$k_B T \Sigma_{min} \bigg|_{T=0} = \frac{\hbar (\Delta \phi)^2}{\pi \tau},$$
 (25)

with  $\phi = \arctan(\mu/\varepsilon)$ . Note that there are multiple (infinitely many) geodesics for any pair of boundary points. This fact prevents us from continuing the expansion to further orders in temperature. Nevertheless, this limit provides analytical insights on optimal protocols with  $\beta\varepsilon$  or  $\beta\mu\gg 1$ . In particular, we note that there is no need for a diverging coupling even when  $\varepsilon(\tau)\to\infty$  as, once  $\mu$  has become large, eq. (25) shows that it is optimal to reduce the coupling while increasing the energy. Furthermore, eq. (25) shows that at zero temperature, while the reversible cost of the operation goes to zero, the dissipation remains strictly

 $^{3}$ The zero temperature limit is achieved whenever the energy gaps of the system are too large for thermal fluctuations to occur between the energy levels. Bringing either  $\beta\varepsilon$  or  $\beta\mu$  to infinity achieves this effect. It is the opposite in the infinite temperature limit, where the thermal fluctuations need to overcome any energy gap, therefore in that limit, both  $\beta\varepsilon$  and  $\beta\mu$  need to be brought to zero.

positive. This result is complementary to the findings of Ref. [13] which demonstrate a finite-size correction to Landauer's bound that does not disappear in the zero-temperature regime.

### 4.3 Weak coupling limit

Lastly, we take take the weak coupling limit to compare to previous erasure results that are obtained via Lindbladian dynamics, a common assumption in previous works on optimal thermodynamic control in the quantum regime [35, 49–54]. In this limit the coupling is taken to be small and constant, therefore the metric becomes a scalar (cf. App. B.2):

$$m_{weak}(\varepsilon) = \frac{\beta \hbar}{\Gamma} f_{\beta}(\varepsilon) (1 - f_{\beta}(\varepsilon)) ,$$
 (26)

which matches with the results of [50, 54] which were also obtained with thermodynamic geometry. Indeed, this metric can be obtained from the rate equation

$$\frac{dp(t)}{dt} = -\Gamma \left( p(t) - \frac{1}{1 + e^{\beta \varepsilon(t)}} \right) , \qquad (27)$$

which can also be obtained by taking the weak coupling limit in the Heisenberg equations that define eq. (14). In this regime protocols that minimize dissipated heat at arbitrary speed were found by [109]. Therefore we will compare the results one obtains in slow driving and the results of [51, 52] to the exact minimization of [109].

We are interested in erasure processes, where  $\varepsilon(t)$  is driven from  $\varepsilon(0) = 0$  to  $\varepsilon(\tau) = \varepsilon_*$  with  $\varepsilon_* \gg k_B T$  in a time  $\tau$ . Optimal finite-time protocols are those which minimize the work cost  $W = \int_0^\tau dt \, \dot{\varepsilon}(t) p(t)$ , and hence the heat dissipated to the environment  $Q = W - \Delta E$ . The results of [109] provide an exact solution to this problem, which is shown in Fig. 1. As it is well-known in finite time stochastic thermodynamics [108], jumps appear in the optimal solution. However, as we approach the quasistatic limit where  $\tau\Gamma \gg 1$ , the jumps progressively disappear. In App. E we prove why the jumps should also disappear in the long times limit at strong coupling. As detailed in App. B.2, and also discussed in previous references [50], the optimal driving solution in this limit has the simple analytical form

$$\varepsilon(t) = 2\beta^{-1} \ln \tan \left[ \frac{\pi}{4} (t/\tau + 1) \right] , \qquad (28)$$

leading to the work cost

$$W = k_B T \left( \ln 2 + \frac{\pi^2}{4\tau \Gamma} \right) , \qquad (29)$$

from where we can directly recover eq. (1) through the first law of thermodynamics (note that  $\Delta E_S \approx 0$ ). In Fig. 1 we notice that the exact solution of [109] agrees well with this analytical form in the slow driving limit. For completeness, we also show recent results of [51, 52]. These results apply more generally to any Markovian master equation (here we apply them to the particular case of eq. (27)), and one can see that they provide a bound to the exact numerical (and approximate analytical) solutions.

# 5 Optimized erasure

We now focus on erasure outside of any approximation, where we will optimize the driving over both the energy and coupling. In what follows, we focus on minimising  $\Sigma$  in an erasure process, which imposes specific boundary conditions to the geodesic equations. We assume that we have no prior knowledge of the system, therefore its initial state is  $\rho_S(0) = 1/2$ . This translates in taking  $\varepsilon(0) = 0$  so that it coincides with the thermal state of  $H_S$ . For the qubit to be erased we want its final state to be  $\rho_S(\tau) \approx |0\rangle\langle 0|$  (i.e.  $p(\tau) \approx 0$ ). Since the driving is done slowly, p(t) is always close to its thermal expectation value. Therefore by choosing  $\beta \varepsilon(\tau) \to \infty$  we ensure  $p(\tau) \approx 0^4$ . For the coupling, the boundary conditions are  $\mu(0) = \mu(\tau) = 0$ , because we want to think of this as an "erasure machine" that the qubit is "brought to" at the start and "retrieved from" at the end. Given this family of protocols, we recognise from eq. (6) that  $W = k_B T(\ln 2 + \Sigma)$ , and similarly  $Q = k_B T(\ln 2 + \Sigma)$ , thus justifying the minimisation of  $\Sigma$  as given in eq. (9). After the qubit has been decoupled (i.e. at  $t > \tau$ ), we bring the Hamiltonian of the system back to its starting value ( $\varepsilon = 0$ ) to close the cycle. Since  $p(\tau) \approx 0$ ,

<sup>4</sup>Strictly speaking, in order to ensure consistency with the slow driving limit,  $\beta \varepsilon(\tau)$  has to remain finite (so that the speed  $\dot{\lambda}$  remain finite). However, the final population  $p(\tau)$  is exponentially small with  $\beta \varepsilon(\tau)$ , leading to exponentially small corrections. Our results are valid up to such corrections, and for sufficiently large  $\tau$  to ensure the validity of the approximation.

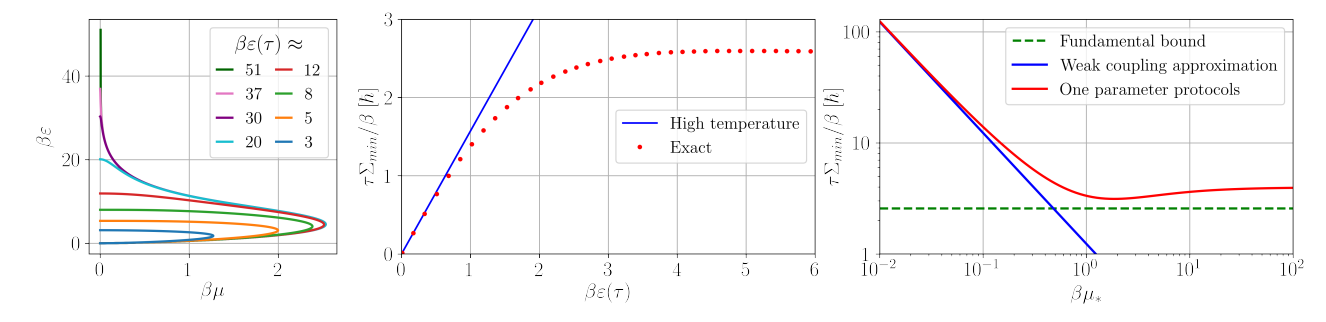


Figure 2: (left) A series of optimal protocols depicted in the  $(\mu,\varepsilon)$  space. They all start with zero energy and coupling and end with finite energy and zero coupling. In the limit of large  $\beta\varepsilon(\tau)$  they can be considered as erasure protocols. (middle) The entropy production of the optimal erasure protocol as a function of the final energy, compared to the high temperature regime cost eq. (23). (right) Comparison of the entropy production for a geodesic protocol in which one parameter is varied at a time (with  $\mu$  being increased until  $\mu^*$ ) and the weak coupling approximation eq. (1); the minimal possible entropy production,  $\tau \Sigma_{min}/\beta = 2.57946 \pm 1 \cdot 10^{-5}$  [ $\hbar$ ], obtained when both parameters are changed simultaneously is also shown.

this step requires no work, and it can be done arbitrarily quickly.

The geodesic equations we obtain for this process are not solvable analytically. The integral of eq. (18) can be solved to give us an expression of the metric in terms of polygamma functions (cf. App. B) but it does not simplify the geodesic equations into an analytically solvable form. We therefore turn to numerical tools to obtain the optimal protocol and compute the dissipated work. Though, in our case, we want to impose the aforementioned boundary conditions; this is known as a Boundary Value Problem (BVP), which is famously hard to solve numerically [114]. Though we can use the fact that the high temperature limit is accurate at the start of an erasure protocol, therefore the initial conditions of the optimal protocol for erasure will match the initial conditions of eq. (21) and eq. (22). This allows us to turn the BVP into an Initial Value Problem (cf. App. G) which is much simpler to solve.

In Fig. 2 we show optimal erasure protocols in the  $(\mu, \varepsilon)$  space for different final values of  $\beta \varepsilon$ . We can notice that the predictions of the high and low temperature limit are verified: at the start of the protocols the coupling is increased but once we reach a certain value there is no more need to increase it, regardless of the final value of  $\beta \varepsilon$  we try to reach. Interestingly, the maximal value reached by  $\beta \mu$  is larger than 1. This shows that reaching the strong coupling is needed to achieve optimal erasure, which is one of the main insights of our work. In the same figure we also show the value of  $\tau \Sigma_{min}/\beta$  for the optimal protocol as a function of the final energy.

We can see that for small values of  $\beta \varepsilon(\tau)$  eq. (23) gives an accurate description of the work cost, but as we reach higher values it saturates around  $\tau \Sigma_{min}/\beta = 2.57946 \pm 1 \cdot 10^{-5} \ [\hbar]$ . This provides a finite-time correction to Landauer's principle in this set-up, thus leading to a generalisation of eq. (1):

$$Q \ge k_B T \left( \ln 2 + a \frac{\tau_{\text{Pl}}}{\tau} \right) + \mathcal{O}\left( \frac{1}{\Gamma^2 \tau^2} \right).$$
 (30)

with  $a \approx 2.57946$  and  $\tau_{\rm Pl} = \beta \hbar$ . This is one of the main results of this work and can be seen as a generalization of eq. (1). As opposed to the results of [51] and [52], eq. (30) is only valid for large protocol times; yet, it has the advantage of taking into account strong coupling effects (including any possible variation of the coupling strength), having a much simpler form for the correction (which is independent of any chosen relaxation timescale), and we provide an explicit protocol to achieve it. By turning around eq. (30) one can highlight a quantum speed limit for erasure of a qubit, furthermore this speed limit is of the order of the Planckian time  $\tau_{\rm Pl} = \hbar/k_B T$  which is conjectured to be the fastest relaxation timescale for thermalization [84]. In particular, one can see that eq. (30) bounds the speed of erasure by the order of  $\tau_{\rm Pl}$  regardless of how large is the coupling strength used in the protocol.

Interestingly, we now argue that the form of the correction eq. (30) is in fact general of any Landauer erasure protocol with control on S and the SB coupling. Indeed, first note that the geodesic length  $\mathcal{L}$  is dimensionless and can only depend on  $\beta$  and the boundary conditions as we optimize over  $\mu$  and  $\varepsilon$ . In an erasure process, the

boundary conditions read:  $\varepsilon(0) = 0$ ,  $\varepsilon(\tau) \to \infty$ , and  $\mu_i(0) = \mu_i(\tau) = 0$  where *i* runs over all the possible control parameters on SB. But this implies that  $\mathcal{L}$  is independent of them and hence of  $\beta$ . Therefore  $k_B T \Sigma_{min}$  will take the form of a constant, independent of any parameter of the system and bath, divided by  $\tau$ . This is a crucial difference from eq. (1).

This simple argument based on dimensional analysis thus shows that eq. (30) is rather general, with the value of a depending on the specific implementation (e.g. the ohmicity of the bath). It is important to highlight that the bound eq. (30) implies that, even when having access to arbitrary strong SB interactions (naively taking  $\Gamma \to \infty$  in eq. (1)), infinite time is still required for perfect erasure due to the quantum-mechanical correction derived here.

Finally, we analyze a scenario where the coupling is kept constant while  $\varepsilon(t)$  is driven, which is motivated both by experimental set-ups and for a comparison with the weakly interacting case. Therefore, we restrict to one-parameter protocols consisting of the three following steps: 1. while keeping  $\varepsilon$  at 0 we turn on the coupling to some value  $\mu_*$ ; 2. while keeping the coupling fixed we bring  $\varepsilon$  from 0 to some value  $\varepsilon_* \gg k_B T$ ; 3. while keeping  $\varepsilon$  constant we turn off the coupling. Each step contributes positively to the entropy production, and its minimisation is discussed in App. F. In Fig. 2, we show  $\Sigma_{\min}$  for different values of  $\mu_*$ , ranging from the weak to the super-strong coupling regime. It can be appreciated how eq. (1) breaks down, and also how such one-parameter protocols become close to the fundamental limit eq. (30) for  $\beta \mu_* > 1$ .

### 6 Conclusions and outlook

Deriving finite-time corrections to the seminal Landauer bound is a challenging endeavour in stochastic and quantum thermodynamics [35, 44–54]. Previous works have focused on markovian systems only, which in the quantum regime is obtained through the weak coupling limit ( $\beta g^2 \rightarrow 0$ ). However, should a general finite-time correction exist, it will require the presence of strong coupling at some point during the process as the dissipation generated in finite time is propor-

tional to  $g^{-2}$  when g is small<sup>5</sup>. Motivated by this observation, we have developed new insights into the form of optimal protocols for erasure beyond the weak coupling limit.

We have focused on a bit encoded in the occupation of a single fermionic mode, which can be strongly coupled to a reservoir. We have derived analytically the thermodynamic metric, which governs the dissipation rate in the slow driving regime, and showed that it takes a simple form in the high and low temperature limits. From the general form of the metric we obtained the optimal erasure protocol, which requires increasing the coupling strength to  $g^2 \sim k_B T$ , which corresponds to a relaxation timescale of the order of the Planckian time  $\tau_{\rm Pl}$ . The corresponding dissipation yields a finite-time correction to Landauer's bound for this setup, which is substantially lower than similar results in the weak coupling regime. Furthermore, by using the obtained bound as a quantum speed limit, this result adds further evidence to the conjecture [84] that  $\tau_{\rm Pl}$  is fastest relaxation timescale many-body systems can achieve.

While our results were derived in a fermionic model there are some general insights that follow from our work. First there is a fundamental quantum correction that prevails, see eq. (30), which can be compared with eq. (1) derived in the weak coupling regime. While the specific value of a in eq. (30) will depend on the specific setup, it will never approach 0 (even for diverging system-bath coupling) due to the inherent cost of changing the interaction strength. Furthermore, to obtain these results we adapted the framework of thermodynamic geometry to system-bath unitary dynamics in which the coupling can be arbitrarily large or small. This is in contrast to recent claims of failure of this approach in closed quantum systems [115]. Finally, as was argued before, our results make evident the need of strong coupling in a general finite-time correction to Landauer's principle.

This work opens exciting directions for the future. On the one hand, the level of experimental control required to implement such protocols is in principle possible in quantum dots [116–119],

<sup>5</sup>This can be seen by expanding the finite time dissipation around  $g^2 = 0$  for long times:  $k_B T \Sigma \propto 1/g^2 \tau$ , which follows by noticing that the relaxation time-scale is of the order of  $g^{-2}$ .

where the energy-level  $\varepsilon(t)$  and coupling g(t) can be independently controlled, even by several orders of magnitude [110]. On the other hand, it would be interesting to characterise the dependence of a in the nature of the bath and the SB coupling (e.g. its spectral density), more generally to derive similar quantum-mechanical finite-time corrections that are independent of the specific implementation, and to gain further insights in the connection between Landauer erasure and the Planckian time.

Acknowledgments. We warmly thank Mark T. Mitchinson, Ludovico Machet, and Gabriel Landi for insightful discussions. We also sincerely thank Luca V. Delacretaz for introducing us to the concept of Planckian time. This work was supported by the Swiss National Science Foundation through an Ambizione Grant No. PZ00P2-186067.

### References

- [1] R. Landauer, IBM Journal of Research and Development 5, 183 (1961).
- [2] T. Sagawa and M. Ueda, Phys. Rev. Lett. 102, 250602 (2009).
- [3] M. Esposito and C. V. den Broeck, EPL (Europhysics Letters) 95, 40004 (2011).
- [4] S. Hilt, S. Shabbir, J. Anders, and E. Lutz, Phys. Rev. E 83, 030102 (2011).
- [5] S. Deffner and C. Jarzynski, Phys. Rev. X 3, 041003 (2013).
- [6] D. Reeb and M. M. Wolf, New Journal of Physics 16, 103011 (2014).
- [7] P. Faist, F. Dupuis, J. Oppenheim, and R. Renner, Nature Communications 6 (2015), 10.1038/ncomms8669.
- [8] S. Lorenzo, R. McCloskey, F. Ciccarello, M. Paternostro, and G. M. Palma, Phys. Rev. Lett. 115, 120403 (2015).
- [9] J. Goold, M. Paternostro, and K. Modi, Phys. Rev. Lett. 114, 060602 (2015).
- [10] A. M. Alhambra, L. Masanes, J. Oppenheim, and C. Perry, Phys. Rev. X 6, 041017 (2016).
- [11] G. Guarnieri, S. Campbell, J. Goold, S. Pi-geon, B. Vacchini, and M. Paternostro, New Journal of Physics 19, 103038 (2017).
- [12] H. J. Miller, G. Guarnieri, M. T. Mitchison, and J. Goold, Physical Review Letters 125 (2020), 10.1103/physrevlett.125.160602.

- [13] A. M. Timpanaro, J. P. Santos, and G. T. Landi, Phys. Rev. Lett. 124, 240601 (2020).
- [14] P. M. Riechers and M. Gu, Phys. Rev. A 104, 012214 (2021).
- [15] L. Buffoni and M. Campisi, Journal of Statistical Physics 186 (2022), 10.1007/s10955-022-02877-8.
- [16] P. Taranto, F. Bakhshinezhad, A. Bluhm, R. Silva, N. Friis, M. P. Lock, G. Vitagliano, F. C. Binder, T. Debarba, E. Schwarzhans, F. Clivaz, and M. Huber, PRX Quantum 4, 010332 (2023).
- [17] C. Browne, A. J. P. Garner, O. C. O. Dahlsten, and V. Vedral, Phys. Rev. Lett. 113, 100603 (2014).
- [18] A. Bérut, A. Arakelyan, A. Petrosyan, S. Ciliberto, R. Dillenschneider, and E. Lutz, Nature 483, 187 (2012).
- [19] Y. Jun, M. Gavrilov, and J. Bechhoefer, Phys. Rev. Lett. 113, 190601 (2014).
- [20] A. Bérut, A. Petrosyan, and S. Ciliberto, J. Stat. Mech. 2015, P06015 (2015).
- [21] M. Gavrilov and J. Bechhoefer, Phys. Rev. Lett. 117, 200601 (2016).
- [22] J. Hong, B. Lambson, S. Dhuey, and J. Bokor, Sci. Adv. 2 (2016), 10.1126/sciadv.1501492.
- [23] L. Martini, M. Pancaldi, M. Madami, P. Vavassori, G. Gubbiotti, S. Tacchi, F. Hartmann, M. Emmerling, S. Höfling, L. Worschech, and G. Carlotti, Nano Energy 19, 108 (2016).
- [24] R. Gaudenzi, E. Burzurí, S. Maegawa, H. S. J. van der Zant, and F. Luis, Nat. Phys. 14, 565 (2018).
- [25] O. Saira, M. H. Matheny, R. Katti, W. Fon, G. Wimsatt, J. P. Crutchfield, S. Han, and M. L. Roukes, Phys. Rev. Res. 2, 013249 (2020).
- [26] S. Dago, J. Pereda, N. Barros, S. Ciliberto, and L. Bellon, Phys. Rev. Lett. 126, 170601 (2021).
- [27] S. Dago and L. Bellon, Phys. Rev. Lett. 128, 070604 (2022).
- [28] M. A. Ciampini, T. Wenzl, M. Konopik, G. Thalhammer, M. Aspelmeyer, E. Lutz, and N. Kiesel, arXiv:2107.04429 (2021).
- [29] M. Scandi, D. Barker, S. Lehmann, K. A. Dick, V. F. Maisi, and M. Perarnau-Llobet, Phys. Rev. Lett. 129, 270601 (2022).

- [30] Nernst, W. Sitzber. Kgl. Preuss. Akad. Wiss. Physik-Math. Kl. 134 (1912), missing.
- [31] L. Masanes and J. Oppenheim, Nature Communications 8 (2017), 10.1038/n-comms14538.
- [32] N. Freitas, R. Gallego, L. Masanes, and J. P. Paz, in *Fundamental Theories of Physics* (Springer International Publishing, 2018) pp. 597–622.
- [33] E. Aurell, C. Mejía-Monasterio, and P. Muratore-Ginanneschi, Phys. Rev. Lett. 106, 250601 (2011).
- [34] E. Aurell, K. Gawędzki, C. Mejía-Monasterio, R. Mohayaee, and P. Muratore-Ginanneschi, Journal of Statistical Physics 147, 487 (2012).
- [35] T. Van Vu and K. Saito, Phys. Rev. X 13, 011013 (2023).
- [36] P. Salamon, B. Andresen, P. D. Gait, and R. S. Berry, J. Chem. Phys. 73, 1001 (1980).
- [37] P. Salamon and R. S. Berry, Phys. Rev. Lett. 51, 1127 (1983).
- [38] J. Nulton, P. Salamon, B. Andresen, and A. Qi, J. Chem. Phys. 83, 334 (1985).
- [39] B. Andresen, R. S. Berry, R. Gilmore, E. Ihrig, and P. Salamon, Phys. Rev. A 37, 845 (1988).
- [40] D. A. Sivak and G. E. Crooks, Phys. Rev. Lett. 108, 190602 (2012).
- [41] S. Deffner and M. V. S. Bonança, EPL (Europhysics Letters) 131, 20001 (2020).
- [42] P. Abiuso, H. J. D. Miller, M. Perarnau-Llobet, and M. Scandi, Entropy 22, 1076 (2020).
- [43] T. V. Vu and Y. Hasegawa, Physical Review Letters 126 (2021), 10.1103/physrevlett.126.010601.
- [44] P. R. Zulkowski and M. R. DeWeese, Phys. Rev. E 89, 052140 (2014).
- [45] K. Proesmans, J. Ehrich, and J. Bechhoefer, Phys. Rev. Lett. 125, 100602 (2020).
- [46] K. Proesmans, J. Ehrich, and J. Bechhoefer, Phys. Rev. E 102, 032105 (2020).
- [47] A. B. Boyd, A. Patra, C. Jarzynski, and J. P. Crutchfield, Journal of Statistical Physics 187, 1 (2022).
- [48] J. S. Lee, S. Lee, H. Kwon, and H. Park, Phys. Rev. Lett. 129, 120603 (2022).
- [49] G. Diana, G. B. Bagci, and M. Esposito, Phys. Rev. E 87, 012111 (2013).

- [50] M. Scandi and M. Perarnau-Llobet, Quantum 3, 197 (2019).
- [51] Y.-Z. Zhen, D. Egloff, K. Modi, and O. Dahlsten, Phys. Rev. Lett. 127, 190602 (2021).
- [52] T. Van Vu and K. Saito, Phys. Rev. Lett. 128, 010602 (2022).
- [53] Y.-Z. Zhen, D. Egloff, K. Modi, and O. Dahlsten, Phys. Rev. E 105, 044147 (2022).
- [54] Y.-H. Ma, J.-F. Chen, C. P. Sun, and H. Dong, Phys. Rev. E 106, 034112 (2022).
- [55] P. Strasberg, G. Schaller, N. Lambert, and T. Brandes, New Journal of Physics 18, 073007 (2016).
- [56] C. Jarzynski, Phys. Rev. X 7, 011008 (2017).
- [57] H. J. D. Miller, in Fundamental Theories of Physics (Springer International Publishing, 2018) pp. 531–549.
- [58] A. Nazir and G. Schaller, in *Fundamental Theories of Physics* (Springer International Publishing, 2018) pp. 551–577.
- [59] P. Talkner and P. Hänggi, Rev. Mod. Phys. 92, 041002 (2020).
- [60] A. Rivas, Phys. Rev. Lett. 124, 160601 (2020).
- [61] M. Brenes, J. J. Mendoza-Arenas, A. Purkayastha, M. T. Mitchison, S. R. Clark, and J. Goold, Phys. Rev. X 10, 031040 (2020).
- [62] N. Pancotti, M. Scandi, M. T. Mitchison, and M. Perarnau-Llobet, Phys. Rev. X 10, 031015 (2020).
- [63] S. Alipour, A. Chenu, A. T. Rezakhani, and A. del Campo, Quantum 4, 336 (2020).
- [64] K. Ptaszyński, Physical Review E **106** (2022), 10.1103/physreve.106.014114.
- [65] M. Carrega, L. M. Cangemi, G. De Filippis, V. Cataudella, G. Benenti, and M. Sassetti, PRX Quantum 3, 010323 (2022).
- [66] F. Cavaliere, M. Carrega, G. D. Filippis, V. Cataudella, G. Benenti, and M. Sassetti, Physical Review Research 4 (2022), 10.1103/physrevresearch.4.033233.
- [67] F. Ivander, N. Anto-Sztrikacs, and D. Segal, Phys. Rev. E 105, 034112 (2022).
- [68] D. Newman, F. Mintert, and A. Nazir, Phys. Rev. E 95, 032139 (2017).
- [69] M. Perarnau-Llobet, H. Wilming, A. Riera, R. Gallego, and J. Eisert, Physical

- Review Letters **120** (2018), 10.1103/physrevlett.120.120602.
- [70] P. Strasberg, G. Schaller, T. L. Schmidt, and M. Esposito, Physical Review B 97 (2018), 10.1103/physrevb.97.205405.
- [71] M. Wiedmann, J. T. Stockburger, and J. Ankerhold, New Journal of Physics 22, 033007 (2020).
- [72] J. Liu, K. A. Jung, and D. Segal, Phys. Rev. Lett. 127, 200602 (2021).
- [73] Y. Shirai, K. Hashimoto, R. Tezuka, C. Uchiyama, and N. Hatano, Phys. Rev. Research 3, 023078 (2021).
- [74] S. Koyanagi and Y. Tanimura, The Journal of Chemical Physics 157, 084110 (2022).
- [75] J. Liu and K. A. Jung, Phys. Rev. E 106, L022105 (2022).
- [76] G. Schaller, Open quantum systems far from equilibrium, Vol. 881 (Springer, 2014).
- [77] M. F. Ludovico, J. S. Lim, M. Moskalets, L. Arrachea, and D. Sánchez, Phys. Rev. B 89, 161306 (2014).
- [78] M. Esposito, M. A. Ochoa, and M. Galperin, Phys. Rev. Lett. 114, 080602 (2015).
- [79] M. Esposito, M. A. Ochoa, and M. Galperin, Phys. Rev. B 92, 235440 (2015).
- [80] A. Bruch, M. Thomas, S. Viola Kusminskiy, F. von Oppen, and A. Nitzan, Phys. Rev. B 93, 115318 (2016).
- [81] P. Haughian, M. Esposito, and T. L. Schmidt, Phys. Rev. B 97, 085435 (2018).
- [82] M. T. Mitchison and M. B. Plenio, New Journal of Physics 20, 033005 (2018).
- [83] K. Tong and W. Dou, Journal of Physics: Condensed Matter **34**, 495703 (2022).
- [84] S. A. Hartnoll and A. P. Mackenzie, Rev. Mod. Phys. 94, 041002 (2022).
- [85] S. Sachdev, Quantum Phase Transitions, 2nd ed. (Cambridge University Press, 2011).
- [86] J. Maldacena, S. H. Shenker, and D. Stanford, Journal of High Energy Physics 2016 (2016), 10.1007/jhep08(2016)106.
- [87] S. Pappalardi and J. Kurchan, SciPost Phys. 13, 006 (2022).
- [88] P. R. Zulkowski, D. A. Sivak, G. E. Crooks, and M. R. DeWeese, Phys. Rev. E 86, 041148 (2012).

- [89] M. V. S. Bonança and S. Deffner, J. Chem. Phys. 140, 244119 (2014).
- [90] G. M. Rotskoff, G. E. Crooks, and E. Vanden-Eijnden, Phys. Rev. E 95, 012148 (2017).
- [91] G. Li, J.-F. Chen, C. P. Sun, and H. Dong, Phys. Rev. Lett. 128, 230603 (2022).
- [92] J. Eglinton and K. Brandner, Phys. Rev. E 105, L052102 (2022).
- [93] A. G. Frim and M. R. DeWeese, Phys. Rev. Lett. 128, 230601 (2022).
- [94] J.-F. Chen, R.-X. Zhai, C. Sun, and H. Dong, arXiv preprint arXiv:2209.07269 (2022), 10.48550/arXiv.2209.07269.
- [95] H. J. D. Miller, M. Scandi, J. Anders, and M. Perarnau-Llobet, Phys. Rev. Lett. 123, 230603 (2019).
- [96] P. Abiuso and M. Perarnau-Llobet, Phys. Rev. Lett. 124, 110606 (2020).
- [97] K. Brandner and K. Saito, Phys. Rev. Lett. 124, 040602 (2020).
- [98] P. Terrén Alonso, P. Abiuso, M. Perarnau-Llobet, and L. Arrachea, PRX Quantum 3, 010326 (2022).
- [99] M. Mehboudi and H. J. D. Miller, Phys. Rev. A 105, 062434 (2022).
- [100] S. Deffner and E. Lutz, Phys. Rev. Lett. 105, 170402 (2010).
- [101] J. Eisert, M. Friesdorf, and C. Gogolin, Nature Physics 11, 124 (2015).
- [102] L. D'Alessio, Y. Kafri, A. Polkovnikov, and M. Rigol, Advances in Physics 65, 239 (2016).
- [103] Y. Subaşı, C. H. Fleming, J. M. Taylor, and B. L. Hu, Physical Review E 86 (2012), 10.1103/physreve.86.061132.
- [104] M. Merkli, Annals of Physics 412, 167996 (2020).
- [105] J. D. Cresser and J. Anders, Phys. Rev. Lett. 127, 250601 (2021).
- [106] A. S. Trushechkin, M. Merkli, J. D. Cresser, and J. Anders, AVS Quantum Science 4, 012301 (2022).
- [107] V. Cavina, A. Mari, and V. Giovannetti, Phys. Rev. Lett. 119, 050601 (2017).
- [108] T. Schmiedl and U. Seifert, Phys. Rev. Lett. 98, 108301 (2007).
- [109] M. Esposito, R. Kawai, K. Lindenberg, and C. Van Den Broeck, EPL 89, 20003 (2010).
- [110] S. Rochette, M. Rudolph, A.-M. Roy, M. J. Curry, G. A. T. Eyck, R. P. Manginell,

- J. R. Wendt, T. Pluym, S. M. Carr, D. R. Ward, M. P. Lilly, M. S. Carroll, and M. Pioro-Ladrière, Applied Physics Letters 114, 083101 (2019).
- [111] F. Evers, R. Korytár, S. Tewari, and J. M. van Ruitenbeek, Rev. Mod. Phys. 92, 035001 (2020).
- [112] F. Covito, F. G. Eich, R. Tuovinen, M. A. Sentef, and A. Rubio, Journal of Chemical Theory and Computation 14, 2495 (2018).
- [113] L. W. Tu, Differential Geometry (Springer International Publishing, 2017).
- [114] L. Fox and D. F. Mayers, Numerical Solution of Ordinary Differential Equations (Springer Netherlands, 1987).
- [115] A. Soriani, E. Miranda, and M. V. S. Bonança, New Journal of Physics 24, 113037 (2022).
- [116] M. Ciorga, A. S. Sachrajda, P. Hawrylak,

- C. Gould, P. Zawadzki, S. Jullian, Y. Feng, and Z. Wasilewski, Phys. Rev. B **61**, R16315 (2000).
- [117] J. M. Elzerman, R. Hanson, J. S. Greidanus, L. H. Willems van Beveren, S. De Franceschi, L. M. K. Vandersypen, S. Tarucha, and L. P. Kouwenhoven, Phys. Rev. B 67, 161308 (2003).
- [118] J. V. Koski, V. F. Maisi, J. P. Pekola, and D. V. Averin, Proceedings of the National Academy of Sciences 111, 13786 (2014).
- [119] J. V. Koski, V. F. Maisi, T. Sagawa, and J. P. Pekola, Phys. Rev. Lett. 113, 030601 (2014).
- [120] S. Ismail-Beigi, Yale notes (2013).
- [121] P. A. Erdman, A. Rolandi, P. Abiuso, M. Perarnau-Llobet, and F. Noé, Phys. Rev. Res. 5, L022017 (2023).

### Contents

1	Introduction	1
2	Framework	2
3	Thermodynamic geometry 3.1 Strongly coupled systems	<b>2</b> 3 3
4	Special limits of the metric 4.1 High temperature limit $(\beta \varepsilon, \beta \mu \ll 1)$	4 5 5 6
5	Optimized erasure	6
6	Conclusions and outlook	8
	References	9
A	Solving the exact dynamics  A.1 Solving the Heisenberg equations  A.2 Relevant observables  A.3 Proof of requirement 1  A.3.1 Infinite time limit in absence of driving  A.3.2 Thermal expectation value	13 13 14 15 16
В	Slow driving expansion  B.1 Deriving the thermodynamic metric	19 19 21 22

C	High temperature limit	24
D	Low temperature limit	26
$\mathbf{E}$	Discontinuities in the protocol	27
F	One-parameter case	28
$\mathbf{G}$	Numerical solution to the general case	30

# Solving the exact dynamics

### Solving the Heisenberg equations

We consider a single fermionic mode coupled to a fermionic bath. Without loss of generality we can set the chemical potential to 0 and the ground state of the two-level system to 0. The Hamiltonians of the system and bath are

$$\hat{H}_S(t) = \varepsilon(t)\hat{a}^{\dagger}\hat{a} , \qquad (31)$$

$$\hat{H}_B = \sum_{k=1}^n \omega_k \hat{b}_k^{\dagger} \hat{b}_k \ , \tag{32}$$

where  $\hat{a}^{\dagger}$  is the creation operator of the two-level system and  $\hat{b}_k^{\dagger}$  is the creation operator of a bath mode with frequency  $\omega_k$ . These ladder operators follow the canonical anticommutation relations. For the interaction between system and bath, the Hamiltonian is

$$\hat{H}_{\text{int}}(t) = g(t)\hat{V} = g(t)\sum_{k=1}^{n} \lambda_k \hat{a}^{\dagger} \hat{b}_k + \lambda_k^* \hat{b}_k^{\dagger} \hat{a} , \qquad (33)$$

where the  $\lambda_k$  are the interaction weights.

Will will consider that  $\varepsilon(t)$  and g(t) are the control parameters to then perform the erasure of information in the single mode of the system. We now proceed to solve the dynamics of the system and bath in the Heisenberg picture.

For an operator  $\hat{A}$  in the Schrödinger picture, we denote by  $\hat{A}_H(t)$  the corresponding operator in the the Heisenberg picture. The evolution of  $\hat{A}_H(t)$  is defined by the Heisenberg equation of motion:

$$\frac{d}{dt}\hat{A}_H(t) = i\left[\hat{H}(t), \hat{A}_H(t)\right] , \qquad (34)$$

where  $\hat{H}(t) = \hat{H}_S(t) + \hat{H}_{int}(t) + \hat{H}_B$  and  $\hbar = 1$ . Applying this equation to the ladder operators  $\hat{a}_H(t)$  and  $\hat{b}_{k,H}(t)$  we find the following system of n+1 equations:

$$\frac{d}{dt}\hat{a}_H(t) = -i\varepsilon(t)\hat{a}_H(t) - ig(t)\sum_k \lambda_k \hat{b}_{k,H}(t) , \qquad (35)$$

$$\frac{d}{dt}\hat{b}_{k,H}(t) = -i\omega_k \hat{b}_{k,H}(t) - ig(t)\lambda_k^* \hat{a}_H(t) . \tag{36}$$

By defining  $\hat{u}_k(t) = e^{i\omega_k t} \hat{b}_{k,H}(t)$  we can see that eq. (36) becomes

$$e^{-i\omega_k t} \frac{d}{dt} \hat{u}_k(t) = -ig(t) \lambda_k^* \hat{a}_H(t) ,$$

which is solved by  $\hat{u}_k(t) = \hat{u}_k(0) - i\lambda_k^* \int_0^t ds \ e^{i\omega_k s} g(s) \hat{a}_H(s)$ . We therefore find

$$\hat{b}_{k,H}(t) = e^{-i\omega_k t} \hat{b}_k - i\lambda_k^* \int_0^t ds \ g(s) \hat{a}_H(s) e^{i\omega_k(s-t)} \ , \tag{37}$$

where we used that  $\hat{u}_k(0) = \hat{b}_{k,H}(0) = \hat{b}_k$ . Therefore

$$\sum_{k} \lambda_{k} \hat{b}_{k,H}(t) = \hat{\xi}(t) - i \int_{0}^{t} ds \ \chi(s-t)g(s)\hat{a}_{H}(s) \ , \tag{38}$$

where we defined the noise operator  $\hat{\xi}(t) = \sum_k e^{-i\omega_k t} \lambda_k \hat{b}_k$  and  $\chi(t) = \sum_k e^{i\omega_k t} |\lambda_k|^2$ . We can notice that  $\chi(t)$  is the (symmetrized) noise correlation function:

$$\left\langle \left\{ \hat{\xi}^{\dagger}(t), \hat{\xi}(0) \right\} \right\rangle = \sum_{j,k} e^{i\omega_k t} \lambda_k^* \lambda_j \left\langle \left\{ \hat{b}_k^{\dagger}, \hat{b}_j \right\} \right\rangle = \sum_k e^{i\omega_k t} |\lambda_k|^2 = \chi(t) ,$$

and its Fourier transform is the (unit-less) spectral density of the bath  $\mathfrak{J}(\omega) = 2\pi \sum_k |\lambda_k|^2 \delta(\omega - \omega_k)$ By inserting eq. (38) into equation eq. (35) we find an equation of motion for  $\hat{a}_H(t)$ :

$$\frac{d}{dt}\hat{a}_H(t) = -i\varepsilon(t)\hat{a}_H(t) - ig(t)\hat{\xi}(t) - g(t)\int_0^t ds \ \chi(s-t)g(s)\hat{a}_H(s) \ . \tag{39}$$

In order to solve eq. (39) we will need to explicitly take the continuum limit so that our bath indeed becomes a bath. We can take its spectral density to be either a Lorentzian  $\mathfrak{J}(\omega) = \frac{\Lambda^2}{\Lambda^2 + \omega^2}$  or a pass-band  $\mathfrak{J}(\omega) = \Theta(\Lambda - |\omega|)$  ( $\Theta$  is the Heaviside step function). We will need to assume that we are working in the wide-band approximation ( $\Lambda \to \infty$ ). More practically, we are assuming that the bath interaction is the same over the energies we are spanning with the system. This limit allows us to say that the noise correlation function is negligible for time differences larger than zero:

$$\lim_{\Lambda \to \infty} \lim_{n \to \infty} \chi(t) = \delta(t) .$$

In this limit eq. (39) becomes considerably simpler:

$$\frac{d}{dt}\hat{a}_H(t) = -\left(i\varepsilon(t) + \frac{1}{2}g(t)^2\right)\hat{a}_H(t) - ig(t)\hat{\xi}(t) . \tag{40}$$

Similarly to how we solved eq. (36), we define  $\hat{u}(t) = \exp\left[\int_0^t z(s)ds\right]\hat{a}_H(t)$  for  $z(t) := i\varepsilon(t) + \frac{1}{2}g(t)^2$ . Now we have

$$e^{-\int_0^t z(s)ds} \frac{d}{dt} \hat{u}(t) = -ig(t)\hat{\xi}(t) ,$$

which is solved by  $\hat{u}(t) = \hat{u}(0) - i \int_0^t ds \ g(s) \exp\left[\int_0^s z(r)dr\right] \hat{\xi}(s)$ . We therefore find the solution of the evolution of the ladder operator of the distinguished mode:

$$\hat{a}_{H}(t) = G(t,0)\hat{a} - i \int_{0}^{t} ds \ g(s)G(t,s)\hat{\xi}(s)$$
(41)

where we defined the propagator  $G(t,s) = \exp\left[-\int_s^t z(r)dr\right]$ . And from eq. (37) we find the solution for the bath modes:

$$\hat{b}_{k,H}(t) = e^{-i\omega_k t} \hat{b}_k - i\lambda_k^* \int_0^t ds \ g(s)G(s,0) \hat{a}e^{i\omega_k(s-t)} - \lambda_k^* \int_0^t ds \int_0^s dr \ g(s)g(r)G(s,r) \hat{\xi}(r)e^{i\omega_k(s-t)} \ . \tag{42}$$

### A.2 Relevant observables

Since we are performing an erasure, we will assume the system starts in a factorized state and that the bath starts in a thermal state at inverse temperature  $\beta$  state with respect to its Hamiltonian:

$$\hat{\rho}(0) = \hat{\rho}_S(0) \otimes \frac{e^{-\beta \hat{H}_B}}{Z_B} , \qquad Z_B = \text{Tr}[e^{-\beta \hat{H}_B}] .$$

We are interested in computing the occupation probability of the excited level  $p(t) = \langle \hat{a}^{\dagger} \hat{a} \rangle$  and the system-bath interaction potential  $v(t) = \langle \hat{V} \rangle$ . From eq. (41) we have

$$p(t) = \text{Tr}\Big[\hat{\rho}(0)\hat{a}_{H}^{\dagger}(t)\hat{a}_{H}(t)\Big] = |G(t,0)|^{2} p(0) + \int_{0}^{t} ds dr \ g(s)g(r)G^{*}(t,s)G(t,r)\text{Tr}\left[\frac{e^{-\beta H_{B}}}{Z_{B}}\hat{\xi}^{\dagger}(s)\hat{\xi}(r)\right],$$
(43)

where we used the CAR to get  $\text{Tr}[\hat{a}^{\dagger}\hat{\xi}(s)] = 0$  and drop the cross terms. Further using the CAR we simplify the remaining trace in the integral:

$$\operatorname{Tr}\left[\frac{e^{-\beta H_B}}{Z_B}\hat{\xi}^{\dagger}(s)\hat{\xi}(r)\right] = \sum_{k} e^{i\omega_k(s-r)}|\lambda_k|^2 \operatorname{Tr}\left[\frac{e^{-\beta H_B}}{Z_B}\hat{b}_k^{\dagger}\hat{b}_k\right] = \sum_{k} e^{i\omega_k(r-s)}|\lambda_k|^2 f_{\beta}(\omega_k) , \qquad (44)$$

where  $f_{\beta}(\omega) = (1 + e^{\beta \omega})^{-1}$  is the Fermi-Dirac distribution. We can apply the continuum limit to eq. (44) by using the equality  $2\pi \sum_{k} |\lambda_{k}|^{2} h(\omega_{k}) = \int d\omega \, \mathfrak{J}(\omega) h(\omega)$ , which holds for any function h by definition of  $\mathfrak{J}$ . We can then apply the wideband limit by using  $\lim_{\Lambda \to \infty} \lim_{n \to \infty} \mathfrak{J}(\omega) = 1$ . We find

$$\operatorname{Tr}\left[\frac{e^{-\beta H_B}}{Z_B}\hat{\xi}^{\dagger}(s)\hat{\xi}(r)\right] = \int_{-\infty}^{\infty} \frac{d\omega}{2\pi} e^{i\omega(s-r)} \mathfrak{J}(\omega) f_{\beta}(\omega) \xrightarrow{\Lambda \to \infty} \int_{-\infty}^{\infty} \frac{d\omega}{2\pi} e^{i\omega(s-r)} f_{\beta}(\omega) . \tag{45}$$

Applying eq. (45) to eq. (43) we get

$$p(t) = |G(t,0)|^2 p(0) + \frac{1}{2\pi} \int_{-\infty}^{\infty} d\omega \ f_{\beta}(\omega) \int_{0}^{t} ds \int_{0}^{t} dr \ g(s)g(r)G^*(t,s)G(t,r)e^{i\omega(s-r)} \ . \tag{46}$$

Using eq. (38), the CAR and eq. (41), we have

$$\begin{split} v(t) &= \operatorname{Tr} \left[ \hat{\rho}(0) \hat{a}_H^{\dagger}(t) \left( \sum_k \lambda_k \hat{b}_H(t) \right) \right] + h.c. \\ &= \operatorname{Tr} \left[ \hat{\rho}(0) \hat{a}_H^{\dagger}(t) \hat{\xi}(t) \right] - i \int_0^t ds \ \chi(s-t) g(s) \operatorname{Tr} \left[ \hat{\rho}(0) \hat{a}_H^{\dagger}(t) \hat{a}_H(s) \right] + h.c. \ , \\ &\xrightarrow{\Lambda \to \infty} \operatorname{Tr} \left[ \hat{\rho}(0) \hat{a}_H^{\dagger}(t) \hat{\xi}(t) \right] - i \frac{g(t)}{2} \operatorname{Tr} \left[ \hat{\rho}(0) \hat{a}_H^{\dagger}(t) \hat{a}_H(t) \right] + h.c. \ , \\ &= \operatorname{Tr} \left[ \hat{\rho}(0) \hat{a}_H^{\dagger}(t) \hat{\xi}(t) \right] + h.c. \ , \\ &= i \int_0^t ds \ g(s) G^*(t,s) \operatorname{Tr} \left[ \frac{e^{-\beta H_B}}{Z_B} \hat{\xi}^{\dagger}(s) \hat{\xi}(t) \right] + h.c. \ , \\ &= \frac{i}{2\pi} \int_{-\infty}^\infty d\omega \ f_{\beta}(\omega) \int_0^t ds \ g(s) G^*(t,s) e^{i\omega(s-t)} + h.c. \ . \end{split}$$

So we have

$$v(t) = \frac{1}{\pi} \Im \int_{-\infty}^{\infty} d\omega \ f_{\beta}(\omega) \int_{0}^{t} ds \ g(s) G(t, s) e^{i\omega(t-s)} \ . \tag{47}$$

### A.3 Proof of requirement 1

We will now proceed to prove that, in absence of driving, p(t) and v(t) thermalize. We do so in two steps, we first simplify the expressions of eq. (46) and eq. (47) for  $\varepsilon(t) = \varepsilon$  and g(t) = g and compute the infinite time limit. Then we compute the thermal expectation value of the corresponding observables and prove that the obtained expressions are the same.

#### A.3.1 Infinite time limit in absence of driving

By assuming that the driving parameters are kept constant the propagator becomes

$$G(t,s) = e^{-(t-s)(\frac{1}{2}g^2 + i\varepsilon)}$$
 (48)

This allows us to compute the time integrals in eq. (46) and eq. (47):

$$p(t) = p(0)e^{-g^2t} + \frac{g^2}{2\pi} \int_{-\infty}^{\infty} d\omega \ f_{\beta}(\omega) \frac{1 - 2e^{-g^2t/2}\cos([\omega - \varepsilon]t) + e^{-g^2t}}{g^4/4 + (\omega - \varepsilon)^2} \ , \tag{49}$$

$$v(t) = \frac{g}{\pi} \int_{-\infty}^{\infty} d\omega \ f_{\beta}(\omega) \frac{(\omega - \varepsilon) \left[ 1 - e^{-g^2 t/2} \cos([\omega - \varepsilon]t) \right] - \frac{1}{2} g^2 e^{-g^2 t/2} \sin([\omega - \varepsilon]t)}{g^4 / 4 + (\omega - \varepsilon)^2} \ . \tag{50}$$

As a side-note, it is interesting to note that the frequency integral of eq. (49) can be solved to give the following expression for the occupation probability

$$p(t) = 1 + p(0)e^{-g^2t} + \frac{\sinh(\beta\varepsilon)}{\cosh(\beta\varepsilon) + \cos(\frac{\beta g^2}{2})} + \left(1 + e^{-g^2t}\right) \left[\frac{1}{2} - \frac{1}{\pi}\Im\psi^{(0)}\left(\frac{1}{2} + \frac{\beta}{2\pi}\left(\frac{g^2}{2} + i\varepsilon\right)\right)\right] + \frac{e^{-g^2t}}{\pi}\Im\left(e^{2\pi t/\beta}; \frac{1}{2} + \frac{\beta}{2\pi}\left(\frac{g^2}{2} - i\varepsilon\right), 0\right) + \frac{1}{\pi}\Im\left(e^{2\pi t/\beta}; \frac{1}{2} - \frac{\beta}{2\pi}\left(\frac{g^2}{2} - i\varepsilon\right), 0\right), \quad (51)$$

where  $\psi^{(0)}(z) = \frac{d}{dz} \ln \Gamma(z)$  is the digamma function (defined as the logarithmic derivative of the Gamma function) and  $B(x; a, b) = \int_0^x ds \ s^{a-1} (1-s)^{b-1}$  is the incomplete beta function. This expression is useful for numerical implementations as it is faster to compute than the integral of eq. (49).

By taking the limit  $t \to \infty$  in eq. (49) and eq. (50) we find

$$\lim_{t \to \infty} p(t) = \int_{-\infty}^{\infty} \frac{d\omega}{\pi} f_{\beta}(\omega) \frac{g^2/2}{g^4/4 + (\omega - \varepsilon)^2} , \qquad (52)$$

$$\lim_{t \to \infty} v(t) = g \int_{-\infty}^{\infty} \frac{d\omega}{\pi} f_{\beta}(\omega) \frac{(\omega - \varepsilon)}{g^4/4 + (\omega - \varepsilon)^2} . \tag{53}$$

Here we can notice that if we take the Laplace transform of the propagator we obtain

$$\tilde{G}(z) := \int_0^\infty dt \ G(t,0)e^{-zt} = \frac{1}{z + i\varepsilon + g^2/2} \ ,$$
 (54)

which allows us to rewrite eq. (52) and eq. (53) as

$$\lim_{t \to \infty} p(t) = \int_{-\infty}^{\infty} \frac{d\omega}{\pi} f_{\beta}(\omega) \Re \left[ \tilde{G}(-i\omega) \right] , \qquad (55)$$

$$\lim_{t \to \infty} v(t) = g \int_{-\infty}^{\infty} \frac{d\omega}{\pi} f_{\beta}(\omega) \Im \left[ \tilde{G}(-i\omega) \right] . \tag{56}$$

#### A.3.2 Thermal expectation value

We now compute the expectation value of  $\hat{a}^{\dagger}\hat{a}$  and  $\hat{V}$  when the state is a Gibbs state

$$\hat{\omega}_{\beta} := \frac{e^{-\beta \hat{H}}}{Z} = \frac{\exp\left[-\beta \varepsilon \hat{a}^{\dagger} \hat{a} - \beta g \hat{V} - \beta \hat{H}_{B}\right]}{Z} , \qquad Z = \text{Tr}[e^{-\beta \hat{H}}] .$$

Therefore we want to find  $p_{th} := \text{Tr}[\hat{\omega}_{\beta}\hat{a}^{\dagger}\hat{a}]$  and  $v_{th} := \text{Tr}[\hat{\omega}_{\beta}\hat{V}]$ . Using the fact that the total Hamiltonian is quadratic, we can diagonalize it to rewrite it in the following way

$$\hat{H} = \sum_{k} \varepsilon_k \hat{c}_k^{\dagger} \hat{c}_k \;, \tag{57}$$

where  $\varepsilon_k$  are eigen-energies and  $\hat{c}_k$  are fermionic ladder operators that follow the CAR:  $\{\hat{c}_j^{\dagger}, \hat{c}_k\} = \delta_{jk}\mathbb{1}$ ,  $\{\hat{c}_j, \hat{c}_k\} = 0$ . They are related to the original ones in the following way

$$\hat{a} = \sum_{k} \langle 0 | \hat{a} | k \rangle \, \hat{c}_k \,\,, \tag{58}$$

$$\hat{b}_j = \sum_k \langle 0 | \hat{b}_j | k \rangle \, \hat{c}_k \ , \tag{59}$$

where  $|k\rangle = \hat{c}_k^{\dagger} |0\rangle$  are 1-particle eigenstates of the Hamiltonian with eigenvalue  $\varepsilon_k$ . Inserting this in the expression for the thermal expectation of the probability of occupation we find

$$p_{th} = \frac{1}{Z} \sum_{jk} \langle j | \hat{a}^{\dagger} | 0 \rangle \langle 0 | \hat{a} | k \rangle \operatorname{Tr} \left[ e^{-\beta \hat{H}} \hat{c}_{j}^{\dagger} \hat{c}_{k} \right] = \sum_{k} \left| \langle k | \hat{a}^{\dagger} | 0 \rangle \right|^{2} \frac{\operatorname{Tr} \left[ e^{-\beta \varepsilon_{k}} \hat{c}_{k}^{\dagger} \hat{c}_{k}} \hat{c}_{k}^{\dagger} \hat{c}_{k} \right]}{\operatorname{Tr} \left[ e^{-\beta \varepsilon_{k}} \hat{c}_{k}^{\dagger} \hat{c}_{k} \right]} = \sum_{k} \left| \langle k | \hat{a}^{\dagger} | 0 \rangle \right|^{2} f_{\beta}(\varepsilon_{k}) . \tag{60}$$

From eq. (41) it is easy to see that we can write the propagator in the following way

$$G(t,0) = \langle 0|\hat{a}_H(t)\hat{a}^{\dagger}|0\rangle = \langle 0|\hat{U}^{\dagger}(t)\hat{a}\hat{U}(t)\hat{a}^{\dagger}|0\rangle = \sum_k e^{-i\varepsilon_k t} \langle 0|\hat{U}^{\dagger}(t)\hat{a}|k\rangle \langle k|\hat{a}^{\dagger}|0\rangle = \sum_k e^{-i\varepsilon_k t} \left|\langle k|\hat{a}^{\dagger}|0\rangle\right|^2 ,$$
(61)

where we used the fact that the vacuum state does not evolve  $\hat{U}(t)|0\rangle = |0\rangle$  and that since we are performing no driving we have  $\hat{U}(t) = e^{-it\sum_k \varepsilon_k \hat{c}_k^{\dagger} \hat{c}_k}$ . Note that the sum needs only to be over 1-particle states as there is a scalar product with the 1-particle state  $\hat{a}^{\dagger}|0\rangle$ . By now defining  $\varphi(\omega) := \sum_k \left| \langle k | \hat{a}^{\dagger} | 0 \rangle \right|^2 \delta(\omega - \varepsilon_k)$  we can identify

$$G(t,0) = \int_{-\infty}^{\infty} d\omega \ \varphi(\omega) e^{-i\omega t} \ , \tag{62}$$

$$p_{th} = \int_{-\infty}^{\infty} d\omega \ f_{\beta}(\omega) \varphi(\omega) \ . \tag{63}$$

Considering eq. (55) it is clear that if  $\varphi(\omega) = \frac{1}{\pi} \Re \left[ \tilde{G}(-i\omega) \right]$  then we have proven  $p_{th} = \lim_{t \to \infty} p(t)$ . Therefore we compute the Laplace transform of G(t,0) using eq. (62)

$$\begin{split} \tilde{G}(-i\omega) &= \int_0^\infty dt \ G(t,0) e^{i\omega t} \ , \\ &= \int_0^\infty dt \int_{-\infty}^\infty d\omega' \ e^{i(\omega - \omega')t} \varphi(\omega') \ , \\ &= \int_{-\infty}^\infty d\omega' \ \varphi(\omega') \int_{-\infty}^\infty dt \ \Theta(t) e^{i(\omega - \omega')t} \ , \\ &= \pi \varphi(\omega) + iP. \int_{-\infty}^\infty d\omega' \ \frac{\varphi(\omega')}{\omega - \omega'} \ , \end{split}$$

where P denotes the Cauchy principal value,  $\Theta(t)$  is the Heaviside step function and we used that its Fourier transform is (in a distributional sense)  $\int dt \ e^{ist}\Theta(t) = \pi\delta(s) + P.\frac{i}{s}$ . Since  $\varphi(\omega)$  is by definition a real function we can see that  $P.\int_{-\infty}^{\infty} d\omega' \frac{\varphi(\omega')}{\omega-\omega'}$  is a real number. Therefore we can conclude  $\varphi(\omega) = \frac{1}{\pi}\Re\left[\tilde{G}(-i\omega)\right]$ . Which concludes the proof of the thermalization of p(t).

To prove the thermalization of v(t) we proceed in a similar fashion. We start by computing  $v_{th}$ 

$$v_{th} = \frac{1}{Z} \sum_{jk} \lambda_j \langle k | \hat{a}^{\dagger} | 0 \rangle \langle 0 | \hat{b}_j | k \rangle \operatorname{Tr} \left[ e^{-\beta \hat{H}} \hat{c}_k^{\dagger} \hat{c}_k \right] + h.c. = \sum_{jk} f_{\beta}(\varepsilon_k) \left( \lambda_j \langle k | \hat{a}^{\dagger} | 0 \rangle \langle 0 | \hat{b}_j | k \rangle + \lambda_j^* \langle k | \hat{b}_j^{\dagger} | 0 \rangle \langle 0 | \hat{a} | k \rangle \right) . \tag{64}$$

To proceed we have to define the following cross-propagators

$$\lambda_j K_j(t) := \langle 0|\hat{a}_H(t)\hat{b}_j^{\dagger}|0\rangle = \sum_k e^{-i\varepsilon_k t} \langle k|\hat{b}_j^{\dagger}|0\rangle \langle 0|\hat{a}|k\rangle = \int_{-\infty}^{\infty} d\omega \ \psi_j(\omega)e^{-i\omega t} \ , \tag{65}$$

$$\lambda_j^* H_j(t) := \langle 0|\hat{b}_{j,H}(t)\hat{a}^{\dagger}|0\rangle = \sum_k e^{-i\varepsilon_k t} \langle k|\hat{a}^{\dagger}|0\rangle \langle 0|\hat{b}_j|k\rangle = \int_{-\infty}^{\infty} d\omega \ \psi_j^*(\omega)e^{-i\omega t} \ , \tag{66}$$

where we defined  $\psi_j(\omega) = \sum_k \langle k | \hat{b}_j^{\dagger} | 0 \rangle \langle 0 | \hat{a} | k \rangle \delta(\omega - \varepsilon_k)$ . By further defining  $\psi_0(\omega) := \sum_k \lambda_k^* \psi_k(\omega)$  and  $\psi(\omega) = \psi_0(\omega) + \psi_0^*(\omega)$  we can see that

$$K(t) := \sum_{j} |\lambda_{j}|^{2} \left( K_{j}(t) + H_{j}(t) \right) = \int_{-\infty}^{\infty} d\omega \ \psi(\omega) e^{-i\omega t} , \qquad (67)$$

$$v_{th} = \int_{-\infty}^{\infty} d\omega \ f_{\beta}(\omega)\psi(\omega) \ . \tag{68}$$

Therefore, similarly to the case of G(t,0), we have

$$\tilde{K}(-i\omega) = \pi\psi(\omega) + iP. \int_{-\infty}^{\infty} d\omega' \frac{\psi(\omega')}{\omega - \omega'}$$

and in particular  $\pi\psi(\omega) = \Re\left[\tilde{K}(-i\omega)\right]$  (since  $\psi(\omega)$  is real by definition). Hence, by eq. (56) and eq. (68), the last step to prove that v(t) thermalizes is to check that  $\Re\left[\tilde{K}(-i\omega)\right] = g\Im\left[\tilde{G}(-i\omega)\right]$ . To do so we start by computing the components of K(t): from eq. (41) we can see that

$$K_{j}(t) = -ig \int_{0}^{t} ds \ G(t,s)e^{-i\omega_{j}s} ,$$

$$= -ig \int_{0}^{t} ds \ e^{-(t-s)(\frac{1}{2}g^{2}+i\varepsilon)}e^{-i\omega_{j}s} ,$$

$$= -ige^{-t(\frac{1}{2}g^{2}+i\varepsilon)} \int_{0}^{t} ds \ e^{s(\frac{1}{2}g^{2}+i(\varepsilon-\omega_{j}))} ,$$

$$= -ig \frac{e^{-i\omega_{j}t} - e^{-(\frac{1}{2}g^{2}+i\varepsilon)t}}{\frac{1}{2}g^{2} + i(\varepsilon-\omega_{j})} = -ig \frac{e^{-i\omega_{j}t} - G(t,0)}{\frac{1}{2}g^{2} + i(\varepsilon-\omega_{j})} ;$$
(69)

and from eq. (42)

$$H_{j}(t) = -ig \int_{0}^{t} ds \, G(s,0) e^{i\omega_{j}(s-t)} = -ig e^{-i\omega_{j}t} \int_{0}^{t} ds \, e^{-(\frac{1}{2}g^{2} + i(\varepsilon - \omega_{j}))s} = -ig \frac{e^{-i\omega_{j}t} - e^{-(\frac{1}{2}g^{2} + i\varepsilon)t}}{\frac{1}{2}g^{2} + i(\varepsilon - \omega_{j})} = K_{j}(t) .$$

$$(70)$$

Since the time dependence is contained in the exponentials, it is straightforward to compute the Laplace transform

$$\tilde{K}_{j}(z) = \tilde{H}_{j}(z) = \frac{-ig}{\frac{1}{2}g^{2} + i(\varepsilon - \omega_{j})} \int_{0}^{\infty} dt \left[ e^{-i\omega_{j}t} - G(t, 0) \right] e^{-zt}$$

$$= \frac{-ig}{\frac{1}{2}g^{2} + i(\varepsilon - \omega_{j})} \left[ \frac{1}{z + i\omega_{j}} - \frac{1}{z + i\varepsilon + g^{2}/2} \right] = \frac{-ig}{z + i\omega_{j}} \tilde{G}(z) . \quad (71)$$

Therefore we find

$$\tilde{K}(-i\omega) = \frac{g}{\pi}\tilde{G}(-i\omega)P.\int_{-\infty}^{\infty} d\omega' \frac{1}{\omega - \omega'} = -ig\tilde{G}(-i\omega) , \qquad (72)$$

which allows us to conclude  $\psi(\omega) = g\Im[\tilde{G}(-i\omega)]$ . This concludes the proof of the thermalization of v(t).

# B Slow driving expansion

### B.1 Deriving the thermodynamic metric

We are interested in performing an erasure protocol and minimizing the work cost of performing it. The erasure protocol is one where  $\varepsilon(0) = 0$ ,  $\varepsilon(\tau) \gg \beta^{-1}$  and  $g(0) = g(\tau) = 0$ , for  $\tau$  the total time of the protocol. The work cost of a protocol where we control  $\varepsilon$  and g is

$$W = \int_0^\tau dt \operatorname{Tr} \left[ \hat{\rho}(t) \frac{d}{dt} \hat{H}(t) \right] = \int_0^\tau dt \, \dot{\varepsilon}(t) p(t) + \dot{g}(t) v(t) . \tag{73}$$

To get a correction to Landauer's bound for finite time protocols, and to work with more tractable expressions, we expand eq. (73) in the long times limit up to first order. To do that we first need to make some notation changes. First we make the time parameter in  $\varepsilon$  and g dimensionless, so that the protocol starts at "time" input parameter 0 and ends at "time" input parameter 1. So we have the following mappings:  $t \to \tau t$ ,  $\int dt \to \tau \int dt$  and  $\frac{d}{dt} \to \tau^{-1} \frac{d}{dt}$ . Second we need to "extract" the evolution timescale of the system in order to make the slow driving expansion. From eq. (46), eq. (47) and the definition of the propagator (or more clearly form eq. (49) and eq. (50)) it is quite clear that the relaxation timescale of the system, at any point of the evolution, is of the order  $(g(t)^2)^{-1}$ . Hence we are going take the average of the square of the coupling as normalizing factor, we therefore define (in normalized time)  $\Gamma := \int_0^1 dt \ g(t)^2$ . We now define a normalized version of our control parameters:

$$\epsilon(t) := \frac{1}{\Gamma} \varepsilon(t) , \qquad \gamma(t) := \frac{1}{2\Gamma} g(t)^2 .$$
(74)

We can therefore write the expression for work cost in this new convention

$$W = \int_0^1 dt \ \dot{\epsilon}(t) \Gamma p(t) + \dot{\gamma}(t) \sqrt{\frac{\Gamma}{2\gamma(t)}} v(t) \ . \tag{75}$$

We can also rewrite the propagator

$$G(t,s) = \exp\left[-\tau\Gamma \int_{s}^{t} dr \, \gamma(r) + i\epsilon(r)\right] , \qquad (76)$$

and the expectation values of the observables

$$p(t) = |G(t,0)|^2 p_0 + \frac{1}{\pi} \int_{-\infty}^{\infty} d\omega \ f_{\beta}(\omega \Gamma) \left| \tau \Gamma \int_0^t ds \ \gamma(s)^{\frac{1}{2}} G(t,s) e^{i\tau \omega \Gamma(t-s)} \right|^2 , \tag{77}$$

$$v(t) = \frac{\tau \Gamma \sqrt{2\Gamma}}{\pi} \Im \int_{-\infty}^{\infty} d\omega \ f_{\beta}(\omega \Gamma) \int_{0}^{t} ds \ \gamma(s)^{\frac{1}{2}} G(t, s) e^{i\tau \Gamma \omega(t-s)} \ , \tag{78}$$

where we were able to insert a phase in the time integral of eq. (77) because of the absolute value and rescaled  $\omega$  by  $\Gamma$ . We can see that we have to expand in  $1/\tau\Gamma$  the same integral for both eq. (77) and eq. (78). To do that we do partial integration. First, we can notice that

$$G_{\omega}(t,s) := G(t,s)e^{i\tau\Gamma\omega(t-s)} = \exp\left[-\tau\Gamma\int_{s}^{t}dr\ \gamma(r) + i(\epsilon(r) - \omega)\right].$$

Furthermore we have

$$\frac{d}{ds}G_{\omega}(t,s) = \tau\Gamma\left[\gamma(s) + i(\epsilon(s) - \omega)\right]G_{\omega}(t,s) .$$

Therefore we can write

$$\tau\Gamma \int_0^t ds \ \gamma(s)^{\frac{1}{2}} G_{\omega}(t,s) = \int_0^t ds \ \frac{\gamma(s)^{\frac{1}{2}}}{\gamma(s) + i(\epsilon(s) - \omega)} \frac{d}{ds} G_{\omega}(t,s) \ ,$$

$$= \frac{\gamma(s)^{\frac{1}{2}}}{\gamma(s) + i(\epsilon(s) - \omega)} G_{\omega}(t,s) \bigg|_{s=0}^t - \int_0^t ds \ G_{\omega}(t,s) \frac{d}{ds} \frac{\gamma(s)^{\frac{1}{2}}}{\gamma(s) + i(\epsilon(s) - \omega)} \ , \quad (79)$$

where we can evaluate the first part as  $\frac{\gamma(s)^{\frac{1}{2}}}{\gamma(s)+i(\epsilon(s)-\omega)}G_{\omega}(t,s)\Big|_{s=0}^{t}=\frac{\gamma(t)^{\frac{1}{2}}}{\gamma(t)+i(\epsilon(t)-\omega)}+\mathcal{O}(e^{-\tau\Gamma})$ . We absorbed the  $G_{\omega}(t,0)$  term in  $\mathcal{O}(e^{-\tau\Gamma})$ . For the second term we evaluate the derivative and continue integrating by parts

$$\int_{0}^{t} ds \, \frac{\frac{\dot{\gamma}(s)}{2} (\gamma(s) + i(\epsilon(s) - \omega)) - \gamma(s)(\dot{\gamma}(s) + i\dot{\epsilon}(s))}{\gamma(s)^{\frac{1}{2}} (\gamma(s) + i(\epsilon(s) - \omega))^{2}} G_{\omega}(t, s) 
= \frac{1}{\tau \Gamma} \frac{\frac{\dot{\gamma}(s)}{2} (\gamma(s) + i(\epsilon(s) - \omega)) - \gamma(s)(\dot{\gamma}(s) + i\dot{\epsilon}(s))}{\gamma(s)^{\frac{1}{2}} (\gamma(s) + i(\epsilon(s) - \omega))^{3}} G_{\omega}(t, s) \Big|_{s=0}^{t} 
- \frac{1}{\tau \Gamma} \int_{0}^{t} ds \, G_{\omega}(t, s) \frac{d}{ds} \frac{\dot{\gamma}(s)}{2} (\gamma(s) + i(\epsilon(s) - \omega)) - \gamma(s)(\dot{\gamma}(s) + i\dot{\epsilon}(s))}{\gamma(s)^{\frac{1}{2}} (\gamma(s) + i(\epsilon(s) - \omega))^{3}} . \quad (80)$$

Similarly as in eq. (79), we keep only the evaluation at s=t for the first term because the evaluation at s=0 is of order  $\mathcal{O}(e^{-\tau\Gamma})$ . Whereas the remaining integral will also have to be evaluated by parts, and in doing so we will obtain another power of  $1/\tau\Gamma$ . But since we are only interested in the first order correction and the integral will only yield terms of order  $\mathcal{O}(1/\tau^2\Gamma^2)$  we don't need to compute it. By combining eq. (79) and eq. (80) we finally find

$$\tau \Gamma \int_0^t ds \ \gamma(s)^{\frac{1}{2}} G_{\omega}(t,s) = \frac{\gamma(t)^{\frac{1}{2}}}{\gamma(t) + i(\epsilon(t) - \omega)} - \frac{1}{\tau \Gamma} \frac{\frac{\dot{\gamma}(t)}{2} (-\gamma(t) + i(\epsilon(t) - \omega)) - i\gamma(t)\dot{\epsilon}(t)}{\gamma(t)^{\frac{1}{2}} (\gamma(t) + i(\epsilon(t) - \omega))^3} + \mathcal{O}(\frac{1}{\tau^2 \Gamma^2}) \ . \tag{81}$$

The absolute value squared of eq. (81) is

$$\left| \tau \Gamma \int_{0}^{t} ds \, \gamma(s)^{\frac{1}{2}} G_{\omega}(t,s) \right|^{2} = \frac{\gamma(t)}{\gamma(t)^{2} + (\epsilon(t) - \omega)^{2}} + \frac{1}{\tau \Gamma} \frac{4\dot{\epsilon}(t)\gamma(t)^{2}(\epsilon(t) - \omega) + \dot{\gamma}(t)\gamma(t) \left(\gamma(t)^{2} - 3(\epsilon(t) - \omega)^{2}\right)}{(\gamma(t)^{2} + (\epsilon(t) - \omega)^{2})^{3}} + \mathcal{O}(\frac{1}{\tau^{2}\Gamma^{2}}) . \quad (82)$$

Combining this with eq. (77) we find the expansion of p(t) in the slow driving regime

$$p(t) = \frac{1}{\pi} \int_{-\infty}^{\infty} d\omega \ f_{\beta}(\omega \Gamma) \frac{\gamma(t)}{\gamma(t)^{2} + (\epsilon(t) - \omega)^{2}} + \frac{1}{\tau \Gamma} \frac{1}{\pi} \int_{-\infty}^{\infty} d\omega \ f_{\beta}(\omega \Gamma) \frac{4\dot{\epsilon}(t)\gamma(t)^{2}(\epsilon(t) - \omega) + \dot{\gamma}(t)\gamma(t) \left(\gamma(t)^{2} - 3(\epsilon(t) - \omega)^{2}\right)}{(\gamma(t)^{2} + (\epsilon(t) - \omega)^{2})^{3}} + \mathcal{O}(\frac{1}{\tau^{2}\Gamma^{2}}) \ . \tag{83}$$

Whereas the imaginary part of eq. (81) is

$$\frac{\tau\Gamma}{\gamma(t)^{\frac{1}{2}}}\Im\int_{0}^{t}ds \ \gamma(s)^{\frac{1}{2}}G_{\omega}(t,s) = -\frac{\epsilon(t)-\omega}{\gamma(t)^{2}+(\epsilon(t)-\omega)^{2}} \\
-\frac{1}{\tau\Gamma}\frac{2\dot{\gamma}(t)(\epsilon(t)-\omega)\left(\gamma(t)^{2}-(\epsilon(t)-\omega)^{2}\right)-\dot{\epsilon}(t)\gamma(t)\left(\gamma(t)^{2}-3(\epsilon(t)-\omega)^{2}\right)}{(\gamma(t)^{2}+(\epsilon(t)-\omega)^{2})^{3}} + \mathcal{O}(\frac{1}{\tau^{2}\Gamma^{2}}) \ . \tag{84}$$

Therefore the slow driving expansion of v(t) is

$$\frac{1}{\sqrt{2\Gamma\gamma(t)}}v(t) = -\frac{1}{\pi} \int_{-\infty}^{\infty} d\omega \ f_{\beta}(\omega\Gamma) \frac{\epsilon(t) - \omega}{\gamma(t)^{2} + (\epsilon(t) - \omega)^{2}} 
- \frac{1}{\tau\Gamma} \frac{1}{\pi} \int_{-\infty}^{\infty} d\omega \ f_{\beta}(\omega\Gamma) \frac{2\dot{\gamma}(t)(\epsilon(t) - \omega) \left(\gamma(t)^{2} - (\epsilon(t) - \omega)^{2}\right) - \dot{\epsilon}(t)\gamma(t) \left(\gamma(t)^{2} - 3(\epsilon(t) - \omega)^{2}\right)}{(\gamma(t)^{2} + (\epsilon(t) - \omega)^{2})^{3}} 
+ \mathcal{O}(\frac{1}{\tau^{2}\Gamma^{2}}) \ . \tag{85}$$

Therefore we can see that we can rewrite the work cost of the protocol as

$$W = W^{(0)} + \frac{1}{\tau \Gamma} W^{(1)} + \mathcal{O}(\frac{1}{\tau^2 \Gamma^2}) . \tag{86}$$

The leading order term is

$$W^{(0)} = \frac{1}{\pi} \int_{-\infty}^{\infty} d\omega \ f_{\beta}(\omega) \int_{0}^{1} dt \ \frac{\dot{\epsilon}(t)\gamma(t) - \dot{\gamma}(t)(\epsilon(t) - \omega/\Gamma)}{\gamma(t)^{2} + (\epsilon(t) - \omega/\Gamma)^{2}}$$
$$= \frac{1}{\pi} \int_{-\infty}^{\infty} d\omega \ f_{\beta}(\omega) \left( \arctan \frac{\gamma(0)}{\epsilon(0) - \omega/\Gamma} - \arctan \frac{\gamma(1)}{\epsilon(1) - \omega/\Gamma} \right) , \quad (87)$$

where we re-scaled  $\omega$  by  $\Gamma$ . Here we were able to perform the integral independently of the function describing the control parameters. Therefore  $W^{(0)}$  only depends on their initial and final value. More importantly, we can identify the instantaneous thermal expectation values of p(t) and v(t) (from eq. (52) and eq. (53)) in the time integral of  $W^{(0)}$ . This implies very directly that  $W^{(0)} = \Delta F$ . We can notice that we can write  $W^{(1)}$  as

$$W^{(1)} = \int_0^1 dt \ \dot{\vec{\lambda}}_t^T m(\vec{\lambda}_t) \dot{\vec{\lambda}}_t \ , \tag{88}$$

with  $\vec{\lambda}_t = (\epsilon(t), \gamma(t))^T$  and the metric

$$m(\vec{\lambda}) = \frac{1}{\pi} \int_{-\infty}^{\infty} d\omega \ f_{\beta}(\omega) m_{\omega}(\epsilon - \omega/\Gamma, \gamma) \ , \tag{89}$$

for

$$m_{\omega}(\epsilon, \gamma) = \frac{1}{(\gamma^2 + \epsilon^2)^3} \begin{pmatrix} 4\epsilon\gamma^2 & \gamma(\gamma^2 - 3\epsilon^2) \\ \gamma(\gamma^2 - 3\epsilon^2) & 2\epsilon(\epsilon^2 - \gamma^2) \end{pmatrix} . \tag{90}$$

Since the leading order is independent of the path taken in parameter space, minimizing the work cost of erasure only implies minimizing  $W^{(1)}$ , i.e., the entropy production  $k_BT\Sigma$ . As we see from eq. (88) it is equivalent to finding the shortest path in a metric space described by the metric  $m(\vec{\lambda})$ . The length of this shortest path is known as thermodynamic length. In the main text eq. (18) and eq. (19) represent the metric when the problem is rewritten in terms of the unit-full parameters.

### B.2 Weak coupling limit

Previous works on optimization of finite-time Landauer erasure have focused on the Markovian regime [44–54], corresponding to the weak coupling limit. We analyze this regime in this section. First we assume that the coupling remains unchanged during the protocol, which means  $\Gamma = g^2$  and  $\gamma = 1$ . We start by rewriting p(t) from eq. (83) in a more convenient manner under this first assumption:

$$p(t) = \frac{1}{2\pi} \int_{-\infty}^{\infty} d\omega \ f_{\beta}(\omega) \frac{\Gamma}{\Gamma^2/4 + (\varepsilon(t) - \omega)^2} + \frac{1}{\tau \Gamma} \frac{1}{2\pi} \int_{-\infty}^{\infty} d\omega \ f_{\beta}(\omega) \frac{\dot{\varepsilon}(t)(\varepsilon(t) - \omega)\Gamma^3}{(\Gamma^2/4 + (\varepsilon(t) - \omega)^2)^3} + \mathcal{O}(\frac{1}{\tau^2 \Gamma^2}) \ , \tag{91}$$

where we used eq. (74) to go back to unit-full parameters and re-scaled  $\omega$  by  $\Gamma$ . Integrating by parts the second integral we get

$$p(t) = \frac{1}{2\pi} \int_{-\infty}^{\infty} d\omega \ f_{\beta}(\omega) \frac{\Gamma}{\Gamma^{2}/4 + (\varepsilon(t) - \omega)^{2}} + \frac{1}{\tau \Gamma} \frac{\beta \dot{\varepsilon}(t)}{8\pi} \int_{-\infty}^{\infty} d\omega \ f_{\beta}(\omega) (1 - f_{\beta}(\omega)) \frac{\Gamma^{3}}{(\Gamma^{2}/4 + (\varepsilon(t) - \omega)^{2})^{2}},$$
(92)

where we used that  $\frac{d}{d\omega}f_{\beta}(\omega) = -\beta f_{\beta}(\omega)(1-f_{\beta}(\omega))$ ,  $\frac{d}{d\omega}\frac{1}{(\Gamma^2/4+(\varepsilon(t)-\omega)^2)^2} = \frac{4(\varepsilon(t)-\omega)}{(\Gamma^2/4+(\varepsilon(t)-\omega)^2)^3}$  and dropped the  $\mathcal{O}(1/\tau^2\Gamma^2)$  to make the notation lighter. We now take the weak coupling limit, but we do so while

keeping the slow driving assumption:  $\tau\Gamma\gg 1$ . Using the results of [120] we get the following

$$\begin{split} &\lim_{\Gamma \to 0} \frac{1}{\pi} \frac{\Gamma/2}{\Gamma^2/4 + (\varepsilon(t) - \omega)^2} = \delta(\varepsilon(t) - \omega) \ , \\ &\lim_{\Gamma \to 0} \frac{1}{\pi} \frac{\Gamma^3/8}{(\Gamma^2/4 + (\varepsilon(t) - \omega)^2)^2} = \frac{1}{2} \delta(\varepsilon(t) - \omega) \ , \end{split}$$

where the equalities are meant in a distributional sense. Therefore we find that the occupation probability in the weak coupling limit is

$$p(t) = f_{\beta}(\varepsilon(t)) + \frac{1}{\tau \Gamma} \beta \dot{\varepsilon}(t) f_{\beta}(\varepsilon(t)) [1 - f_{\beta}(\varepsilon(t))] . \tag{93}$$

This result coincides with applying a slow driving expansion to a simple exponential relaxation model with characteristic time  $\Gamma$  ( $\dot{p} = -\tau \Gamma[p - f_{\beta}(\epsilon(t))]$ ). Computing the work cost yields

$$W = \Delta F + \frac{1}{\tau \Gamma} \beta \int_0^1 dt \ \dot{\varepsilon}(t)^2 f_{\beta}(\varepsilon(t)) [1 - f_{\beta}(\varepsilon(t))] \ , \tag{94}$$

with  $\Delta F = \beta^{-1} \ln \frac{1+e^{-\beta\varepsilon(0)}}{1+e^{-\beta\varepsilon(1)}}$ . We will now minimize the work cost of the erasure protocol, similar optimizations have been done before in [50, 109, 121]. From variational calculus we know that the extremal function of the integral in eq. (94) will keep the integrand constant. So we can solve the variational problem as follows:

$$\dot{\varepsilon}(t)\sqrt{f_{\beta}(\varepsilon(t))[1-f_{\beta}(\varepsilon(t))]} = K_{w} ,$$

$$\int_{\varepsilon(0)}^{\varepsilon(t)} \frac{e^{-\beta\varepsilon/2}}{1+e^{-\beta\varepsilon}} d\varepsilon = K_{w} \int_{0}^{t} dt' ,$$

$$2\arctan(e^{\beta\varepsilon(t)/2}) - \frac{\pi}{2} = \beta K_{w}t ,$$

$$\varepsilon(t) = 2\beta^{-1} \ln \tan \left(\beta K_{w}t/2 + \frac{\pi}{4}\right) ,$$
(95)

with  $K_w = 2\beta^{-1}(\arctan(e^{\beta\varepsilon(1)/2}) - \frac{\pi}{4}) \xrightarrow{\beta\epsilon(1)\to\infty} \frac{\pi}{2}\beta^{-1}$ . We therefore find

$$\varepsilon_{weak}(t) = 2\beta^{-1} \ln \tan \left(\frac{\pi}{4}(t+1)\right) ,$$
 (96)

and recover the result of eq. (1) from the main text:

$$W = k_B T \left( \ln 2 + \frac{\pi^2}{4\tau\Gamma} \right) . \tag{97}$$

### B.3 Solving the integral of the thermodynamic metric and finding the symmetry

We will now try to find a more tractable version of the metric in eq. (89). First we notice that

$$m_{\omega}(\epsilon, \gamma) = -\frac{d}{d\epsilon} \frac{1}{(\gamma^2 + \epsilon^2)^2} \begin{pmatrix} \gamma^2 & -\epsilon \gamma \\ -\epsilon \gamma & \epsilon^2 \end{pmatrix} =: -\frac{d}{d\epsilon} m_0(\epsilon, \gamma) . \tag{98}$$

We can remark that  $m_0$  coincides with a metric of an angle distance in the  $(\epsilon, \gamma)$  space. To solve the integral of eq. (89) we will go in Fourier space. For a function  $h(\epsilon)$  its Fourier transform  $\tilde{h}(\xi)$  has the defining property

$$h(\epsilon) = \frac{1}{2\pi} \int_{-\infty}^{\infty} d\xi \ \tilde{h}(\xi) e^{i\xi\epsilon} \ . \tag{99}$$

Even though  $f_{\beta}(\omega)$  is not an integrable function we can find its Fourier transform in a distributional sense

$$\tilde{f}_{\beta}(\xi) = \pi \delta(\xi) + \frac{\pi i}{\beta \sinh(\pi \xi/\beta)} . \tag{100}$$

For  $m_0$  we find

$$\tilde{m}_0(\xi,\gamma) = \frac{\pi}{2}\Theta(\xi)e^{-\xi\gamma} \begin{pmatrix} \gamma^{-1} + \xi & i\xi \\ i\xi & \gamma^{-1} - \xi \end{pmatrix} + \frac{\pi}{2}\Theta(-\xi)e^{\xi\gamma} \begin{pmatrix} \gamma^{-1} - \xi & i\xi \\ i\xi & \gamma^{-1} + \xi \end{pmatrix} , \qquad (101)$$

with  $\tilde{m}_0(0,\gamma) = \frac{\pi}{2\gamma}\mathbb{1}$ . Therefore we can rewrite eq. (89) as

$$m(\vec{\lambda}) = -\frac{1}{4\pi^3} \frac{d}{d\epsilon} \int_{-\infty}^{\infty} d\omega d\xi d\xi' \ \tilde{f}_{\beta}(\xi') \tilde{m}_0(\xi, \gamma) e^{i\omega\xi'} e^{i(\epsilon - \omega/\Gamma)\xi} \ ,$$

$$= -\frac{i}{4\pi^3} \int_{-\infty}^{\infty} d\omega d\xi d\xi' \ \xi \tilde{f}_{\beta}(\xi') \tilde{m}_0(\xi, \gamma) e^{i\epsilon\xi} e^{i\omega(\xi' - \xi/\Gamma)} \ ,$$

$$= -\frac{i}{2\pi^2} \int_{-\infty}^{\infty} d\xi d\xi' \ \xi \tilde{f}_{\beta}(\xi') \tilde{m}_0(\xi, \gamma) \delta(\xi' - \xi/\Gamma) e^{i\epsilon\xi} \ ,$$

$$= -\frac{i}{2\pi^2} \int_{-\infty}^{\infty} d\xi \ \xi \tilde{f}_{\beta}(\xi/\Gamma) \tilde{m}_0(\xi, \gamma) e^{i\epsilon\xi} \ ,$$

$$= \frac{1}{2\beta\pi} \int_{-\infty}^{\infty} d\xi \ \xi \frac{\tilde{m}_0(\xi, \gamma)}{\sinh(\frac{\pi\xi}{\beta\Gamma})} e^{i\epsilon\xi} \ ,$$

$$(102)$$

where we used eq. (99), eq. (100) and the fact that  $\int_{-\infty}^{\infty} d\omega \ e^{i\omega x} = 2\pi\delta(x)$ . If we now insert eq. (101) and flip the sign in the second integral we find

$$\begin{split} m(\vec{\lambda}) &= \frac{1}{4\beta} \int_{0}^{\infty} d\xi \, \frac{\xi e^{-\xi(\gamma-i\epsilon)}}{\sinh(\frac{\pi\xi}{\beta\Gamma})} \begin{pmatrix} \gamma^{-1} + \xi & i\xi \\ i\xi & \gamma^{-1} - \xi \end{pmatrix} + \frac{1}{4\beta} \int_{-\infty}^{0} d\xi \, \frac{\xi e^{\xi(\gamma+i\epsilon)}}{\sinh(\frac{\pi\xi}{\beta\Gamma})} \begin{pmatrix} \gamma^{-1} - \xi & i\xi \\ i\xi & \gamma^{-1} + \xi \end{pmatrix} \,, \\ &= \frac{1}{4\beta} \int_{0}^{\infty} d\xi \, \frac{\xi e^{-\xi(\gamma-i\epsilon)}}{\sinh(\frac{\pi\xi}{\beta\Gamma})} \begin{pmatrix} \gamma^{-1} + \xi & i\xi \\ i\xi & \gamma^{-1} - \xi \end{pmatrix} + \frac{1}{4\beta} \int_{0}^{\infty} d\xi \, \frac{\xi e^{-\xi(\gamma+i\epsilon)}}{\sinh(\frac{\pi\xi}{\beta\Gamma})} \begin{pmatrix} \gamma^{-1} + \xi & -i\xi \\ -i\xi & \gamma^{-1} - \xi \end{pmatrix} \,, \\ &= \frac{1}{4\beta} \int_{0}^{\infty} d\xi \, \frac{\xi e^{-\xi\gamma}}{\sinh(\frac{\pi\xi}{\beta\Gamma})} \left[ e^{i\xi\epsilon} \begin{pmatrix} \gamma^{-1} + \xi & i\xi \\ i\xi & \gamma^{-1} - \xi \end{pmatrix} + e^{-i\xi\epsilon} \begin{pmatrix} \gamma^{-1} + \xi & -i\xi \\ -i\xi & \gamma^{-1} - \xi \end{pmatrix} \right] \,, \\ &= \frac{1}{4\beta} \int_{0}^{\infty} d\xi \, \frac{\xi e^{-\xi\gamma}}{\sinh(\frac{\pi\xi}{\beta\Gamma})} \begin{pmatrix} (\gamma^{-1} + \xi)(e^{i\xi\epsilon} + e^{-i\xi\epsilon}) & -i\xi(e^{-i\xi\epsilon} - e^{i\xi\epsilon}) \\ -i\xi(e^{-i\xi\epsilon} - e^{i\xi\epsilon}) \end{pmatrix} \begin{pmatrix} \gamma^{-1} - \xi (e^{-i\xi\epsilon} - e^{i\xi\epsilon}) \end{pmatrix} \,, \\ &= \frac{1}{4\beta\gamma} \int_{0}^{\infty} d\xi \, \frac{\xi e^{-\xi\gamma}(e^{i\xi\epsilon} + e^{-i\xi\epsilon})}{\sinh(\frac{\pi\xi}{\beta\Gamma})} \mathbb{1} + \frac{1}{4\beta} \int_{0}^{\infty} d\xi \, \frac{\xi^{2}e^{-\xi\gamma}}{\sinh(\frac{\pi\xi}{\beta\Gamma})} \begin{pmatrix} e^{i\xi\epsilon} + e^{-i\xi\epsilon} & \frac{e^{-i\xi\epsilon} - e^{i\xi\epsilon}}{i} \\ -e^{i\xi\epsilon} - e^{-i\xi\epsilon} & -e^{i\xi\epsilon} \end{pmatrix} \,, \\ &= \frac{1}{2\beta\gamma} \mathbb{1} \Re \int_{0}^{\infty} d\xi \, \frac{\xi e^{-\xi(\gamma+i\epsilon)}}{\sinh(\frac{\pi\xi}{\beta\Gamma})} + \frac{1}{2\beta} \begin{pmatrix} \Re & \Im \\ \Im & -\Re \end{pmatrix} \int_{0}^{\infty} d\xi \, \frac{\xi^{2}e^{-\xi(\gamma+i\epsilon)}}{\sinh(\frac{\pi\xi}{\beta\Gamma})} \,. \end{split}$$

We will now be able to compute these integrals in terms of poly-gamma functions. The poly-gamma function of order  $m \geq 0$  is defined as  $\psi^{(m)}(z) := \frac{d^{m+1}}{dz^{m+1}} \ln \Gamma(z)$ . For m > 0 and  $\Re[z] > 0$  they have an integral representation:

$$\psi^{(m)}(z) = (-1)^{m+1} \int_0^\infty d\xi \, \frac{\xi^m e^{-\xi z}}{1 - e^{-\xi}} \,. \tag{104}$$

Using the fact that  $\frac{1}{\sinh(x)} = \frac{2e^{-x}}{1-e^{-2x}}$ , a change of variable and eq. (104) we find

$$m(\vec{\lambda}) = \frac{1}{\beta\gamma} \mathbb{1}\Re \int_0^\infty d\xi \, \frac{\xi e^{-\xi(\frac{\pi}{\beta\Gamma} + \gamma + i\epsilon)}}{1 - e^{-2\frac{\pi\xi}{\beta\Gamma}}} + \frac{1}{\beta} \begin{pmatrix} \Re & \Im \\ \Im & -\Re \end{pmatrix} \int_0^\infty d\xi \, \frac{\xi^2 e^{-\xi(\frac{\pi}{\beta\Gamma} + \gamma + i\epsilon)}}{1 - e^{-2\frac{\pi\xi}{\beta\Gamma}}} \,,$$

$$= \frac{\beta\Gamma^2}{4\pi^2\gamma} \mathbb{1}\Re \int_0^\infty d\xi \, \frac{\xi e^{-\xi[\frac{1}{2} + \frac{\beta\Gamma}{2\pi}(\gamma + i\epsilon)]}}{1 - e^{-\xi}} + \frac{\beta^2\Gamma^3}{8\pi^3} \begin{pmatrix} \Re & \Im \\ \Im & -\Re \end{pmatrix} \int_0^\infty d\xi \, \frac{\xi^2 e^{-\xi[\frac{1}{2} + \frac{\beta\Gamma}{2\pi}(\gamma + i\epsilon)]}}{1 - e^{-\xi}} \,, \qquad (105)$$

$$= \frac{\beta\Gamma^2}{4\pi^2\gamma} \mathbb{1}\Re \psi^{(1)} \left(\frac{1}{2} + \frac{\beta\Gamma}{2\pi}(\gamma + i\epsilon)\right) - \frac{\beta^2\Gamma^3}{8\pi^3} \begin{pmatrix} \Re & \Im \\ \Im & -\Re \end{pmatrix} \psi^{(2)} \left(\frac{1}{2} + \frac{\beta\Gamma}{2\pi}(\gamma + i\epsilon)\right) \,.$$

We can notice that the metric explicitly depends on  $\Gamma$  in such a way that it seems that the solution for the geodesic should depend on this scale factor. Though this dependence disappears if we reparameterize the problem in terms of its original unit-full parameters. We start by rewriting the work as

$$W = \Delta F + W^{(1)} + \mathcal{O}(\frac{1}{\tau^2 \Gamma^2}) , \qquad (106)$$

where we redefined  $W^{(1)}$  with the unit-full parameters  $\vec{\lambda}_t = (\varepsilon(t), \mu(t))^T$  (with  $\mu(t) := \frac{1}{2}g(t)^2 = \Gamma \gamma(t)$ ):

$$W^{(1)} = \frac{1}{\tau} \int_0^1 dt \ \dot{\vec{\lambda}}_t^T m(\vec{\lambda}_t) \dot{\vec{\lambda}}_t, \tag{107}$$

$$m(\vec{\lambda}) = \frac{\beta}{4\pi^2 \mu} \mathbb{1} \Re \psi^{(1)} \left( \frac{1}{2} + \frac{\beta}{2\pi} z \right) - \frac{\beta^2}{8\pi^3} \begin{pmatrix} \Re & \Im \\ \Im & -\Re \end{pmatrix} \psi^{(2)} \left( \frac{1}{2} + \frac{\beta}{2\pi} z \right) . \tag{108}$$

We remind the reader that  $z = \mu + i\varepsilon$ . This metric is the same as the one presented in the main text. Despite not looking very approachable, eq. (108) is a much more tractable version of eq. (18) from the main text when it comes to numerical implementations (as the polygamma functions are computed much faster than integrals) and analytical studies of the geometric properties of thermodynamic protocols.

We can notice from eq. (107) and eq. (108) is that there is a symmetry in the corrective term. If we perform the following transformation:

$$\varepsilon(t) \to \lambda \varepsilon(t) ,$$

$$\mu(t) \to \lambda \mu(t) ,$$

$$\beta \to \lambda^{-1} \beta ,$$
(109)

for  $\lambda > 0$ ; then  $W^{(1)}$  remains unchanged. This symmetry allows us to conclude that the minimal value of  $W^{(1)}$  to perform Landauer erasure will be of the form  $c/\tau$  where c is a constant that does not depend on any physical quantity.

# C High temperature limit

In order to find the minimal dissipation in the multi-variable case we need to numerically solve the equations of motion given by the exact metric, which (unsurprisingly) are very untractable analytically. But instead of solving an initial value problem (which we can always solve by numerical integration, in principle) we are trying to solve a boundary value problem. Generically, to solve a BVP numerically, the solver will try many IVPs until the wanted BVP is reached. But here we can notice that we can turn the BVP into an IVP by taking an analytical approximation of the problem around the point  $(\varepsilon, \mu) = (0,0)$ .

As we have seen in eq. (109) there is an underlying symmetry in this problem, so a limit where  $\varepsilon$  and  $\mu$  are infinitesimal is the same as a limit where  $\beta$  is infinitesimal but  $\varepsilon$  and  $\mu$  finite. Formally we

are requiring  $\beta | \mu + i \varepsilon | \ll 1$ , which is a high-temperature limit. It is important to note that despite the fact that this approximation will yield some analytical results on how to optimize a protocol in the high temperature regime it will not give us a result that is relevant for Landauer erasure because to perform erasure we are assuming that we reach  $\beta \varepsilon \gg 1$ , which is a low temperature limit.

One way to obtain an analytical result in this framework is by going back to eq. (89) and apply the high-temperature expansion of the Fermi-Dirac distribution:  $f_{\beta}(\omega) = \frac{1}{2} - \frac{1}{4}\beta\omega + \mathcal{O}(\beta^3\omega^3)$ . Since  $m_0(\pm\infty,\gamma) = 0$  the first term of the metric in this expansion is 0. But from the next order we find (in unit-full parameters)

$$m_{HT}(\vec{\lambda}) = \frac{\beta}{4\pi} \int_{-\infty}^{\infty} d\omega \, \frac{\omega - \varepsilon}{(\mu^2 + \omega^2)^3} \begin{pmatrix} 4\omega\mu^2 & \mu(\mu^2 - 3\omega^2) \\ \mu(\mu^2 - 3\omega^2) & 2\omega(\omega^2 - \mu^2) \end{pmatrix} = \frac{\beta}{8\mu} \mathbb{1} . \tag{110}$$

It might not be immediate why we also require  $\beta\mu \ll 1$ , but it becomes clear that it is required when we want to obtain the same result by applying the same expansion on eq. (108) (which would also allow us to get further orders). We will now compute and solve the equations of motion:

$$\ddot{\lambda}^i + \Gamma^i_{jk}\dot{\lambda}^j\dot{\lambda}^k = 0 , \qquad (111)$$

where we assumed the Einstein tensorial notation and  $\Gamma^i_{jk}$  are the Christoffel symbols

$$\Gamma_{jk}^{i} := \frac{1}{2} m^{il} (\partial_{j} m_{kl} + \partial_{k} m_{jl} - \partial_{l} m_{jk}) . \tag{112}$$

Here we have  $m^{il} = \frac{8\mu}{\beta} \delta^{il}$  and  $\partial_a m_{bc} = -\frac{\beta}{8\mu^2} \delta_{a\mu} \delta_{bc}$ . We therefore find

$$\Gamma^{i}_{jk} = -\frac{1}{2\mu} (\delta_{j\mu} \delta^{i}_{k} + \delta_{k\mu} \delta^{i}_{j} - \delta^{i\mu} \delta_{jk}) , \qquad (113)$$

which can be rewritten as

$$\Gamma^{\varepsilon} = -\frac{1}{2\mu} \begin{pmatrix} 0 & 1 \\ 1 & 0 \end{pmatrix} \quad , \quad \Gamma^{\mu} = \frac{1}{2\mu} \begin{pmatrix} 1 & 0 \\ 0 & -1 \end{pmatrix} . \tag{114}$$

We get the following differential equations for  $\mu$  and  $\varepsilon$ :

$$\ddot{\varepsilon}\mu = \dot{\varepsilon}\dot{\mu} \quad , \quad 2\mu\ddot{\mu} = \dot{\mu}^2 - \dot{\varepsilon}^2. \tag{115}$$

From the first equation we can see that  $\int d\dot{\varepsilon}/\dot{\varepsilon} = \int d\mu/\mu$ , therefore  $\dot{\varepsilon} = C\mu$  for some constant C (we can already see as a sanity check that  $\dot{\varepsilon}$  never changes sign in an optimal protocol). The equation for  $\mu$  becomes

$$2\mu\ddot{\mu}=\dot{\mu}^2-C^2\mu^2\ ,$$

when we consider that  $\mu = g^2/2$  and  $\ddot{\mu} = \dot{g}^2 + g\ddot{g}$  we can see that

$$\ddot{g} = -C^2 g/4 \ .$$

Taking into account that the boundary conditions for g are g(0) = g(1) = 0 we find that  $g(t) = A\sin(k\pi t)$  for some constant  $A, k \in \mathbb{N}^*$  and  $C = 2k\pi$ . By choosing  $\varepsilon(0) = 0$  and  $\varepsilon(1) = \varepsilon_*$  we have  $\varepsilon(t) = k\pi A^2 \int_0^t ds \sin(k\pi s)^2$ , therefore  $A^2 = \frac{2\varepsilon_*}{k\pi}$ . Thus the optimal protocol, portrayed in Fig. 3, is

$$\varepsilon(t) = \varepsilon_* \left( t - \frac{\sin(2k\pi t)}{2k\pi} \right) \quad , \quad \mu(t) = \frac{\varepsilon_*}{k\pi} \sin(k\pi t)^2 .$$
 (116)

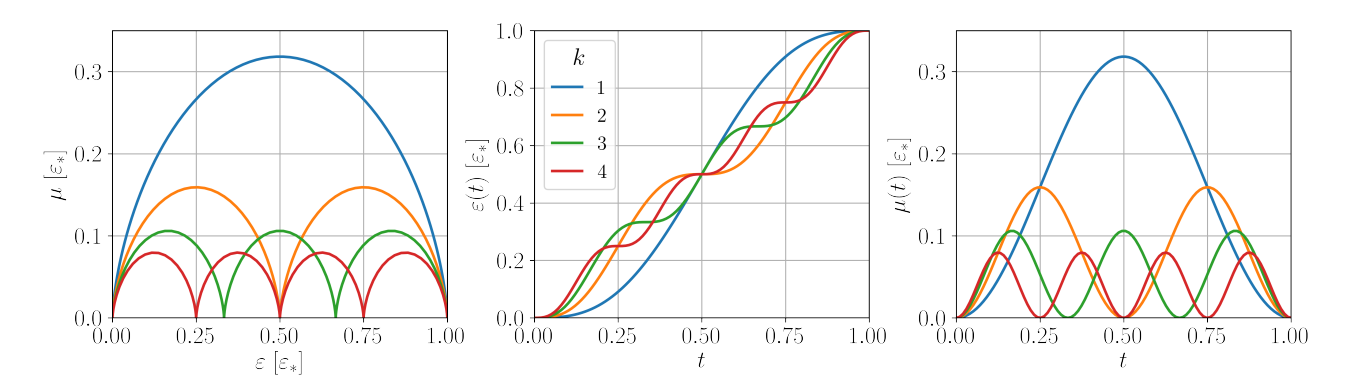


Figure 3: Parametrization of  $\mu(t)$  and  $\varepsilon(t)$  described by eq. (116) for multiple values of k. Shown in the parameter space (left) and as a function of time (centre and right).

From eq. (116) we can compute the integrand of the dissipated work:

$$\dot{\vec{\lambda}}_t^T m_{HT}(\vec{\lambda}_t) \dot{\vec{\lambda}}_t = \frac{\beta}{8\mu} (4k^2 \pi^2 \mu^2 + \dot{\mu}^2)$$

$$= \frac{\beta \varepsilon_*^2}{2\mu} \left( \sin(k\pi t)^4 + \sin(k\pi t)^2 \cos(k\pi t)^2 \right)$$

$$= \frac{k\pi \beta \varepsilon_*}{2} .$$
(117)

We therefore find the dissipated work for the high temperature limit by inserting this in eq. (107) and taking k = 1:

$$W_{HT}^{(1)} = \frac{\pi \beta \varepsilon_*}{2\tau}.\tag{118}$$

We can see that in this scenario the corrective term grows extensively with the final energy  $\varepsilon_*$ , combining this with the fact that the exact metric goes to 0 faster than  $\mathcal{O}(|z^{-1}|)$  we can presume that most of the dissipation in the exact protocol is caused by the part of the protocol that matches with the high temperature regime.

# D Low temperature limit

We will now study the limit of  $T \to 0$  we have  $f_{\beta}(\omega) \to f_{\infty}(\omega) = \Theta(-\omega)$ , where  $\Theta$  is the Heaviside step function. Therefore the integral of eq. (89) becomes (in unit-full parameters)

$$m_{T=0}(\vec{\lambda}) = \frac{1}{\pi} \int_{-\infty}^{\infty} d\omega \ \Theta(-\omega) m_{\omega}(\varepsilon - \omega, \mu) \ ,$$

$$= \frac{1}{\pi} \int_{\varepsilon}^{\infty} d\omega \ m_{\omega}(\omega, \mu) \ ,$$

$$= -\frac{1}{\pi} \int_{\varepsilon}^{\infty} d\omega \ \frac{d}{d\omega} m_{0}(\omega, \mu) \ ,$$

$$= \frac{1}{\pi} m_{0}(\varepsilon, \mu) \ .$$
(119)

where we used eq. (98) and the fact that  $m_0(+\infty, \mu) = 0$ . Thus we have

$$m_{T=0}(\vec{\lambda}) = \frac{1}{\pi} \frac{1}{(\mu^2 + \varepsilon^2)^2} \begin{pmatrix} \mu^2 & -\varepsilon\mu \\ -\varepsilon\mu & \varepsilon^2 \end{pmatrix} . \tag{120}$$

We can compute the integrand of  $W^{(1)}$  to find

$$\dot{\vec{\lambda}}^T m_{T=0}(\vec{\lambda}) \dot{\vec{\lambda}} = \frac{1}{\pi} \frac{\dot{\varepsilon}^2 \mu^2 - 2\dot{\varepsilon}\dot{\mu}\varepsilon\mu + \dot{\mu}^2 \varepsilon^2}{(\mu^2 + \varepsilon^2)^2} = \frac{1}{\pi} \left(\frac{\varepsilon\dot{\mu} - \dot{\varepsilon}\mu}{\mu^2 + \varepsilon^2}\right)^2$$
(121)

By defining the coordinates  $\vec{\lambda}_{r,\phi} = (r,\phi)^T$ , such that  $\varepsilon = r\cos\phi$  and  $\mu = r\sin\phi$ , we have  $\phi = \arctan\frac{\mu}{\varepsilon}$ . Therefore

$$\dot{\vec{\lambda}}^T m_{T=0}(\vec{\lambda})\dot{\vec{\lambda}} = \frac{\dot{\phi}^2}{\pi} , \qquad (122)$$

From which we can deduce the metric in these new coordinates

$$m_{T=0}^{(r,\phi)}(\vec{\lambda}_{r,\phi}) = \frac{1}{\pi} \begin{pmatrix} 0 & 0\\ 0 & 1 \end{pmatrix}$$
 (123)

Crucially, we can notice that this metric is singular: here changes in the coordinate r do not cause an increase in the work cost. Therefore we can parameterize geodesics at zero temperature as follows

$$\varepsilon(t) = r(t)\cos(\phi(0)(1-t) + \phi(1)t) \quad , \quad \mu(t) = r(t)\sin(\phi(0)(1-t) + \phi(1)t) \quad , \tag{124}$$

where r(t) is any function that satisfies the boundary conditions. By using eq. (107) we can find the dissipated work

$$W_{T=0}^{(1)} = \frac{(\Delta\phi)^2}{\pi\tau} , \qquad (125)$$

for  $\Delta \phi = \phi(1) - \phi(0)$ .

# E Discontinuities in the protocol

As is mentioned in the main text, it is well known [108] that, at weak coupling, discontinuities appear at the beginning and at the end in optimal finite-time protocols. In the main text we gave numerical evidence to the fact that these jumps disappear as one approaches the quasistatic limit. Here we make an a posteriori argument as to why these jumps should also disappear for the system we studied in the strong coupling regime.

We can start by immediately discarding jumps in the coupling because these lead to a diverging work cost in the wideband limit. Then, if one makes a jump in the energy at the start of the protocol from 0 to  $\varepsilon_*$  its work cost is

$$W_{jump} = p(0)\varepsilon_* = \frac{1}{2}\varepsilon_* , \qquad (126)$$

where p(0) is the probability of occupation at t = 0 and is set to be 1/2. We can compare it to the work cost given by an optimal continuous protocol with the same boundary conditions:

$$W_{cont} = \Delta F + \frac{a(\beta \varepsilon_*)\hbar}{\tau} = k_B T \ln\left(\frac{2}{1 + e^{-\beta \varepsilon_*}}\right) + \frac{a(\beta \varepsilon_*)\hbar}{\tau} , \qquad (127)$$

where  $a(\beta \varepsilon_*)$  is a bounded function of  $\beta \varepsilon_*$  (c.f. figure in the main text). We note that by expanding  $\Delta F$  around  $\beta = 0$  we find

$$\Delta F = \frac{1}{2}\varepsilon_* - \frac{1}{8}\beta\varepsilon_*^2 + \mathcal{O}(\beta^3) \ . \tag{128}$$

Therefore at  $\beta > 0$  and small enough one finds that  $\Delta F < W_{jump}$ . But one can also note that  $\lim_{\beta \to \infty} \Delta F = 0$ , and since  $\Delta F$  is a monotonous function of  $\beta$  we conclude that  $\Delta F < W_{jump}$  for any temperature and any  $\varepsilon_* > 0$ . At this point it is immediate that there exists  $\tau$  large enough such that  $W_{cont} < W_{jump}$ .

We finally consider jumps in the energy at the end of the protocol. These jumps would have to be performed once the coupling is very close to zero since it is at the end of the protocol. In this limit optimal protocols are found by [109]. These optimal protocols feature jumps whose magnitude is controlled by a constant of integration K, in particular the magnitude of these jumps is  $\mathcal{O}(\sqrt{K})$ . This constant is defined as follows (in terms of our notation with unit-less time)

$$K = \frac{1}{\tau^2 \Gamma^2} \frac{\dot{p}^2}{(p + \dot{p}/\tau \Gamma)(1 - p - \dot{p}/\tau \Gamma)} \ . \tag{129}$$

From which it is clear that K goes to 0 in the limit of  $\tau\Gamma\gg 1$  and therefore the jumps disappear. This behavior is also confirmed in Fig. 1 where these optimal protocols are shown.

### F One-parameter case

Because of the metric we obtain in eq. (108) it is quite clear that, in the two-parameter case, we will not be able to solve analytically the geodesics for the full problem. This even prevents us form finding an analytical expression for the distance between two points in the parameter space, as it is the length of the shortest path (for which we have no expression). But by fixing one parameter to an arbitrary value and solving for the other we can use the fact that geodesics always have a conserved quantity along their path (the integrand:  $\vec{\lambda}_t^T m(\vec{\lambda}_t) \dot{\vec{\lambda}}_t$ ) to avoid solving the geodesic equation and finding an explicit formula for the length and geodesic. We point out the fact that the symmetry mentioned in App. B does not lead to a conserved quantity because  $\beta$  is a constant of the system instead of a function of time for which we are solving.

Here we will take the erasure protocol to be made of three parts, which will be optimized separately: 1. we turn on the coupling to some value  $\mu_*$  while keeping the energy at zero; 2. while keeping the coupling at  $\mu_*$  we increase the energy from zero to infinity; 3. we turn the coupling off. Incidentally, this type of protocols are more realistic for an experimental realization as often setups are not able to control optimally energy an coupling at the same time. And even if the control over the coupling is only to turn it on to some value and turn it off, step 2 will remain valid. Furthermore, previous studies done at weak coupling essentially are described by this type of protocol; but they are in a regime where step 1 and 3 can be neglected. Therefore we can compare the results of this section to those of the weak coupling limit.

We start by looking at step 3, in the limit of  $\beta \varepsilon \to \infty$  we actually reach a scenario described by the T=0 limit. Therefore the length of this step is described by eq. (123), for any finite value of  $\mu_*$  the angle span of this step is trivially 0. Therefore, up to first order, this step will not cause any extra dissipation, no matter how it is realized.

We notice that we can write the length of the first step as follows

$$L_1 = \int_0^1 dt \ |\dot{\mu}(t)| m_{\mu\mu}(0,\mu(t))^{1/2} = \int_0^{\mu(1)} d\mu \ m_{\mu\mu}(0,\mu)^{1/2} \ , \tag{130}$$

where we used the fact that, since the metric is not explicitly time-dependent, the sign of  $\dot{\mu}$  has to be always positive for this step. With eq. (108) we find the following expression for the length

$$L_1 = \frac{1}{\sqrt{2\pi}} \int_0^{\beta \mu_*/2\pi} \sqrt{\Re\left[\frac{1}{x}\psi^{(1)}\left(\frac{1}{2} + x\right) + \psi^{(2)}\left(\frac{1}{2} + x\right)\right]} dx . \tag{131}$$

Now that we have an expression for  $L_1$  we can recover an equation for  $\mu(t)$ . We can use the fact that the integrand of the time integral in eq. (130) is constant to obtain

$$tL_1 = \frac{1}{\sqrt{2\pi}} \int_0^{\beta\mu(t)/2\pi} \sqrt{\Re\left[\frac{1}{x}\psi^{(1)}\left(\frac{1}{2} + x\right) + \psi^{(2)}\left(\frac{1}{2} + x\right)\right]} dx , \qquad (132)$$

which gives an implicit definition of  $\mu(t)$ , or rather an explicit definition of its inverse  $t(\mu)$ .

By following the same procedure as in step 1 we can recover the length of step 2

$$L_2 = \frac{1}{\sqrt{2\pi}} \int_0^\infty \sqrt{\Re\left[\frac{2\pi}{\beta\mu_*}\psi^{(1)}\left(\frac{1}{2} + \frac{\beta\mu_*}{2\pi} + iy\right) - \psi^{(2)}\left(\frac{1}{2} + \frac{\beta\mu_*}{2\pi} + iy\right)\right]} dy , \qquad (133)$$

and the implicit definition of  $\varepsilon(t)$ 

$$L_2 t = \frac{1}{\sqrt{2\pi}} \int_0^{\beta \varepsilon(t)/2\pi} \sqrt{\Re \left[ \frac{2\pi}{\beta \mu_*} \psi^{(1)} \left( \frac{1}{2} + \frac{\beta \mu_*}{2\pi} + iy \right) - \psi^{(2)} \left( \frac{1}{2} + \frac{\beta \mu_*}{2\pi} + iy \right) \right]} dy . \tag{134}$$

These implicit definitions of  $\varepsilon(t)$  and  $\mu(t)$  can be solved numerically, the results are shown in Fig. 4.

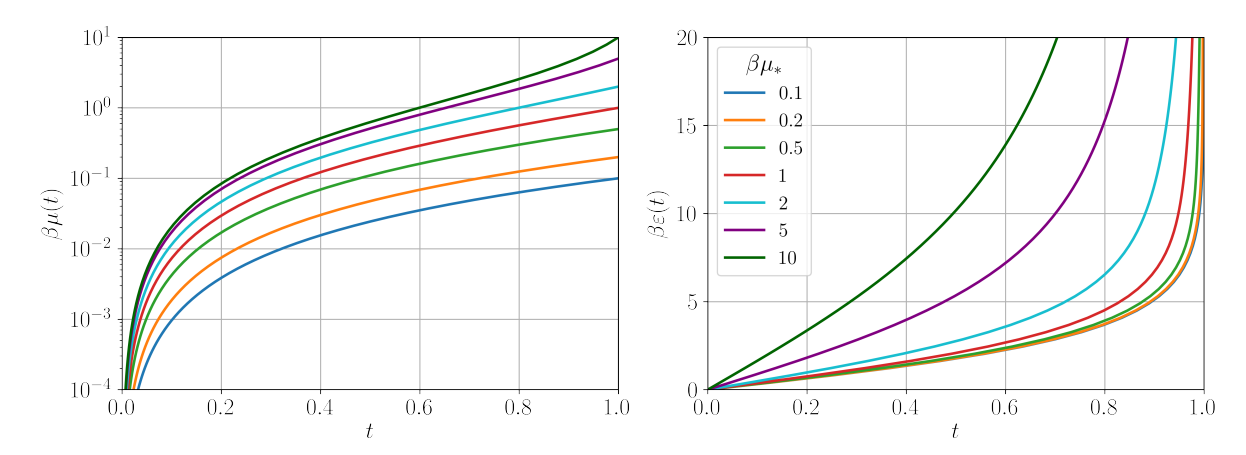


Figure 4: Parametrization of  $\mu(t)$  and  $\varepsilon(t)$  described by eq. (132) and eq. (134) for multiple values of  $\beta\mu_*$ .

The question remains about how to subdivide optimally the protocol times of step 1 ( $\tau_1$ ) and step 2 ( $\tau_2 = \tau - \tau_1$ ). The total excess work is given by  $W^{(1)} = L_1^2/\tau_1 + L_2^2/\tau_2$ , by taking the derivative and imposing it to be zero we find

$$\tau_1 = \frac{L_1}{L_2 + L_1} \tau \ . \tag{135}$$

And therefore we find

$$W^{(1)} = \frac{1}{\tau} (L_1 + L_2)^2 , \qquad (136)$$

which is indeed what was to be expected, as  $L_1 + L_2$  is the total length of the protocol.

We now discuss how we can obtain an exact version of eq. (1) of the main text, so that it applies also in the strong coupling regime. First we can notice that since  $L_1 > 0$  and  $L_2 > 0$  we have  $W^{(1)} \ge L_2^2/\tau$ . Then by considering that  $m_{\varepsilon\varepsilon}(\varepsilon, \mu_*)$  is a one-dimensional metric it has to be positive by definition. Therefore the integrand of eq. (133) is always positive. Next we can consider the fact that

$$\lim_{\mu_* \to \infty} \frac{2\pi}{\beta \mu_*} \psi^{(1)} \left( \frac{1}{2} + \frac{\beta \mu_*}{2\pi} + iy \right) - \psi^{(2)} \left( \frac{1}{2} + \frac{\beta \mu_*}{2\pi} + iy \right) = 0 . \tag{137}$$

Therefore, for all  $\mu_*$  and all  $\varepsilon$ 

$$m_{\varepsilon\varepsilon}(\varepsilon, \mu_*) \ge \lim_{n \to \infty} m_{\varepsilon\varepsilon}(\varepsilon, \mu_*) ,$$
 (138)

which allows us to conclude  $L_2 \ge \lim_{\mu_* \to \infty} L_2$ . For any finite  $\mu_*$  large enough  $m_{\varepsilon\varepsilon}(\varepsilon, \mu_*)$  can be approximated by  $[m_{T=0}]_{\varepsilon\varepsilon}(\varepsilon, \mu_*)$ . The angle spanned by the integral of  $L_2$  is  $\pi/2$ . Therefore for all  $\mu_*$ 

$$\int_0^\infty d\varepsilon \ [m_{T=0}(\varepsilon, \mu_*)]_{\varepsilon\varepsilon}^{1/2} = \frac{\sqrt{\pi}}{2} \ , \tag{139}$$

and since the approximation becomes exact in the limit  $\mu_* \to \infty$  we have  $\lim_{\mu_* \to \infty} L_2 = \sqrt{\pi}/2$ . Therefore,

$$W^{(1)} \ge \frac{\pi}{4\tau} \ .$$
 (140)

In Fig. 5 we show the minimal value of  $W^{(1)}$  for step 2 as a function of  $\beta\mu_*$ , and we compare it to eq. (1) of the main text and to eq. (140). We can see how, when the coupling becomes small, the exact curve agrees with eq. (1).

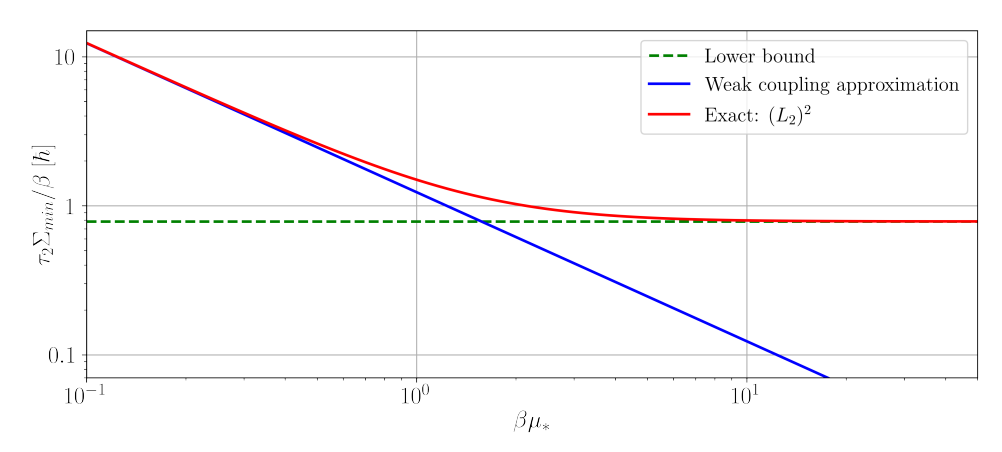


Figure 5: Comparison of the excess work  $W^{(1)} = k_B T \Sigma$  for a slow erasure protocol at constant coupling in the exact description (eq. (133)) with the weak coupling approximation (eq. (1) of the main text) and the lower bound of eq. (140).

## G Numerical solution to the general case

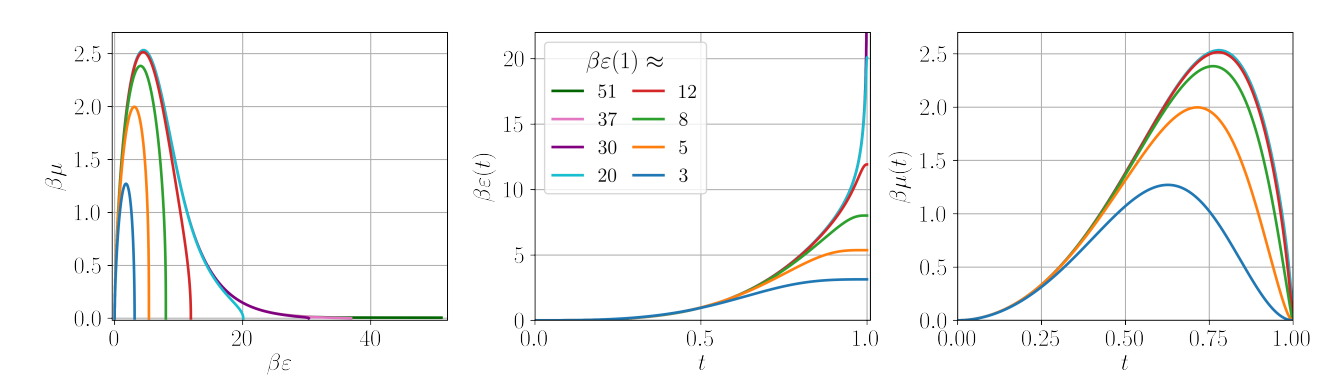


Figure 6: A series of optimal protocols depicted for multiple values of  $\beta \varepsilon(1)$ . They all start with zero energy and coupling and end with finite energy and zero coupling. In the limit of large  $\beta \varepsilon(1)$  they can be considered as erasure protocols. Shown in the parameter space (left) and as a function of time (centre and right).

We now discuss how the numerical problem of finding the optimal erasure protocol was approached. Having found the metric eq. (108), all we have to do to find the optimal erasure protocol is to solve the geodesic equations

$$0 = \ddot{\varepsilon} + \Gamma^{\varepsilon}_{\varepsilon\varepsilon}\dot{\varepsilon}^{2} + 2\Gamma^{\varepsilon}_{\varepsilon\mu}\dot{\varepsilon}\dot{\mu} + \Gamma^{\mu}_{\mu\mu}\dot{\mu}^{2} ,$$

$$0 = \ddot{\varepsilon} + \Gamma^{\mu}_{\varepsilon\varepsilon}\dot{\varepsilon}^{2} + 2\Gamma^{\mu}_{\varepsilon\mu}\dot{\varepsilon}\dot{\mu} + \Gamma^{\mu}_{\mu\mu}\dot{\mu}^{2} ;$$

$$(141)$$

with the Christoffel symbols defined as in eq. (112). Though the differential equations we get are quite untractable and cannot be solved analytically, we won't even write them here as they are very long and will not bring any insight. Therefore we will solve them numerically, and indeed eq. (141) is quite practical for numerical integration since the second derivative of the parameters can be easily isolated. The boundary conditions we impose for the erasure protocol are  $\{\varepsilon(0) = \mu(0) = \mu(1) = 0, \varepsilon(1) \gg k_B T\}$ . Indeed we cannot impose  $\beta \varepsilon(1) = \infty$  because we are performing numerics, therefore we set it to be an arbitrarily large value.

But at this point we can notice that close to t=0, by continuity, we are satisfying the conditions for the high temperature approximation. And at t=0 the approximation becomes exact. Therefore the initial conditions of an optimal erasure protocol in the general case must match with the initial conditions of the protocols that we previously studied in the high-temperature regime. From a numerical perspective it is much more preferable to solve an initial value problem instead of a boundary value problem. Therefore we used the numerical solver DOP853, implemented in the scipy library in python, to solve eq. (141) with the initial conditions given by eq. (116).

To be precise, we cannot start the integration from t=0 as the metric is formally divergent at  $(\varepsilon,\mu)=(0,0)$ , therefore we evaluate eq. (116) at an infinitesimal time and integrate from there. The specific value we choose for  $\varepsilon_*$  sets the value of  $\varepsilon(1)$  that is reached in a monotonous way. When  $\varepsilon_*$  is chosen small the protocol closes matches with those of eq. (116) (as long as  $\varepsilon(1)$  is also small). Then for larger values of  $\varepsilon_*$  we get more interesting behavior, as is shown in Fig. 6.

When one changes the value of k in eq. (116) the value of  $\varepsilon(1)$  that is reached is different. But, as is shown in Fig. 7, by numerically searching values of  $\varepsilon_*$  such that the same  $\varepsilon(1)$  is reached for different values of k we find that the protocols end up being the same.

Finally we thought it might be interesting to compare the best one-parameter protocol to the geodesic erasure protocol we find numerically. And we can see from Fig. 8 that, despite seeming very different in the path taken in the parameter space, when we look at the functions of time they are actually quite similar. The apparent difference happens because the part of the protocol for  $\beta \varepsilon \gg 1$  is done very quickly since the metric is vanishing in that region.

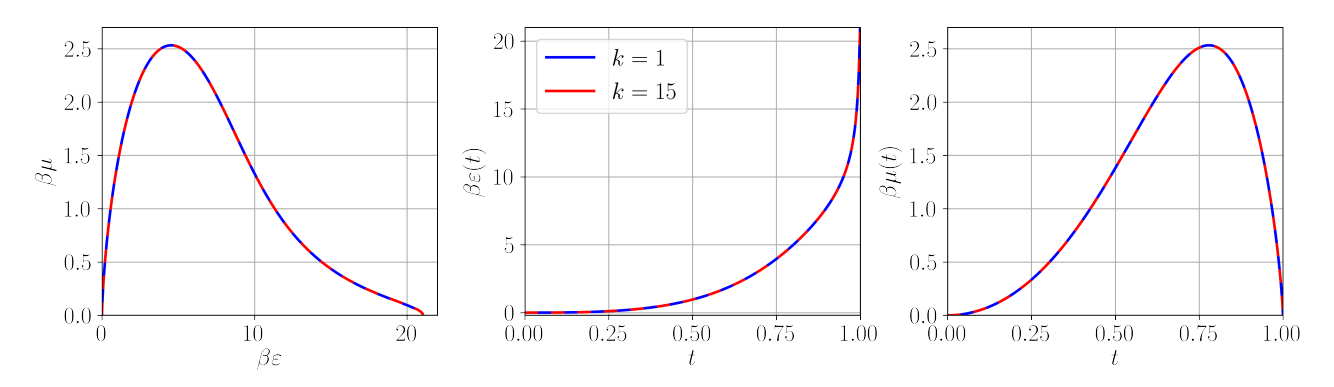


Figure 7: Comparing two optimal erasure protocol with  $\beta \varepsilon(1) \approx 21$  for two different values of k. The same is found for other values of k.

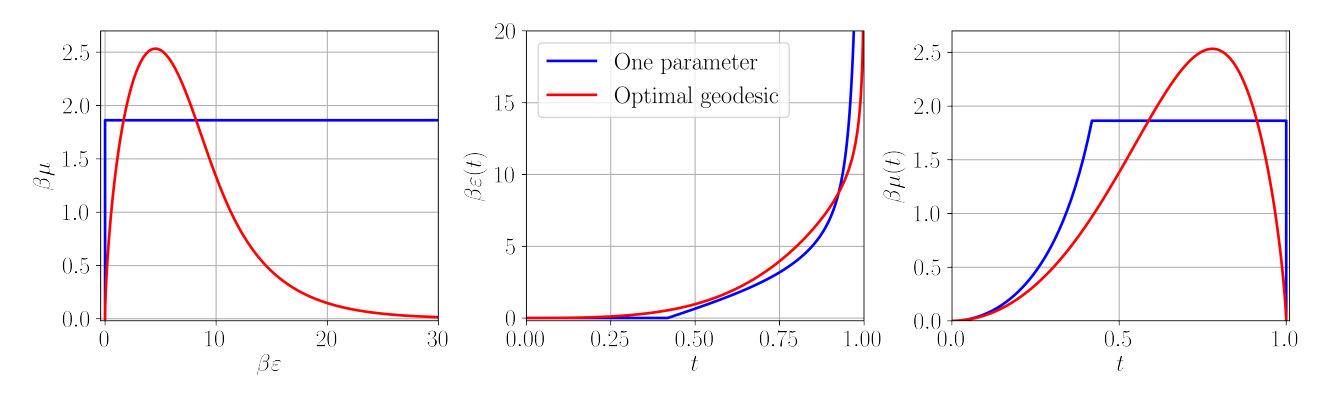


Figure 8: Comparing an optimal erasure protocol ( $\beta\varepsilon(1)\approx 50$ ) to an optimized ( $\beta\mu_*\approx 1.863$ ) erasure protocol where we change only one parameter at a time.

## **Collective Advantages in Finite-Time Thermodynamics**

Alberto Rolandi<sup>®</sup>, <sup>1,\*</sup> Paolo Abiuso<sup>®</sup>, <sup>2,†</sup> and Martí Perarnau-Llobet<sup>®</sup>, <sup>1</sup>Département de Physique Appliquée, Université de Genève, 1211 Genève, Switzerland <sup>2</sup>Institute for Quantum Optics and Quantum Information—IQOQI, Vienna, Austrian Academy of Sciences, Boltzmanngasse 3, A-1090 Vienna, Austria

(Received 5 July 2023; accepted 23 October 2023; published 22 November 2023)

A central task in finite-time thermodynamics is to minimize the excess or dissipated work  $W_{\rm diss}$  when manipulating the state of a system immersed in a thermal bath. We consider this task for an N-body system whose constituents are identical and uncorrelated at the beginning and end of the process. In the regime of slow but finite-time processes, we show that  $W_{\rm diss}$  can be dramatically reduced by considering collective protocols in which interactions are suitably created along the protocol. This can even lead to a sublinear growth of  $W_{\rm diss}$  with N:  $W_{\rm diss} \propto N^x$  with x < 1; to be contrasted to the expected  $W_{\rm diss} \propto N$  satisfied in any noninteracting protocol. We derive the fundamental limits to such collective advantages and show that x = 0 is in principle possible; however, it requires long-range interactions. We explore collective processes with spin models featuring two-body interactions and achieve noticeable gains under realistic levels of control in simple interaction architectures. As an application of these results, we focus on the erasure of information in finite time and prove a faster convergence to Landauer's bound.

DOI: 10.1103/PhysRevLett.131.210401

Introduction.—Collective effects play a central role in physics, ranging from phase transitions to quantum entanglement. Often, they can be exploited for a useful task, such as ultraprecise measurements [1], leading to the notion of a collective advantage [2]. In the growing fields of stochastic and quantum thermodynamics [3–9], such advantages have received notable attention: relevant examples are found in quantum batteries [10–17], where entangling operations have been proven to enable faster charging [10–17]; in many-body thermal engines [18], whose performance can be enhanced via phase transitions [19–25], many-body effects [26–30], or superradiance [31–34]; and in quantum transport [35–40].

In this Letter, we uncover a new collective advantage in a crucial task in nonequilibrium thermodynamics: the minimization of dissipation in finite time [41–52]. In general, the thermodynamic work W required to transform a system, in contact with an environment, in a finite-time  $\tau$  can be split into two contributions (see e.g., [4])

$$W = \Delta F + W_{\rm diss} \tag{1}$$

a reversible contribution  $\Delta F$ , the free energy change, and an irreversible positive contribution  $W_{\rm diss}$ , the excess or dissipated work (the latter is directly proportional to the entropy production [53]). Whereas  $\Delta F$  is extensive with the size N of the system, we will show here that  $W_{\rm diss}$  can grow sublinearly in N. This is proven in the regime of slow-but-finite-time processes and becomes possible by exploiting many-body interactions suitably created along the process.

The advantage is dramatic: in principle, collective processes enable an N-fold reduction of  $W_{\rm diss}$  when

compared to local processes (see Fig. 1). While we will show that reaching this limit requires highly nonlocal or long-range interactions, a sublinear growth of  $W_{\rm diss}$  can be achieved with two-body interactions and realistic control.

To obtain these results, we rely on the framework of thermodynamic geometry [42,46,54,55], which has recently found numerous applications in mesoscopic and quantum systems [23,56–64]. In this approach, which is valid in the slow-driving regime, finite-time protocols are identified with curves in the thermodynamic parameter space, so that geodesics are those protocols that minimize  $W_{\rm diss}$ . Our results show that geodesic protocols generically explore highly interacting Hamiltonians, even if interactions are absent at the beginning and end of the process. As an application, we focus on finite-time information erasure [65–75] of N qubits. We show that collective processing can substantially reduce dissipation in this relevant task, leading to a faster convergence to Landauer's bound.

Overall, these results uncover a genuine collective advantage in stochastic and quantum thermodynamics, which is not linked to standard collective phenomena such as quantum entanglement, phase transitions, or collective system-baths couplings (e.g., superradiance).

Framework.—Let us consider a system in a d-dimensional Hilbert space  $\mathbb{C}^d$  with an externally driven Hamiltonian  $\hat{h}(t)$ . It can be parametrized as  $\hat{h}(t) = \sum_{j=1}^n \lambda^j(t) \hat{x}_j$ ,  $\{\lambda^j\}$  are externally controllable parameters, and  $\{\hat{x}_j\}$  are the corresponding observables. These control parameters can be constrained, and we will denote by  $M \subseteq \mathbb{R}^n$  the manifold

of the allowed values for these parameters. Additionally, the system is in contact with a thermal bath at inverse temperature  $\beta$ .

We focus on the task of driving  $\hat{h}(t)$  from an initial configuration  $\hat{h}(0) = \hat{h}_A$  to a final one  $\hat{h}(\tau) = \hat{h}_B$  in a time  $t \in [0, \tau]$ . External energy is needed to realize this transformation, quantified by the (average) thermodynamic work:

$$W = \int_0^{\tau} dt \operatorname{Tr} \left[ \frac{d\hat{h}(t)}{dt} \hat{\rho}(t) \right], \tag{2}$$

where  $\hat{\rho}(t)$  is the state of the system. This expression can be split as in Eq. (1), where  $\Delta F = \beta^{-1} \ln \mathcal{Z}(0)/\mathcal{Z}(\tau)$  and  $\mathcal{Z}(t) = \mathrm{Tr}[e^{-\beta \hat{h}(t)}]$ . Whereas  $\Delta F$  depends only on the end points of the process, W depends on the protocol, i.e., the specific driving  $\lambda\colon [0,\tau]\to M$ . The minimal dissipated work  $W_{\mathrm{diss}}$  in a finite time  $\tau$  can then be found by optimizing for  $\{\lambda_j(t)\}$  over the space of curves in M connecting  $\hat{h}_A$  to  $\hat{h}_B$ :  $W^*_{\mathrm{diss}} \equiv \min_{\lambda\in\mathcal{C}_{A,B}(M)}W_{\mathrm{diss}}$ . To address the nontrivial optimization we make some assumptions.

First, we assume that the driving  $(d/dt)\hat{h}(t)$  is slow compared to the relaxation rate. Then  $W_{\rm diss}$  can be expressed as a quadratic form at leading order in  $\tau^{-1}$  [23,42,46,54]:

$$W_{\text{diss}} = k_B T \int_0^{\tau} dt \, \dot{\lambda}^i(t) \dot{\lambda}^j(t) g_{ij}(\lambda(t)) + \mathcal{O}(\tau^{-2}), \quad (3)$$

where  $g_{ij}(\lambda)$  is the so-called thermodynamic metric, and we adopted the Einstein summation convention. The metric allows us to define the length of a line element in M by  $ds^2 = g_{ij}d\lambda^i d\lambda^j$ , which is used to assign a length to a curve  $\lambda$  in M:  $L[\lambda] = \int_{\lambda} ds = \int_0^{\tau} dt \sqrt{\dot{\lambda}^i(t)\dot{\lambda}^j(t)g_{ij}(\lambda(t))}$ . It is related to the dissipated work via a Cauchy-Schwartz inequality [42]:  $\beta W_{\rm diss} \geq L^2/\tau$ , where equality is satisfied by protocols with constant dissipation rate. The shortest length  $\mathcal L$  corresponds to the protocol that minimizes dissipation:  $\beta W_{\rm diss}^* = \mathcal L^2/\tau$ . We can then find  $W_{\rm diss}^*$  by solving the geodesic equation for the thermodynamic metric [23,42,46].

As a second simplification, we assume there is a single relaxation timescale  $\tau_{eq}$  [76], so that the metric becomes [55]

$$g_{ij} = \tau_{eq} \frac{\partial^2 \ln \mathcal{Z}}{\partial \lambda^i \partial \lambda^j}.$$
 (4)

Note that  $g_{ij}$  then becomes the standard thermodynamic metric for macroscopic systems [54,77,78], which can also describes step processes [79,80]. In what follows, without loss of generality, we set  $\tau_{eq} = 1$ .

As a last simplification, we will assume that the initial and final Hamiltonian commute  $[\hat{h}_A, \hat{h}_B] = 0$ . This allows us to conclude that at all times  $[(d/dt)\hat{h}(t), \hat{h}(t)] = 0$ , as

changes in the eigenbasis can only increase dissipation in the linear response regime [49,81].

Let us now consider a scenario in which we perform the driving on N copies of the system. We denote by  $\hat{H}(t)=\hat{H}_0(t)+\hat{H}_{\rm int}(t)$  the total Hamiltonian for all the copies, where  $\hat{H}_0(t)=\sum_{j=1}^N\hat{h}^{(j)}(t)$  and  $\hat{H}_{\rm int}(t)$  contains the interaction between the copies. We parametrize  $\hat{H}(t)$  similarly to  $\hat{h}(t)$ :  $\hat{H}(t)=\sum_{i=1}^n\gamma^i(t)\hat{X}_i$ , where the sum can have up to  $n=d^N$  terms. The problem at hand imposes the following boundary conditions on the protocol:  $\hat{H}_{\rm int}(0)=\hat{H}_{\rm int}(\tau)=0$ ,  $\hat{h}^{(j)}(0)=\hat{h}_A$ , and  $\hat{h}^{(j)}(\tau)=\hat{h}_B$   $\forall$  j. Furthermore, by the same reasoning as in the case for a single copy, we have that  $[(d/dt)\hat{H}(t),\hat{H}(t)]=0$  for the geodesic protocol.

Fundamental limit of collective advantages.—Let us first note that  $\Delta F$  is extensive with N which directly follows from the boundary conditions. Instead,  $W_{\rm diss}$  depends on the process and can exhibit a nontrivial behavior whenever  $\hat{H}_{\rm int}(t) \neq 0$ . Indeed, we find that, in general, geodesic paths explore highly interacting Hamiltonians if the constraints allow for it.

To reach the fundamental limit of  $W^*_{\rm diss}$  we can assume full control on  $\hat{H}(t)$ , so that the  $n=d^N$  different eigenenergies  $\{\gamma^i\}$  can be externally controlled at will—the corresponding  $\{\hat{X}_i\}$  are chosen to be the corresponding projectors. In this case, the thermodynamic metric is given by  $\beta^{-2}g_{ij}=\omega_i\delta_{ij}-\omega_i\omega_j$ , where  $\omega_i=e^{-\beta\gamma_i}/\mathcal{Z}$  are the eigenvalues of the thermal state  $\hat{\omega}_\beta=e^{-\beta\hat{H}}/\mathcal{Z}$ , for which the distance function is known to be the quantum Hellinger angle:  $\mathcal{L}=2\arccos {\rm Tr}[\sqrt{\hat{\omega}_\beta(0)}\sqrt{\hat{\omega}_\beta(\tau)}]$  (cf. Supplemental Material A [82] and [23,83]), leading to

$$\beta W_{\rm diss}^* = \frac{1}{\tau} \left( 2 \arccos \operatorname{Tr} \left[ \sqrt{\hat{\omega}_{\beta}(0)} \sqrt{\hat{\omega}_{\beta}(\tau)} \right] \right)^2. \quad (5)$$

Since trivially  $\arccos(x) \le \pi/2$  for x > 0, the minimal dissipation of an N-body system is bounded by a constant  $W_{\rm diss}^* \le (1/\tau)\pi^2$  independent of N. This is somehow astonishing, as we expect the dissipation generated when driving a many-body system to increase extensively with its size. In Supplemental Material A [82] we derive the protocol that achieves this limit, obtaining

$$\beta \hat{H}(t) = -2\log \left[ \sin \left[ \frac{\mathcal{L}(\tau - t)}{2\tau} \right] \sqrt{\hat{\omega}_{\beta}(0)} + \sin \left[ \frac{\mathcal{L}t}{2\tau} \right] \sqrt{\hat{\omega}_{\beta}(\tau)} \right]. \tag{6}$$

Crucially, this protocol generally requires all possible interacting terms available in the Hamiltonian space, including highly nonlocal N-body interactions (see proof in Supplemental Material A [82]). This is illustrated in what follows for the paradigmatic task of erasing N bits of information.

Collective erasure.—Let us consider N qubits, each with local Hamiltonian  $\hat{h}(t) = \varepsilon(t)\hat{\sigma}_z$ . We want to drive  $\varepsilon(t)$  from  $\varepsilon(0) = 0$  to  $\varepsilon(\tau) = E$  with  $E \gg k_B T$ , so that the state of each qubit evolves from a fully mixed state  $\hat{\omega}_{\beta}(0) = \frac{1}{2}\mathbb{1}$  to an (almost) pure state  $\hat{\omega}_{\beta}(\tau) \approx |0\rangle\langle 0|$  due to the action of the external bath. We have  $\Delta F = Nk_B T \ln 2$ , corresponding to Landauer's bound.

Consider first the independent scenario, so that during the whole protocol  $\hat{H}_{\rm int}(t)=0$ . For each qubit, the dissipation generated via an optimal driving can be computed from Eq. (5) with the aforementioned boundary conditions, yielding  $\beta W_{\rm diss}^* = \pi^2/4\tau$ , see also [42,72,75]. The total dissipation of N qubits then reads

$$\beta W_{\rm diss}^{*,\rm local} = N \frac{\pi^2}{4\tau},\tag{7}$$

which grows linearly with N. The corresponding optimal driving reads  $\beta \varepsilon(t) = \ln \tan \left[ \pi (t + \tau) / 4\tau \right]$ , which has been implemented experimentally in a single-energy driven dot [73].

If we now allow for full control of the Hamiltonian, we can again use Eq. (5) to compute the minimal dissipation, but this time we use the global states  $\hat{\omega}_{\beta}(0) = (1/2^N)\mathbb{1}$  and  $\hat{\omega}_{\beta}(\tau) \approx |0\rangle\langle 0|^{\otimes N}$  instead of the local ones. This leads to

$$\beta W_{\rm diss}^{*,\rm global} = \frac{1}{\tau} \left( 2 \arccos \left[ \frac{1}{2^{N/2}} \right] \right)^2 = \frac{\pi^2}{\tau} + \mathcal{O}(e^{-N/2}). \quad (8)$$

Therefore, an *N*-fold advantage can potentially be achieved by global processes, as illustrated in Fig. 1.

Let us now discuss the implications of this result for the reachability of Landauer's bound. From Eq. (1) we have  $\Delta F = Nk_BT \ln 2$  whereas  $W_{\rm diss}$  can reach Eq. (8) at leading order in  $\tau^{-1}$  [recall that our results are based on the slow driving assumption where the expansion Eq. (3) is well justified]. Hence, the work cost per qubit of erasure can be written as

$$\beta W_{\text{qubit}}^* = \ln 2 + \frac{\pi^2}{\tau N} + \mathcal{O}(\tau^{-2}). \tag{9}$$

Hence, in the thermodynamic limit  $N \to \infty$ , we can approach Landauer's bound with an error that scales as  $\tau^{-2}$  instead of the standard  $\tau^{-1}$  [65–75,84].

We note that a collective *N*-qubit erasure based upon spontaneous symmetry breaking has been recently reported in Ref. [85]. Furthermore, a link between complexity, as in higher level *k*-body interactions and faster information erasure has been suggested in Ref. [86]. While being based on different collective phenomena or operations, these results share conceptual similarities to the collective erasure developed here.

The optimal driving achieving the limit Eq. (8) can be computed from Eq. (6):

$$\beta \hat{H}(t) = \gamma(t) \sum_{j=1}^{N} (-1)^{j+1} \sum_{i_1 < i_2 < \dots < i_j}^{N} \hat{x}^{(i_1)} \hat{x}^{(i_2)} \dots \hat{x}^{(i_j)}, \quad (10)$$

where  $\hat{x} = \hat{\sigma}_+ \hat{\sigma}_-$  and the control function can be written as  $\gamma(t) = 2\log\left[1 + 2^{N/2}\sin(\frac{\pi t}{2\tau})\sin^{-1}(\frac{\pi(\tau-t)}{2\tau})\right]$ . It follows that highly nonlocal *N*-body interactions are required to saturate the bound Eq. (8). More specifically, one needs to activate every possible (classical) interaction present in the system. This makes reaching the fundamental bound Eq. (8) highly challenging in practice, and opens the question as to whether collective advantages beyond the local bound Eq. (7) can be achieved via more realistic driven manybody systems featuring (local) few-body interactions. We address this relevant question in what follows.

Collective advantage in driven many-body systems.—To seek collective advantages in a more realistic model, in this section, we constrain the total system to only feature at most two-body interactions. Specifically, we consider a spin system with Hamiltonian of the form

$$\hat{H}(t) = \sum_{i=1}^{N} \varepsilon_i(t) \hat{\sigma}_z^{(i)} + \frac{1}{2} \sum_{i,j=1}^{N} J_{ij}(t) \hat{\sigma}_z^{(i)} \hat{\sigma}_z^{(j)}.$$
 (11)

We thus examine different degrees of control, reflected in the topologies represented in Fig. 1: (i) an all-to-all spin model, (ii) a 1D spin chain with nearest neighbor interaction (with periodic boundary conditions), (iii) a star-shaped design, which we generalize to (iv) a multilayer pyramid scheme. In practice, the energies  $\varepsilon_i(t)$  could be tuned via an external magnetic field whereas the interaction strength  $J_{ij}(t)$  could be controlled by changing the distance between the spins interacting via dipole-dipole coupling. Current quantum annealers have the capacity of tuning generic Hamiltonians of the form Eq. (11) [87].

The all-to-all model corresponds to taking uniform magnetic fields and spin interactions, i.e.,  $\varepsilon_i(t) \equiv \varepsilon(t)$  and  $J_{ij}(t) \equiv J(t)$  in Eq. (11). We can compute the partition function as follows,

$$\mathcal{Z}_{\text{all}} = \sum_{k=0}^{N} \binom{N}{k} e^{-\beta E_k},\tag{12}$$

where  $E_k = \varepsilon(2k - N) + \frac{1}{2}J(2k - N)^2$ . The standard 1D Ising model corresponds to uniform local terms  $\varepsilon$ , and  $J_{i,i+1} \equiv J$  for nearest neighbors and 0 elsewhere. The partition function can be found by making use of the transfer matrix method:

$$\mathcal{Z}_{\text{chain}} = z_+^N + z_-^N, \tag{13}$$

where  $z_{\pm} = e^{-\beta J/2} \cosh \beta \varepsilon \pm \sqrt{e^{-\beta J}} \sinh \beta \varepsilon + e^{\beta J}$ . Third, we consider a star topology corresponding to a central spin  $\hat{\sigma}_z^{(1)}$  with local magnetic field  $\varepsilon_0(t)$  and uniform elsewhere

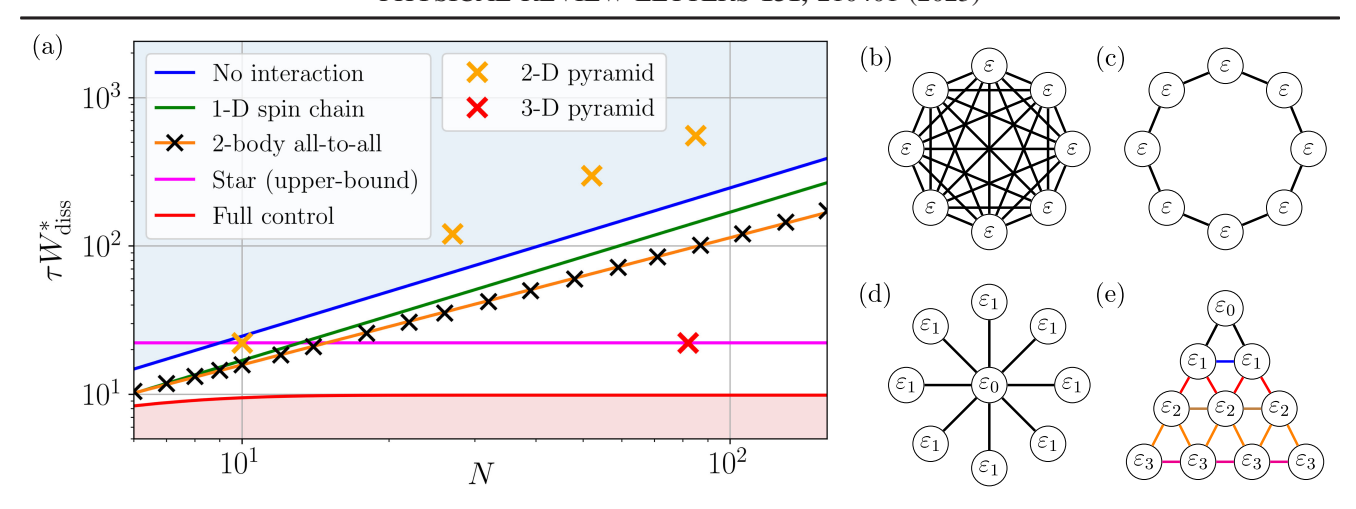


FIG. 1. (a) Minimal dissipation for the erasure of N spins for different control designs analyzed in this Letter. These are compared with the dissipations that are achievable with no interactions [Eq. (7), blue shaded area], and with the dissipations that are not achievable regardless of the protocol [Eq. (8), red shaded area]. We find  $\tau W_{\rm diss}^{*,{\rm chain}} \approx 1.69N$ ,  $\tau W_{\rm diss}^{*,{\rm all}} \approx 2.20N^{0.857}$ , while  $\tau W_{\rm diss}^{*,{\rm Star}} \leq 9\pi^2/4$  (cf. Supplemental Material B [82]). Single points are provided for 2D and 3D Pyramids with few layers and an aperture of 8 (cf. Supplemental Material B [82]). (b)–(e) Depiction of the geometries of the interactions in Eq. (11) (equal colors/labels correspond to equal values of the local fields). (b) All-to-all model with N=8, (c) 1D spin chain with N=8, (d) the star model with N=9, (e) 2D pyramid model with four layers and an aperture of 1.

 $\varepsilon_i(t) \equiv \varepsilon_1(t) \ \forall \ i > 1$ , and uniform "radial" interaction  $J_{1j}(t) \equiv J(t)$ , and 0 elsewhere. The partition function is easily computed as

$$\mathcal{Z}_{\rm star} = e^{-\beta\varepsilon} (2\cosh\beta\lambda_+)^{N-1} + e^{\beta\varepsilon} (2\cosh\beta\lambda_-)^{N-1}, \quad \ (14)$$

where  $\lambda_{\pm} = \varepsilon_1 \pm J$ .

For the models above, given the partition function, we compute the metric according to Eq. (4), from which we can obtain the geodesic equations. Their solution provides us with the minimal length for given boundary conditions, from which we find the minimal dissipation. This is implemented numerically for the task of approximate erasure (see details in Supplemental Material C [82]); we take  $\varepsilon(0) = 0$  and  $\varepsilon(\tau) = 5k_BT$  [recall  $J(0) = J(\tau) = 0$ ] which corresponds to an erasure process with an error of  $4.5 \times 10^{-5}$ .

In Fig. 1 we present the resulting minimal dissipation for the different many-body models. The results are contrasted with the optimal noninteracting protocol Eq. (7) and the fundamental bound obtained with full-control Eq. (8) (i.e., arbitrarily complex interactions).

First, we observe that the nearest neighbor model displays a linear increase of the dissipation with N, but with a better prefactor than the noninteracting case  $(W_{\rm diss}^{*,{\rm chain}}/W_{\rm diss}^{*,{\rm local}} \approx 0.686)$ . On the other hand, the all-to-all model displays a sublinear dependence on N:  $W_{\rm diss}^{*,{\rm all}} = \alpha N^x$  with  $x \approx 6/7$ . Furthermore, the exponent x displays a nontrivial dependence on the specific boundary conditions (cf. Supplemental Material C [82]). Finally, quite remarkably, the star model can achieve *a finite value of the dissipation, independent of N*. This feature is enabled by a three-step protocol (cf. Supplemental Material B [82])

that suppresses specific terms in the otherwise-extensive  $\log \mathcal{Z}_{Star}$ . Interestingly, the star model was found to be optimal in the context of two-body probes used for thermometry [88].

The sublinearity of the all-to-all's and star-model's dissipation is remarkable as it allows for the same effect as in Eq. (9): it is possible to reach Landauer's bound in finite-time with an error that scales as  $\tau^{-2}$  instead of  $\tau^{-1}$  as one approaches the thermodynamic limit. However, both of these models use long-range interactions between arbitrarily far spins as N grows, and their scaling properties might thus be seen as inconsequential. For this reason, in Supplemental Material B [82] we generalized the star model to a multilayer structure, i.e., a pyramid model (see Fig. 1 and Supplemental Material B [82]). By generalizing the star protocol, we prove that such model can achieve  $W_{\rm diss}^{\rm Pyr} \propto \ell^2$ ,  $\ell$  being the number of layers of the pyramid. Given that  $N \propto \ell^D$  for pyramids in D dimensions,  $W_{\rm diss}^{\rm Pyr} \propto N^{2/D}$  follows asymptotically.

TABLE I. All models studied in this Letter are based on two-body interactions (11). The all-to-all and star model feature long-range interactions that enable a sublinear scaling of  $W_{\rm diss}$ , i.e., a collective advantage. The pyramid models can achieve such advantage in D=3 spatial dimensions using short-range interactions only (cf. Supplemental Material B [82]).

Model	1D chain	All-to-all	Star	Pyramid
Asymptotic $W_{\rm diss}$	$\mathcal{O}(N)$	$\mathcal{O}(N^x)$	$\mathcal{O}(1)$	$\mathcal{O}(N^{2/D})$
Short-range	✓	X	X	✓

Conclusions and discussion.—In this Letter, we considered the task of minimizing dissipated work,  $W_{\rm diss}$ , for an N-body system. We showed that, in contrast to  $\Delta F$ ,  $W_{\rm diss}$  can grow sublineraly with N by suitably creating interactions between the N systems along the process. This leads to a finite-time reduction of dissipation induced by collective processes and has a clear potential for improving various thermodynamic tasks ranging from quantum and stochastic engines [5,9,89] to the estimation of equilibrium free energy via nonequilibrium work measurements [90]; or, as is shown here, for the erasure of information in finite time. There are several observations to be made about these collective processes.

First, the derived collective processes are a genuine effect of finite-time thermodynamic protocols, which cannot be directly linked to other well-known collective phenomena such as entanglement, phase transitions, or superradiance. Indeed, (i) they do not require the presence of quantum correlations or coherence, but rather arise due to the interplay between interactions and dissipation to an external thermal environment, and (ii) they are process dependent, i.e., they depend on the whole driving protocol  $\hat{H}(t)$ , unlike phase transitions which take place in a particular point in the parameter space.

Second, our results suggest an interesting interplay between the complexity of the interactions and the associated reductions in dissipation, see also Ref. [86]. In particular, we argued that reaching the maximal advantage requires highly nonlocal N-body interactions. Despite this, we showed that similar reductions (in scaling) can be achieved with only two-body long-range interactions via the star model. A sublinear growth of  $W_{\rm diss}$  was found in the all-to-all model and, crucially, in the pyramid model that only features short-range strong interactions. See Table I for a compact summary.

Third, being derived in the linear response regime, the dissipated work is directly related to the work fluctuations  $\sigma_W^2$  via the work fluctuation-dissipation relation  $(\beta/2)\sigma_W^2 = W_{\rm diss}$  [91–94]. This implies that the collective gains also lead to a reduction of work fluctuations, a desired property in stochastic thermodynamics [95,96].

Finally, it is important to stress that our results have been derived in the slow driving regime, i.e., for the leading order contribution of  $W_{\rm diss}$  in  $\tau^{-1}$ . For a finite (large) time  $\tau$ , the next order contributions of  $\mathcal{O}(\tau^{-2})$  can become relevant when increasing N. An exciting future endeavor is to generalize such collective advantages for arbitrary non-equilibrium protocols. For this, it might be useful to exploit recent results on minimal dissipation and the Wasserstein distance [48,51,52,97–100] as well as new tools such as reinforcement learning [101,102] or fast-driving expansions [102–104] for finding optimal protocols.

Another future challenge is to understand how the collective advantages are modified beyond the simple model of thermalization used in Eq. (4) and by adding

constraints on the strength of the couplings in Eq. (11). In particular, for more realistic thermalization models where the relaxation timescale(s) is(are) modified in the presence of interactions, which can lead, e.g., to a critical slowdown of relaxation.

We warmly thank Nicolas Brunner, Harry J. D. Miller, and Maja Milas for their insightful discussions. This work was supported by the Swiss National Science Foundation through Ambizione Grant No. PZ00P2-186067. P. A. is supported by the QuantERA II program, that has received funding from the European Union's Horizon 2020 research and innovation program under Grant Agreement No. 101017733, and from the Austrian Science Fund (FWF), project No. I-6004.

- \*alberto.rolandi@unige.ch †paolo.abiuso@oeaw.ac.at
- <sup>‡</sup>marti.perarnaullobet@unige.ch
- [1] V. Giovannetti, S. Lloyd, and L. Maccone, Phys. Rev. Lett. 96, 010401 (2006).
- [2] The outcome of a task is improved when performed globally on a collection of systems than when realized on each system individually.
- [3] M. Esposito, U. Harbola, and S. Mukamel, Rev. Mod. Phys. 81, 1665 (2009).
- [4] C. Jarzynski, Annu. Rev. Condens. Matter Phys. 2, 329 (2011).
- [5] U. Seifert, Rep. Prog. Phys. 75, 126001 (2012).
- [6] J. Goold, M. Huber, A. Riera, L. del Rio, and P. Skrzypczyk, J. Phys. A 49, 143001 (2016).
- [7] S. Vinjanampathy and J. Anders, Contemp. Phys. **57**, 545 (2016).
- [8] M. T. Mitchison, Contemp. Phys. **60**, 164 (2019).
- [9] N. M. Myers, O. Abah, and S. Deffner, AVS Quantum Sci. 4, 027101 (2022).
- [10] F. Campaioli, F. A. Pollock, and S. Vinjanampathy, in *Fundamental Theories of Physics* (Springer International Publishing, New York, 2018), pp. 207–225.
- [11] S. Bhattacharjee and A. Dutta, Eur. Phys. J. B 94, 1 (2021).
- [12] K. V. Hovhannisyan, M. Perarnau-Llobet, M. Huber, and A. Acín, Phys. Rev. Lett. 111, 240401 (2013).
- [13] F. C. Binder, S. Vinjanampathy, K. Modi, and J. Goold, New J. Phys. 17, 075015 (2015).
- [14] F. Campaioli, F. A. Pollock, F. C. Binder, L. Céleri, J. Goold, S. Vinjanampathy, and K. Modi, Phys. Rev. Lett. 118, 150601 (2017).
- [15] S. Julià-Farré, T. Salamon, A. Riera, M. N. Bera, and M. Lewenstein, Phys. Rev. Res. 2, 023113 (2020).
- [16] D. Rossini, G. M. Andolina, D. Rosa, M. Carrega, and M. Polini, Phys. Rev. Lett. 125, 236402 (2020).
- [17] J.-Y. Gyhm, D. Šafránek, and D. Rosa, Phys. Rev. Lett. 128, 140501 (2022).
- [18] V. Mukherjee and U. Divakaran, J. Phys. Condens. Matter 33, 454001 (2021).
- [19] M. Campisi and R. Fazio, Nat. Commun. 7, 11895 (2016).

- [20] H. Vroylandt, M. Esposito, and G. Verley, Europhys. Lett. 120, 30009 (2017).
- [21] V. Holubec and A. Ryabov, Phys. Rev. E 96, 030102(R) (2017).
- [22] T. Herpich, J. Thingna, and M. Esposito, Phys. Rev. X 8, 031056 (2018).
- [23] P. Abiuso and M. Perarnau-Llobet, Phys. Rev. Lett. 124, 110606 (2020).
- [24] T. Fogarty and T. Busch, Quantum Sci. Technol. 6, 015003 (2020).
- [25] F. Barra, K. V. Hovhannisyan, and A. Imparato, New J. Phys. 24, 015003 (2022).
- [26] L. d. S. Souza, G. Manzano, R. Fazio, and F. Iemini, Phys. Rev. E 106, 014143 (2022).
- [27] A. Solfanelli, G. Giachetti, M. Campisi, S. Ruffo, and N. Defenu, New J. Phys. 25, 033030 (2023).
- [28] G. Watanabe, B. P. Venkatesh, P. Talkner, M.-J. Hwang, and A. del Campo, Phys. Rev. Lett. **124**, 210603 (2020).
- [29] F. S. Filho, G. A. L. Forão, D. M. Busiello, B. Cleuren, and C. E. Fiore, Phys. Rev. Res. 5, 043067 (2023).
- [30] J Jaramillo, M Beau, and A del Campo, New J. Phys. 18, 075019 (2016).
- [31] W. Niedenzu and G. Kurizki, New J. Phys. 20, 113038 (2018).
- [32] M. Kloc, P. Cejnar, and G. Schaller, Phys. Rev. E 100, 042126 (2019).
- [33] D. Kolisnyk and G. Schaller, Phys. Rev. Appl. 19, 034023 (2023).
- [34] N. Jaseem, S. Vinjanampathy, and V. Mukherjee, Phys. Rev. A 107, L040202 (2023).
- [35] G. T. Landi, D. Poletti, and G. Schaller, Rev. Mod. Phys. 94, 045006 (2022).
- [36] K. Brandner, T. Hanazato, and K. Saito, Phys. Rev. Lett. **120**, 090601 (2018).
- [37] C. Chiaracane, M. T. Mitchison, A. Purkayastha, G. Haack, and J. Goold, Phys. Rev. Res. 2, 013093 (2020).
- [38] T. Ehrlich and G. Schaller, Phys. Rev. B 104, 045424 (2021).
- [39] M. Gerry and D. Segal, Phys. Rev. B **105**, 155401 (2022).
- [40] S. Kamimura, K. Yoshida, Y. Tokura, and Y. Matsuzaki, Phys. Rev. Lett. 131, 090401 (2023).
- [41] B. Andresen and P. Salamon, Entropy 24, 690 (2022).
- [42] P. Salamon and R. S. Berry, Phys. Rev. Lett. 51, 1127 (1983).
- [43] T. Schmiedl and U. Seifert, Phys. Rev. Lett. 98, 108301 (2007).
- [44] M. Esposito, R. Kawai, K. Lindenberg, and C. V. den Broeck, Europhys. Lett. **89**, 20003 (2010).
- [45] E. Aurell, C. Mejía-Monasterio, and P. Muratore-Ginanneschi, Phys. Rev. Lett. 106, 250601 (2011).
- [46] D. A. Sivak and G. E. Crooks, Phys. Rev. Lett. **108**, 190602 (2012) (2012).
- [47] M. V. S. Bonança and S. Deffner, Phys. Rev. E 98, 042103 (2018).
- [48] A. Dechant and Y. Sakurai, arXiv:1912.08405.
- [49] P. Abiuso, H. J. D. Miller, M. Perarnau-Llobet, and M. Scandi, Entropy 22, 1076 (2020).
- [50] S. Deffner and M. V. S. Bonança, Europhys. Lett. 131, 20001 (2020).

- [51] T. Van Vu and Y. Hasegawa, Phys. Rev. Lett. 126, 010601 (2021).
- [52] T. Van Vu and K. Saito, Phys. Rev. X 13, 011013 (2023).
- [53] G. T. Landi and M. Paternostro, Rev. Mod. Phys. 93, 035008 (2021).
- [54] G. E. Crooks, Phys. Rev. Lett. 99, 100602 (2007).
- [55] M. Scandi and M. Perarnau-Llobet, Quantum 3, 197 (2019).
- [56] P. R. Zulkowski, D. A. Sivak, G. E. Crooks, and M. R. DeWeese, Phys. Rev. E 86, 041148 (2012).
- [57] G. M. Rotskoff, G. E. Crooks, and E. Vanden-Eijnden, Phys. Rev. E 95, 012148 (2017).
- [58] K. Brandner and K. Saito, Phys. Rev. Lett. 124, 040602 (2020).
- [59] G. Li, J.-F. Chen, C. P. Sun, and H. Dong, Phys. Rev. Lett. 128, 230603 (2022).
- [60] J. Eglinton and K. Brandner, Phys. Rev. E 105, L052102 (2022).
- [61] A. G. Frim and M. R. DeWeese, Phys. Rev. Lett. 128, 230601 (2022).
- [62] P. Terrén Alonso, P. Abiuso, M. Perarnau-Llobet, and L. Arrachea, PRX Quantum 3, 010326 (2022).
- [63] M. Mehboudi and H. J. D. Miller, Phys. Rev. A 105, 062434 (2022).
- [64] J. Eglinton, T. Pyhäranta, K. Saito, and K. Brandner, New J. Phys. 25, 043014 (2023).
- [65] P. R. Zulkowski and M. R. DeWeese, Phys. Rev. E 89, 052140 (2014).
- [66] K. Proesmans, J. Ehrich, and J. Bechhoefer, Phys. Rev. Lett. 125, 100602 (2020).
- [67] A. B. Boyd, A. Patra, C. Jarzynski, and J. P. Crutchfield, J. Stat. Phys. 187, 1 (2022).
- [68] J. S. Lee, S. Lee, H. Kwon, and H. Park, Phys. Rev. Lett. 129, 120603 (2022).
- [69] G. Diana, G. B. Bagci, and M. Esposito, Phys. Rev. E 87, 012111 (2013).
- [70] Y.-Z. Zhen, D. Egloff, K. Modi, and O. Dahlsten, Phys. Rev. Lett. 127, 190602 (2021).
- [71] Y.-Z. Zhen, D. Egloff, K. Modi, and O. Dahlsten, Phys. Rev. E 105, 044147 (2022).
- [72] Y.-H. Ma, J.-F. Chen, C. P. Sun, and H. Dong, Phys. Rev. E 106, 034112 (2022).
- [73] M. Scandi, D. Barker, S. Lehmann, K. A. Dick, V. F. Maisi, and M. Perarnau-Llobet, Phys. Rev. Lett. 129, 270601 (2022).
- [74] M. Konopik, T. Korten, E. Lutz, and H. Linke, Nat. Commun. 14, 447 (2023).
- [75] A. Rolandi and M. Perarnau-Llobet, Quantum 7, 1161 (2023).
- [76] We assume that all driven observables decay exponentially to equilibrium with the same timescale [23,49].
- [77] F. Schlögl, Z. Phys. B Condens. Matter 59, 449 (1985).
- [78] P. Salamon, J. D. Nulton, and R. S. Berry, J. Chem. Phys. 82, 2433 (1985).
- [79] J. Nulton, P. Salamon, B. Andresen, and Q. Anmin, J. Chem. Phys. 83, 334 (1985).
- [80] M. Scandi, H. J. D. Miller, J. Anders, and M. Perarnau-Llobet, Phys. Rev. Res. 2, 023377 (2020).
- [81] K. Brandner, M. Bauer, and U. Seifert, Phys. Rev. Lett. 119, 170602 (2017).

- [82] See Supplemental Material at http://link.aps.org/ supplemental/10.1103/PhysRevLett.131.210401 for the more technical proofs of the claims in the letter and a description of the numerical techniques employed for some of the many-body models.
- [83] A. Jenčová, J. Math. Phys. (N.Y.) 45, 1787 (2004).
- [84] Y.-H. Ma, R.-X. Zhai, J. Chen, C. P. Sun, and H. Dong, Phys. Rev. Lett. 125, 210601 (2020).
- [85] L. Buffoni and M. Campisi, Quantum 7, 961 (2023).
- [86] P. Taranto, F. Bakhshinezhad, A. Bluhm, R. Silva, N. Friis, M. P. Lock, G. Vitagliano, F. C. Binder, T. Debarba, E. Schwarzhans, F. Clivaz, and M. Huber, PRX Quantum 4, 010332 (2023).
- [87] See for example D-wave systems.
- [88] P. Abiuso, P. A. Erdman, M. Ronen, F. Noé, G. Haack, and M. Perarnau-Llobet, arXiv:2211.01934.
- [89] S. Blaber and D. A. Sivak, J. Chem. Phys. 153, 244119 (2020).
- [90] S. Blaber and D. A. Sivak, J. Chem. Phys. 153, 244119 (2020).
- [91] J. Hermans, J. Phys. Chem. 95, 9029 (1991).
- [92] C. Jarzynski, Phys. Rev. Lett. 78, 2690 (1997).

- [93] D. Mandal and C. Jarzynski, J. Stat. Mech. (2016) 063204.
- [94] H. J. D. Miller, M. Scandi, J. Anders, and M. Perarnau-Llobet, Phys. Rev. Lett. 123, 230603 (2019).
- [95] H. J. D. Miller and M. Mehboudi, Phys. Rev. Lett. 125, 260602 (2020).
- [96] G. Watanabe and Y. Minami, Phys. Rev. Res. 4, L012008 (2022).
- [97] Y. Chen, T. T. Georgiou, and A. Tannenbaum, IEEE Trans. Autom. Control 65, 2979 (2020).
- [98] M. Nakazato and S. Ito, Phys. Rev. Res. 3, 043093 (2021).
- [99] A. Dechant, J. Phys. A 55, 094001 (2022).
- [100] P. Abiuso, V. Holubec, J. Anders, Z. Ye, F. Cerisola, and M. Perarnau-Llobet, J. Phys. Commun. 6, 063001 (2022).
- [101] P. A. Erdman and F. Noé, npj Quantum Inf. 8, 1 (2022).
- [102] P. A. Erdman, A. Rolandi, P. Abiuso, M. Perarnau-Llobet, and F. Noé, Phys. Rev. Res. 5, L022017 (2023).
- [103] S. Blaber, M. D. Louwerse, and D. A. Sivak, Phys. Rev. E 104, L022101 (2021).
- [104] A. Rolandi, M. Perarnau Llobet, and H. J. D. Miller, New J. Phys. 25, 073005 (2023).

## Supplemental Material for "Collective advantages in finite-time thermodynamics"

Alberto Rolandi, 1, \* Paolo Abiuso, 2, † and Martí Perarnau-Llobet 1, ‡

Département de Physique Appliquée, Université de Genève, 1211 Genève, Switzerland Institute for Quantum Optics and Quantum Information - IQOQI Vienna, Austrian Academy of Sciences, Boltzmanngasse 3, A-1090 Vienna, Austria

## A. FULL CONTROL SCENARIO

We consider N copies of a d-dimensional system, with an externally driven Hamiltonian  $\hat{H}(t) = \hat{H}_0(t) + \hat{H}_{int}(t)$ , where  $\hat{H}_0(t) = \sum_{j=1}^N \hat{h}^{(j)}(t)$  (with each  $\hat{h}^{(j)}$  acting only on the d-dimensional Hilbert space of the j-th site) and  $\hat{H}_{int}(t)$  contains the interaction terms. We can always parameterize the total Hamiltonian by  $\hat{H}(t) = \sum_{i=1}^n \gamma^i(t) \hat{X}_i$  with  $n = d^{2N}$ .

We focus on the task of driving each copy from an initial configuration  $\hat{h}(0) = \hat{h}_A$  to a final one  $\hat{h}(\tau) = \hat{h}_B$  in a time  $t \in [0, \tau]$ , where at the beginning and the end of the protocol the copies are non-interacting. This translates to the following boundary conditions

$$\hat{H}_{\text{int}}(0) = \hat{H}_{\text{int}}(\tau) = 0 , \quad \hat{h}^{(j)}(0) = \hat{h}_A , \quad \hat{h}^{(j)}(\tau) = \hat{h}_B \quad \forall j .$$
 (A1)

Since we are considering only protocols in which the initial and final Hamiltonian commute (cf. main text), the driving will not require us to change the eigenbasis of  $\hat{H}(t)$ . Therefore we can reduce the number of needed parameters to  $n = d^N$  parameters to describe  $\hat{H}(t)$  by choosing  $\{\gamma^j(t)\}$  to be its eigenvalues at time t, and  $\hat{X}_j$  to be the projector associated to  $\gamma^j(t)$ . The average work cost of the operation can be computed by:

$$W = \int_0^{\tau} dt \operatorname{Tr} \left[ \frac{d\hat{H}(t)}{dt} \hat{\rho}(t) \right] , \qquad (A2)$$

where  $\hat{\rho}(t)$  is the state of the system. We can split this expression into  $W = \Delta F + W_{\text{diss}}$ , where  $\Delta F = \beta^{-1} \ln \mathcal{Z}(0)/\mathcal{Z}(\tau)$  (with  $\mathcal{Z}(t) = \text{Tr}\left[e^{-\beta \hat{H}(t)}\right]$ ) is the reversible contribution and depends only on the endpoints. Whereas the dissipative term  $W_{\text{diss}}$  depends on the specific driving  $\hat{H}(t)$ , at first order in the slow driving regime, it is quantified by

$$W_{\text{diss}} = k_B T \int_0^{\tau} dt \ d\gamma^i(t) d\gamma^j(t) g_{ij}(\gamma(t)) + \mathcal{O}(\tau^{-2}) \ , \tag{A3}$$

where  $g_{ij}(\gamma)$  is a metric over the manifold M of the control parameters  $\{\gamma^i\}$ . This metric allows us to quantify the length of a line element ds over the manifold M:  $ds^2 = g_{ij}d\gamma^i d\gamma^j$ . By integrating ds over a curve  $\gamma(t)$  we can find the length of the curve:

$$L[\gamma] = \int_{\gamma} ds = \int_{0}^{\tau} dt \sqrt{d\gamma^{i}(t)d\gamma^{j}(t)g_{ij}(\gamma(t))} . \tag{A4}$$

The length of the curve and the dissipation of the corresponding driving are related by a Cauchy-Schwartz inequality

$$\beta W_{\rm diss} \ge \frac{1}{\tau} L^2 \,,$$
 (A5)

where equality is satisfied whenever the integrand is constant. Since geodesics – curves of minimal length connecting two points – have a constant integrand for the length, they also minimize dissipation. Therefore we can find protocols that minimize the dissipation by solving the geodesic equations:

$$\ddot{\gamma}^i(t) + \Gamma^i_{ik}\dot{\gamma}^j(t)\dot{\gamma}^k(t) = 0 , \qquad (A6)$$

<sup>\*</sup> alberto.rolandi@unige.ch

 $<sup>^{\</sup>dagger}$ paolo.abiuso@oeaw.ac.at

<sup>†</sup> marti.perarnaullobet@unige.ch

where  $\Gamma^{i}_{jk}$  are the Christoffel symbols

$$\Gamma_{jk}^{i} = \frac{1}{2}g^{il}\left(\frac{\partial g_{lk}}{\partial \gamma^{j}} + \frac{\partial g_{jl}}{\partial \gamma^{k}} - \frac{\partial g_{jk}}{\partial \gamma^{l}}\right) , \qquad (A7)$$

for  $q^{il}$  the inverse of the metric.

In this work, we focus on a simple model of thermalization with a single time-scale  $\tau_{eq}$ , which is described by the rate equation

$$\frac{d}{dt}\hat{\rho}(t) = \frac{\hat{\omega}_{\beta}(t) - \hat{\rho}(t)}{\tau_{\text{eq}}} , \qquad (A8)$$

where  $\hat{\omega}_{\beta}(t) = e^{-\beta \hat{H}(t)}/\mathcal{Z}(t)$  is the instantaneous thermal state. Without loss of generality, we can absorb the time scale in the total time of the protocol, which allows us to drop it for simplicity. This model guarantees us the following form for the metric [1]

$$g_{ij} = \frac{\partial^2 \ln \mathcal{Z}}{\partial \gamma^i \partial \gamma^j} \ . \tag{A9}$$

Given the full control assumed here, and choosing the parametrization to be such that  $\{\gamma^i\}$  correspond to the eigenenergies of  $\hat{H}$ , this leads to

$$\beta^{-2}g_{ij} = \omega_i \delta_{ij} - \omega_i \omega_j , \qquad (A10)$$

where  $\omega_i = e^{-\beta \gamma_i}/\mathcal{Z}$  is the thermal probability of the eigenstate corresponding to the energy  $\gamma^i$ .

#### 1. Recovering the quantum Hellinger angle

We now show that the distance function induced by the metric eq. (A10) is the quantum Hellinger angle

$$d(\gamma, \gamma') = 2 \arccos \operatorname{Tr} \left[ \sqrt{\hat{\omega}_{\beta}(\gamma)} \sqrt{\hat{\omega}_{\beta}(\gamma')} \right] , \qquad (A11)$$

where  $\gamma$  and  $\gamma'$  are two points in M,  $\hat{\omega}_{\beta}(\gamma)$  and  $\hat{\omega}_{\beta}(\gamma')$  are the corresponding thermal states. Let us notice that we can rewrite the Hellinger angle as  $d(\gamma, \gamma') = 2 \arccos \sqrt{\omega^i \omega_i'}$  since the thermal states have the same eigenbasis.

Let us now consider the radius 2 sphere embedded in  $\mathbb{R}^n$ , we can describe it with Cartesian coordinates  $\{r^i\}_{i=1}^n$  subject to the constraint  $r^i r_i = 4$ . With the Euclidean metric, the line element in  $\mathbb{R}^n$  is  $dl^2 = \delta_{ij} dr^i dr^j$ , this naturally induces the notion of Euclidean distance over  $\mathbb{R}^n$ . By restricting ourselves to the radius 2 sphere it is clear that the Euclidean distance between a point r and r' on the sphere is given by the angle between these two points times the radius, which gives us

$$d(r,r') = 2\arccos\frac{r^i r_i'}{4} , \qquad (A12)$$

where  $r^i r_i'$  is the scalar product of r and r'. We can notice that if we identify  $r^i = 2\sqrt{\omega^i}$  we recover the Hellinger angle, and the constraint is naturally satisfied by the thermal probabilities since it becomes  $\sum_i \omega^i = 1$ . Therefore by applying a coordinate transformation, we can recover the line element (or equivalently the metric) that induces the Hellinger angle as its distance in terms of variations of the eigenenergies instead of variations of the square root of the thermal probabilities. We start by transforming to the thermal probabilities as coordinates, we have

$$dl^2 = \frac{\delta_{ij}}{\omega^i} d\omega^i d\omega^j , \qquad (A13)$$

where we used  $dr^i = \frac{1}{\sqrt{\omega^i}}d\omega^i$ . Using the definition of the thermal probabilities we can easily find  $d\omega^i = \beta(\omega^i\omega^j - \delta^{ij}\omega^i)d\gamma_j$ , with eq. (A13) and the constraint  $\sum_i \omega^i = 1$  we find  $dl^2 = \beta^2(\omega_i\delta_{ij} - \omega_i\omega_j)d\gamma^i d\gamma^j$ , which corresponds to the metric we found in eq. (A10). This reveals that the manifold M is the positive quadrant of the n-dimensional sphere of radius 2. It confirms that the thermodynamic length is given by the Hellinger angle and allows us to find the corresponding optimal protocols over the space of parameters.

#### 2. Geodesics

For this subsection, we will take  $\tau = 1$  for lightness of notation, as the results can be trivially generalized to  $\tau \neq 1$ . Since M is the positive quadrant of the n-dimensional sphere of radius 2 equipped with the Euclidean metric, it is very simple to find the geodesics. In terms of the coordinates  $\{r^i\}_i$  the geodesic connecting r(0) to r(1) is given by

$$r(t) = 2\frac{(1 - u(t))r(0) + u(t)r(1)}{\|(1 - u(t))r(0) + u(t)r(1)\|},$$
(A14)

where  $u:[0,1] \to [0,1]$  is a bijective and increasing function that we choose such that  $\|\dot{r}(t)\|$  is a constant, as this is equivalent to  $\frac{ds}{dt}$  being constant. This trajectory follows a great circle of the *n*-dimensional sphere. To compute u(t) we can start by noticing that, because of the normalization,  $\mathcal{L} = d(r(0), r(1)) = \frac{ds}{dt} = \dot{r}^i(t)\dot{r}_i(t)$  for a geodesic. Therefore we get the following differential equation for u(t)

$$\mathcal{L} = \frac{2\dot{u}(t)\sin\frac{\mathcal{L}}{2}}{1 - 2u(t)(1 - u(t))(1 - \cos\frac{\mathcal{L}}{2})} , \qquad (A15)$$

which can be solved by integration. We thus find

$$u(t) = \frac{1}{2} \left( 1 + \frac{\tan\left[\frac{\mathcal{L}}{4}(2t-1)\right]}{\tan\frac{\mathcal{L}}{4}} \right) . \tag{A16}$$

Plugging this result in eq. (A14) and transforming the coordinates we find the geodesic in terms of the thermal state

$$\hat{\omega}_{\beta}(t) = \frac{1}{\sin^2 \frac{\mathcal{L}}{2}} \left( \sin \left[ \frac{\mathcal{L}}{2} (1 - t) \right] \sqrt{\hat{\omega}_{\beta}(0)} + \sin \left[ \frac{\mathcal{L}}{2} t \right] \sqrt{\hat{\omega}_{\beta}(1)} \right)^2 . \tag{A17}$$

At this point, it is immediate that the geodesic trajectory for the Hamiltonian is

$$\hat{H}(t) = -2k_B T \log \left[ \sin \left[ \frac{\mathcal{L}(\tau - t)}{2\tau} \right] \frac{e^{-\frac{\beta}{2}\hat{H}(0)}}{\mathcal{Z}(0)^{\frac{1}{2}}} + \sin \left[ \frac{\mathcal{L}t}{2\tau} \right] \frac{e^{-\frac{\beta}{2}\hat{H}(\tau)}}{\mathcal{Z}(\tau)^{\frac{1}{2}}} \right] , \tag{A18}$$

where we neglected terms proportional to the identity. The geodesic of eq. (A18) describes the optimal trajectory that every energy level should follow, one can notice that if two distinct energy levels have the same boundary conditions then they follow the same trajectory. Therefore, by permutation invariance, the number of distinct trajectories is given by the number of different (i.e. without counting the degeneracies) energy levels in the initial and final Hamiltonian. By taking into account that the initial and final Hamiltonian do not have interaction terms and are permutation invariant we can conclude that there are at most only  $n = \binom{N+d-1}{N} = \mathcal{O}(N^{d-1})$  distinct control parameters instead of  $d^N$ .

Let us now consider the question of what orders of interaction are present in the trajectory described by eq. (A18). The following argument is made for spins- $\frac{1}{2}$ , but its generalization is immediate. Let us suppose that there is no k-th order interaction term (i.e. that it involves k sites) in the trajectory in eq. (A18), then we denote by  $\varepsilon_k(t)$  an eigenenergy of  $\hat{H}$  that corresponds to k distinct excitations at time t. Then  $\varepsilon_k(t)$  can be written as a linear combination of eigen-energies corresponding to fewer excitations:  $\varepsilon_k(t) = \sum_{j=1}^{k-1} \sum_{l}^{N_j} \alpha_{j,l} \varepsilon_{j,l}(t)$ , where  $\varepsilon_{j,l}(t)$  are the eigen-energies corresponding to j distinct excitations (we are supposing w.l.o.g. that there are  $N_j$  of them) and  $\alpha_{j,l}$  are the real numbers composing the linear combination. Inserting this into eq. (A18) we get that the following must be satisfied for all  $t \in [0, \tau]$ 

$$\sum_{i,l} \alpha_{j,l} \log \left[ A(t) e^{-\beta \varepsilon_{j,l}(0)/2} + B(t) e^{-\beta \varepsilon_{j,l}(\tau)/2} \right] = \log \left[ A(t) e^{-\beta \sum_{j,l} \alpha_{i,j} \varepsilon_{j,l}(0)/2} + B(t) e^{-\beta \sum_{j,l} \alpha_{i,j} \varepsilon_{j,l}(\tau)/2} \right] . \tag{A19}$$

By defining  $\Delta \varepsilon_{j,l} := \varepsilon_{j,l}(\tau) - \varepsilon_{j,l}(0)$  we can turn this last equation into

$$\sum_{j,l} \alpha_{j,l} \log \left[ A(t) + B(t)e^{-\beta \Delta \varepsilon_{j,l}/2} \right] = \log \left[ A(t) + B(t)e^{-\beta \sum_{j,l} \alpha_{j,l} \Delta \varepsilon_{j,l}/2} \right] . \tag{A20}$$

Since the function  $\log (A + B \exp[\cdot])$  is non-linear, this equality generally cannot be satisfied for all times for a given set of boundary conditions  $\{\varepsilon_{j,l}(0), \varepsilon_{j,l}(\tau)\}_{j,l}$ . It is worth noting that there are some examples in which  $\varepsilon_k(t)$  is diverging for all times where this equality will be satisfied and k-th order interactions are not needed. Furthermore, let us point out that permutation invariance is not necessary here, we only need to require that  $\hat{h}^{(j)}(0) \neq \hat{h}^{(j)}(\tau)$  for all j. Therefore, generally eq. (A20) cannot be satisfied. The only way to solve the contradiction is by removing the assumption that the k-th order terms are missing. We conclude that, generally, all orders of interactions (from 2-body to N-body) are necessary to realize the geodesic trajectory.

## B. FISHER METRIC AND MINIMUM HELLINGER ANGLE ON CONDITIONAL PROBABILITIES

We analyze here the metric eq. (A13), also known as Fisher metric, for generic probability distributions having 1-way conditional dependence. That is, consider a probability vector of the form

$$p_{i_1,i_2,i_3,\dots,i_m} = p_{i_1}^{(1)} p_{i_2|i_1}^{(2)} p_{i_3|i_2}^{(3)} \dots p_{i_m|i_{m-1}}^{(m)},$$
(B1)

where  $p_{i_l|i_{l-1}}^{(l)}$  is the conditional probability of outcome  $i_l$  given the value of  $i_{l-1}$ . Moreover, we will use the intuitive notation for marginal probabilities, that is, for example

$$p_{i_2,i_5} := \sum_{i_1,i_3,i_4,i_6,\dots,i_m} p_{i_1,i_2,i_3,\dots,i_m} . \tag{B2}$$

Notice in particular that with this notation  $p_{i_1}^{(1)} \equiv p_{i_1}$ . For conditioned probabilities of the kind above eq. (B1), the Fisher metric takes a special decomposition, that is

$$\sum_{\vec{i}} \frac{dp_{\vec{i}}^2}{p_{\vec{i}}} = \sum_{i_1} \frac{dp_{i_1}^2}{p_{i_1}} + \sum_{i_1, i_2} p_{i_1} \frac{dp_{i_2|i_1}^{(2)^2}}{p_{i_2|i_1}} + \sum_{i_2, i_3} p_{i_2} \frac{dp_{i_3|i_2}^{(3)^2}}{p_{i_3|i_2}} + \dots + \sum_{i_{m-1}, i_m} p_{i_{m-1}} \frac{dp_{i_m|i_{m-1}}^{(m)^2}}{p_{i_m|i_{m-1}}} .$$
 (B3)

This equation will be our central observation in the following, and can be derived explicitly. *Proof of eq. (B3)*. We show here the case m=3, which can be generalized trivially. One has

$$\sum_{i_1,i_2,i_3} \frac{dp_{i_1,i_2,i_3}^2}{p_{i_1,i_2,i_3}} = \sum_{i_1,i_2,i_3} \frac{\left(dp_{i_1}^{(1)}p_{i_2|i_1}^{(2)}p_{i_3|i_2}^{(3)} + p_{i_1}^{(1)}dp_{i_2|i_1}^{(2)}p_{i_3|i_2}^{(3)} + p_{i_1}^{(1)}p_{i_2|i_1}^{(2)}dp_{i_3|i_2}^{(3)}\right)^2}{p_{i_1}^{(1)}p_{i_2|i_1}^{(2)}p_{i_3|i_2}^{(3)}},$$
(B4)

from which the numerator yields

$$\begin{split} \sum_{i_1,i_2,i_3} \frac{dp_{i_1}^{(1)^2}p_{i_2|i_1}^{(2)^2}p_{i_3|i_2}^{(3)^2} + p_{i_1}^{(1)^2}dp_{i_2|i_1}^{(2)^2}p_{i_3|i_2}^{(3)^2} + p_{i_1}^{(1)^2}p_{i_2|i_1}^{(2)^2}dp_{i_3|i_2}^{(3)^2}}{p_{i_1}^{(1)}p_{i_2|i_1}^{(2)}p_{i_3|i_2}^{(3)}} + & \text{cross-terms} \\ &= \sum_{i_1,i_2,i_3} \frac{dp_{i_1}^{(1)^2}}{p_{i_1}^{(1)}}p_{i_2|i_1}^{(2)}p_{i_3|i_2}^{(3)} + p_{i_1}^{(1)}\frac{dp_{i_2|i_1}^{(2)^2}}{p_{i_2|i_1}^{(2)}}p_{i_3|i_2}^{(3)} + p_{i_1}^{(1)}p_{i_2|i_1}^{(2)}p_{i_3|i_2}^{(3)} + cross-terms \\ &= \sum_{i_1} \frac{dp_{i_1}^{(2)^2}}{p_{i_1}} + \sum_{i_1,i_2} p_{i_1}\frac{dp_{i_2|i_1}^{(2)^2}}{p_{i_2|i_1}^{(2)}} + \sum_{i_2,i_3} p_{i_2}\frac{dp_{i_3|i_2}^{(3)^2}}{p_{i_3|i_2}^{(3)}} + \sum_{i_1,i_2,i_3} \text{cross-terms} \;, \quad \text{(B5)} \end{split}$$

where we simplified the expression by partially summing on the indices, using the identification  $p_{i_1}^{(1)} \equiv p_{i_1}$ , noticing that  $\sum_{i_1} p_{i_1} p_{i_2|i_1}^{(2)} = p_{i_2}$ , and using the normalization constraints on conditional probabilities.

To conclude the proof of eq. (B3) one needs to show that the cross-terms are null. This is indeed the case as

$$\sum_{i_1, i_2, i_3} dp_{i_1}^{(1)} dp_{i_2|i_1}^{(2)} p_{i_3|i_2}^{(3)} = 0 \text{ by summing on } i_3 \text{ first, and then on } i_2,$$
(B6)

$$\sum_{i_1, i_2, i_3} dp_{i_1}^{(1)} p_{i_2|i_1}^{(2)} dp_{i_3|i_2}^{(3)} = 0 \text{ by summing on } i_3,$$
(B7)

$$\sum_{i_1, i_2, i_3} p_{i_1}^{(1)} dp_{i_2|i_1}^{(2)} dp_{i_3|i_2}^{(3)} = 0 \text{ by summing on } i_3.$$
 (B8)

This concludes the proof.

## 1. Bounds on the Fisher distance between conditional probabilities

In this section, we prove a simple bound on the geodesic Fisher distance between probabilities with conditional dependence, for a specific form of eq. (B3). Namely, consider a probability vector of the form

$$p_{i_1,i_2,i_3} = p_{i_1}^{(1)} p_{i_2|i_1}^{(2)} p_{i_3}^{(3)}. (B9)$$

In the following we will assume full control on  $p_{i_1}^{(1)}$ , while  $p_{i_2|i_1}^{(2)}$  might be constrained to belong to a submanifold of conditional probabilities; finally the index  $i_3$  includes all the degrees of freedom that are uncorrelated to  $p_{i_1,i_2}$ . Moreover, our results will be general to any cardinality of the various indexes. As we are interested in Landauer erasures, and as a tool for simplification, we consider the distance to partially deterministic distributions. That is, probability vectors representing a deterministic outcome for  $i_1$  and  $i_2$ , which without loss of generality can be expressed (via re-indexing) always as

$$p_{i_1,i_2}^{\text{det}} = \delta_{i_1,0}\delta_{i_2,0} \ . \tag{B10}$$

where  $\delta_{i,j}$  is the Kronecker product. Notice that  $p^{\text{det}}$  is a particular case of the conditional form eq. (B1). We can now state our main Lemma

**Lemma 1.** The geodesic Fisher distance between any p of the form eq. (B9), when fixing  $p^{(3)}$  and assuming full control on  $p^{(1)}$ , is bounded by  $3\pi$ . When the final point is deterministic on  $i_1$  and  $i_2$ , the bound can be reduced to  $2\pi$ . That is, for fixed boundary conditions

$$p_{\vec{i}}(0) \equiv p_{i_1}^{(1)}(0) \, p_{i_2|i_1}^{(2)}(0) \, p_{i_3}^{(3)} \,, \quad \text{and} \quad p_{\vec{i}}(1) \equiv p_{i_1}^{(1)}(1) \, p_{i_2|i_1}^{(2)}(1) \, p_{i_3}^{(3)} \,, \tag{B11}$$

and assuming full control on  $p^{(1)}$  only, one has

$$\min_{p_{\vec{i}}(t) \equiv p_{i_1}^{(1)}(t) \, p_{i_2|i_1}^{(2)}(t) \, p_{i_3}^{(3)}} \int_0^1 dt \, \frac{\dot{p}_{\vec{i}}^2}{p_{\vec{i}}} \, \le 3\pi \, . \tag{B12}$$

Moreover, if the final point is of the form eq. (B10), the same bound reads

$$\min_{p_{\vec{i}}(t) \equiv p_{i_1}^{(1)}(t) \, p_{i_{3}|i_{1}}^{(2)}(t) \, p_{i_{3}}^{(3)}} \int_{0}^{1} dt \, \frac{\dot{p}_{\vec{i}}^{2}}{p_{\vec{i}}} \leq 2\pi \quad \text{when} \quad p_{\vec{i}}(1) \equiv \delta_{i_{1},0} \delta_{i_{2},0} p_{i_{3}}^{(3)} \,. \tag{B13}$$

As we are mainly interested in Landauer erasure, in the following applications we will mainly use the second inequality eq. (B13). The proof of the Lemma is constructive. That is, we show an explicit trajectory p(t) that satisfies eq. (B12) and eq. (B13).

*Proof of Lemma 1.* To prove Lemma 1, we consider a trajectory  $p^{\text{step}}(t)$  of the form eq. (B9)

$$p_{\vec{i}}^{\text{step}}(t) = p_{i_1}^{(1)}(t) \, p_{i_2|i_1}^{(2)}(t) \, p_{i_3}^{(3)} \tag{B14}$$

and use eq. (B3) specialized to such case as

$$\sum_{\vec{i}} \frac{dp_{\vec{i}}^2}{p_{\vec{i}}} = \sum_{i_1} \frac{dp_{i_1}^2}{p_{i_1}} + \sum_{i_1, i_2} p_{i_1} \frac{dp_{i_2|i_1}^{(2)^2}}{p_{i_2|i_1}} . \tag{B15}$$

We consider  $p^{\text{step}}(t)$  to follow 5 steps. In steps 1, 3, and 5, the distance traveled is bounded by  $\pi$ , while in steps 2 and 4 the distance is null. By the triangular inequality, the Lemma is then proven. In particular, if the final point is deterministic on  $i_1$  and  $i_2$ , Step 5 is not needed and the  $2\pi$  bound eq. (B13) follows. For more general endpoints Step 5 is needed, proving eq. (B12).

• Step 1. First  $p_{i_1}^{(1)}(t)$  goes to a deterministic distribution, w.l.o.g.

$$p_{i_1}^{(1)}(0) \to \delta_{i_1,1}$$
 (B16)

while  $p^{(2)}$  and (by hypothesis)  $p^{(3)}$  do not change. It follows from eq. (B15) that the distance consumed during this step is given only by  $\int \sum_{i_1} dt \frac{\dot{p}_{i_1}^{(1)^2}}{p_{i_1}}$ , and therefore by choosing the geodesic path between  $p_{i_1}^{(1)}(0)$  and  $\delta_{i_1,1}$ , one travels a distance that is bounded by  $d(p_{i_1}^{(1)}, \delta_{i_1,1}) \leq \pi$ .

• Step 2. Secondly,  $p_{i_2|i_1}^{(2)}$  is modified to its final value for all values of  $i_1$  except  $i_1 = 1$ ,

$$p_{i_2|i_1}^{(2)} \to p_{i_2|i_1}^{(2)}(1) \quad \forall i_1 \neq 1 ,$$
 (B17)

while all other probabilities are fixed. Notice that in the case of an erasure protocol, one has  $p_{i_2|i_1}^{(2)}(1) \equiv \delta_{i_2,0}$ . Due to  $p_{i_1}^{(1)} = \delta_{i_1,1}$  and eq. (B3) it follows that the distance traveled by the whole probability distribution is null (as the weight associated with  $i_1 \neq 1$  is null).

• Step 3. As a third step, one modifies again  $p_{i_1}^{(1)}$ , bringing it to a different deterministic value eq. (B10), i.e.

$$p_{i_1}^{(1)} = \delta_{i_1,1} \to \delta_{i_1,0}$$
 (B18)

Once again, the distance cost of this step is bounded by  $\pi$ , when taking the geodesic path from  $\delta_{i_1,1}$  to  $\delta_{i_1,0}$ .

 $\bullet$  Step 4. The fourth step takes  $p_{i_2|i_1=1}^{(2)}$  to its final value

$$p_{i_2|1}^{(2)} \to p_{i_2|1}^{(2)}(1)$$
 (B19)

at zero distance cost, due to  $p_{i_1=1}=0$ . Notice that at this point the full vector  $p_{i_2|i_1}^{(2)}(t)$  is in its final point and  $p^{(1)}$  is in a deterministic configuration.

• Step 5 (only for non-deterministic  $p_{i_1}^{(1)}(1)$ ). If the final desired point is non-deterministic in the  $i_1$  index, a final step is needed to complete

$$p_{i_1}^{(1)} = \delta_{i_1,0} \to p_{i_1}^{(1)}(1)$$
 (B20)

This step consists again of traveling a distance smaller than  $\pi$ .

Summarizing, the total effect of the above steps is that of transforming

$$p^{\text{step}}(0) = p_{i_1}^{(1)}(0)p_{i_2|i_1}^{(2)}(0)p_{i_3}^{(3)} \rightarrow p^{\text{step}}(1) = p_{i_1}^{(1)}(1)p_{i_2|i_1}^{(2)}(1)p_{i_3}^{(3)} \tag{B21}$$

at a distance cost bounded by  $2\pi$  for deterministic final points (erasure protocols), or  $3\pi$  otherwise. This proves Lemma 1.

## 2. Star Model

Consider the following Star-shaped Hamiltonian, featuring a central spin interacting with all the remaining ones, as depicted in Fig. B1

$$\hat{H}_{\text{star}}(t) = \varepsilon(t)\hat{\sigma}_z^{(1)} + \lambda_1(t)\sum_{i=2}^N \hat{\sigma}_z^{(i)} + \lambda_2(t)\sum_{i=2}^N \hat{\sigma}_z^{(1)}\hat{\sigma}_z^{(i)}.$$
 (B22)

This particular choice of interactions creates on the N-1 external spins an effective uniform magnetic field that is equal to  $\lambda_1 + \lambda_2$  when  $\hat{\sigma}_z^{(1)} = +1$ , while  $\lambda_1 - \lambda_2$  when  $\hat{\sigma}_z^{(1)} = -1$ . For this reason, the change of variable

$$\lambda_{+} = \lambda_1 + \lambda_2 , \quad \lambda_{-} = \lambda_1 - \lambda_2 , \qquad (B23)$$

makes the computation of the thermal probabilities and the partition function particularly easy. In particular, choosing temperature units in which  $\beta = 1$ ,

$$\mathcal{Z}_{\text{star}} = e^{-\varepsilon} (2\cosh\lambda_{+})^{N-1} + e^{\varepsilon} (2\cosh\lambda_{-})^{N-1} . \tag{B24}$$

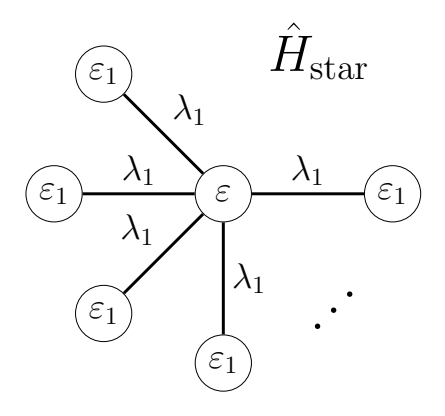


FIG. B1. Star model: a central spin

Moreover, one can notice how the Hamiltonian eq. (B22) leads to a thermal state  $\omega_{i_1,i_2}$  of the form eq. (B1) for m=2. In this case,  $i_1=\pm 1$  represents the two possible configurations of the central spin  $\hat{\sigma}_z^{(1)}$ , while  $\vec{i_2}=\{+1,-1\}^{N-1}$  labels the configuration of the remaining N-1 spins. It is straightforward to compute the probabilities of the central spin

$$\omega_{i_1=+1} = p_{i_1=+1}^{(1)} = \frac{e^{-\varepsilon} (2\cosh\lambda_+)^{N-1}}{e^{-\varepsilon} (2\cosh\lambda_+)^{N-1} + e^{\varepsilon} (2\cosh\lambda_-)^{N-1}} ,$$
 (B25)

$$\omega_{i_1=-1} = p_{i_1=-1}^{(1)} = \frac{e^{\varepsilon} (2\cosh\lambda_-)^{N-1}}{e^{-\varepsilon} (2\cosh\lambda_+)^{N-1} + e^{\varepsilon} (2\cosh\lambda_-)^{N-1}}.$$
 (B26)

Similarly, once the central spin is fixed i.e.  $\hat{\sigma}_z^{(1)} = i_1$ , the statistics of the remaining spins are defined by a homogeneous local magnetic field equal to  $\lambda_{i_1}$ ,

$$\omega_{\vec{i_2}|i_1} = p_{\vec{i_2}|i_1}^{(2)} = \frac{e^{-\lambda_{i_1} \sum_{i=2}^{N} \sigma_z^{(i)}}}{(2\cosh \lambda_{i_1})^{N-1}},$$
(B27)

which can be seen to factorize in parallel, that is

$$\omega_{\vec{i_2}|i_1} = \omega_{i_2|i_1}^{\otimes N-1} \ . \tag{B28}$$

The resulting metric becomes of the form

$$\sum_{i_1} \frac{d\omega_{i_1}^2}{\omega_{i_1}} + \sum_{i_1, \vec{i_2}} \omega_{i_1} \frac{d\omega_{\vec{i_2}|i_1}^2}{\omega_{\vec{i_2}|i_1}} = \sum_{i_1} \frac{d\omega_{i_1}^2}{\omega_{i_1}} + (N-1) \sum_{i_1, i_2} \omega_{i_1} \frac{d\omega_{i_2|i_1}^2}{\omega_{i_2|i_1}} . \tag{B29}$$

The above discussion clarifies how the Hamiltonian control eq. (B22) induces a control on the thermal statistics  $\hat{\omega}$  which is of the form eq. (B9). To bound the dissipation for such a model, we can therefore invoke Lemma 1, which provides the existence of an erasure protocol, starting from any initial thermal state  $\hat{\omega}$  to a final deterministic  $\hat{\omega}^{\text{det}}$ , with Fisher distance bounded by bound

$$L^{\text{Star}}(\omega, \omega^{\text{det}}) \le 2\pi$$
 , (B30)

which is translated to an upper bound on the dissipation

$$\tau \beta W_{\text{diss}} \equiv L^{\text{Star}}(\omega, \omega^{\text{det}})^2 \le 4\pi^2 \ .$$
 (B31)

## 3. Pyramid scheme

In this section, we generalize the Star model above and its minimally-dissipating protocol to a multi-layer structure, which importantly features only *short-range* interactions. Consider the pyramidal structure presented in Fig. B2,

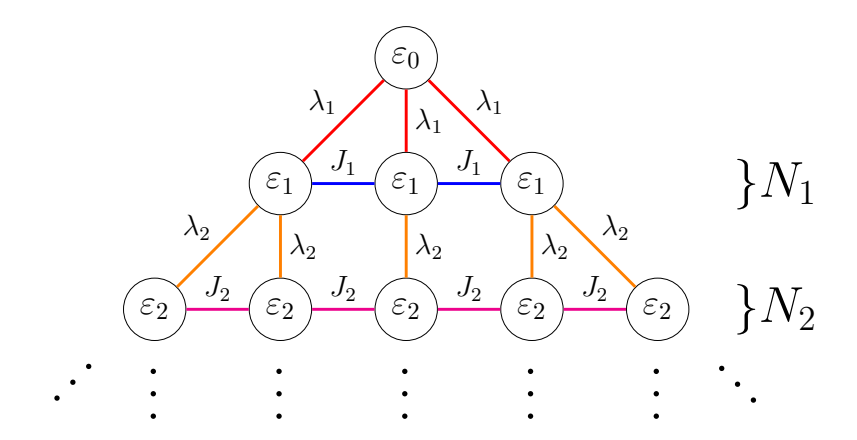


FIG. B2. Pyramid model with  $N_i = 1 + 2i$  (cf. eq. (B38)), in dimension D = 2.

which can be ascribed to a Hamiltonian of the form

$$\hat{H}_{\text{pyr}}(t) = \varepsilon(t)\hat{\sigma}_{z}^{(1)} + \varepsilon_{1}(t) \sum_{i_{1}=1}^{N_{1}} \hat{\sigma}_{z}^{(i_{1})} + \varepsilon_{2}(t) \sum_{i_{1}=1}^{N_{2}} \hat{\sigma}_{z}^{(i_{2})} + \dots + \varepsilon_{m-1}(t) \sum_{i_{m-1}=1}^{N_{m-1}} \hat{\sigma}_{z}^{(i_{m-1})}$$

$$+ \lambda_{1}(t) \sum_{i_{1}=1}^{N_{1}} \hat{\sigma}_{z}^{(1)} \hat{\sigma}_{z}^{(i_{1})} + \lambda_{2}(t) \sum_{i_{1},i_{2}=1,1}^{N_{1},N_{2}} \hat{\sigma}_{z}^{(i_{1})} \hat{\sigma}_{z}^{(i_{2})} + \dots + \lambda_{m-1} \sum_{i_{m-2},i_{m-1}=1,1}^{N_{m-2},N_{m-1}} \hat{\sigma}_{z}^{(i_{m-2})} \hat{\sigma}_{z}^{(i_{m-1})}$$

$$+ J_{1}(t) \sum_{i_{1}=1}^{N_{1}} \hat{\sigma}_{z}^{(i_{1})} \hat{\sigma}_{z}^{(i_{1}+1)} + J_{2}(t) \sum_{i_{2}=1}^{N_{2}} \hat{\sigma}_{z}^{(i_{2})} \hat{\sigma}_{z}^{(i_{2}+1)} + \dots + J_{m-1}(t) \sum_{i_{m-1}=1}^{N_{m-1}} \hat{\sigma}_{z}^{(i_{m-1})} \hat{\sigma}_{z}^{(i_{m-1}+1)} . \quad (B32)$$

We now consider an erasure protocol for the such pyramid model, starting from a completely uncorrelated thermal state of the form

$$\omega_{i_0,i_1,i_2,\dots,i_{m-1}}^{\text{initial}} = \omega_{i_0}\omega_{i_1}\omega_{i_2}\dots\omega_{i_{m-1}}, \qquad (B33)$$

corresponding to all  $\lambda_i = 0$  and  $J_i = 0$  in the Hamiltonian eq. (B32), to a final deterministic configuration

$$\omega_{i_0,i_1,i_2,\dots,i_{m-1}}^{\text{final}} = \delta_{i_0,0}\delta_{i_1,0}\delta_{i_2,0}\dots\delta_{i_{m-1},0} . \tag{B34}$$

To bound the total dissipation, we consider a step protocol of the form

$$\omega_{i_0}\omega_{i_1}\omega_{i_2}\dots\omega_{i_{m-1}} \to \delta_{i_0,0}\delta_{i_1,0}\omega_{i_2}\dots\omega_{i_{m-1}} \to \delta_{i_0,0}\delta_{i_1,0}\delta_{i_2,0}\dots\omega_{i_{m-1}} \to \cdots \to \delta_{i_0,0}\delta_{i_1,0}\delta_{i_2,0}\dots\delta_{i_{m-1},0} \ . \tag{B35}$$

That is, at each step k, an erasure is completed for the (k-1)-th and k-th layer, while the other layers are left untouched, for a total of m-1 steps. We now claim that each of the m-1 steps fulfills the hypothesis of Lemma 1 when appropriately using the controls of the Pyramid Hamiltonian eq. (B32). In fact, each k-step has boundary conditions of the form eq. (B11), by identifying  $p_{i_1}^{(1)} \leftrightarrow \omega_{i_{k-1}}^{\text{initial/final}}, p_{i_2|i_1}^{(2)} \leftrightarrow \omega_{i_k}^{\text{initial/final}}$ , and all the untouched degrees of freedom  $i_3 \leftrightarrow i_0, \ldots, i_{k-2}, i_{k+1}, \ldots, i_{m-1}$ . For the Lemma to be valid at each step, one needs to assume full-control on the  $i_{k-1}$  degrees of freedom. This is not the case in general, as each layer corresponds to a uniform Ising-like control. However, this is resolved with the following care: after step k-1, layer k-1 is in a deterministic  $\omega_{i_{k-1}} = \delta_{i_{k-1},0}$ . In such case, it is possible to modify the couplings  $J_{k-1} \to \infty$  to a fully ferromagnetic configuration without modifying  $\hat{\omega}$ . This produces an effective two-level system, i.e. all the spins up or all spins down at layer k-1, on which the local magnetic fields act as an effective full-control for such a two-level system.

Given the above discussion, we can bound the dissipation in the Pyramid model using the (m-1)-step protocol therein described, which corresponds to a total Fisher distance  $L \leq 2(m-1)\pi$ . It then follows that the dissipations are bounded by

$$\tau \beta W_{\text{diss}} \equiv L^2 \le 4(m-1)^2 \pi^2 \,,$$
 (B36)

while the total number of spins is

$$N = N_0 + \dots + N_{m-1} + N_{m-1} . \tag{B37}$$

In standard pyramids with spatial dimension D, we can assume that

$$N_i = (c + a(i-1))^{D-1}$$
(B38)

for some positive integers c and a. This corresponds to a pyramid-shaped Hamiltonian in spatial dimension D having the first layer increase with size a. For example, the pyramid in Fig. B2 corresponds to c = 1 and a = 2. In such a model the total number of spins scales as

$$N = \sum_{i=0}^{m-1} N_i = \sum_{i=0}^{m-1} (1+ai)^{D-1} \approx \frac{a^{D-1}}{D} m^D$$
(B39)

at leading order.

It follows that the dissipation eq. (B36) can be expressed, at leading order,

$$\tau \beta W_{\rm diss} \approx \frac{4\pi^2}{a^2} (aDN)^{\frac{2}{D}}$$
 (B40)

The above expression shows that the scaling of the dissipation in such models is sub-linear in N as soon as D > 2, (e.g. if the pyramid is 3-dimensional D = 3). The obtained dissipation for D = 2 and D = 3 is showcased in Fig. B3 where it's contrasted to the minimal dissipation found for the other models.

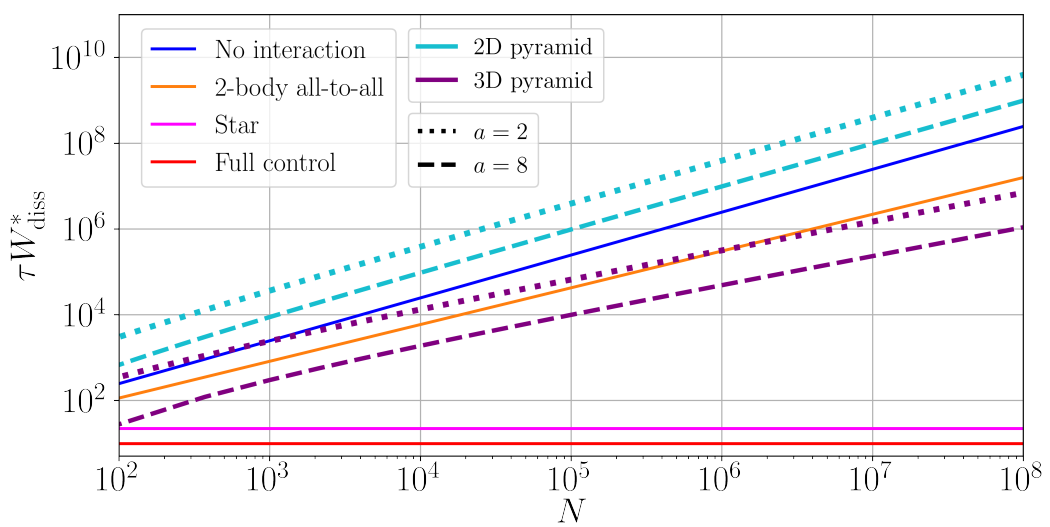


FIG. B3. Minimal dissipation for the erasure of N spins in the non-interacting case and full control scenario. The dissipation of the protocol described in Lemma 1 for the erasure of N spins in the star model, and its repeated application for pyramid models in 2-D and 3-D with apertures a=2 and a=8. And an extrapolation of the fit of the minimal dissipation in the all-to-all model (to compare the scaling)  $W_{\rm diss}^{*,\rm all}=\alpha N^x$  with x=0.857 and  $\alpha=2.20$ .

## C. NUMERICS FOR MANY-BODY SYSTEMS

In this section, we explain the techniques used to find the protocols that minimize dissipation for the two-body all-to-all system of spins and the 1-D Ising chain. The Hamiltonians of these systems are the following

$$\hat{H}_{\text{all}}(t) = \varepsilon(t) \sum_{i=1}^{N} \hat{\sigma}_{z}^{(i)} + \frac{1}{2} J(t) \sum_{i,j=1}^{N} \hat{\sigma}_{z}^{(i)} \hat{\sigma}_{z}^{(j)} , \qquad (C1)$$

$$\hat{H}_{\rm nn}(t) = \varepsilon(t) \sum_{i=1}^{N} \hat{\sigma}_z^{(i)} + \frac{1}{2} J(t) \sum_{i=1}^{N} \hat{\sigma}_z^{(i)} \hat{\sigma}_z^{(i+1)} . \tag{C2}$$

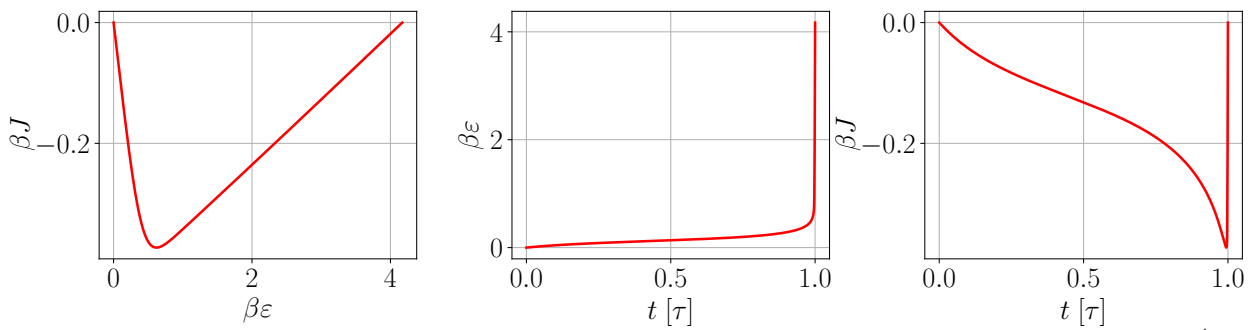


FIG. C4. Optimal finite-time protocol for approximate erasure ( $\varepsilon(\tau) = 4k_BT$  which has an erasure error of  $3 \cdot 10^{-4}$ ) in the all-to-all spin model. This protocol is computed for N = 10.

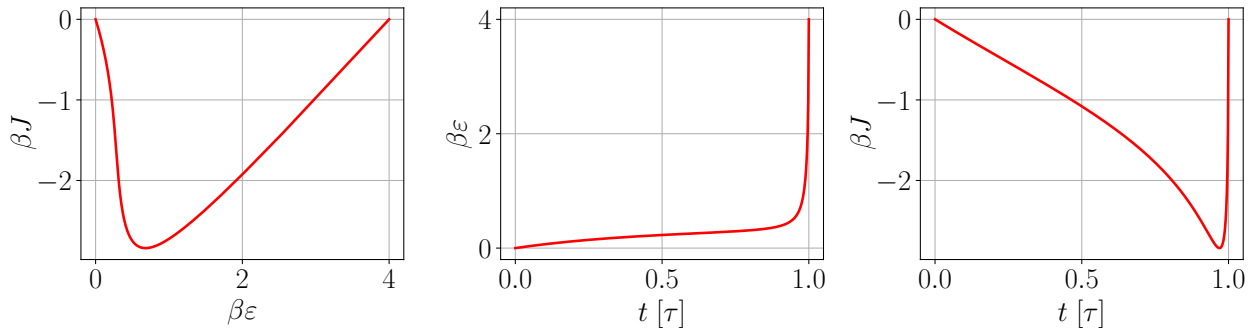


FIG. C5. Optimal finite-time protocol for approximate erasure  $(\varepsilon(\tau) = 4k_BT)$  which has an erasure error of  $3 \cdot 10^{-4}$ ) in the 1-D Ising chain model. This protocol is the same for all values of N.

To find the optimal driving we use the formalism of geometric thermodynamics which explained in the Sec. A. In particular, the optimal driving protocols solve the geodesic equation eq. (A6). To compute it we need the Christoffel symbols, which can be computed from derivatives of the partition function eq. (A9). In both scenarios at hand, the geodesic equation cannot be solved analytically. Therefore we want to be able to express the partition function (in particular its derivatives) in numerically tractable ways. For the all-to-all case, we can write the partition function and its derivatives as follows

$$\mathcal{Z}_{\text{all}} = \sum_{k=0}^{N} \binom{N}{k} e^{-\beta E_k} , \qquad (C3)$$

$$\beta^{-2} \frac{\partial^2 \ln \mathcal{Z}_{\text{all}}}{\partial \gamma^i \partial \gamma^j} = \langle \hat{X}_i \hat{X}_j \rangle - \langle \hat{X}_i \rangle \langle \hat{X}_j \rangle , \qquad (C4)$$

$$-\beta^{-3} \frac{\partial^{3} \ln \mathcal{Z}_{\text{all}}}{\partial \gamma^{i} \partial \gamma^{j} \partial \gamma^{k}} = \langle \hat{X}_{i} \hat{X}_{j} \hat{X}_{k} \rangle - \langle \hat{X}_{i} \hat{X}_{j} \rangle \langle \hat{X}_{k} \rangle - \langle \hat{X}_{i} \hat{X}_{k} \rangle \langle \hat{X}_{j} \rangle - \langle \hat{X}_{k} \hat{X}_{j} \rangle \langle \hat{X}_{i} \rangle + 2 \langle \hat{X}_{i} \rangle \langle \hat{X}_{k} \rangle \langle \hat{X}_{k} \rangle ,$$
(C5)

where we defined  $E_k = \varepsilon(2k-N) + \frac{1}{2}J(2k-N)^2$ ,  $\gamma = (\varepsilon, J)$ ,  $\hat{X}_1 = \sum_{k=1}^N \hat{\sigma}_z^{(k)}$ ,  $\hat{X}_2 = \frac{1}{2}\sum_{k,l=1}^N \hat{\sigma}_z^{(k)}\hat{\sigma}_z^{(l)}$ , and the expectation values are computed with respect to the thermal state. Thanks to eq. (C3) we can efficiently compute (for large N) these expectation values, as we get the following expression

$$\langle \hat{X}_{i_1} \hat{X}_{i_2} \dots \hat{X}_{i_j} \rangle = \frac{1}{\mathcal{Z}_{\text{all}}} \sum_{k=0}^{N} \binom{N}{k} \frac{\partial E_k}{\partial \gamma^{i_1}} \frac{\partial E_k}{\partial \gamma^{i_2}} \dots \frac{\partial E_k}{\partial \gamma^{i_j}} e^{-\beta E_k} . \tag{C6}$$

Whereas for the 1-D Ising chain we can compute the partition function in a more contained analytical expression thanks to the transfer matrix formalism (with exponentially small corrections in N)

$$\log \mathcal{Z}_{\rm nn} = -\frac{\beta J N}{2} + N \log \left[ \cosh(\beta \varepsilon) + \sqrt{\sinh(\beta \varepsilon)^2 + e^{2\beta J}} \right], \tag{C7}$$

from which we can compute analytically the expression for its derivatives and solve the geodesic equations efficiently with numerical tools. Let us remark here that since  $\log \mathcal{Z}_{nn}$  is linear in N it is immediate that the same is true for

its derivatives and therefore the dissipated work. Furthermore, it is quite clear from eq. (A7) that the differential equations will not depend on N, therefore the geodesic will also be independent of N.

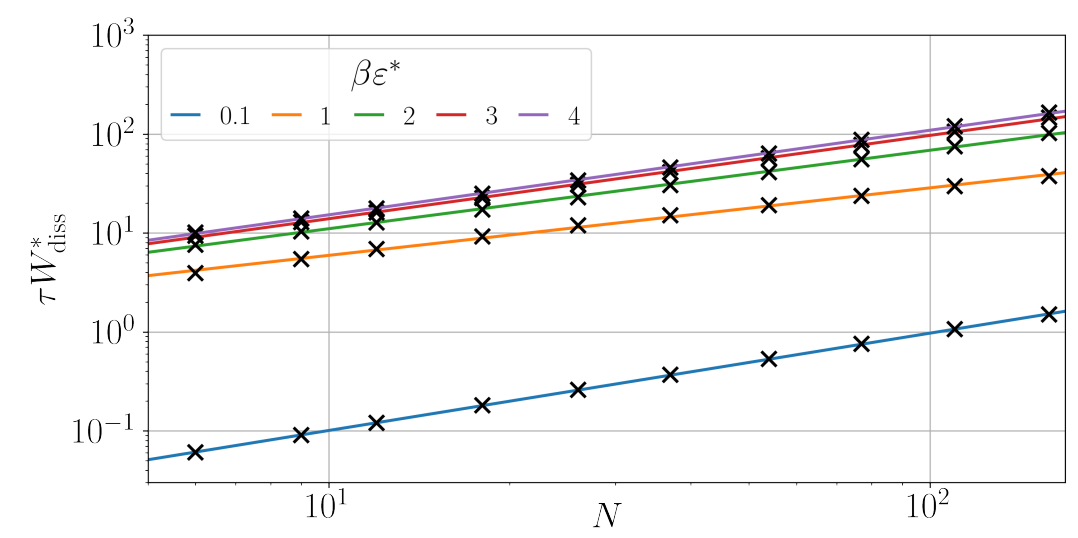


FIG. C6. Scaling of the dissipation with respect to N for different values of  $\varepsilon^*$ .

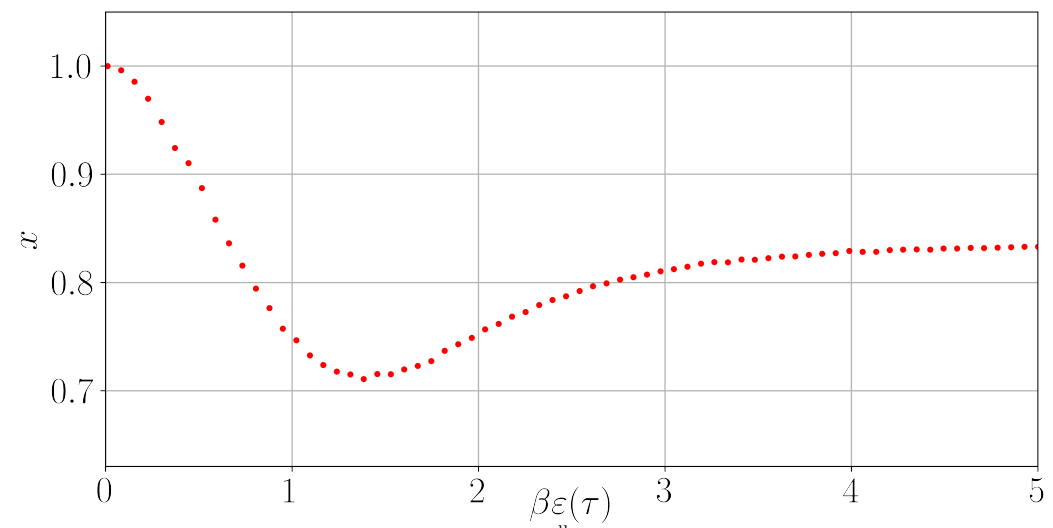


FIG. C7. Dependence of the exponent x of the dissipation  $W_{\text{diss}}^{*,\text{all}} = \alpha N^x$  on the boundary condition  $\beta \varepsilon(\tau)$  (with  $\varepsilon(0) = 0$ ). The fit is achieved for numerical data up to N = 150.

For both models, we end up with a system of two second-order non-linear differential equations. By the structure of the geodesic equations, we can turn it into a system of four first-order non-linear differential equations of the type  $\frac{d\vec{x}}{dt} = \vec{f}(\vec{x})$  with  $\vec{x} = (\varepsilon, J, \dot{\varepsilon}, \dot{J})$ . Here we want to enforce the boundary conditions  $\varepsilon(0) = J(0) = J(\tau)$  and  $\varepsilon(\tau) = \varepsilon^*$  (where  $\varepsilon^* \gg k_B T$  for erasure), but famously boundary value problems are very difficult to solve numerically. In this particular case, we can exploit the fact that we have only two parameters and that geodesics never cross paths (they describe a flow in the parameter space). Therefore there is a bijection between the ratio of the initial velocities  $\dot{\varepsilon}(0)/\dot{J}(0)$  and the final value  $\varepsilon^*$ , this allows us to turn the boundary value problem into solving multiple initial value problems for different ratios of the initial velocities until we find the initial conditions that match the desired boundary conditions.

Using these techniques we can find the geodesics for (approximate) erasure in both models, an example for each is showcased in Fig. C4 and Fig. C5. As is explained in the main text, in the case of the all-to-all spin model the dissipation scales sub-linearly with respect to N. To quantify this effect we compute the dissipation for multiple values of N (19 values for Fig. 1 and 10 values for Fig. 2, all between N = 5 and N = 150) and fit a power law. The relative errors of all the fits showcased in this study are 0.5% or less. In Fig. C6 we showcase more examples of this

sub-linear scaling for different values of  $\varepsilon^*$  and how they are each well described by a power law. Then, in Fig. C7 we collect all the fitted exponents to showcase the dependence on the boundary conditions. Where x is plotted as a function of  $\beta\varepsilon(\tau)$ , which illustrates that the collective effects developed here are genuinely process-dependent.

[1] P. Abiuso, H. J. D. Miller, M. Perarnau-Llobet, and M. Scandi, Entropy 22, 1076 (2020).

Letter

## Pareto-optimal cycles for power, efficiency and fluctuations of quantum heat engines using reinforcement learning

Paolo A. Erdman , <sup>1</sup> Alberto Rolandi , <sup>2</sup> Paolo Abiuso , <sup>3</sup> Martí Perarnau-Llobet , <sup>2</sup>, \* and Frank Noé , <sup>6</sup>,1,4,5,† 

<sup>1</sup>Department of Mathematics and Computer Science, Freie Universität Berlin, Arnimallee 6, 14195 Berlin, Germany 

<sup>2</sup>Department of Applied Physics, University of Geneva, 1211 Geneva, Switzerland 

<sup>3</sup>ICFO Institut de Ciències Fotòniques, The Barcelona Institute of Science and Technology, 08860 Castelldefels (Barcelona), Spain 

<sup>4</sup>Department of Physics, Freie Universität Berlin, Arnimallee 6, 14195 Berlin, Germany 

<sup>5</sup>Department of Chemistry, Rice University, Houston, Texas 77005, USA 

<sup>6</sup>Microsoft Research Al4Science, Karl-Liebknecht Str. 32, 10178 Berlin, Germany



(Received 2 August 2022; revised 4 December 2022; accepted 15 March 2023; published 27 April 2023)

The full optimization of a quantum heat engine requires operating at high power, high efficiency, and high stability (i.e., low power fluctuations). However, these three objectives cannot be simultaneously optimized—as indicated by the so-called thermodynamic uncertainty relations—and a systematic approach to finding optimal balances between them including power fluctuations has, as yet, been elusive. Here we propose such a general framework to identify Pareto-optimal cycles for driven quantum heat engines that trade off power, efficiency, and fluctuations. We then employ reinforcement learning to identify the Pareto front of a quantum dot-based engine and find abrupt changes in the form of optimal cycles when switching between optimizing two and three objectives. We further derive analytical results in the fast- and slow-driving regimes that accurately describe different regions of the Pareto front.

DOI: 10.1103/PhysRevResearch.5.L022017

Introduction. Stochastic heat engines are devices that convert between heat and work on the nanoscale [1-3]. Steady-state heat engines (SSHEs) perform work against external thermodynamic forces (e.g., a chemical potential difference) after reaching a nonequilibrium steady state [4], whereas periodically driven heat engines (PDHEs) perform work against external driving fields through time-dependent cycles [5]. The performance of heat engines is usually characterized by the output power and efficiency, and their optimization has been thoroughly addressed in literature [6–30]. However, in contrast to their macroscopic counterpart, the performance of quantum and microscopic engines is strongly influenced by power fluctuations. Although early works have started optimizing power fluctuation [31–35], a framework to fully optimize the performance of microscopic heat engines that accounts for power fluctuations is currently lacking; this Letter fills this void.

An ideal engine operates at high power, high efficiency, and low-power fluctuations; however, such quantities usually cannot be optimized simultaneously, but one must seek tradeoffs. In SSHEs, a rigorous manifestation of this trade-off is given by the thermodynamic uncertainty relations [36–44].

Published by the American Physical Society under the terms of the Creative Commons Attribution 4.0 International license. Further distribution of this work must maintain attribution to the author(s) and the published article's title, journal citation, and DOI.

For "classical" stochastic SSHEs (i.e., in the absence of quantum coherence) operating between two Markovian reservoirs at inverse temperatures  $\beta_{\rm C}$  (cold) and  $\beta_{\rm H}$  (hot), they read [38]

$$\xi \equiv \frac{2}{\beta_{\rm C}} \frac{\langle P \rangle}{\langle \Delta P \rangle} \frac{\eta}{\eta_{\rm c} - \eta} \leqslant 1, \tag{1}$$

where  $\langle P \rangle$  and  $\langle \Delta P \rangle$  are, respectively, the average power and power fluctuations,  $\eta$  is the efficiency, and  $\eta_c \equiv 1 - \beta_H/\beta_C$  is the Carnot efficiency. Such thermodynamic uncertainty relations imply, for example, that high efficiency can only be attained at the expense of low-power or high-power fluctuations. The thermodynamic uncertainty relation inequality (1) can be violated with quantum coherence [45–53] and in PDHEs [54–59]. This has motivated various generalized thermodynamic uncertainty relations [60–65], in particular, for time-symmetric driving [40,55] and slowly driven stochastic engines [66,67].

Despite their importance, thermodynamic uncertainty relations provide an incomplete picture of the trade-off: whereas high values of  $\xi$  may appear more favorable, this does not give us any information on the individual objectives. Indeed, Refs. [56,66] have shown that high values of  $\xi$  can be achieved in the limit of vanishing power, whereas often the goal is to operate at high power or efficiency.

In this Letter, we propose a framework to optimize arbitrary trade-offs among power, efficiency and power fluctuations in arbitrary PDHEs described by Lindblad dynamics [68–71]; this framework enables the use of various optimization techniques, such as the Pontryagin minimum principle [72] or reinforcement learning (RL) [73] to find Pareto-optimal cycles, i.e., those cycles where no objective can be

<sup>\*</sup>marti.perarnaullobet@unige.ch

<sup>†</sup>frank.noe@fu-berlin.de

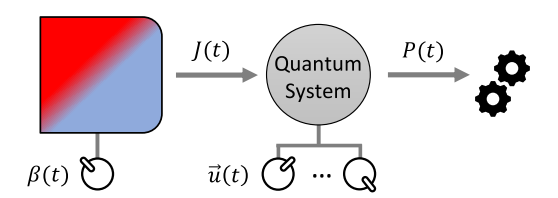


FIG. 1. A quantum system (gray circle) is coupled to a thermal bath (left box) characterized by a controllable inverse temperature  $\beta(t)$ . The coupling produces a heat flux J(t). Control parameters  $\vec{u}(t)$  allow us to control the state of the system and the power P(t) extracted from the system.

further improved without sacrificing another one. We then employ RL to fully optimize a quantum dot- (QD-) based heat engine [74]. We characterize the Pareto front, i.e., the set of values  $\{\langle P \rangle, \langle \Delta P \rangle, \eta \}$  corresponding to Pareto-optimal cycles, and evaluate the thermodynamic uncertainty relation ratio  $\xi$  on such optimal cycles. Furthermore, we derive analytical results for the Pareto front and  $\xi$  in the fast- [6,8,20,23,27,75,76] and slow- [9,26,77–88] driving regimes, i.e., when the period of the cycle is, respectively, much shorter or much longer than the thermalization timescale of the system.

Multiobjective optimization of quantum heat engines. We describe a PDHE as a quantum system coupled to a heat bath whose inverse temperature  $\beta(t)$  can be tuned in time between two extremal values  $\beta_H$  and  $\beta_C$  with  $\beta_H \leq \beta_C$  (Fig. 1). The coupling produces a heat flux J(t) from the bath to the quantum system. The PDHE is further controlled by timedependent control parameters  $\vec{u}(t)$  that allow exchanging work with the system, producing power P(t). A thermodynamic cycle is then described by periodic functions  $\beta(t)$  and  $\vec{u}(t)$ with period  $\tau$ . This framework includes standard PDHEs in which the system is sequentially put in contact with two baths [by abruptly changing the values of  $\beta(t)$ ] and cases where  $\beta(t)$  varies smoothly in time [66,84,87,89–92]. We assume that the dynamics of the system is described by a Markovian master equation, i.e., that the reduced density matrix  $\rho_t$  of the quantum system satisfies

$$\dot{\rho}_t = \mathcal{L}_{\vec{u}(t),\beta(t)}\rho_t,\tag{2}$$

where  $\mathcal{L}_{\vec{u}(t),\beta(t)}$  is the Lindbladian describing the evolution of the system [70].

We are interested in characterizing the performance of PDHEs computing the average power  $\langle P \rangle$ , average irreversible entropy production  $\langle \Sigma \rangle$ , and average power fluctuations  $\langle \Delta P \rangle$  in the asymptotic limit cycle [66,89,90], i.e., in the limit of infinite repetitions of the cycle. In such a limit,  $\rho_t$  becomes periodic with the same periodicity  $\tau$  of the control (see the Supplemental Material [93]).

Given the density-matrix  $\rho_t$ , the calculation of  $\langle P \rangle$  and  $\langle \Sigma \rangle$  can be performed using the standard approach first put forward in Ref. [94] (see the Supplemental Material [93] for details). Defining the time-average  $\langle O \rangle$  of an arbitrary quantity O(t) as  $\langle O \rangle \equiv \tau^{-1} \int_0^\tau O(t) dt$ , we can calculate  $\langle P \rangle$  and  $\langle \Sigma \rangle$  by averaging

$$P(t) = -\text{Tr}[\rho_t \dot{H}_{\vec{u}(t)}], \qquad \Sigma(t) = -\text{Tr}[\dot{\rho}_t H_{\vec{u}(t)}]\beta(t). \quad (3)$$

Note that we compute the entropy production  $\Sigma(t) \equiv -J(t)\beta(t)$  neglecting the entropy variation  $\Delta S$  of the quantum system since the periodicity of the state in the limiting cycle implies that  $\Delta S = 0$  after each repetition of the cycle.

The average fluctuations  $\langle \Delta P \rangle$ , however, cannot be expressed as a time average of a function of the state  $\rho_t$  since they involve a two-point correlation function. Indeed, from Ref. [82], we can express them as

$$\langle \Delta P \rangle = \lim_{T \to \infty} \frac{1}{T} \int_0^T dt \, \text{Tr}[s_t \dot{H}_{\vec{u}(t)}], \tag{4}$$

where we define

$$s_t \equiv \int_0^t dt' P(t, t') [\dot{H}_{\vec{u}(t')} \rho_{t'}] + \langle w \rangle_t \rho_t + \text{H.c.}$$
 (5)

In Eq. (5)  $P(t,t') \equiv \overleftarrow{T} \exp[\int_{t'}^{t} dt'' \mathcal{L}_{\vec{u}(t''),\beta(t'')}]$  is the propagator,  $\langle w \rangle_t \equiv -\int_0^t dt' \operatorname{Tr}[\rho_{t'} \dot{H}_{\vec{u}(t')}]$  is the total average work extracted between time 0 and t, and H.c. represents the complex conjugate of the right-hand side.

Here, we overcome the difficulty of computing nested integrals and two-point correlation function in Eqs. (4) and (5) by noting that  $s_t$  is a traceless Hermitian operator that satisfies

$$\dot{s}_t = \mathcal{L}_{\vec{u}(t), \beta(t)} s_t + \{ \rho_t, \dot{H}_{\vec{u}(t)} \} - 2 \operatorname{Tr}[\rho_t \dot{H}_{\vec{u}(t)}] \rho_t, \tag{6}$$

and becomes periodic with period  $\tau$  in the limiting cycle (see the Supplemental Material [93]).

Therefore, by considering  $(\rho_t, s_t)$  as an "extended state" satisfying the equations of motion in (2) and (6) in the time-interval  $[0, \tau]$  with periodic boundary conditions, we can compute  $\langle P \rangle$ ,  $\langle \Sigma \rangle$ , and  $\langle \Delta P \rangle$  as time averages of P(t),  $\Sigma(t)$ , and  $\Delta P(t)$ , where P(t) and  $\Sigma(t)$  are defined in Eq. (3), and where

$$\Delta P(t) \equiv \text{Tr}[s_t \dot{H}_{\vec{u}(t)}]. \tag{7}$$

Note that these are now linear functionals of the extended state.

To identify Pareto-optimal cycles, we introduce the dimensionless figure of merit

$$\langle F \rangle = a \frac{\langle P \rangle}{P_{\text{max}}} - b \frac{\langle \Delta P \rangle}{\Delta P(P_{\text{max}})} - c \frac{\langle \Sigma \rangle}{\Sigma(P_{\text{max}})},$$
 (8)

where  $a, b, c \ge 0$  are three scalar weights, satisfying a + b + c = 1, that determine how much we are interested in each of the three objectives, and  $P_{\text{max}}$ ,  $\Delta P(P_{\text{max}})$ , and  $\Sigma(P_{\text{max}})$  are, respectively, the average power, fluctuations and entropy production of the cycle that maximizes the power. Note that, given the relation between entropy production and efficiency, cycles that are Pareto optimal for  $\{\langle P \rangle, \langle \Delta P \rangle, \eta \}$ , are also Pareto optimal for  $\{\langle P \rangle, \langle \Delta P \rangle, \eta \}$ , see the Supplemental Material [93]). The positive sign in front of  $\langle P \rangle$  in Eq. (8) ensures that we are maximizing the power, while the negative sign in front of  $\langle \Delta P \rangle$  and  $\langle \Sigma \rangle$  ensures that we are minimizing power fluctuations and the entropy production. Interestingly, if convex, it has been shown that the full Pareto front can be identified repeating the optimization of  $\langle F \rangle$  for many values of a, b, and c [95,96].

Since  $\langle F \rangle$  is a linear combination of the average thermodynamic quantities, using Eqs. (3) and (7) we can express  $\langle F \rangle$  as a time integral of a function of the extended state  $(\rho_t, s_t)$  and

of the controls  $\vec{u}(t)$  and  $\beta(t)$ ,

$$\langle F \rangle = \int_0^\tau G[\rho_t, s_t, \vec{u}(t), \beta(t)] dt, \tag{9}$$

where  $G[\rho_t, s_t, \vec{u}(t), \beta(t)]$  is a suitable function. The optimization of  $\langle F \rangle$  in this form is precisely the type of problem that can be readily tackled using optimization techniques, such as the Pontryagin minimum principle [72] or RL [73]. In this Letter, we employ the latter.

*QD heat engine.* In the following, we compute Paretooptimal cycles in a minimal heat engine consisting of a two-level system coupled to a fermionic bath with flat density of states. This represents a model of a single-level QD [6,10,74]. The Hamiltonian reads

$$H_{u(t)} = u(t)\frac{E_0}{2}\sigma_z,\tag{10}$$

where u(t) is our single control parameter,  $E_0$  is a fixed energy scale, and  $\sigma_z$  is a Pauli matrix. Denoting with  $|1\rangle$  the excited state of  $H_{u(t)}$ , and defining  $p_t \equiv \langle 1|\rho_t|1\rangle$  as the probability of being in the excited state, the Lindblad equation (2) becomes  $\dot{p}_t = -\gamma(p_t - \pi_{\bar{u}(t),\beta(t)})$ , where  $\gamma^{-1}$  is the thermalization timescale arising from the coupling between system and bath, and  $\pi_{\bar{u}(t),\beta(t)} = f[\beta(t)E_0u(t)]$  is the excited level population of the instantaneous Gibbs state, with  $f(x) \equiv (1+e^x)^{-1}$  [23].

Optimal cycles with RL and analytical results. We optimize  $\langle F \rangle$  of the QD heat engine using three different tools: RL, analytics in the fast-driving regime, and analytics in the slow-driving regime.

The RL-based method allows us to numerically optimize  $\langle F \rangle$  without making any approximations on the dynamics, exploring all possible (time-discretized) time-dependent controls  $\beta(t)$  and u(t) subject to the constraints  $\beta(t) \in [\beta_H, \beta_C]$  and  $u(t) \in [u_{\min}, u_{\max}]$  (thus, beyond fixed structures, such as Otto cycles), and identifying automatically the optimal period. The RL method, based on the soft actor-critic algorithm [97–99] and generalized from [100,101], additionally includes the crucial impact of power fluctuations and identifies Pareto-optimal cycles (see the Supplemental Material [93] for technical details and for benefits of using RL). Machine learning methods have been employed for other quantum thermodynamic [102–104] and quantum control [105–117] tasks.

The fast-driving regime assumes that  $\tau \ll \gamma^{-1}$ . Interestingly, without any assumption on the driving speed, we show [93] that any trade-off between power and entropy production [b=0 in Eq. (8)] in the QD engine is maximized by Otto cycles in the fast-driving regime, i.e., switching between two values of  $\beta(t)$  and u(t) "as fast as possible" [23,27]. We thus expect such "fast-Otto cycles" to be nearly optimal in the high power or efficiency regime. Moreover, we derive analytical expressions to compute and optimize  $\{\langle P \rangle, \langle \Delta P \rangle, \langle \Sigma \rangle\}$  efficiently in arbitrary systems in the fast-driving regime [93].

The slow-driving regime corresponds to the opposite limit, i.e.,  $\tau \gg \gamma^{-1}$ . Since entropy production and power fluctuations can be minimized by considering quasistatic cycles (see, e.g., Refs. [56,66]), we expect this regime to be nearly optimal in the low-power regime, i.e., for low values of a in Eq. (8). To make analytical progress in this regime, we maximize Eq. (8) assuming a finite-time Carnot cycle (see

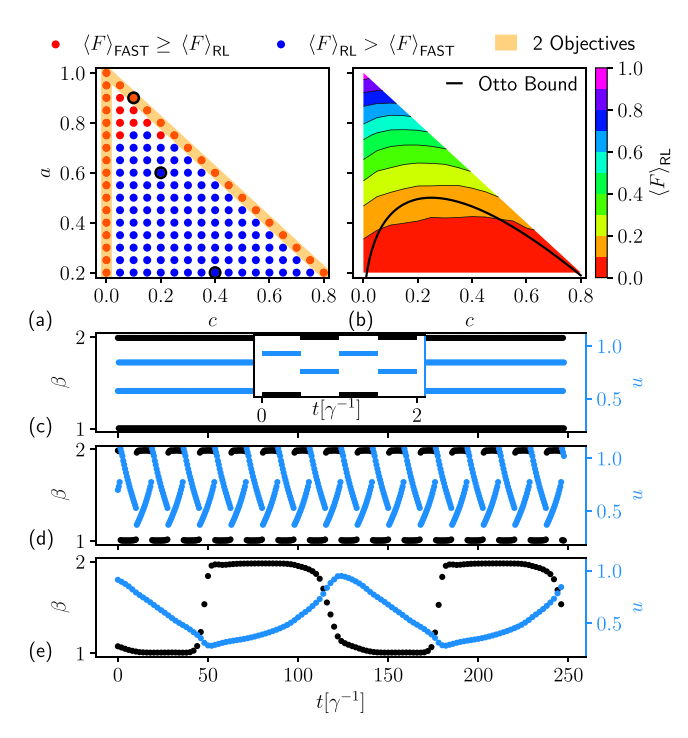


FIG. 2. Optimization of  $\langle F \rangle$  at different values of a and c with b=1-a-c, for a QD-based PDHE. Each dot in panel (a) displays, as a function of c and a, whether  $\langle F \rangle_{RL} > \langle F \rangle_{FAST}$  (blue dots) or not (red dots). Points with  $a \sim 0$  are not displayed since, in such a regime, optimal cycles become infinitely long (to minimize entropy production and fluctuations) and the RL method does not converge reliably [93]. (b) Contour plot of  $\langle F \rangle_{RL}$ , as a function of c and a, using the data points of (a). The black line represents the curve below which  $\langle F \rangle_{FAST} = 0$ . (c)—(e) cycles, described by piecewise constant values of  $\beta$  (black dots) and a (blue dots) as a function of a, identified at the three values of a and a highlighted in black in panel (a) (respectively, from top to bottom). The inset in panel (c) represents a zoom into the corresponding cycle, which is a fast-Otto cycle. Parameters: a0 and a1, a1, a2, a3, a4, a5.

the Supplemental Material [93]). The obtained results naturally generalize previous considerations for low-dissipation engines [9,10,13,14,21,22,26] to account for the role of fluctuations (see also Ref. [32]). The main technical tool is the geometric concept of "thermodynamic length" [77,86], which yields the first-order correction in  $(\gamma \tau)^{-1}$  from the quasistatic limit.

We now present the results. Each point in Fig. 2(a) corresponds to a separate optimization of  $\langle F \rangle$  with weights c and a displayed on the x-y axis. Since b=1-a-c, points lying on the sides of the triangle (highlighted in yellow) correspond to optimizing the trade-off between two objectives, whereas points inside the triangle take all three objectives into account. Denoting the figure of merit optimized with RL and with fast-Otto cycles with  $\langle F \rangle_{RL}$  and  $\langle F \rangle_{FAST}$ , in Fig. 2(a), we show blue (red) dots when  $\langle F \rangle_{RL} > \langle F \rangle_{FAST}$  ( $\langle F \rangle_{RL} \le \langle F \rangle_{FAST}$ ), whereas Fig. 2(b) is a contour plot of  $\langle F \rangle_{RL}$ . As expected, there are red dots when b=0 (along the hypotenuse), but it turns out that fast-Otto cycles are optimal also when c=0. However, as soon as all three weights are finite, the optimal cycles identified with RL change abruptly and

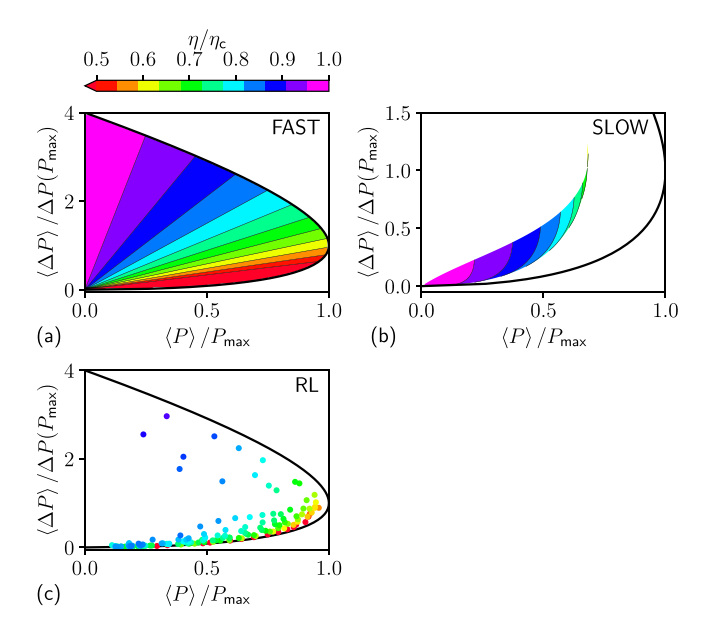


FIG. 3. Pareto front found optimizing  $\langle F \rangle$  with fast-Otto cycles in the limit of small temperature differences [panel (a)], optimizing  $\langle F \rangle$  in the slow-driving regime [panel (b)], and numerically using RL [panel (c)]. The system parameters are as in Fig. 2. All panels display  $\langle \Delta P \rangle / \Delta P (P_{\text{max}})$  as a function of  $\langle P \rangle / P_{\text{max}}$  (x axis) and of  $\eta/\eta_c$  (color). The black curve represents the outer border of the Pareto front derived analytically in the Supplemental Material [93].

outperform fast-Otto cycles. Furthermore, we note that whereas  $\langle F \rangle_{RL}$  is positive for all values of the weights,  $\langle F \rangle_{FAST} = 0$  below the black curve shown in Fig. 2(b) (see the Supplemental Material [93] for its analytic expression).

To visualize the changes in protocol space, in Figs. 2(c)-2(e) we show the cycles identified with RL at the three different values of the weights highlighted by a black circle in Fig. 2(a) (respectively, from top to bottom). Since RL identifies piecewise constant controls, the cycle is displayed as dots corresponding to the value of  $\beta(t)$  (black dots) and u(t) (blue dots) at each small time step. First, we note that the inverse temperature abruptly switches between  $\beta_{\rm H}$  and  $\beta_{\rm C}$ for all values of the weights so that, in this engine, no gain arises when smoothly varying the temperature. As expected, the cycle identified by RL in Fig. 2(c), corresponding to the black point on the hypotenuse in Fig. 2(a), is a fast-Otto cycle (a "zoom" in a short-time interval is shown in the inset). However, moving down in weight space to the black dot at a = 0.6and c = 0.2, we see that the corresponding cycle [Fig. 2(d)] now displays a finite period with linear modulations of u(t) at fixed temperatures and a discontinuity of u(t) when switching between  $\beta_H$  and  $\beta_C$ . The cycle in Fig. 2(e), corresponding to the lowest black dot at a = 0.2 and c = 0.4, displays an extremely long period  $\tau \approx 125 \gamma^{-1}$ , which is far in the slowdriving regime. Optimal cycles, therefore, interpolate between the fast- and the slow-driving regimes as we move in weight space [Fig. 2(a)] from the sides to the lower and central region (i.e., switching from two to three objectives).

In Fig. 3, we display the Pareto front, i.e., we plot the value of  $P/P_{\text{max}}$ ,  $\Delta P/\Delta P(P_{\text{max}})$ , and of the efficiency  $\eta/\eta_c$ , found maximizing  $\langle F \rangle$  for various values of the weights.

Figure 3(a) is derived in the fast-driving regime assuming a small temperature difference, whereas Fig. 3(b) is derived in the slow-driving regime. The RL results, shown in Fig. 3(c), correspond to the points in Fig. 2(a). First, we note that, by definition of the Pareto front, the "outer border" corresponds to points where we only maximize the trade-off between the two objectives  $\langle P \rangle$  and  $\langle \Delta P \rangle$ . Since these points are optimized by fast-Otto cycles, the black border of Fig. 3(a), also shown in Figs. 3(b) and 3(c), is exact and given by (see the Supplemental Material [93] for details)

$$\frac{\langle P \rangle}{P_{\text{max}}} = 2\sqrt{\frac{\langle \Delta P \rangle}{\Delta P (P_{\text{max}})}} - \frac{\langle \Delta P \rangle}{\Delta P (P_{\text{max}})}.$$
 (11)

Moreover, in this setup, we can establish an exact mapping between the performance of a SSHE and of our PDHE operated with fast-Otto cycles (see the Supplemental Material [93]). Since SSHEs satisfy Eq. (1), also fast-Otto cycles have  $\xi \leq 1$ . Furthermore, for small temperature differences  $\xi = 1$ . This allows us to fully determine the internal part of the Pareto front in the fast-driving regime using the thermodynamic uncertainty relations, i.e.,  $P/P_{\text{max}} = [\Delta P/\Delta P(P_{\text{max}})](\eta_c - \eta)/\eta$ . Indeed, the linear contour lines in Fig. 3(a) stem from the linearity between P and  $\Delta P$ , the angular coefficient being determined by the efficiency.

Comparing Figs. 3(a) and 3(b), we see where the fastand slow-driving regimes are optimal. As expected, the slowdriving Pareto front cannot reach the black border, especially in the high-power area where fast-Otto cycles are optimal. However, in the low-power and low fluctuation regime, cycles in the slow driving substantially outperform fast-Otto cycles by delivering a higher efficiency [purple and blue regions in Fig. 3(b)].

Interestingly, the RL points in Fig. 3(c) capture the best features of both regimes. RL can describe the high-power and low fluctuation regime displaying both red and blue/green dots near the lower border. The red dots are fast-Otto cycles that are optimal exactly along the border but deliver a low efficiency. The blue/green dots instead are finite-time cycles that deliver a much higher efficiency by sacrificing a very small amount of power and fluctuations. This dramatic enhancement of the efficiency as we depart from the lower border is another signature of the abrupt change in optimal cycles.

Violation of thermodynamic uncertainty relation. At last, we analyze the behavior of the thermodynamic uncertainty relation ratio  $\xi$ , which represents a relevant quantity combining the three objectives, computing it on Pareto-optimal cycles (recall that  $\xi \leq 1$  for classical stochastic SSHEs but PDHEs can violate this bound [54-59]). In Fig. 4(a), we show a contour plot of  $\xi$ , computed with RL as a function of a and c. Because of the mapping between SSHEs and fast-Otto cycles [93], we have  $\xi = 1$  along the sides of the triangle where only two objectives are optimized. However, this mapping breaks down for finite-time cycles, allowing us to observe a strong increase in  $\xi$  in the green/purple region in Fig. 4(a). As shown in Fig. 2, this region corresponds to long cycles operated in the slow-driving regime where violations of thermodynamic uncertainty relations had already been reported [56,66]. In Figs. 4(b)–4(d) we show a log-log plot of  $\xi$ , respectively, as a function of  $P/P_{\text{max}}$ ,  $\Delta P/\Delta P(P_{\text{max}})$ , and  $\Sigma/\Sigma(P_{\text{max}})$  with

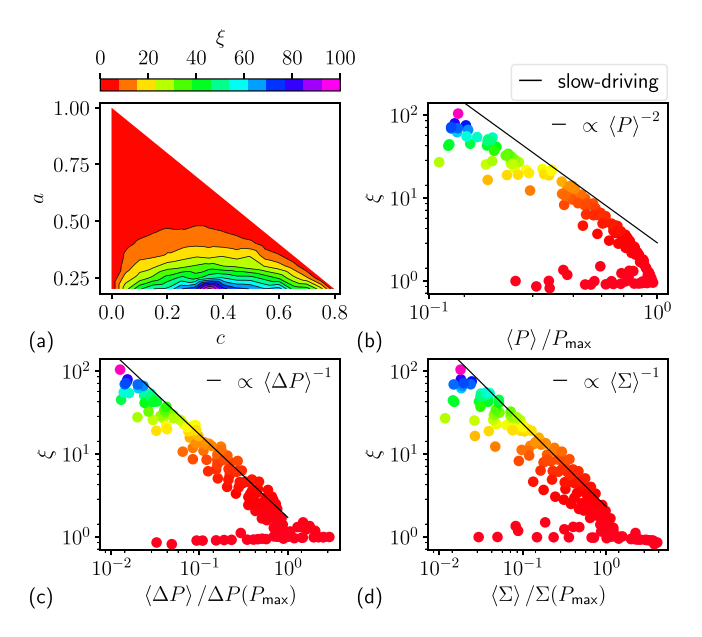


FIG. 4. (a) Contour plot of the SSHE thermodynamic uncertainty relationship ratio  $\xi$  as a function of c and a. (b)–(d) log-log plot of  $\xi$ , color mapped as in panel (a) as a function of  $\langle P \rangle/P_{\text{max}}$ ,  $\langle \Delta P \rangle/\Delta P(P_{\text{max}})$ , and  $\langle \Sigma \rangle/\Sigma(P_{\text{max}})$ , respectively. Every point corresponds to the same RL optimization performed in Fig. 2. The black line is the behavior of  $\xi$  derived analytically in the Supplemental Material [93] in the slow-driving regime for small values of  $\langle P \rangle$ ,  $\langle \Delta P \rangle$ , and  $\langle \Sigma \rangle$ .

the same color map as in Fig. 4(a). We see that  $\xi$  diverges in the limit of low power, low fluctuations, and low entropy production as a power law. Indeed, using the slow-driving approximation, we analytically prove that  $\xi$  diverges as  $\langle P \rangle^{-2}$ ,  $\langle \Delta P \rangle^{-1}$ , and  $\langle \Sigma \rangle^{-1}$ . Such relations, plotted as black lines, nicely agree with our RL results.

Conclusions. We introduced a general framework to identify Pareto-optimal cycles among power, efficiency, and power fluctuations in quantum or classical stochastic heat engines, paving the way for their systematic optimization using optimal control techniques, such as the Pontryagin minimum principle [72] or reinforcement learning [73]. As opposed to previous literature reviewed above, we account for the crucial impact of power fluctuations. We then employed RL to optimize a quantum dot-based heat engine, solving its exact finite-time and out-of-equilibrium dynamics, providing us with new physical insights. We observe an abrupt change in Pareto-optimal cycles when switching from the optimization of two objectives where Otto cycles in the fast-driving regime are optimal, to three objectives where the optimal cycles have a finite period. This feature, which shares analogies with the phase transition in protocol space observed in Ref. [96], corresponds to a large enhancement of one of the objectives whereas only slightly decreasing the other ones. Furthermore, we find an exact mapping between Otto cycles in the fastdriving regime and SSHEs, implying that a violation of the thermodynamic uncertainty relation ratio  $\xi$  in Eq. (1) requires the optimization of all three objectives. We then find that  $\xi$ becomes arbitrarily large in the slow-driving regime. Cycles found with RL display the best features analytically identified in the fast- and slow-driving regimes.

Acknowledgments. F.N. gratefully acknowledges funding by the BMBF (Berlin Institute for the Foundations of Learning and Data—BIFOLD), the European Research Commission (Grant No. ERC CoG 772230) and the Berlin Mathematics Center MATH+ (Grant No. AA1-6, AA2-8). P.A.E. gratefully acknowledges funding by the Berlin Mathematics Center MATH+ (AA1-6, AA2-18). A.R. and M.P.L. acknowledge funding from Swiss National Science Foundation through an Ambizione Grant No. PZ00P2-186067. P.A. is supported by la Caixa Foundation (ID 100010434, Grant No. LCF/BQ/DI19/11730023), and by the Government of Spain (Grants No. FIS2020-TRANQI and No. Severo Ochoa CEX2019-000910-S), Fundacio Cellex, Fundacio Mir-Puig, Generalitat de Catalunya (Grant No. CERCA, AGAUR SGR 1381).

<sup>[1]</sup> F. Giazotto, T. T. Heikkilä, A. Luukanen, A. M. Savin, and J. P. Pekola, Opportunities for mesoscopics in thermometry and refrigeration: Physics and applications, Rev. Mod. Phys. **78**, 217 (2006).

<sup>[2]</sup> J. P. Pekola, Towards quantum thermodynamics in electronic circuits, Nat. Phys. 11, 118 (2015).

<sup>[3]</sup> S. Vinjanampathy and J. Anders, Quantum thermodynamics, Contemp. Phys. **57**, 545 (2016).

<sup>[4]</sup> G. Benenti, G. Casati, K. Saito, and R. S. Whitney, Fundamental aspects of steady-state conversion of heat to work at the nanoscale, Phys. Rep. 694, 1 (2017).

<sup>[5]</sup> F. Binder, L. Correa, C. Gogolin, J. Anders, and G. Adesso, Thermodynamics in the Quantum Regime: Fundamental Aspects and New Directions (Springer International Publishing, Cham, Switzerland, 2019).

<sup>[6]</sup> E. Geva and R. Kosloff, A quantum-mechanical heat engine operating in finite time. a model consisting of spin-1/2 systems as the working fluid, J. Chem. Phys. 96, 3054 (1992).

<sup>[7]</sup> T. Feldmann and R. Kosloff, Performance of discrete heat engines and heat pumps in finite time, Phys. Rev. E **61**, 4774 (2000).

<sup>[8]</sup> T. Schmiedl and U. Seifert, Efficiency at maximum power: An analytically solvable model for stochastic heat engines, Europhys. Lett. 81, 20003 (2008).

<sup>[9]</sup> M. Esposito, R. Kawai, K. Lindenberg, and C. V. den Broeck, Efficiency at Maximum Power of Low-Dissipation Carnot Engines, Phys. Rev. Lett. 105, 150603 (2010).

<sup>[10]</sup> M. Esposito, R. Kawai, K. Lindenberg, and C. Van den Broeck, Quantum-dot carnot engine at maximum power, Phys. Rev. E 81, 041106 (2010).

<sup>[11]</sup> A. E. Allahverdyan, K. V. Hovhannisyan, A. V. Melkikh, and S. G. Gevorkian, Carnot Cycle at Finite Power: Attainability of Maximal Efficiency, Phys. Rev. Lett. 111, 050601 (2013).

<sup>[12]</sup> S. Juergens, F. Haupt, M. Moskalets, and J. Splettstoesser, Thermoelectric performance of a driven double quantum dot, Phys. Rev. B 87, 245423 (2013).

- [13] V. Holubec and A. Ryabov, Efficiency at and near maximum power of low-dissipation heat engines, Phys. Rev. E 92, 052125 (2015).
- [14] V. Holubec and A. Ryabov, Maximum efficiency of low-dissipation heat engines at arbitrary power, J. Stat. Mech.: Theory Exp. (2016) 073204.
- [15] B. Karimi and J. P. Pekola, Otto refrigerator based on a superconducting qubit: Classical and quantum performance, Phys. Rev. B 94, 184503 (2016).
- [16] M. Campisi and R. Fazio, The power of a critical heat engine, Nat. Commun. 7, 11895 (2016).
- [17] K. Yamamoto, O. Entin-Wohlman, A. Aharony, and N. Hatano, Efficiency bounds on thermoelectric transport in magnetic fields: The role of inelastic processes, Phys. Rev. B 94, 121402(R) (2016).
- [18] R. Kosloff and Y. Rezek, The quantum harmonic otto cycle, Entropy 19, 136 (2017).
- [19] V. Patel, V. Savsani, and A. Mudgal, Many-objective thermodynamic optimization of Stirling heat engine, Energy 125, 629 (2017).
- [20] V. Cavina, A. Mari, A. Carlini, and V. Giovannetti, Optimal thermodynamic control in open quantum systems, *Phys. Rev.* A **98**, 012139 (2018).
- [21] P. Abiuso and V. Giovannetti, Non-markov enhancement of maximum power for quantum thermal machines, Phys. Rev. A 99, 052106 (2019).
- [22] Y.-H. Ma, D. Xu, H. Dong, and C.-P. Sun, Universal constraint for efficiency and power of a low-dissipation heat engine, Phys. Rev. E **98**, 042112 (2018).
- [23] P. A. Erdman, V. Cavina, R. Fazio, F. Taddei, and V. Giovannetti, Maximum power and corresponding efficiency for two-level heat engines and refrigerators: Optimality of fast cycles, New J. Phys. 21, 103049 (2019).
- [24] P. Menczel, T. Pyhäranta, C. Flindt, and K. Brandner, Two-stroke optimization scheme for mesoscopic refrigerators, Phys. Rev. B 99, 224306 (2019).
- [25] J.-F. Chen, C.-P. Sun, and H. Dong, Boosting the performance of quantum otto heat engines, Phys. Rev. E 100, 032144 (2019).
- [26] P. Abiuso and M. Perarnau-Llobet, Optimal Cycles for Low-Dissipation Heat Engines, Phys. Rev. Lett. 124, 110606 (2020).
- [27] V. Cavina, P. A. Erdman, P. Abiuso, L. Tolomeo, and V. Giovannetti, Maximum-power heat engines and refrigerators in the fast-driving regime, Phys. Rev. A 104, 032226 (2021).
- [28] R. A. Vargas-Hernández, R. T. Q. Chen, K. A. Jung, and P. Brumer, Fully differentiable optimization protocols for non-equilibrium steady states, New J. Phys. 23, 123006 (2021).
- [29] P. Terrén Alonso, P. Abiuso, M. Perarnau-Llobet, and L. Arrachea, Geometric optimization of nonequilibrium adiabatic thermal machines and implementation in a qubit system, PRX Quantum 3, 010326 (2022).
- [30] Z. Ye, F. Cerisola, P. Abiuso, J. Anders, M. Perarnau-Llobet, and V. Holubec, Optimal finite-time heat engines under constrained control Phys. Rev. Res. 4, 043130 (2022).
- [31] V. Holubec, An exactly solvable model of a stochastic heat engine: Optimization of power, power fluctuations and efficiency, J. Stat. Mech.: Theory Exp. (2014) P05022.

- [32] H. J. D. Miller and M. Mehboudi, Geometry of Work Fluctuations Versus Efficiency in Microscopic Thermal Machines, Phys. Rev. Lett. **125**, 260602 (2020).
- [33] T. Denzler and E. Lutz, Power fluctuations in a finite-time quantum carnot engine, Phys. Rev. Res. 3, L032041 (2021).
- [34] S. Saryal and B. K. Agarwalla, Bounds on fluctuations for finite-time quantum otto cycle, Phys. Rev. E 103, L060103 (2021).
- [35] M. Mehboudi and H. J. D. Miller, Thermodynamic length and work optimisation for gaussian quantum states, Phys. Rev. A 105, 062434 (2022).
- [36] A. C. Barato and U. Seifert, Thermodynamic Uncertainty Relation for Biomolecular Processes, Phys. Rev. Lett. 114, 158101 (2015).
- [37] T. R. Gingrich, J. M. Horowitz, N. Perunov, and J. L. England, Dissipation Bounds All Steady-State Current Fluctuations, Phys. Rev. Lett. 116, 120601 (2016).
- [38] P. Pietzonka and U. Seifert, Universal Trade-Off between Power, Efficiency, and Constancy in Steady-State Heat Engines, Phys. Rev. Lett. **120**, 190602 (2018).
- [39] G. Guarnieri, G. T. Landi, S. R. Clark, and J. Goold, Thermodynamics of precision in quantum nonequilibrium steady states, Phys. Rev. Res. 1, 033021 (2019).
- [40] A. M. Timpanaro, G. Guarnieri, J. Goold, and G. T. Landi, Thermodynamic Uncertainty Relations from Exchange Fluctuation Theorems, Phys. Rev. Lett. 123, 090604 (2019).
- [41] G. Falasco, M. Esposito, and J.-C. Delvenne, Unifying thermodynamic uncertainty relations, New J. Phys. 22, 053046 (2020).
- [42] H. M. Friedman, B. K. Agarwalla, O. Shein-Lumbroso, O. Tal, and D. Segal, Thermodynamic uncertainty relation in atomic-scale quantum conductors, Phys. Rev. B **101**, 195423 (2020).
- [43] J. M. Horowitz and T. R. Gingrich, Thermodynamic uncertainty relations constrain non-equilibrium fluctuations, Nat. Phys. 16, 15 (2020).
- [44] S. Saryal, M. Gerry, I. Khait, D. Segal, and B. K. Agarwalla, Universal Bounds on Fluctuations in Continuous Thermal Machines, Phys. Rev. Lett. 127, 190603 (2021).
- [45] B. K. Agarwalla and D. Segal, Assessing the validity of the thermodynamic uncertainty relation in quantum systems, Phys. Rev. B **98**, 155438 (2018).
- [46] K. Brandner, T. Hanazato, and K. Saito, Thermodynamic Bounds on Precision in Ballistic Multiterminal Transport, Phys. Rev. Lett. **120**, 090601 (2018).
- [47] K. Ptaszyński, Coherence-enhanced constancy of a quantum thermoelectric generator, Phys. Rev. B 98, 085425 (2018).
- [48] F. Carollo, R. L. Jack, and J. P. Garrahan, Unraveling the Large Deviation Statistics of Markovian Open Quantum Systems, Phys. Rev. Lett. 122, 130605 (2019).
- [49] J. Liu and D. Segal, Thermodynamic uncertainty relation in quantum thermoelectric junctions, Phys. Rev. E 99, 062141 (2019).
- [50] A. Arash Sand Kalaee, A. Wacker, and P. P. Potts, Violating the thermodynamic uncertainty relation in the three-level maser, Phys. Rev. E 104, L012103 (2021).
- [51] A. Rignon-Bret, G. Guarnieri, J. Goold, and M. T. Mitchison, Thermodynamics of precision in quantum nanomachines, Phys. Rev. E **103**, 012133 (2021).

- [52] T. Ehrlich and G. Schaller, Broadband frequency filters with quantum dot chains, Phys. Rev. B 104, 045424 (2021).
- [53] M. Gerry and D. Segal, Absence and recovery of costprecision tradeoff relations in quantum transport, Phys. Rev. B 105, 155401 (2022).
- [54] A. C. Barato and U. Seifert, Cost and Precision of Brownian Clocks, Phys. Rev. X 6, 041053 (2016).
- [55] K. Proesmans and C. V. den Broeck, Discrete-time thermodynamic uncertainty relation, Europhys. Lett. 119, 20001 (2017).
- [56] V. Holubec and A. Ryabov, Cycling Tames Power Fluctuations near Optimum Efficiency, Phys. Rev. Lett. 121, 120601 (2018).
- [57] L. M. Cangemi, V. Cataudella, G. Benenti, M. Sassetti, and G. De Filippis, Violation of thermodynamics uncertainty relations in a periodically driven work-to-work converter from weak to strong dissipation, Phys. Rev. B 102, 165418 (2020).
- [58] P. Menczel, E. Loisa, K. Brandner, and C. Flindt, Thermodynamic uncertainty relations for coherently driven open quantum systems, J. Phys. A: Math. Theor. 54, 314002 (2021).
- [59] J. Lu, Z. Wang, J. Peng, C. Wang, J.-H. Jiang, and J. Ren, Geometric thermodynamic uncertainty relation in a periodically driven thermoelectric heat engine, Phys. Rev. B 105, 115428 (2022).
- [60] T. Koyuk, U. Seifert, and P. Pietzonka, A generalization of the thermodynamic uncertainty relation to periodically driven systems, J. Phys. A: Math. Theor. **52**, 02LT02 (2019).
- [61] T. Koyuk and U. Seifert, Operationally Accessible Bounds on Fluctuations and Entropy Production in Periodically Driven Systems, Phys. Rev. Lett. 122, 230601 (2019).
- [62] T. Koyuk and U. Seifert, Thermodynamic Uncertainty Relation for Time-Dependent Driving, Phys. Rev. Lett. 125, 260604 (2020).
- [63] T. Van Vu and Y. Hasegawa, Thermodynamic uncertainty relations under arbitrary control protocols, Phys. Rev. Res. 2, 013060 (2020).
- [64] E. Potanina, C. Flindt, M. Moskalets, and K. Brandner, Thermodynamic Bounds on Coherent Transport in Periodically Driven Conductors, Phys. Rev. X 11, 021013 (2021).
- [65] Y. Hasegawa, Irreversibility, Loschmidt Echo, and Thermodynamic Uncertainty Relation, Phys. Rev. Lett. 127, 240602 (2021).
- [66] H. J. D. Miller, M. H. Mohammady, M. Perarnau-Llobet, and G. Guarnieri, Thermodynamic Uncertainty Relation in Slowly Driven Quantum Heat Engines, Phys. Rev. Lett. 126, 210603 (2021).
- [67] H. J. D. Miller, M. H. Mohammady, M. Perarnau-Llobet, and G. Guarnieri, Joint statistics of work and entropy production along quantum trajectories, Phys. Rev. E 103, 052138 (2021).
- [68] V. Gorini, A. Kossakowski, and E. C. G. Sudarshan, Completely positive dynamical semigroups of N-level systems, J. Math. Phys. 17, 821 (1976).
- [69] G. Lindblad, On the generators of quantum dynamical semigroups, Commun. Math. Phys. 48, 119 (1976).
- [70] H. Breuer and F. Petruccione, *The Theory of Open Quantum systems* (Oxford University Press, New York, 2002).
- [71] M. Yamaguchi, T. Yuge, and T. Ogawa, Markovian quantum master equation beyond adiabatic regime, Phys. Rev. E 95, 012136 (2017).
- [72] D. E. Kirk, Optimal Control Theory: an Introduction (Dover, New York, 2004).

- [73] R. S. Sutton and A. G. Barto, *Reinforcement Larning: An Introduction* (MIT Press, Cambridge, MA, 2018).
- [74] B. Sothmann, R. Sánchez, and A. N. Jordan, Thermoelectric energy harvesting with quantum dots, Nanotechnology 26, 032001 (2015).
- [75] J. P. Pekola, B. Karimi, G. Thomas, and D. V. Averin, Supremacy of incoherent sudden cycles, Phys. Rev. B 100, 085405 (2019).
- [76] L. M. Cangemi, M. Carrega, A. De Candia, V. Cataudella, G. De Filippis, M. Sassetti, and G. Benenti, Optimal energy conversion through antiadiabatic driving breaking time-reversal symmetry, Phys. Rev. Res. 3, 013237 (2021).
- [77] P. Salamon and R. S. Berry, Thermodynamic Length and Dissipated Availability, Phys. Rev. Lett. 51, 1127 (1983).
- [78] J. Wang, J. He, and X. He, Performance analysis of a two-state quantum heat engine working with a single-mode radiation field in a cavity, Phys. Rev. E 84, 041127 (2011).
- [79] J. E. Avron, M. Fraas, G. M. Graf, and P. Grech, Adiabatic theorems for generators of contracting evolutions, Commun. Math. Phys. 314, 163 (2012).
- [80] M. F. Ludovico, F. Battista, F. von Oppen, and L. Arrachea, Adiabatic response and quantum thermoelectrics for ac-driven quantum systems, Phys. Rev. B 93, 075136 (2016).
- [81] V. Cavina, A. Mari, and V. Giovannetti, Slow Dynamics and Thermodynamics of Open Quantum Systems, Phys. Rev. Lett. 119, 050601 (2017).
- [82] H. J. D. Miller, M. Scandi, J. Anders, and M. Perarnau-Llobet, Work Fluctuations in Slow Processes: Quantum Signatures and Optimal Control, Phys. Rev. Lett. 123, 230603 (2019).
- [83] M. Scandi and M. Perarnau-Llobet, Thermodynamic length in open quantum systems, Quantum 3, 197 (2019).
- [84] K. Brandner and K. Saito, Thermodynamic Geometry of Microscopic Heat Engines, Phys. Rev. Lett. 124, 040602 (2020).
- [85] B. Bhandari, P. T. Alonso, F. Taddei, F. von Oppen, R. Fazio, and L. Arrachea, Geometric properties of adiabatic quantum thermal machines, Phys. Rev. B **102**, 155407 (2020).
- [86] P. Abiuso, H. J. D. Miller, M. Perarnau-Llobet, and M. Scandi, Geometric optimisation of quantum thermodynamic processes, Entropy **22**, 1076 (2020).
- [87] A. G. Frim and M. R. DeWeese, Geometric Bound on the Efficiency of Irreversible Thermodynamic Cycles, Phys. Rev. Lett. 128, 230601 (2022).
- [88] J. Eglinton and K. Brandner, Geometric bounds on the power of adiabatic thermal machines, Phys. Rev. E **105**, L052102 (2022).
- [89] K. Brandner, K. Saito, and U. Seifert, Thermodynamics of Micro- and Nano-Systems Driven by Periodic Temperature Variations, Phys. Rev. X 5, 031019 (2015).
- [90] K. Brandner and U. Seifert, Periodic thermodynamics of open quantum systems, Phys. Rev. E 93, 062134 (2016).
- [91] O. Movilla Miangolarra, R. Fu, A. Taghvaei, Y. Chen, and T. T. Georgiou, Underdamped stochastic thermodynamic engines in contact with a heat bath with arbitrary temperature profile, Phys. Rev. E 103, 062103 (2021).
- [92] O. Movilla Miangolarra, A. Taghvaei, R. Fu, Y. Chen, and T. T. Georgiou, Energy harvesting from anisotropic fluctuations, Phys. Rev. E 104, 044101 (2021).
- [93] See Supplemental Material at http://link.aps.org/supplemental/ 10.1103/PhysRevResearch.5.L022017 for details on the the

- general framework, the reinforcement learning method, and the fast and slow driving regimes.
- [94] R. Alicki, The quantum open system as a model of the heat engine, J. Phys. A 12, L103 (1979).
- [95] L. F. Seoane and R. Solé, Multiobjective optimization and phase transitions, in *Proceedings of ECCS 2014*, edited by S. Battiston, F. De Pellegrini, G. Caldarelli, and E. Merelli (Springer, Cham, 2016), pp. 259-270.
- [96] A. P. Solon and J. M. Horowitz, Phase Transition in Protocols Minimizing Work Fluctuations, Phys. Rev. Lett. 120, 180605 (2018).
- [97] T. Haarnoja, A. Zhou, K. Hartikainen, G. Tucker, S. Ha, J. Tan, V. Kumar, H. Zhu, A. Gupta, P. Abbeel, and S. Levine, Soft actor-critic algorithms and applications, arXiv:1812.05905.
- [98] O. Delalleau, M. Peter, E. Alonso, A. Logut, Discrete and continuous action representation for practical RL in video games, arXiv:1912.11077.
- [99] T. Haarnoja, A. Zhou, P. Abbeel, and S. Levine, Soft actor-critic: Off-policy maximum entropy deep reinforcement learning with a stochastic actor, *International Conference on Machine Learning*, Vol. 80 (PMLR, Birmingham, UK, 2018), p. 1861.
- [100] P. A. Erdman and F. Noé, Identifying optimal cycles in quantum thermal machines with reinforcement-learning, npj Quantum Inf 8, 1 (2022).
- [101] P. A. Erdman and F. Noé, Driving black-box quantum thermal machines with optimal power/efficiency trade-offs using reinforcement learning, arXiv:2204.04785.
- [102] P. Sgroi, G. M. Palma, and M. Paternostro, Reinforcement Learning Approach to Nonequilibrium Quantum Thermodynamics, Phys. Rev. Lett. 126, 020601 (2021).
- [103] I. Khait, J. Carrasquilla, and D. Segal, Optimal control of quantum thermal machines using machine learning, Phys. Rev. Res. 4, L012029 (2022).
- [104] Y. Ashida and T. Sagawa, Learning the best nanoscale heat engines through evolving network topology, Commun. Phys. 4, 45 (2021).
- [105] M. Bukov, A. G. R. Day, D. Sels, P. Weinberg, A. Polkovnikov, and P. Mehta, Reinforcement Learning in

- Different Phases of Quantum Control, Phys. Rev. X 8, 031086 (2018).
- [106] T. Fösel, P. Tighineanu, T. Weiss, and F. Marquardt, Reinforcement Learning with Neural Networks for Quantum Feedback, Phys. Rev. X 8, 031084 (2018).
- [107] Z. An and D. Zhou, Deep reinforcement learning for quantum gate control, Europhys. Lett. 126, 60002 (2019).
- [108] M. Y. Niu, S. Boixo, V. N. Smelyanskiy, and H. Neven, Universal quantum control through deep reinforcement learning, npj Quantum Inf 5, 33 (2019).
- [109] X.-M. Zhang, Z. Wei, R. Asad, X.-C. Yang, and X. Wang, When does reinforcement learning stand out in quantum control? A comparative study on state preparation, npj Quantum Inf 5, 85 (2019).
- [110] M. Dalgaard, F. Motzoi, J. J. Sørensen, and J. Sherson, Global optimization of quantum dynamics with alphazero deep exploration, npj Quantum Inf 6, 6 (2020).
- [111] J. Mackeprang, D. B. R. Dasari, and J. Wrachtrup, A reinforcement learning approach for quantum state engineering, Quantum Mach. Intell. 2, 5 (2020).
- [112] F. Schäfer, M. Kloc, C. Bruder, and N. Lörch, A differentiable programming method for quantum control, Mach. Learn.: Sci. Technol. 1, 035009 (2020).
- [113] R. Sweke, M. S. Kesselring, E. P. L. van Nieuwenburg, and J. Eisert, Reinforcement learning decoders for fault-tolerant quantum computation, Mach. Learn.: Sci. Technol. 2, 025005 (2021).
- [114] F. Schäfer, P. Sekatski, M. Koppenhöfer, C. Bruder, and M. Kloc, Control of stochastic quantum dynamics by differentiable programming, Mach. Learn.: Sci. Technol. 2, 035004 (2021).
- [115] R. Porotti, A. Essig, B. Huard, and F. Marquardt, Deep reinforcement learning for quantum state preparation with weak nonlinear measurements, Quantum 6, 747 (2022).
- [116] F. Metz and M. Bukov, Self-correcting quantum many-body control using reinforcement learning with tensor networks, arXiv:2201.11790.
- [117] L. Coopmans, S. Campbell, G. De Chiara, and A. Kiely, Optimal control in disordered quantum systems, Phys. Rev. Res. 4, 043138 (2022).

# Supplemental Material for "Pareto-optimal cycles for power, efficiency and fluctuations of quantum heat engines using reinforcement learning"

Paolo A. Erdman, Alberto Rolandi, Paolo Abiuso, Martí Perarnau-Llobet, and Frank Noé

#### I. GENERAL FRAMEWORK AND REINFORCEMENT LEARNING APPROACH

In this section we describe a general framework to compute the power, entropy production and power fluctuations of a quantum thermal machine. We then show how it allows us to use RL to optimize the trade-off between these three objectives. Assuming that the dynamics is Markovian, the reduced state evolves according to Eq. (2) of the main text, i.e.

$$\dot{\rho}_t = \mathcal{L}_{\vec{u}(t),\beta(t)}\rho_t. \tag{S1}$$

As usual, we employ the first law to split the internal energy  $U(t) = \text{Tr}[\rho_t H_{\vec{u}(t)}]$  of the system into absorbed heat and output work [1]:

$$dU = dQ - dW , \quad dQ = \text{Tr} \left[ d\rho_t H_{\vec{u}(t)} \right] , \quad dW = -\text{Tr} \left[ \rho_t dH_{\vec{u}(t)} \right] . \tag{S2}$$

The instantaneous power *output* is thus given by Eq. (3) of the main text, i.e.

$$P(t) = -\operatorname{Tr}\left[\rho_t \dot{H}_{\vec{u}(t)}\right] \tag{S3}$$

and, according to Clausius theorem for cycles (in which we set  $\Delta S = 0$  of the quantum system since we consider a periodic driving in the limiting cycle), the instantaneous irreversible entropy production is given by Eq. (3) of the main text, i.e.

$$\Sigma(t) = -\beta(t) \operatorname{Tr} \left[ \dot{\rho}_t H_{\vec{u}(t)} \right]. \tag{S4}$$

For what concerns power fluctuations, let  $\langle \sigma^2 \rangle_t$  be the work fluctuations between time 0 at t. Using Eq. (2) of Ref. [2], we can write the fluctuations as

$$\langle \sigma^2 \rangle_t = \int_0^t dt_1 \operatorname{Tr} \left[ \dot{H}_{\vec{u}(t_1)} s_{t_1} \right], \tag{S5}$$

where we introduce

$$s_{t_1} \equiv \int_0^{t_1} dt_2 P(t_1, t_2) [\dot{H}_{\vec{u}(t_2)} \rho_{t_2}] + \langle w \rangle_{t_1} \rho_{t_1} + h.c. .$$
 (S6)

Here  $P(t_1,t_2) \equiv \overleftarrow{T} \exp\left[\int_{t_2}^{t_1} d\tau \mathcal{L}_{\vec{u}(\tau),\beta(\tau)}\right]$  is the propagator,  $\langle w \rangle_{t_1} \equiv -\int_0^{t_1} dt_2 \operatorname{Tr}\left[\rho_{t_2} \dot{H}_{\vec{u}(t_2)}\right]$  is the total average work extracted between time 0 and  $t_1$ , h.c. represents the complex conjugate of the whole right-hand-side, and in deriving Eq. (S5) we used that  $[P(t_1,t_2)O]^{\dagger} = P(t_1,t_2)O^{\dagger}$ , which stems from  $[\mathcal{L}_{\vec{u}(\tau),\beta(\tau)}O]^{\dagger} = \mathcal{L}_{\vec{u}(\tau),\beta(\tau)}O^{\dagger}$ . Taking the time-derivative of  $s_t$ , we find that it satisfies the equation of motion given in Eq. (6) of the main text, i.e.

$$\dot{s}_t = \mathcal{L}_{\vec{u}(t),\beta(t)} s_t + \{\rho, \dot{H}_{\vec{u}(t)}\} - 2 \operatorname{Tr} \left[ \rho_t \dot{H}_{\vec{u}(t)} \right] \rho_t, \tag{S7}$$

where  $\{\cdot,\cdot\}$  denotes the anti-commutator. Using the definition of  $s_t$  given in Eq. (S6), we see that  $s_t$  is an Hermitian operator, and that  $\text{Tr}[s_t] = 0$ . This last property stems from the fact that  $P(t_1, t_2)[\cdot]$  is trace-preserving.

## A. "Extended state" and formulation of the optimization problem

We now define  $(\rho_t, s_t)$  as an "extended state". We have just shown that the equation of motion of the extended state is a set of first-order differential equations [see Eqs. (S1) and (S7)]. Furthermore, the average power  $\langle P \rangle \equiv \langle w \rangle_{\tau} / \tau$ ,

the average fluctuations  $\langle \Delta P \rangle \equiv \langle \sigma^2 \rangle_{\tau}/\tau$  and the average entropy production  $\langle \Sigma \rangle \equiv (1/\tau) \int_0^{\tau} \Sigma(t) dt$  can be expressed as a time-average of the extended state and of the controls  $\vec{u}(t)$  and  $\beta(t)$ , i.e.

$$\langle P \rangle = -\frac{1}{\tau} \int_0^{\tau} dt \operatorname{Tr} \left[ \rho_t \dot{H}_{\vec{u}(t)} \right] = \frac{1}{\tau} \int_0^{\tau} dt \operatorname{Tr} \left[ \dot{\rho}_t H_{\vec{u}(t)} \right],$$

$$\langle \Delta P \rangle = \frac{1}{\tau} \int_0^{\tau} dt \operatorname{Tr} \left[ s_t \dot{H}_{\vec{u}(t)} \right],$$

$$\langle \Sigma \rangle = -\frac{1}{\tau} \int_0^{\tau} dt \operatorname{Tr} \left[ \dot{\rho}_t H_{\vec{u}(t)} \right] \beta(t).$$
(S8)

Therefore, also the figure of merit  $\langle F \rangle$  in Eq. (8) of the main text can be expressed as a time integral of a function of the extended state  $(\rho_t, s_t)$  and of the controls  $\vec{u}(t)$  and  $\beta(t)$ , i.e.

$$\langle F \rangle = \int_0^\tau G(\rho_t, s_t, \vec{u}(t), \beta(t)) dt, \tag{S9}$$

where  $G(\rho_t, s_t, \vec{u}(t), \beta(t))$  is a suitable function. This is precisely the type of problem that can readily tackled using optimal control techniques such as Pontryagin Minimum Principle [3] or Reinforcement Learning [4].

As a final remark, one can study heat engines in the limiting cycle imposing periodic boundary conditions for the extended state, i.e.  $(\rho_0, s_0) = (\rho_\tau, s_\tau)$ . Indeed, we are interested in studying thermodynamic cycles, i.e. when both the control and the quantum state  $\rho_t$  are periodic with period  $\tau$ . Assuming that the Lindbladian  $\mathcal{L}_{\vec{u}(t),\beta(t)}$  has a single fixed point, it can be shown that a periodic control eventually drives the state  $\rho_t$  towards the limiting cycle solution, where  $\rho_t$  becomes periodic with the same period  $\tau$  of the driving [5]. Furthermore, the equation of motion of  $s_t$  has the same homogeneous part  $(\mathcal{L}_{\vec{u}(t),\beta(t)}[s_t])$  as  $\rho_t$ , and the non-homogeneous term becomes periodic once  $\rho_t$  reaches the limiting cycle. Therefore, also  $s_t$  naturally reaches a limiting cycle solution where it is periodic with the same period  $\tau$ .

#### B. Optimizing the entropy production instead of the efficiency

Here we discuss the relation between minimizing the entropy production or maximizing the efficiency. We generalize the discussion of Ref. [6], where power fluctuations are not considered. We start by noticing that we can express the efficiency of a heat engine in terms of the average power and entropy production, i.e.

$$\eta = \eta_{\rm c} \left[ 1 + \langle \Sigma \rangle / (\beta_{\rm C} \langle P \rangle) \right]^{-1}. \tag{S10}$$

We show that, thanks to this dependence of  $\eta$  on  $\langle P \rangle$  and  $\langle \Sigma \rangle$ , optimizing a trade-off between high power, low fluctuations and high efficiency yields all the Pareto optimal trade-offs between high power, low fluctuations, and low entropy-production up to a change of the weights (a, b, c).

First, we provide a non-rigorous argument as follows: notice that a point  $\{\langle P \rangle, \langle \Delta P \rangle, \langle \Sigma \rangle\}$  belongs to the Pareto front iff there exists no cycle outperforming it in all 3 quantities, i.e. larger power, smaller fluctuations and smaller entropy production. Due to the functional dependence of  $\eta(\langle \Sigma \rangle, \langle P \rangle)$  (S10), the corresponding point  $\{\langle P \rangle, \langle \Delta P \rangle, \eta(\langle \Sigma \rangle, \langle P \rangle)\}$  will belong to the power-fluctuations-efficiency Pareto front. In fact, if the point  $\{\langle P \rangle, \langle \Delta P \rangle, \eta(\langle \Sigma \rangle, \langle P \rangle)\}$  is not on the Pareto front, then a cycle  $\{\langle P \rangle', \langle \Delta P \rangle', \eta'\}$  exists such that one of the following statements holds

(Case 1) 
$$\langle P \rangle' > \langle P \rangle$$
,  $\langle \Delta P \rangle' = \langle \Delta P \rangle$ ,  $\eta' = \eta(\langle \Sigma \rangle, \langle P \rangle)$ ; (S11)

(Case 2) 
$$\langle P \rangle' = \langle P \rangle$$
,  $\langle \Delta P \rangle' < \langle \Delta P \rangle$ ,  $\eta' = \eta(\langle \Sigma \rangle, \langle P \rangle)$ ; (S12)

(Case 3) 
$$\langle P \rangle' = \langle P \rangle$$
,  $\langle \Delta P \rangle' = \langle \Delta P \rangle$ ,  $\eta' > \eta(\langle \Sigma \rangle, \langle P \rangle)$ . (S13)

Notice that in (Case 2) the corresponding  $\{\langle P \rangle', \langle \Delta P \rangle', \langle \Sigma \rangle (\langle P \rangle', \eta')\} \equiv \{\langle P \rangle, \langle \Delta P \rangle', \langle \Sigma \rangle\}$  clearly violates the power-fluctuations-entropy production Pareto front, i.e. outperforms the point  $\{\langle P \rangle, \langle \Delta P \rangle, \langle \Sigma \rangle\}$  because of smaller fluctuations. Similarly, by inverting (S10)

$$\Sigma(P,\eta) = \frac{\eta_{\rm c} - \eta}{\eta} \beta_{\rm C} P \tag{S14}$$

we see that in (Case 3) the corresponding point violates the Pareto front via a reduction of  $\langle \Sigma \rangle$ . Finally (Case 1) is non trivial, but it is intuitive (and empirically verified) that in power-fluctuations-efficiency trade-offs it is always possible to reduce the power in favor of efficiency and fluctuations, (typically by slowing down the whole cycle, i.e. increasing  $\tau$ ). This means that the occurrence of (Case 1) induces the existence of (Case 2) and (Case 3), closing the argument.

Besides the above intuitive argument, to prove such equivalence mathematically, we can prove that the cycles that maximize

$$\langle G \rangle \equiv a \frac{\langle P \rangle}{P_{\text{max}}} - b \frac{\langle \Delta P \rangle}{\Delta P(P_{\text{max}})} + c \frac{\eta}{\eta_{\text{c}}}$$
 (S15)

for some values of the weights  $a \ge 0$ ,  $b \ge 0$ ,  $c \ge 0$  such that a+b+c=1, also maximize the figure of merit in Eq. (8) of the main text for some (possibly different) non-negative values of the weights summing to one. To simplify the proof and the notation, we consider the following two functions

$$F(a, b, c; \theta) = aP(\theta) - b\Delta P(\theta) - c\Sigma(P(\theta), \eta(\theta)),$$
  

$$G(a, b, c; \theta) = aP(\theta) - b\Delta P(\theta) + c\eta(\theta),$$
(S16)

where  $P(\theta)$ ,  $\Delta P(\theta)$ , and  $\eta(\theta)$  represent the average power, fluctuations and efficiency of a cycle parameterized by a set of parameters  $\theta$ , and  $\Sigma(P, \eta)$  is given by Eq. (S14).

We wish to prove the following. Given three fixed scalars  $a_1, b_1, c_1 > 0$ , that do not necessarily sum to 1, let  $\theta_1$  be the value of  $\theta$  that locally maximizes  $G(a_1, b_1, c_1; \theta)$ . Then, it is always possible to identify three positive scalars  $a_2, b_2, c_2 > 0$ , such that the same parameters  $\theta_1$  (i.e. the same cycle) is a local maximum for  $F(a_2, b_2, c_2; \theta)$ . In the following, we will use that

$$\partial_P \Sigma \ge 0,$$
  $\partial_n \Sigma < 0,$  (S17)

and that the Hessian  $H^{(\Sigma)}$  of  $\Sigma(P,\eta)$  is given by

$$H^{(\Sigma)} = \begin{pmatrix} 0 & -\beta_{\mathcal{C}} \frac{\eta_{\mathcal{C}}}{\eta^2} \\ -\beta_{\mathcal{C}} \frac{\eta_{\mathcal{C}}}{\eta^2} & 2\beta_{\mathcal{C}} P \frac{\eta_{\mathcal{C}}}{\eta^3} \end{pmatrix}. \tag{S18}$$

Proof: by assumption,  $\theta_1$  is a local maximum for  $G(a_1, b_1, c_1; \theta)$ . Denoting with  $\partial_i$  the partial derivative in  $(\theta)_i$ , we thus have

$$0 = \partial_i G(a_1, b_1, c_1; \theta_1) = a_1 \partial_i P(\theta_1) - b_1 \partial_i \Delta P(\theta) + c_1 \partial_i \eta(\theta_1). \tag{S19}$$

Now we compute the derivative in  $\theta$  of  $F(a_2, b_2, c_2; \theta)$ , where  $a_2, b_2, c_2 > 0$  are three arbitrary scalars, and we evaluate it in  $\theta_1$ . We have

$$\partial_i F(a_2, b_2, c_2; \theta_1) = (a_2 - c_2 \partial_P \Sigma) \partial_i P(\theta_1) - b_2 \partial_i \Delta P(\theta) - (c_2 \partial_\eta \Sigma) \partial_i \eta(\theta_1). \tag{S20}$$

Therefore, if we choose  $a_2, b_2, c_2$  such that

$$\begin{pmatrix} a_1 \\ b_1 \\ c_1 \end{pmatrix} = \begin{pmatrix} 1 & 0 & -\partial_P \Sigma \\ 0 & 1 & 0 \\ 0 & 0 & -\partial_\eta \Sigma \end{pmatrix} \begin{pmatrix} a_2 \\ b_2 \\ c_2 \end{pmatrix},$$
(S21)

thanks to Eq. (S19) we have that

$$0 = \partial_i F(a_2, b_2, c_2; \theta_1), \tag{S22}$$

meaning that the same parameters  $\theta_1$  that nullifies the gradient of G, nullifies also the gradient of F at a different choice of the weights, given by Eq. (S21). The invertibility of Eq. (S21) (i.e. a non-null determinant of the matrix) is guaranteed by Eq. (S17). We also have to make sure that if  $a_1, b_1, c_1 > 0$ , then also  $a_2, b_2, c_2 > 0$ . To do this, we invert Eq. (S21), finding

$$\begin{pmatrix} a_2 \\ b_2 \\ c_2 \end{pmatrix} = \begin{pmatrix} 1 & 0 & -\partial_P \Sigma / (\partial_\eta \Sigma) \\ 0 & 1 & 0 \\ 0 & 0 & -1/(\partial_\eta \Sigma) \end{pmatrix} \begin{pmatrix} a_1 \\ b_1 \\ c_1 \end{pmatrix}. \tag{S23}$$

It is now easy to see that also the weights  $a_2, b_2, c_2$  are positive using Eq. (S17).

To conclude the proof, we show that  $\theta_1$  is a local maximum for  $F(a_2, b_2, c_2; \theta)$  by showing that its Hessian is negative semi-definite. Since, by hypothesis,  $\theta_1$  is a local maximum for  $G(a_1,b_1,c_1;\theta)$ , we have that the Hessian matrix

$$H_{ij}^{(G)} \equiv \partial_{ij}G(a_1, b_1, c_1; \theta_1) = a_1\partial_{ij}P - b_1\partial_{ij}\Delta P + c_1\partial_{ij}\eta$$
(S24)

is negative semi-definite. We now compute the Hessian  $H^{(F)}$  of  $F(a_2, b_2, c_2; \theta)$  in  $\theta = \theta_1$ :

$$H_{ij}^{(F)} = a_2 \partial_{ij} P - b_2 \partial_{ij} \Delta P - c_2 \left[ \partial_P \Sigma \partial_{ij} P + \partial_\eta \Sigma \partial_{ij} \eta + Q_{ij} \right], \tag{S25}$$

where

$$Q_{ij} = (\partial_i P \ \partial_i \eta) H^{(\Sigma)} \begin{pmatrix} \partial_j P \\ \partial_j \eta \end{pmatrix}, \tag{S26}$$

and  $H^{(\Sigma)}$  is the Hessian of  $\Sigma(P,\eta)$  computed in  $P(\theta_1)$  and  $\eta(\theta_1)$ . Since we are interested in studying the Hessian of  $F(a_2, b_2, c_2; \theta_1)$  in the special point  $(a_2, b_2, c_2)$  previously identified, we substitute Eq. (S23) into Eq. (S25), yielding

$$H_{ij}^{(F)} = H_{ij}^{(G)} + \frac{b_1}{\partial_{\eta} \Sigma} Q_{ij}. \tag{S27}$$

We now prove that  $H_{ij}^{(F)}$  is negative semi-definite since it is the sum of negative semi-definite matrices. By hypothesis  $H_{ij}^{(G)}$  is negative semi-definite. Recalling Eq. (S17) and that  $b_1 > 0$ , we now need to show that  $Q_{ij}$  is positive semi-definite. Plugging Eq. (S18) into Eq. (S26) yields

$$Q_{ij} = \beta_{\rm C} \frac{\eta_{\rm c}}{\eta^2} \partial_i \eta \, \partial_j \eta \, R_{ij}, \tag{S28}$$

where

$$R_{ij} \equiv 2P + S_{ij} + S_{ij}^{T}, \qquad S_{ij} = -\frac{\partial_i P}{\partial_i \eta}.$$
 (S29)

We now show that if  $R_{ij}$  is positive semi-definite, then also  $Q_{ij}$  is positive semi-definite. By definition,  $Q_{ij}$  is positive semi-definite if, for any set of coefficient  $a_i$ , we have that  $\sum_{ij} a_i Q_{ij} a_j \geq 0$ . Assuming  $R_{ij}$  to be positive semi-definite, and using that  $\beta_{\rm C}$ ,  $\eta_{\rm c}$ ,  $\eta > 0$ , we have

$$\sum_{ij} a_i Q_{ij} a_j = \beta_{\mathcal{C}} \frac{\eta_c}{\eta^2} \sum_{ij} x_i R_{ij} x_j \ge 0, \tag{S30}$$

where we define  $x_i \equiv \partial_i \eta \, a_i$ . We thus have to prove the positivity of  $R_{ij}$ . We prove this showing that it is the sum of 3 positive semi-definite matrices. Indeed, the first term in Eq. (S29), 2P, is proportional to a matrix with 1 in all entries. Trivially, this matrix has 1 positive eigenvalue, and all other ones are null, so it is positive semi-definite. At last,  $S_{ij}$  and its transpose have the same positivity, so we focus only on  $S_{ij}$ .  $S_{ij}$  is a matrix with all equal columns. This means that it has all null eigenvalues, except for a single one that we denote with  $\lambda$ . Since the trace of a matrix is equal to the sum of the eigenvalues, we have  $\lambda = \text{Tr}[S] = \sum_i S_{ii}$ . Using the optimality condition in Eq. (S19), we see that each entry of S is positive, i.e.  $S_{ij} > 0$ . Therefore  $\lambda > 0$ , thus S is positive semi-definite, concluding the proof that  $H_{ij}^{(F)}$  is negative semi-definite. To conclude, we notice that we can always renormalize  $a_2, b_2, c_2$ , such that they sum to 1, preserving the same exact

optimization problem.

## Identifying optimal cycles with reinforcement learning

In this subsection we show how the formulation of the optimization problem given in Sec. IA in terms of an extended state allows us to use RL to optimize a figure of merit containing power fluctuations, and we provide details on the RL implementation. The RL method that we use is based on the Soft Actor-Critic algorithm [7], introduced in the context of robotics and video-games [8-11], generalized to optimize multiple objectives. RL has received great attention for its success at mastering tasks beyond human-level such as playing games [12-14], for robotic applications [8, 9], and for controlling plasmas in a tokamak [15]. RL has been recently used for quantum control [16–23], outperforming previous state-of-the-art methods [24, 25], for fault-tolerant quantum computation [26, 27], and in the field of quantum thermodynamics [6, 28–30]. RL also allows to optimize "blackbox systems", i.e. to perform an optimization without requiring any explicit knowledge of the dynamics of the system being optimized, thus potentially applicable to experimental devices [6, 29]. In light of this, we expect RL to be a powerful tool also in this context. Furthermore, since RL is based on the Markovian Decision Process framework (see below and Ref. [4] for details), it is a natural choice for systems described by Markovian dynamics. In principle, also other optimization methods, such as Pontryagin's Minimum Principle, could be used [3]. However, this method only provides, in general, necessary conditions for an optimal control. Furthermore, it could in practice get stuck in local maxima, and it requires some hand-tuning in the case of non-analytic controls. As we see from our results, optimal cycles are often given by of piece-wise continuous function, which are not analytic. This would complicate the use of Pontryagin's Minimum Principle.

The method here described is an extension of the methods described in Refs. [6, 30]. We therefore refer to the Ref. [30] for an explanation of the RL method, and we adopt its notation to explain all the differences and generalizations that we put forward in this paper.

First, we define the optimization problem detailing the choice of the state space, the action space, and of the reward. Let us discretize time in time steps  $t_i = i\Delta t$ . In Ref. [30] just the power is optimized, so the state of the environment is described by the density matrix  $\rho$ . Indeed, RL is based on the Markov Decision Process assumption, meaning that the reward at a given time-step must be a function of the last state and action. In Ref. [30], the reward is the power averaged over the last time-step, which can be computed from the density matrix and from the value of the control at the last time-step. However, power fluctuations cannot be computed solely from the knowledge of  $\rho$ . Here, to optimize also power fluctuations, we employ the extended state as state of the environment, i.e. we choose as state space  $\mathcal{S} = \{(\rho, s, \vec{u}) | \rho \in \mathcal{D}, s \in \mathcal{E}, \vec{u} \in \mathcal{U}\}$ , where  $\mathcal{D} = \{\rho | \rho \geq 0, \text{Tr}[\rho] = 1\}$  is the space of density matrices,  $\mathcal{E} = \{s | s = s^{\dagger}, \text{Tr}[s] = 0\}$  is the space of traceless Hermitian operators, and  $\mathcal{U}$  is the continuous set of allowed control parameters. The state at time-step i is then given by  $s_i = (\rho_{t_i}, s_{t_i}, \vec{u}(t_{i-1}))$ . The action space is given by  $\mathcal{A} = \{(\vec{u}, \beta) | \vec{u} \in \mathcal{U}, \beta \in [\beta_H, \beta_C]\}$ , such that the action at time-step  $t_i$  is  $a_i = (\vec{u}_i, \beta_i)$ . The controls  $\vec{u}(t)$  and  $\beta(t)$  are then kept constant at  $\vec{u}_i$  for the current time-step. The reward is given by

$$r_{i} = \frac{1}{\Delta t} \int_{t_{i-1}}^{t_{i}} \left[ a \frac{P(t)}{P_{\text{max}}} - b \frac{\Delta P(t)}{\Delta P(P_{\text{max}})} - c \frac{\Sigma(t)}{\Sigma(P_{\text{max}})} \right] dt, \tag{S31}$$

which corresponds to the figure of merit averaged only over the last time-step. Together with Eqs. (3) and (7) of the main text, we see that this choice satisfies the Markov Decision Process assumption.

As in Ref. [30], we formulate the optimization problem as a discounted, continuing RL task, where the aim is to learn a policy  $\pi(a|s)$  that, at each time step  $t_i$ , maximizes the return, i.e. the long-term average of the rewards:

$$r_{i+1} + \gamma r_{i+2} + \gamma^2 r_{i+3} + \dots = \sum_{k=0}^{\infty} \gamma^k r_{i+1+k},$$
 (S32)

where  $\gamma \in [0,1)$  is the discount factor which determines how much we are interested in future rewards, as opposed to immediate rewards. By choosing  $\gamma$  close enough to 1, we are optimizing the figure of merit averaged over a long time-scale, such that the method should automatically discover to perform cycles (see Refs. [6, 30] for additional details).

In this work, we employ the soft actor-critic method [8, 9] as implemented in Ref. [30] with the following changes.

- Policy parameterization. Here we do not have a discrete action, but we have multiple continuous actions given by  $\vec{\xi} \equiv (\vec{u}, \beta)$ . We therefore need to parameterize the policy  $\pi(\vec{\xi}|s)$  as a multi-variate distribution function. We use the same approach as in Ref. [30], but we replace the normal distribution with a multivariate normal distribution. To this end, we employ a Neural Network (NN) that takes the state s as input, and outputs a vector  $\vec{\mu}$  and a matrix M. We use a multilayer perceptron NN with 2 hidden layer. We then produce samples from the multivariate normal distribution with mean  $\vec{\mu}$  and covariance matrix  $M^TM + \lambda \mathbb{1}$ , where  $\lambda > 0$  is a small real number added for numerical stability. Then, as in Ref. [30], we determine a sample of  $\pi(\vec{\xi}|s)$  applying a "squash function", in this case a hyperbolic tangent, to each variable of the multivariate distribution. This ensures that each action lies in the specified continuous interval  $\mathcal{U}$ .
- Automatic "temperature" tuning. In the soft-actor critic method, the exploration-exploitation balance is governed by the hyper-parameter  $\varepsilon$ , known in the RL literature as the "temperature" parameter. In Ref. [30],  $\varepsilon$  was scheduled during training. However, its value depends on the magnitude of the reward, making it quite model-dependent. Here, instead, we follow Ref. [8] to automatically tune  $\varepsilon$  during training. The idea is to change  $\varepsilon$  during training as to set the average entropy of the policy to a target value  $\bar{H}$ . Large values of  $\bar{H}$

produce an exploratory policy, while smaller values of  $\bar{H}$  produce a more deterministic policy. As detailed in Ref. [8] and implemented in Ref. [6], the tuning of  $\varepsilon$  is done by minimizing the following loss function

$$L_{H}(\varepsilon) \equiv \underset{s \sim \mathcal{B}}{\varepsilon} \left[ H(\pi(\cdot|s)) - \bar{H} \right], \tag{S33}$$

where  $H(P) \equiv \underset{x \sim P}{\mathbb{E}}[-\ln P(x)]$  is the entropy of the distribution P(x). For numerical stability, if  $\varepsilon$  becomes negative during training, we reset it to a small positive number. To favour exploration in the early phases of the training, while still obtaining a final policy that is nearly deterministic, we exponentially schedule the target entropy  $\bar{H}$  during training as follows

$$\bar{H}(n_{\text{steps}}) = \bar{H}_{\text{end}} + (\bar{H}_{\text{start}} - \bar{H}_{\text{end}}) \exp(-n_{\text{steps}}/\bar{H}_{\text{decay}}),$$
 (S34)

where  $\bar{H}_{\text{start}}$ ,  $\bar{H}_{\text{end}}$  and  $\bar{H}_{\text{decay}}$  are training hyperparameters.

- Training steps. The training steps are performed as in Ref. [30], i.e. repeatedly using the ADAM algorithm to minimize the loss functions  $L_{\pi}$  and  $L_{Q}$  computed over a batch of experience drawn from the replay buffer  $\mathcal{B}$ . Here, in addition, every time an optimization step of  $L_{\pi}$  and  $L_{Q}$  is performed, we also update  $\varepsilon$  performing one optimization step of  $L_{H}$  computed over the same batch of experience.
- Optimal cycle evaluation. Once the training is complete, all cycles and values of the power, power fluctuations, entropy production and efficiency reported in the main text are computed evaluating the deterministic policy. More specifically, we determine the optimal cycle using the deterministic policy, i.e. choosing actions according to the *mean* of the multivariate normal distribution, instead of sampling from it. This turns the stochastic policy into a deterministic one that typically performs better.

## II. FAST-DRIVING FOR GENERIC SYSTEMS

In this section we derive analytic expressions for the main quantities (S8) in the regime of fast-driving, i.e. when the period  $\tau$  of the cycle is small compared to the relaxation timescales of the system. As this regime is rigorously justified for stochastic dynamics, and for easiness of presentation, we will assume diagonal operators that commute at all times (cf. Ref. [31]).

First, for what concerns power and entropy production, notice, from (S8) that both can be computed from the integral of

$$\operatorname{Tr}\left[\dot{\rho}_{t}H_{\vec{u}(t)}\right] = \operatorname{Tr}\left[\mathcal{L}_{\vec{u}(t),\beta(t)}[\rho_{t}]H_{\vec{u}(t)}\right]. \tag{S35}$$

In the fast driving approximation, the cycle is much quicker than the relaxation time of the system. The consequence is that  $\rho_t \simeq \rho^{(0)}$  tends to a steady-state solution, which can be computed as the leading order of a perturbative expansion [31]. It follows that power and entropy production can be computed as

$$\langle P \rangle = \frac{1}{\tau} \int_0^{\tau} dt \operatorname{Tr} \left[ \mathcal{L}_{\vec{u}(t),\beta(t)}[\rho^{(0)}] H_{\vec{u}(t)} \right], \tag{S36}$$

$$\langle \Sigma \rangle = -\frac{1}{\tau} \int_0^{\tau} dt \operatorname{Tr} \left[ \mathcal{L}_{\vec{u}(t),\beta(t)} [\rho^{(0)}] H_{\vec{u}(t)} \right] \beta(t). \tag{S37}$$

The generic expression for  $\rho^{(0)}$  is given in Ref. [31]. At the same time, for the purposes of the present work, it is enough to consider the simple case in which the dynamics is described by a scalar master equation  $\mathcal{L}[...] = \gamma \pi_t \operatorname{Tr}[...] - \gamma \mathbb{1}$ , where

$$\pi_t = \frac{e^{-\beta(t)H_{\vec{u}(t)}}}{\text{Tr}[e^{-\beta(t)H_{\vec{u}(t)}}]}$$
 (S38)

is the instantaneous steady state and  $\gamma^{-1}$  the relaxation timescale. In such case it is clear that, as  $\rho^{(0)}$  is the steady state, it satisfies

$$\int_0^\tau dt \gamma \left( \pi_t - \rho^{(0)} \right) = 0 , \qquad (S39)$$

leading to

$$\rho^{(0)} = \frac{\int_0^{\tau} dt \ \pi_t}{\tau} = \langle \pi \rangle \ , \tag{S40}$$

and therefore

$$\langle P \rangle = \frac{1}{\tau} \int_0^\tau dt \gamma \operatorname{Tr} \left[ (\pi_t - \langle \pi \rangle) H_{\vec{u}(t)} \right], \tag{S41}$$

$$\langle \Sigma \rangle = -\frac{1}{\tau} \int_0^{\tau} dt \gamma \operatorname{Tr} \left[ (\pi_t - \langle \pi \rangle) H_{\vec{u}(t)} \right] \beta(t). \tag{S42}$$

The most general expression for the heat current in the fast-driving regime is given in Ref. [31]. In the following, we derive new analytical expressions that allow to efficiently compute also the power fluctuations in the same regime.

## Fluctuations in the Fast driving regime for arbitrary stochastic (classical) systems

As mentioned above, we will simplify the discussion by considering semi-classical systems represented by commuting operators at all time.

## 1. Simple Lindbladian

First, we start again by considering the simple scalar master equation  $\mathcal{L}[...] = \gamma \pi_t \operatorname{Tr}[...] - \gamma \mathbb{1}$ , with  $\pi_t =$  $e^{-\beta(t)H_{\vec{u}(t)}}/\operatorname{Tr}[e^{-\beta(t)H_{\vec{u}(t)}}]$ . In such case, the equations for  $\rho_t$  (S1) and  $s_t$  (S7) become (from now on we simplify the notation as  $H_{\vec{u}(t)} \equiv H_t$ )

$$\dot{\rho}_t = \gamma(\pi_t - \rho_t) \,, \tag{S43}$$

$$\dot{s}_t = -\gamma s_t + 2\rho_t \dot{H}_t - 2\operatorname{Tr}\left[\rho_t \dot{H}_t\right]\rho_t \equiv -\gamma s_t + 2\rho_t \tilde{\dot{H}}_{\rho_t}, \qquad (S44)$$

where we defined

$$\tilde{A}_{\rho} = A - \rho \operatorname{Tr}[\rho A] . \tag{S45}$$

The asymptotic solutions for  $\pi_t$  and  $s_t$ , in the case of periodic driving with period  $\tau$ , are

$$\rho_t = \frac{\int_{t-\tau}^t dt' \, \gamma \pi_{t'} e^{\gamma(t'-t)}}{1 - e^{-\gamma \tau}} \,, \tag{S46}$$

$$s_t = \frac{\int_{t-\tau}^t dt' \ 2\rho_{t'} \tilde{\dot{H}}_{\rho_{t'}} e^{\gamma(t'-t)}}{1 - e^{-\gamma\tau}} \ . \tag{S47}$$

Notice that until now, no approximation has been used. To compute all relevant quantities, we will use the fast-driving condition  $\gamma \tau \ll 1$  and expand in powers of  $\gamma \tau$ . That is,

$$\rho_t = \rho_t^{(0)} + \rho_t^{(1)} + \dots \quad \rho_t^{(i)} \sim \mathcal{O}(\gamma^i \tau^i) ,$$
(S48)

$$s_t = s_t^{(0)} + s_t^{(1)} + \dots \quad s_t^{(i)} \sim \mathcal{O}(\gamma^i \tau^i)$$
 (S49)

It is easy to verify, from (S46),

$$\rho_t^{(0)} \equiv \rho^{(0)} = \langle \pi \rangle \tag{S50}$$

$$\dot{\rho}_t^{(0)} = 0 \,, \tag{S51}$$

$$\dot{\rho}_t^{(0)} = 0 , \qquad (S51)$$

$$\dot{\rho}_t^{(1)} = \gamma (\pi_t - \rho^{(0)}) . \qquad (S52)$$

The expansion of  $s_t$  is slightly more complex, but for our purposes we only need  $s^{(0)}$ , which can be found integrating by parts (S47),

$$s_{t} = \frac{\int_{t-\tau}^{t} ds \ 2\rho_{s} \tilde{H}_{\rho_{s}} e^{\gamma(s-t)}}{1 - e^{-\gamma\tau}} = 2\rho_{t} \tilde{H}_{\rho_{t}} - \frac{2}{1 - e^{-\gamma\tau}} \int_{t-\tau}^{t} dt' \left( \dot{\rho}_{t'} \tilde{H}_{\rho_{t'}} e^{\gamma(t'-t)} + \gamma \rho_{t'} \tilde{H}_{\rho_{t'}} e^{\gamma(t'-t)} - \rho_{t'} \operatorname{Tr}[H_{t'} \dot{\rho}_{t'}] e^{\gamma(t'-t)} \right) . \tag{S53}$$

In this expression we can substitute all the quantities at the leading order, obtaining, using the fluctuations notation  $\delta A := A - \langle A \rangle$ ,

$$s_t^{(0)} = 2\rho^{(0)}\tilde{H}_{\rho^{(0)}} - \frac{2}{\gamma\tau} \int_{t-\tau}^t dt' \left( \gamma \delta \pi_{t'} \tilde{H}_{\rho^{(0)}} + \gamma \rho^{(0)} \tilde{H}_{\rho^{(0)}} - \gamma \rho^{(0)} \operatorname{Tr}[H_{t'} \delta \pi_{t'}] \right)$$
 (S54)

Notice that although  $\rho^{(0)}$  is constant, the quantity  $\tilde{H}_{\rho^{(0)}}$  (cf. Eq. (S45)) is time-dependent as  $H_t$  is time dependent. The above expression can be further simplified by dropping all the time-dependence in the notation and expanding the time-average at leading order

$$s^{(0)} = 2\left(\rho^{(0)}\tilde{H}_{\rho^{(0)}} - \langle \rho^{(0)}\tilde{H}_{\rho^{(0)}}\rangle\right) + 2\left\langle\rho^{(0)}\operatorname{Tr}[\delta H \delta \pi] + \delta \pi \operatorname{Tr}\left[\delta H \rho^{(0)}\right] - \delta \pi \delta H\right\rangle. \tag{S55}$$

Fluctuations. The fluctuations become, integrating by parts (S8),

$$\Delta P = \frac{1}{\tau} \int_0^{\tau} dt \operatorname{Tr} \left[ \dot{H}_t s_t \right] = -\frac{1}{\tau} \int_0^{\tau} dt \operatorname{Tr} \left[ H_t \dot{s}_t \right] = \frac{1}{\tau} \int_0^{\tau} dt \operatorname{Tr} \left[ H_t (\gamma s_t - 2\tilde{H}_{\rho_t}) \right]. \tag{S56}$$

Therefore we want to compute

$$I_2 = -\frac{1}{\tau} \int_0^{\tau} dt \operatorname{Tr} \left[ 2H_t \tilde{H}_{\rho_t} \right], \tag{S57}$$

$$I_1 = \frac{1}{\tau} \int_0^\tau dt \operatorname{Tr}[\gamma H_t s_t] , \qquad (S58)$$

at leading order. Let's compute the two terms

$$I_{2} = -\frac{1}{\tau} \int_{0}^{\tau} dt \operatorname{Tr} \left[ 2H_{t} \tilde{\dot{H}}_{\rho_{t}} \right] = -\frac{1}{\tau} \int_{0}^{\tau} dt \operatorname{Tr} \left[ 2H_{t} (\dot{H}_{t} \rho_{t} - \rho_{t} \operatorname{Tr} \left[ \dot{H}_{t} \rho_{t} \right]) \right] = \frac{1}{\tau} \int_{0}^{\tau} dt \operatorname{Tr} \left[ H_{t}^{2} \dot{\rho}_{t} - 2 \operatorname{Tr} \left[ \rho_{t} H_{t} \right] \operatorname{Tr} \left[ \dot{\rho}_{t} H_{t} \right] \right] = \frac{1}{\tau} \int_{0}^{\tau} dt \operatorname{Tr} \left[ H_{t}^{2} \dot{\rho}_{t} - 2 \operatorname{Tr} \left[ \rho_{t} H_{t} \right] \operatorname{Tr} \left[ \dot{\rho}_{t} H_{t} \right] \right] = \frac{1}{\tau} \int_{0}^{\tau} dt \operatorname{Tr} \left[ H_{t}^{2} \dot{\rho}_{t} - 2 \operatorname{Tr} \left[ H_{t} \partial_{t} \right] \operatorname{Tr} \left[ \dot{\rho}_{t} H_{t} \right] \right] = \frac{1}{\tau} \int_{0}^{\tau} dt \operatorname{Tr} \left[ H_{t}^{2} \dot{\rho}_{t} - 2 \operatorname{Tr} \left[ \rho_{t} H_{t} \right] \operatorname{Tr} \left[ \dot{\rho}_{t} H_{t} \right] \right] = \frac{1}{\tau} \int_{0}^{\tau} dt \operatorname{Tr} \left[ H_{t}^{2} \dot{\rho}_{t} - 2 \operatorname{Tr} \left[ \rho_{t} H_{t} \right] \operatorname{Tr} \left[ \dot{\rho}_{t} H_{t} \right] \right] = \frac{1}{\tau} \int_{0}^{\tau} dt \operatorname{Tr} \left[ H_{t}^{2} \dot{\rho}_{t} - 2 \operatorname{Tr} \left[ \rho_{t} H_{t} \right] \operatorname{Tr} \left[ \dot{\rho}_{t} H_{t} \right] \right] = \frac{1}{\tau} \int_{0}^{\tau} dt \operatorname{Tr} \left[ H_{t}^{2} \dot{\rho}_{t} - 2 \operatorname{Tr} \left[ \dot{\rho}_{t} H_{t} \right] \operatorname{Tr} \left[ \dot{\rho}_{t} H_{t} \right] \right] = \frac{1}{\tau} \int_{0}^{\tau} dt \operatorname{Tr} \left[ H_{t}^{2} \dot{\rho}_{t} - 2 \operatorname{Tr} \left[ \dot{\rho}_{t} H_{t} \right] \operatorname{Tr} \left[ \dot{\rho}_{t} H_{t} \right] \right] = \frac{1}{\tau} \int_{0}^{\tau} dt \operatorname{Tr} \left[ H_{t}^{2} \dot{\rho}_{t} - 2 \operatorname{Tr} \left[ \dot{\rho}_{t} H_{t} \right] \operatorname{Tr} \left[ \dot{\rho}_{t} H_{t} \right] \right] = \frac{1}{\tau} \int_{0}^{\tau} dt \operatorname{Tr} \left[ H_{t}^{2} \dot{\rho}_{t} - 2 \operatorname{Tr} \left[ \dot{\rho}_{t} H_{t} \right] \operatorname{Tr} \left[ \dot{\rho}_{t} H_{t} \right] \right] = \frac{1}{\tau} \int_{0}^{\tau} dt \operatorname{Tr} \left[ H_{t}^{2} \dot{\rho}_{t} - 2 \operatorname{Tr} \left[ \dot{\rho}_{t} H_{t} \right] \operatorname{Tr} \left[ \dot{\rho}_{t} H_{t} \right] \right] = \frac{1}{\tau} \int_{0}^{\tau} dt \operatorname{Tr} \left[ H_{t}^{2} \dot{\rho}_{t} - 2 \operatorname{Tr} \left[ \dot{\rho}_{t} H_{t} \right] \operatorname{Tr} \left[ \dot{\rho}_{t} H_{t} \right] \right] = \frac{1}{\tau} \int_{0}^{\tau} dt \operatorname{Tr} \left[ H_{t}^{2} \dot{\rho}_{t} - 2 \operatorname{Tr} \left[ \dot{\rho}_{t} H_{t} \right] \operatorname{Tr} \left[ \dot{\rho}_{t} + 2 \operatorname{Tr} \left[ \dot{\rho}_{t} H_{t} \right] \right] = \frac{1}{\tau} \int_{0}^{\tau} dt \operatorname{Tr} \left[ H_{t}^{2} \dot{\rho}_{t} + 2 \operatorname{Tr} \left[ \dot{\rho}_{t} + 2 \operatorname{Tr} \left[ \dot{\rho}_{t} \right] \right] \right] + \frac{1}{\tau} \int_{0}^{\tau} dt \operatorname{Tr} \left[ H_{t}^{2} \dot{\rho}_{t} + 2 \operatorname{Tr} \left[ \dot{\rho}_{t} + 2 \operatorname{Tr} \left[ \dot{\rho}_{t} \right] \right] + \frac{1}{\tau} \int_{0}^{\tau} dt \operatorname{Tr} \left[ H_{t}^{2} \dot{\rho}_{t} + 2 \operatorname{Tr} \left[ \dot{\rho}_{t} + 2 \operatorname{Tr} \left[ \dot{\rho}_{t} + 2 \operatorname{Tr} \left[ \dot{\rho}_{t} \right] \right] \right]$$

where for the last equality we used the equation of motions  $\dot{\rho}_t = \gamma(\pi_t - \rho_t)$  a the leading order, where  $\rho_t \sim \rho^{(0)} = \langle \pi \rangle$ . We remind that we use the notation  $\delta A := A - \langle A \rangle$ . Notice that for  $I_1$  we only need s at order  $\mathcal{O}(\gamma^0 \tau^0)$ .  $I_1$  can therefore be computed as

$$I_1 = \gamma \langle \text{Tr} \left[ H s^{(0)} \right] \rangle , \qquad (S60)$$

and the total fluctuations are, after substituting  $s^{(0)}$  (S55) and some tedious algebra,

$$\frac{\Delta P}{2\gamma} = \frac{I_2 + I_1}{2\gamma} = \left\langle \text{Tr} \left[ \rho^{(0)} H^2 \right] - \text{Tr} \left[ \rho^{(0)} H \right]^2 \right\rangle - \left( \text{Tr} \left[ \rho^{(0)} \langle H \rangle^2 \right] - \text{Tr} \left[ \rho^{(0)} \langle H \rangle \right]^2 \right) + \frac{1}{2} \langle \text{Tr} \left[ \delta H^2 \delta \pi \right] \rangle - \langle \text{Tr} \left[ \delta H \delta \pi \right] \text{Tr} \left[ \delta H \rho^{(0)} \right] \rangle .$$
(S61)

Under the same assumptions, the power (S41) can be expressed as

$$P = \gamma \langle \text{Tr}[(\pi - \langle \pi \rangle)(H - \langle H \rangle)] \rangle \equiv \gamma \, \text{Tr}[\text{Cov}[\pi, H]], \tag{S62}$$

and similarly the entropy production (S42)

$$\Sigma = \gamma \langle \text{Tr}[(\pi - \langle \pi \rangle)(\beta H - \langle \beta H \rangle)] \rangle \equiv \gamma \text{Tr}[\text{Cov}[\pi, \beta H]], \tag{S63}$$

where the covariance is with respect to time.

Moving to the case of a general Lindbladian, the expression for power and entropy production can be found as from Reference [31]. For what concerns the fluctuations, these can be again expressed as (see (S56))

$$\Delta P = -\frac{1}{\tau} \int_0^{\tau} dt \operatorname{Tr}[H_t \dot{s}_t] = -\frac{1}{\tau} \int_0^{\tau} dt \operatorname{Tr}\left[H_t(\mathcal{L}_t[s_t] + 2\tilde{H}_{\rho_t})\right] = I_1 + I_2.$$
 (S64)

In the next expressions we drop all the time-dependencies to simplify the notation. The computation of  $I_1$  and  $I_2$  is in this case

$$I_{2} = -\frac{1}{\tau} \int_{0}^{\tau} dt \operatorname{Tr} \left[ 2H \tilde{H}_{\rho} \right] = \langle \operatorname{Tr} \left[ H^{2} \mathcal{L}[\rho^{(0)}] \right] \rangle - 2 \langle \operatorname{Tr} \left[ H \mathcal{L}[\rho^{(0)}] \right] \operatorname{Tr} \left[ H \rho^{(0)} \right] \rangle , \tag{S65}$$

$$I_1 = -\frac{1}{\tau} \int_0^{\tau} dt \operatorname{Tr}[H\mathcal{L}[s_0]] , \qquad (S66)$$

where the first expression can be obtained integrating by parts, and everything is expanded at the leading order in  $|\mathcal{L}|\tau$ ,  $\rho^{(0)}$  is the steady state of the fast driving (see [31] for an analytical expression) and  $s_0$  is the leading order term of s, which can be computed from the analytical solution

$$s_t = \int_{-\infty}^t dt' \ U_{t,t'}[2\rho_{t'}\tilde{H}_{\rho_{t'}}] \ , \tag{S67}$$

 $U_{t,t'}$  being the propagator, i.e. time-ordered exponential of  $\mathcal{L}$  between t' and  $t \geq t'$ . Expanding the leading term one obtains

$$s_0 = 2\rho^{(0)}\tilde{H}_{\rho^{(0)}} + 2\langle \mathcal{L} \rangle^{-1} \left( \langle \mathcal{L}[\rho^{(0)}]\tilde{H}_{\rho^{(0)}} \rangle - \rho^{(0)} \operatorname{Tr} \left[ \langle H\mathcal{L}[\rho^{(0)}] \rangle \right] - \langle \mathcal{L}[\rho^{(0)}\tilde{H}_{\rho^{(0)}}] \rangle \right). \tag{S68}$$

#### III. QUANTUM DOT BASED HEAT ENGINE

#### A. Optimality of the Otto cycle in the fast driving for power and entropy production trade-offs

Here we prove that, among all possible cycles described by  $\beta(t)$  and u(t), Otto cycles in the fast driving regime maximize an arbitrary trade-off between power and entropy production. The proof stems from a simple generalization of Appendix A of Ref. [32], where it is shown that, among all possible Otto cycles, Otto cycles in the fast driving regime maximize the power.

To this end, we consider the figure of merit  $\langle F \rangle$  with b=0:

$$\langle F \rangle = a \frac{\langle P \rangle}{P_{\text{max}}} - c \frac{\langle \Sigma \rangle}{\Sigma(P_{\text{max}})}.$$
 (S69)

By neglecting fluctuations, we no not need the extended state, so we can write  $\langle F \rangle$  as the time average of a function of the state  $p_t$  (defined in the main text) and of the controls  $\beta(t)$  and u(t), i.e. as

$$\langle F \rangle = \frac{1}{\tau} \int_0^\tau f(p_t, u(t), \beta(t)) dt, \tag{S70}$$

where  $f(p, u, \beta)$  is a suitable function. This assumption is sufficient to use the argument of [32], with  $\langle F \rangle$  replacing the average power, to prove that optimal cycles are Otto cycles in the fast-driving regime. Here we outline the general idea, referring to [32] for additional details. As argued here and in [32], given a cycle with period  $\tau$ , also the state  $p_t$  will become periodic with the same period  $\tau$ . We can thus represent an arbitrary cycle cycle as a closed curve in the u-p plane and in the  $\beta-p$  plane. It can be shown that, given any fixed cycle u(t) and  $\beta(t)$ , we can always define two sub-cycles such that one of the two has a larger or equal  $\langle F \rangle$  than the original one. The two sub-cycles are defined by introducing quenches in the control, i.e. "cutting vertically" the cycle represented in the u-p and  $\beta-p$  plane. By reiterating this process over and over, we end up with an Otto cycle in the fast driving regime, thus concluding the proof.

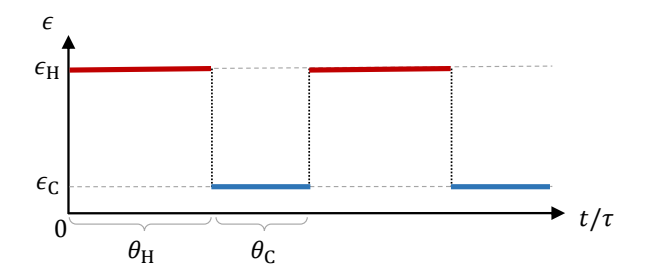


FIG. S1. Schematic representation of the Otto cycle. The value of the gap  $\epsilon(t) \equiv u(t)E_0$  is plotted as a function of  $t/\tau$ . The red segment corresponds to setting  $\beta(t) = \beta_{\rm H}$ , and the blue segment to  $\beta(t) = \beta_{\rm C}$ .

#### B. Fast driving regime

Using Eqs. (S61,S62,S63), we can easily compute the power, entropy production and fluctuations of a generic Otto cycle in the fast driving regime. We fix an Otto cycle as in Fig. S1, where  $\epsilon_{\rm H}$  and  $\epsilon_{\rm C}$  are the values of  $u(t)E_0$  while in contact respectively with the hot (H) and cold (C) bath, and  $\theta_{\rm H}$  and  $\theta_{\rm C}$  represent the time fraction of the cycle spent in contact with the respective bath ( $\theta_{\rm C} + \theta_{\rm H} = 1$ ). This yields

$$\langle P \rangle = \gamma \theta_{\rm H} \theta_{\rm C} (\epsilon_{\rm H} - \epsilon_{\rm C}) (f_{\rm H} - f_{\rm C}),$$

$$\langle \Delta P \rangle = 2\gamma \, \theta_{\rm H} \theta_{\rm C} (\epsilon_{\rm H} - \epsilon_{\rm C})^2 \left[ \bar{f} (1 - \bar{f}) + (\frac{f_{\rm C} + f_{\rm H}}{2} - \bar{f}) (1 - 2\bar{f}) \right],$$

$$\langle \Sigma \rangle = -\gamma \theta_{\rm H} \theta_{\rm C} (\beta_{\rm H} \epsilon_{\rm H} - \beta_{\rm C} \epsilon_{\rm C}) (f_{\rm H} - f_{\rm C}),$$
(S71)

where we define  $f_{\alpha} = f(\beta_{\alpha}\epsilon_{\alpha})$ , for  $\alpha = H, C$  and the average excited state occupation  $\bar{f} = \theta_H f_H + \theta_C f_C$ . Without loss of generality, in the heat engine regime we can assume  $\epsilon_{\alpha} \geq 0$ . This condition, together with the heat engine condition  $P \geq 0$ , can be expressed as

$$0 < x_{\rm H} < x_{\rm C} < x_{\rm H} (1 + dT),$$
 (S72)

where we introduce the dimensionless quantities  $x_{\alpha} = \beta_{\alpha} \epsilon_{\alpha}$ , and where we define the dimensionless temperature difference

$$dT \equiv \beta_{\mathcal{C}}(\beta_{\mathcal{H}}^{-1} - \beta_{\mathcal{C}}^{-1}). \tag{S73}$$

For simplicity, in this appendix we define a figure of merit G with a different normalization, i.e.

$$\langle G \rangle = a \left( \frac{\langle P \rangle}{\gamma T} \right) - b \left( \frac{\langle \Delta P \rangle}{\gamma T^2} \right) - c \left( \frac{\langle \Sigma \rangle}{\gamma} \right),$$
 (S74)

where  $T = \beta_{\rm C}^{-1}$  and  $k_B = 1$ .

We now assume that the temperature difference is small, i.e. that  $dT \ll 1$ . We therefore study  $\langle G \rangle$  to leading order in dT. We carry out the optimization with respect to the time fractions  $\theta_{\alpha}$  and with respect to the dimensionless energy gaps  $x_{\alpha}$ . We expand  $x_{\rm C}$  as

$$x_{\rm C} = x_{\rm H}(1 + \delta x_{\rm C}). \tag{S75}$$

Imposing the heat engine condition in Eq. (S72), we find that  $\delta x_{\rm C}$  must satisfy

$$0 \le \delta x_{\rm C} \le dT; \tag{S76}$$

therefore,  $\delta x_{\rm C}$  is a first order quantity in dT. Expanding  $\langle P \rangle$ ,  $\langle \Delta P \rangle$  and  $\langle \Sigma \rangle$  to leading order in dT, we find

$$\langle P \rangle / (\gamma T) = \theta_{\rm C} \theta_{\rm H} g(x_{\rm H}) \delta x_{\rm C} (dT - \delta x_{\rm C}),$$

$$\langle \Delta P \rangle / (\gamma T^2) = 2\theta_{\rm C} \theta_{\rm H} g(x_{\rm H}) (dT - \delta x_{\rm C})^2,$$

$$\langle \Sigma \rangle / \gamma = \theta_{\rm C} \theta_{\rm H} g(x_{\rm H}) \delta x_{\rm C}^2,$$
(S77)

where we define

$$g(x) \equiv \frac{x^2}{2(1 + \cosh x)}. ag{S78}$$

Plugging this expansion into Eq. (S74) yields

$$\langle G \rangle = \theta_{\rm H} \theta_{\rm C} g(x_{\rm H}) \left[ \delta x_{\rm C} \left( a dT - (a+c) \delta x_{\rm C} \right) - 2b \left( dT - \delta x_{\rm C} \right)^2 \right]. \tag{S79}$$

First, we notice that  $\langle P \rangle$ ,  $\langle \Delta P \rangle$  and  $\langle \Sigma \rangle$  in Eq. (S77), valid in the small temperature difference regime, exactly saturate the steady-state thermodynamic uncertainty relation even before performing any optimization, i.e.  $\xi = 1$ , where, combining Eqs. (1) of the main text and (S10)

$$\xi = 2 \frac{\langle P \rangle^2}{\langle \Sigma \rangle \langle \Delta P \rangle}.$$
 (S80)

We now maximize  $\langle G \rangle$  as written in Eq. (S79). The optimization over  $\theta_{\alpha}$  and  $x_{\rm H}$  depends on the term in the square parenthesis. We therefore distinguish two cases:

1. Case 1

If the term in square parenthesis is non-null, then we trivially have that  $\theta_{\alpha} = 1/2$  and  $x_{\rm H} = x_{\rm max}$ , where  $x_{\rm max}$  is the value that maximizes g(x). It is implicitly defined by  $x_{\rm max} > 0$  and by solving the transcendental equation

$$x_{\text{max}} \tanh(x_{\text{max}}/2) = 2. \tag{S81}$$

We can then determine  $\delta x_{\rm C}$  by taking the derivative of G and setting it to zero. This yields

$$\delta x_{\rm C}^{*1} = \frac{a+4b}{2a+4b+2c}dT. \tag{S82}$$

It is easy to see that this solution always satisfies the heat engine condition in Eq. (S76). In this point we have that

$$\langle G \rangle^{*1} = g_{\text{max}} \frac{a^2 - 8bc}{16(a+2b+c)} dT^2,$$
 (S83)

where we define  $g_{\text{max}} \equiv g(x_{\text{max}}) \approx 2.40$ , and

$$\langle P \rangle^{*1} / (\gamma T) = g_{\text{max}} \frac{(a+4b)(a+2c)}{16(a+2b+c)^2} dT^2, \qquad \langle \Delta P \rangle^{*1} / (\gamma T^2) = g_{\text{max}} \frac{(a+2c)^2}{8(a+2b+c)^2} dT^2,$$

$$\langle \Sigma \rangle^{*1} / \gamma = g_{\text{max}} \frac{(a+4b)^2}{16(a+2b+c)^2} dT^2, \qquad \frac{\eta^{*1}}{\eta_c} = \frac{a+2c}{2a+4b+2c}.$$
(S84)

We thus see that if  $a^2 - 8bc > 0$ , then the figure of merit is positive. In the opposite case, the figure of merit is negative, so doing nothing becomes more convenient (since doing nothing, or doing Carnot cycles, gives  $\langle G \rangle = 0$ ). Notice that if  $a^2 = 8bc$ , then any value of  $\theta_{\alpha}$  and  $x_{\rm H}$  gives the same figure of merit, so all these solutions must be included in the Pareto front.

Setting a = 1 and b = c = 0, we find the maximum power solution:

$$\frac{P_{\text{max}}}{\gamma T} = \frac{g_{\text{max}}}{16} dT^2, \qquad \frac{\Delta P(P_{\text{max}})}{\gamma T^2} = \frac{g_{\text{max}}}{8} dT^2, \qquad \frac{\Sigma(P_{\text{max}})}{\gamma} = \frac{g_{\text{max}}}{16} dT^2, \qquad \frac{\eta}{\eta_{\text{c}}} = \frac{1}{2}. \tag{S85}$$

These relations imply

$$\Delta P(P_{\text{max}}) = 2TP_{\text{max}}.\tag{S86}$$

Setting c = 0 and b = 1 - a in Eq. (S84), we can find the Pareto front between power and power fluctuations, i.e. the outer border of Fig. 3 of the main text. After some algebra, it can be shown that

$$\frac{\langle P \rangle}{P_{\text{max}}} = 2\sqrt{\frac{\langle \Delta P \rangle}{\Delta P(P_{\text{max}})}} - \frac{\langle \Delta P \rangle}{\Delta P(P_{\text{max}})}.$$
 (S87)

This corresponds to the black border shown in Fig. 3 of the main text

We now consider the case where the term in the square parenthesis of Eq. (S79) is zero. This happens in two cases, i.e. when

$$\delta x_{\rm C}^{*2} = \frac{a + 4b - \sqrt{a^2 - 8bc}}{2a + 4b + 2c} dT,$$

$$\delta x_{\rm C}^{*3} = \frac{a + 4b + \sqrt{a^2 - 8bc}}{2a + 4b + 2c} dT.$$
(S88)

These solutions hold when  $a^2 - 8bc \ge 0$ . In the opposite case, there is no solution. Both solutions can be shown to always satisfy the heat engine condition in Eq. (S76), and in this point we have

$$\langle G \rangle^{*2,3} = 0. \tag{S89}$$

However, this zero value of the figure of merit occurs delivering a positive power that is compensated by the negative sign in front of the finite fluctuations and of the finite entropy production. It can be shown that such solutions either lie on the boundary Eq. (S87), or inside. We further notice that, looking at the figure of merit, both these solutions are suboptimal with respect to case 1, except for being equivalent in the special case when  $a^2 = 8bc$ .

#### 3. Fast driving Pareto front

As we have seen, Otto cycles in the fast driving, expanded to leading order in the temperature difference, exactly satisfy the steady-state thermodynamic uncertainty relation  $\xi = 1$ . Furthermore, the trade-off between power and power fluctuations is given by Eq. (S87). Therefore, the entire Pareto front, plotted in Fig. 3a of the main text, is simply obtained by imposing the thermodynamic uncertainty relation, together with the boundary of Eq. (S87).

However, it could in principle be possible that points inside the boundary of Eq. (S87) may not be reached, i.e. there may not be any Otto cycle in the fast driving regime reaching some of these points. Using the results of the previous subsections, it can be verified that this is not the case, i.e. that there is an Otto cycle in the fast driving regime corresponding to all points shown in Fig. 3a of the main text.

4. Positive figure of merit boundary for Otto cycles in the fast-driving regime

In this section we derive the expression for the black boundary shown in Fig. 2b of the main text. As we have seen in the previous two subsections, the condition

$$a^2 = 8bc, (S90)$$

with b=1-a-c, determines the boundary between positive and zero value of the optimized figure of merit in the fast-driving regime. However, this condition was found with the normalization of  $\langle P \rangle$ ,  $\langle \Delta P \rangle$  and  $\langle \Sigma \rangle$  defined as in Eq. (S74), while the boundary shown in Fig. 2 of the main text is relative to the normalization chosen in Eq. (8) of the main text. To account for this, we need to "change the coordinate system" from  $(a_0, b_0, c_0)$  to  $(a_1, b_1, c_1)$ . Let us define

$$\langle G_0 \rangle \equiv a_0 \langle P \rangle - b_0 \langle \Delta P \rangle - c_0 \langle \Sigma \rangle,$$
 (S91)

and let us consider a given cycle that maximize  $G_0$  at given  $(a_0, b_0, c_0)$ . We want to see how the coefficients  $(a_1, b_1, c_1)$  must be chosen in order to find the *same* cycle when maximizing

$$\langle G_1 \rangle = a_1 \left( \frac{\langle P \rangle}{\lambda_a} \right) - b_1 \left( \frac{\langle \Delta P \rangle}{\lambda_b} \right) - c_1 \left( \frac{\langle \Sigma \rangle}{\lambda_c} \right),$$
 (S92)

where  $\lambda_a$ ,  $\lambda_b$  and  $\lambda_c$  are given coefficients.

It can be shown that the following identity holds:

$$\langle G_0 \rangle = N \langle G1 \rangle, \tag{S93}$$

where we choose

$$(a_1, b_1, c_1) = (\lambda_a a_0, \lambda_b b_0, \lambda_c c_0)/N,$$
 (S94)

with

$$N = \lambda_a a_0 + \lambda_b b_0 + \lambda_c c_0. \tag{S95}$$

Since N is just a proportionality factor, they will share the same maximums. Therefore Eq. (S94) defines the "change of coordinates". In order to transform the boundary in Eq. (S90) to the "new coordinate system", we need to invert Eq. (S94). Using that b = 1 - a - c in both coordinate systems, we find

$$\begin{pmatrix} a_0 \\ c_0 \end{pmatrix} = \frac{\lambda_b}{a_1 \lambda_c (\lambda_b - \lambda_a) + c_1 \lambda_a (\lambda_b - \lambda_c) + \lambda_a \lambda_c} \begin{pmatrix} \lambda_c a_1 \\ \lambda_a c_1 \end{pmatrix}. \tag{S96}$$

Plugging this into Eq. (S90) yields

$$a_1^2 = \frac{\lambda_a^2}{\lambda_b \lambda_c} 8c_1 (1 - a_1 - c_1). \tag{S97}$$

Using Eq. (S85), we choose

$$\lambda_a = \frac{g_{\text{max}}}{16} dT^2, \qquad \lambda_b = \frac{g_{\text{max}}}{8} dT^2, \qquad \lambda_c = \frac{g_{\text{max}}}{16} dT^2, \qquad (S98)$$

and solve for a. Retaining the correct solution, we find

$$a = 2(c - \sqrt{c}). \tag{S99}$$

This corresponds to the black curve shown in Fig. 2b of the main text.

#### C. Slow driving regime

Here we optimize the trade-off between power, entropy production and power fluctuations for the quantum dot engine in the slow-driving regime. For this regime we split the protocol of the cycle into four steps: (i) we fix the bath at a cold temperature  $T_{\rm C}$  and we slowly vary the dot energy  $\epsilon(t) \equiv u(t)E_0$  for a time  $\tau_C$  from  $\epsilon(0) = \epsilon_A$  to  $\epsilon(\tau_C^-) = \epsilon_B$ . (ii) We now change the bath temperature to  $T_{\rm H}$  (>  $T_{\rm C}$ ), all while we are changing the energy to  $\epsilon_B T_{\rm H}/T_{\rm C}$  in such a way that the populations of the dot levels remain constant all along the process (because  $[H_{u(t)}, H_{u(t')}] = 0 \ \forall t, t'$ ). This property allows us to perform this step arbitrarily fast without affecting the objectives. (iii) while keeping the bath temperature at  $T_{\rm H}$  we slowly vary the dot energy from  $\epsilon(\tau_C^+) = \epsilon_B T_{\rm H}/T_{\rm C}$  to  $\epsilon(\tau^-) = \epsilon_A T_{\rm H}/T_{\rm C}$  in a time  $\tau_H = \tau - \tau_C$ . (iv) A second quench is performed (in the same manner as step (ii)) to bring the temperature to  $T_{\rm C}$  and the dot energy to  $\epsilon_A$ , which closes the cycle.

During each isotherm we can divide the heat exchange in the following manner:

$$Q_x = T_x \Delta S_x - W_x^{\text{diss}}, \quad x = (H, C) \tag{S100}$$

where  $T_x \Delta S_x$  is the reversible contribution and corresponds to the quasistatic limit  $\tau_x \to \infty$ . The reversible term is given by  $\Delta S \equiv \Delta S_H = -\Delta S_C = S(\pi_0) - S(\pi_{\tau_C})$  with  $S(\pi)$  the Von Neumann entropy. Crucially, we will from now on assume the *slow driving* regime (aka. *low dissipation*). That is, we assume that the relaxation time scale  $\gamma^{-1}$  of the system is much smaller than the time it takes to complete the protocol. This allows us to expand the relevant quantities in orders of  $1/(\gamma \tau_x)$  and keep only the leading terms. In this regime the state can be written as

$$\rho_t = \pi_t + \frac{1}{\tau \gamma} \rho_t^{(1)} + \mathcal{O}(\frac{1}{\gamma^2 \tau^2}). \tag{S101}$$

It is important to note that when the quenches of steps (ii) and (iv) are performed the adiabatic term  $\pi_t$  only contributes reversible work, but the corrective term  $\frac{1}{\tau\gamma}\rho_t^{(1)}$  will cause dissipated work of order  $\frac{1}{\tau\gamma}$ . For simplicity we want to neglect those terms, in order to do so we can add a waiting time  $\tau_w = \tau \Delta s$  at the end of each isotherm. By using the same Lindbladian model as in the fast driving regime (S43), it is clear that during this waiting time the corrective term is exponentially suppressed. Therefore the total protocol time is now  $\tau = \tau_C + \tau_H + 2\tau_w = \frac{\tau_C + \tau_H}{12 + 2\lambda s}$ .

As a result of the slow driving expansion, for each isotherm the irreversible terms can be written as [33–42]:

$$W_x^{\text{diss}} = \frac{T_x}{\tau_x} \int ds \ m_{\epsilon\epsilon} \dot{\epsilon}(s)^2 \equiv T_x \frac{\sigma_x}{\tau_x} + \mathcal{O}(\frac{1}{\gamma^2 \tau_x^2}), \tag{S102}$$

where  $m_{\epsilon\epsilon} = \gamma^{-1}\partial^2 \ln \text{Tr} \left[e^{-\beta H_u}\right]/\partial \epsilon^2$  is the thermodynamic metric. Furthermore, since we only change the temperature of the bath without affecting its spectral density we have that the optimal protocol verifies  $\sigma_H = \sigma_C$  [34, 41]. We will therefore drop this index going forward. In a cycle the work extracted is  $W = Q_C + Q_H$ , therefore the power of the engine reads

$$\langle P \rangle = \frac{1}{\tau} \Delta T \Delta S - \frac{\sigma}{\tau} \left( \frac{T_{\rm H}}{\tau_H} + \frac{T_{\rm C}}{\tau_C} \right),$$
 (S103)

with  $\Delta = T_{\rm H} - T_{\rm C}$ . The slow driving regime allows us to use fluctuation dissipation relations [2, 43–47] to compute the fluctuations of the work: in particular we have  $\frac{1}{2} {\rm Var}(W_x) = T_x W_x^{\rm diss}$ . Instead over the quenches we get  ${\rm Var}(W_y) = \Delta T^2 C_y$ , where  $C_y = -\beta^2 \partial^2 \ln {\rm Tr} \left[ e^{-\beta H_{u_y}} \right] / \partial \beta^2$  is the heat capacity, for y = A, B. Therefore the power fluctuations of the full cycle are

$$\langle \Delta P \rangle = \frac{\text{Var}(W)}{\tau} = \frac{1}{\tau} \Delta T^2 \left( C_A + C_B \right) + \frac{2\sigma}{\tau} \left( \frac{T_H^2}{\tau_H} + \frac{T_C^2}{\tau_C} \right). \tag{S104}$$

The entropy production rate is, by definition,

$$\langle \Sigma \rangle = \frac{\sigma}{\tau} \left( \frac{1}{\tau_H} + \frac{1}{\tau_C} \right). \tag{S105}$$

In this appendix we define a figure of merit where the normalization has been absorbed in the weights

$$G = a\langle P \rangle - \frac{b}{2} \langle \Delta P \rangle - c \langle \Sigma \rangle = \frac{1}{\tau} \left[ \Delta T A - \sigma \left( \frac{\delta_H^2}{\tau_H} + \frac{\delta_C^2}{\tau_C} \right) \right]$$
 (S106)

with  $A = a\Delta S - \frac{1}{2}b\Delta T(C_A + C_B)$  and  $\delta_x^2 = aT_x + bT_x^2 + c$ .

#### 1. Optimization of the cycle

From (S106) we can see that, for given bath temperatures, A depends only on the boundary values  $\epsilon_A$  and  $\epsilon_B$  and  $\sigma$  only depends on the protocol's geometric shape between those boundaries. Therefore all the dependence on protocol time has been rendered explicit and we can optimize over it by setting the derivatives with respect to  $\tau_C$  and  $\tau_C$  to zero: we find

$$\tau_H = 2\left(\delta_H + \delta_C\right) \frac{\delta_H \sigma}{\Delta T A},\tag{S107}$$

$$\tau_C = 2\left(\delta_H + \delta_C\right) \frac{\delta_C \sigma}{\Delta T A},\tag{S108}$$

$$\tau = 2\frac{\left(\delta_H + \delta_C\right)^2}{1 - 2\Delta s} \frac{\sigma}{\Delta T A}.$$
 (S109)

It is important to note that, for the time optimization to be valid, we require that A is strictly positive. If A is negative we can see that G is also negative. But a cycle in which we do nothing results in G=0 which is "better" than a cycle where G is negative, therefore we can always assume A to be positive. We must now check the positivity of A. It is quite easy to see that if a=0 then A is negative and therefore the optimal cycle is to do nothing. But if a>0 we then have that A is strictly larger than zero if and only if

$$\frac{\Delta S}{C_A + C_B} > \frac{b}{2a} \Delta T. \tag{S110}$$

It is clear that this equation can always be satisfied by choosing endpoints of the protocol ( $\epsilon_A$  and  $\epsilon_B$ ) that have vanishing heat capacity.

When we insert the optimal times into the figure of merit we find

$$G = \frac{A^2 \Delta T^2}{4\sigma} \frac{1 - 2\Delta s}{(\delta_H + \delta_C)^2}.$$
 (S111)

During the waiting time at the end of each isotherm, the decay towards the thermal state goes as  $e^{-\tau\gamma\Delta s}$ , to be able to neglect the correction we have to set  $\tau\gamma\Delta s=r$ , where r is some arbitrary  $\mathcal{O}(1)$  constant that is sufficiently large. Therefore we find  $\Delta s=\frac{1}{2}\frac{rA}{rA+(\delta_H+\delta_C)^2\sigma}$ , which leads to a new form of G:

$$G = \frac{1}{4} \frac{A^2 \Delta T^2}{rA + (\delta_H + \delta_C)^2 \sigma}.$$
 (S112)

At this point, the only term that depends on the protocol shape (given its boundaries) is  $\sigma$ . As one would expect, G is maximized when  $\sigma$  is minimized. It has been shown [48, 49] that  $\sigma$  is minimized by the thermodynamic length  $\sigma_{min} = L^2 = 4\arccos\left(\sqrt{p_A p_B} + \sqrt{(1-p_A)(1-p_B)}\right)^2$ , where  $p_{A,B} = (1+e^{\beta_C \epsilon_{A,B}})^{-1}$  is the occupation probability of the excited state at the endpoints of the isotherms.

Now we only have to optimize over the endpoints of the protocol the figure of merit  $G = \frac{1}{4} \frac{A^2 \Delta T^2}{rA + (\delta_H + \delta_C)^2 L^2}$ . By taking derivatives with respect to  $\epsilon_A$  and  $\epsilon_B$  we find two transcendental equations that cannot be solved analytically. Equivalently, we can optimize with respect to  $p_A$  and  $p_B$ , though the same problem persists. But these variables are more practical for numerical optimization as they are defined on the finite range [0,0.5]. Therefore we do a numerical maximization of G for this last step, from the form of G it can be seen that the couple  $(p_A, p_B)$  that maximizes G depends only on two parameters (assuming the temperatures are given):  $\alpha := b\Delta T/a$  and  $\alpha' := c/a$ . We can note that a choice of these parameters defines which trade-off of the objectives we want. Furthermore we have to satisfy the constraint  $\frac{\Delta S}{C_A + C_B} > \alpha/2$  (see eq. (S110)). From a numerical point of view, in order to plot the Pareto front, we are interested in a range of values of  $\alpha$  and  $\alpha'$  that range from  $10^{-2}$  to  $10^2$ . The optimization was done using a Mathematica script and is shown in Fig. S2, then we can use this to compute the power, efficiency, and power fluctuations for different trade-off ratios  $\alpha$  and  $\alpha'$  with which we obtain the Pareto front shown in panel b of Fig. 3 of the main text.

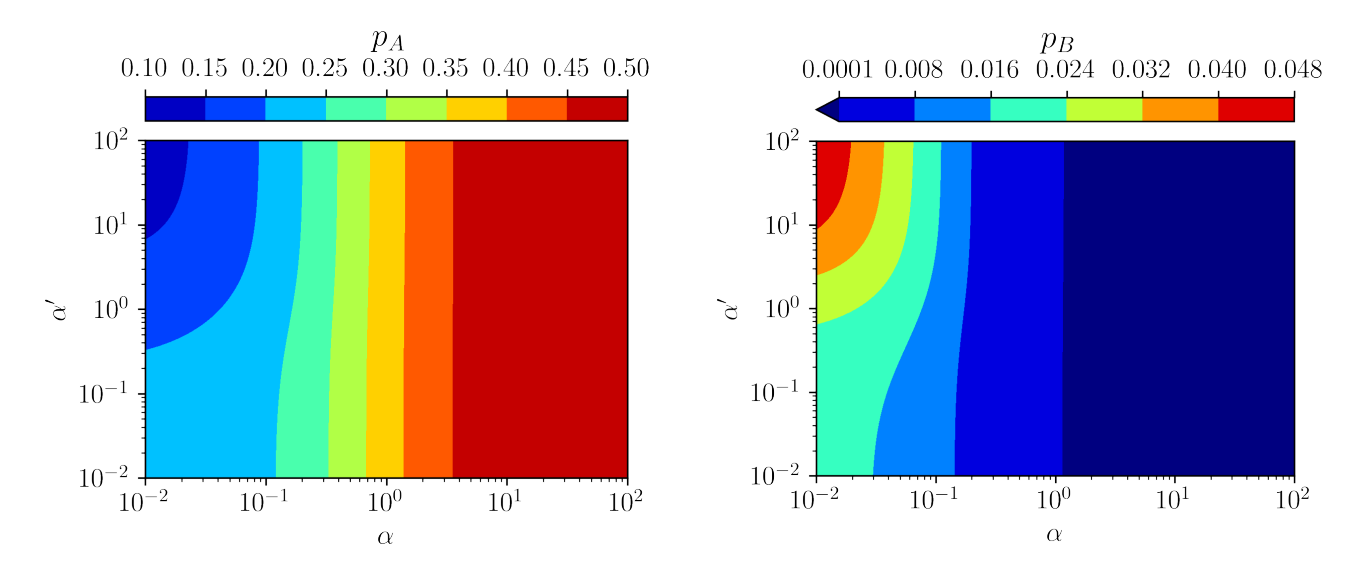


FIG. S2. Probabilities of occupation of the excited state at the endpoints of the isotherms (A and B) that maximize G in the slow-driving regime. These are displayed as a function of  $\alpha = b\Delta T/a$  and  $\alpha' = c/a$  (parameters:  $\beta_C = 2$ ,  $\beta_H = 1$  and r = 2). These values are used to produce the Pareto front in panel b of Fig. 3 of the main text.

#### 2. Violation of thermodynamic uncertainty relation.

In the low power limit it is known that PDHE can violate thermodynamic uncertainty relations [50–55]. We reach this limit by not optimizing for power but instead prioritizing the other two objectives. We take the limit of low power by taking  $a \ll b, c$ ; this implies that  $\alpha, \alpha' \gg 1$ , by Eq. (S110) this implies that we need vanishing heat capacity at A and B (because  $\Delta S$  is upper-bounded by  $\ln 2$ ). This is seen in Fig. S2:  $p_A$  approaches the largest values it can while  $p_B$  approaches the smallest values it can, which both minimize heat capacity. Furthermore, this also implies that the thermodynamic distance is as large as it can be (since it is a measure of the distance between the states at A and B),

but crucially it remains finite. By applying this to Eq. (S109) it is clear that the magnitude of the protocol time is

determined by the ratio  $\frac{L^2}{A} = \frac{1}{a} \frac{L^2}{\Delta S - \alpha (C_A + C_B)/2}$ , it is thus clear that the protocol time diverges in this limit. The fact that the protocol time diverges in this limit also explains the fact that for large  $\alpha$  we see a loss of the dependence on  $\alpha'$  in Fig. S2: in this limit we don't need to fix  $\tau \gamma \Delta s$  to a constant, we only need to fix  $\Delta s$  to an arbitrarily low constant since  $\tau$  goes to infinity. This allows us to keep a simpler form of the figure of merit:  $G = \frac{A^2 \Delta T^2}{4L^2} \frac{1-2\Delta s}{(\delta_H + \delta_C)^2}$ , in which we can note that the optimization over the protocol endpoints only has to be done over the ratio  $A^2/L^2$ ; that does not depend on  $\alpha'$ . To maximize this ratio we can take the derivatives with respect to  $p_A$ and  $p_B$ . As before we end up with transcendental equations:

$$\frac{\alpha^{-1}\Delta S - (C_A + C_B)/2}{\Delta T L} = \beta_C \epsilon_A \sqrt{p_A (1 - p_A)} \left[ \alpha^{-1} + 1 - \frac{1}{2} \beta_C \epsilon_A (1 - 2p_A) \right], \tag{S113}$$

$$\frac{\alpha^{-1}\Delta S - (C_A + C_B)/2}{\Delta T L} = \beta_C \epsilon_B \sqrt{p_B (1 - p_B)} \left[ \alpha^{-1} - 1 + \frac{1}{2} \beta_C \epsilon_B (1 - 2p_B) \right].$$
 (S114)

For  $\alpha^{-1}=0$  we can see that  $p_A=\frac{1}{2}$  and  $p_B=0$  solves the equations, which is coherent with the numerical results of the previous section. We can now expand around  $\alpha^{-1} = 0$  by setting  $p_A = \frac{1}{2} + p_A^{(1)} \alpha^{-1} + \mathcal{O}(\alpha^{-2})$  and  $p_B = 0 + p_B^{(1)} \alpha^{-1} + \mathcal{O}(\alpha^{-2})$ . We therefore find

$$p_A = \frac{1}{2} - \frac{\ln 2}{\pi} \alpha^{-1} + \mathcal{O}(\alpha^{-2}),$$
 (S115)

$$p_B = \mathcal{O}(\alpha^{-2}). \tag{S116}$$

With this result we can compute the values of the objectives analytically to leading order in the low power limit:

$$\langle P \rangle = 2\alpha^{-1} \left( \frac{\ln 2}{\pi} \right)^2 \frac{\Delta T^2}{\left( \sqrt{\frac{c}{b} + T_{\rm H}^2} + \sqrt{\frac{c}{b} + T_{\rm C}^2} \right)^2} + \mathcal{O}(\alpha^{-2}), \tag{S117}$$

$$\langle \Delta P \rangle = 2\alpha^{-2} \left( \frac{\ln 2}{\pi} \right)^2 \frac{\Delta T^2}{\left( \sqrt{\frac{c}{b} + T_{\rm H}^2} + \sqrt{\frac{c}{b} + T_{\rm C}^2} \right)^3} \left( \frac{T_{\rm H}^2}{\sqrt{\frac{c}{b} + T_{\rm H}^2}} + \frac{T_{\rm C}^2}{\sqrt{\frac{c}{b} + T_{\rm C}^2}} \right) + \mathcal{O}(\alpha^{-3}), \tag{S118}$$

$$\langle \Sigma \rangle = \alpha^{-2} \left( \frac{\ln 2}{\pi} \right)^2 \frac{1}{\sqrt{\frac{c}{b} + T_{\rm H}^2} \sqrt{\frac{c}{b} + T_{\rm C}^2}} \frac{\Delta T^2}{\left( \sqrt{\frac{c}{b} + T_{\rm H}^2} + \sqrt{\frac{c}{b} + T_{\rm C}^2} \right)^2} + \mathcal{O}(\alpha^{-3}). \tag{S119}$$

In particular we notice that  $P \propto \alpha^{-1}$ ,  $\Delta P \propto \alpha^{-2}$ ,  $\langle \Sigma \rangle \propto \alpha^{-2}$ . Which results in  $\xi \propto \alpha^2$ , therefore we can violate the thermodynamic uncertainty relations arbitrarily. Therefore we can write, in this limit,  $\xi$  in terms of  $\langle P \rangle$ ,  $\langle \Delta P \rangle$  and  $\langle \Sigma \rangle$ 

$$\xi = \frac{16\left(\frac{\ln 2}{\pi}\right)^4 P^{-2} \Delta T^4}{\left(\sqrt{\frac{c}{b} + T_{\rm H}^2} + \sqrt{\frac{c}{b} + T_c^2}\right)^3} \frac{\left(\frac{c}{b} + T_{\rm H}^2\right) \left(\frac{c}{b} + T_c^2\right)}{T_{\rm C}^2 \sqrt{\frac{c}{b} + T_{\rm H}^2} + T_{\rm H}^2 \sqrt{\frac{c}{b} + T_c^2}},\tag{S120}$$

$$\xi = \frac{4\left(\frac{\ln 2}{\pi}\right)^2 \langle \dot{\Sigma} \rangle^{-1} \Delta T^2}{\sqrt{\frac{c}{b} + T_{\rm H}^2} + \sqrt{\frac{c}{b} + T_c^2}} \frac{\sqrt{\frac{c}{b} + T_{\rm H}^2} \sqrt{\frac{c}{b} + T_c^2}}{T_{\rm C}^2 \sqrt{\frac{c}{b} + T_{\rm H}^2} + T_{\rm H}^2 \sqrt{\frac{c}{b} + T_c^2}},$$
 (S121)

$$\xi = 8 \left(\frac{\ln 2}{\pi}\right)^2 \Delta P^{-1} \Delta T^2 \frac{\sqrt{\frac{c}{b} + T_{\rm H}^2} \sqrt{\frac{c}{b} + T_c^2}}{\left(\sqrt{\frac{c}{b} + T_{\rm H}^2} + \sqrt{\frac{c}{b} + T_c^2}\right)^2}.$$
 (S122)

By maximising over the choice of b and c for a given  $\alpha$  we can then obtain the black lines in Fig. 4 of the main text.

#### D. Numerical Optimization using RL

Here we provide the training details and hyperparameters used to produce all RL results presented in the main text in Figs. 2, 3, and 4 of the main text. The method is described in Sec. IC. A separate training was performed for all values of the weights (a, c) reported in Fig. 2 of the main text. Since the cycles vary dramatically based on the choice of (a, c), we mainly employed two sets of hyperparameters, denoted with v1 and v2, shown in Table I. The hyperparameter names in Table I not defined in this paper are defined as in Ref. [30], except for  $n_{\text{train-steps}}$  that represents the number of steps that were performed during training. For values of a in [0.4, 1], we used v1 and performed a single training. The only two exceptions are (a, c) = (1, 0) and (0.55, 0), where we obtained better cycles training a second time respectively with  $n_{\text{train-steps}} = 340k$  and 280k. Instead, training for values of a in [0.2, 0.35] was less stable, since the low power regime produces much longer cycles that require more "long-term planning". Furthermore, the maximum value of the figure of merit becomes closer to 0 as a decreases. Since also "doing nothing" (i.e. setting  $\vec{u}(t)$  and  $\beta(t)$  to a time-independent constant) produces a null figure of merit, it becomes harder and harder for the RL method to distinguish optimal cycles from these trivial solutions. To overcome these difficulties, we mainly used v2, and we repeated the training up to 3 times for some values of (a, c) - choosing then the cycle with the largest figure of merit. In total, we repeated 54 trainings, some of which trained with v1. At last, in some cases we trained for more steps, up to  $n_{\text{train-steps}} = 471k$  steps, and we set  $\Delta t = 0.5$  in some other trains, including the cases with c = 0 or c = 1 - a.

Hyperparameter name	v1	v2
Hidden layers	2	"
Hidden layers units	256	"
Initial random steps	6k	"
First update at step	1000	"
Batch size	256	"
Learning rate	0.001	"
$ar{H}_{ ext{start}}$	0.4	0.28
$ar{H}_{\mathrm{end}}$	-7	"
$ar{H}_{ m decay}$	108k	162k
$n_{ m updates}$	50	"
$ ho_{ m polyak}$	0.995	"
$\mathcal{B}_{ ext{size}}$	200k	"
$\Delta t$	0.5	2
Discount factor $\gamma$	0.9997	0.9998
$n_{ m train-steps}$	240k	360k

TABLE I. Hyperparameters used to produce the results shown in the main text. The columns v1 and v2 correspond to two different sets of hyperparameters used in different regimes. The values not specified in v2 are the same as in v1.

#### E. Equivalence between SSHE and Fast-Otto PDHE for a two-level system

In this section we show that there is mapping between power, fluctuations, and entropy production produced by a two-level system in a steady-state heat engine (SSHE) and the same system periodically driven (PDHE) in a fast-Otto cycle. This affinity can be explained, intuitively speaking, as in both cases the state of the system relaxes to a fixed point (cf. [31]), and the work exchanges are defined by a single variation of energy level (chemical potential for the SSHE, energy gap quench for the PDHE, see details below).

This mapping explains why, among other things, the Fast-Otto cycle satisfies the SSHE thermodynamic uncertainty relations, as shown in the main text.

Specifically, consider a two-level system connected to two thermal baths, modeled via a simple rate master equation, that is

$$\dot{\vec{p}}_t = \gamma_i (\vec{\pi}_i - \vec{p}_t) \tag{S123}$$

where  $\gamma_i$  is the rate of bath i,  $\vec{p}$  the populations vector, and  $\vec{\pi}_i := (f_i, 1 - f_i)$ , with  $f_i = \frac{1}{1 + e^{-\beta_i \epsilon_i}}$ . Notice that due to normalization  $\vec{p} = (p, 1 - p)$  and the dynamical equation can be equivalently written as  $\dot{p}_t = \gamma_i (f_i - p_t)$ . Both in the steady state case and the fast driving cycle, the state tends to a fixed value

$$p_t \to p$$
 . (S124)

It is possible to compute the steady state p, and the resulting power, efficiency and fluctuations for such system when driven on a Fast-Otto cycle, made by two quenches rapidly alternating. The analytic expressions can be obtained as from Appendix II (cf. Eq. (S71), but we also allow different rates for the two baths now).

	SSHE	Fast-Otto PDHE
$f_i$	$(1 + e^{-\beta_i(\epsilon - \mu_i)})^{-1}$	$(1+e^{-\beta_i\epsilon_i})^{-1}$
p	$ar{f}:=rac{\gamma_1f_1+\gamma_2f_2}{\gamma_1+\gamma_2}$	$ar{f} := rac{ heta_1 \gamma_1 f_1 + \hat{ heta}_2 \gamma_2 f_2}{ heta_1 \gamma_1 +  heta_1 \gamma_2}$
P	$\frac{\gamma_1\gamma_2}{\gamma_1+\gamma_2}(f_1-f_2)(\mu_1-\mu_2)$	$\frac{\theta_1\theta_2\gamma_1\gamma_2}{\theta_1\gamma_1+\theta_2\gamma_2}(f_1-f_2)(\epsilon_2-\epsilon_1)$
$\eta$	$1-rac{\epsilon-\mu_1}{}$	$1-\frac{\epsilon_1}{}$
$\Delta P$	$\left  2 \frac{\gamma_1 \gamma_2}{\gamma_1 + \gamma_2} (\epsilon_1 - \epsilon_2)^2 \left[ \bar{f} (1 - \bar{f}) + \left( \frac{f_1 + f_2}{2} - \bar{f} \right) (1 - 2\bar{f}) \right] \right $	$\left  2 \frac{\gamma_1 \theta_1 \gamma_2 \theta_2}{\gamma_1 \theta_1 + \gamma_2 \theta_2} (\epsilon_1 - \epsilon_2)^2 \left[ \bar{f} (1 - \bar{f}) + \left( \frac{f_1 + f_2}{2} - \bar{f} \right) (1 - 2\bar{f}) \right] \right $

TABLE II. Mapping between a steady-state engine and a fast-Otto cycle for the case of a two-level system.

The resulting expressions are given in Table IIIE (right column), in terms of the rates  $\gamma_i$ , the chosen gaps  $\epsilon_i$ , the fraction of time  $\theta_i$  spent on each bath i ( $\theta_1 + \theta_2 = 1$ ). It turns out that such expressions become formally equivalent to those of a SSHE based on a two-level system in a chemical potential gradient between the two baths  $\mu_i$  (the gap  $\epsilon$  of the qubit is in this case fixed), for which the standard expressions in the left column of Table IIIE can be obtained from standard references. In particular, for  $\Delta P$  it is possible to consider Eq. (14) of [56] and substitute Eq. (24) of [57] for the values of the  $\mathcal{T}$ -coefficients in the weak coupling limit.

By looking at Table IIIE, it is possible to see how each quantity is formally equivalent between the two columns, via the following mapping

$$\gamma_i \to \theta_i \gamma_i$$
, (S125)

$$\epsilon - \mu_i \to \epsilon_i$$
 (S126)

Finally, let us notice that the expression for the fluctuations  $\Delta P$  can equivalently be expressed in other forms, such as (we express it for the SSHE case, although it can be expressed similarly for the Fast-Otto case, via the above mapping)

$$\Delta P = \frac{2\gamma_1 \gamma_2}{\gamma_1 + \gamma_2} (\mu_1 - \mu_2)^2 \left( f_+ (1 - f_+) + (\bar{f} - f_+)^2 \right) , \qquad (S127)$$

where  $f_+ := (f_1 + f_2)/2$ . Such expression shows immediately the positiveness of the fluctuations. Another equivalent expression, which is typically obtained in SSHE calculations is

$$\Delta P = \frac{\gamma_1 \gamma_2}{\gamma_1 + \gamma_2} (\mu_1 - \mu_2)^2 \left( f_1 (1 - f_2) + f_2 (1 - f_1) \right) - \frac{2\gamma_1^2 \gamma_2^2}{(\gamma_1 + \gamma_2)^3} (\mu_1 - \mu_2)^2 \left( f_1 - f_2 \right)^2 . \tag{S128}$$

- [1] R. Alicki, The quantum open system as a model of the heat engine, J. Phys. A: Math. Gen. 12, L103 (1979).
- [2] H. J. D. Miller, M. Scandi, J. Anders, and M. Perarnau-Llobet, Work fluctuations in slow processes: Quantum signatures and optimal control, Phys. Rev. Lett. 123, 230603 (2019).
- [3] D. E. Kirk, Optimal Control Theory: an Introduction (Dover, 2004).
- [4] R. S. Sutton and A. G. Barto, Reinforcement learning: An introduction (MIT press, 2018).
- [5] P. Menczel and K. Brandner, Limit cycles in periodically driven open quantum systems, J. Phys. A Math. Theor. 52, 43LT01 (2019).
- [6] P. A. Erdman and F. Noé, Driving black-box quantum thermal machines with optimal power/efficiency trade-offs using reinforcement learning, arXiv:2204.04785 (2022).
- [7] T. Haarnoja, A. Zhou, P. Abbeel, and S. Levine, Soft actor-critic: Off-policy maximum entropy deep reinforcement learning with a stochastic actor, in *International Conference on Machine Learning*, Vol. 80 (PMLR, 2018) p. 1861.
- [8] T. Haarnoja, A. Zhou, K. Hartikainen, G. Tucker, S. Ha, J. Tan, V. Kumar, H. Zhu, A. Gupta, P. Abbeel, et al., Soft actor-critic algorithms and applications, arXiv:1812.05905 (2018).
- [9] T. Haarnoja, S. Ha, A. Zhou, J. Tan, G. Tucker, and S. Levine, Learning to walk via deep reinforcement learning, arXiv:1912.11077 (2018).
- [10] P. Christodoulou, Soft actor-critic for discrete action settings, arXiv:1910.07207 (2019).
- [11] O. Delalleau, M. Peter, E. Alonso, and A. Logut, Discrete and continuous action representation for practical rl in video games, arXiv:1912.11077 (2019).
- [12] V. Mnih, K. Kavukcuoglu, D. Silver, A. A. Rusu, J. Veness, M. G. Bellemare, A. Graves, M. Riedmiller, A. K. Fidjeland, G. Ostrovski, et al., Human-level control through deep reinforcement learning, Nature 518, 529 (2015).
- [13] D. Silver, J. Schrittwieser, K. Simonyan, I. Antonoglou, A. Huang, A. Guez, T. Hubert, L. Baker, M. Lai, A. Bolton, et al., Mastering the game of go without human knowledge, Nature 550, 354 (2017).

- [14] O. Vinyals, I. Babuschkin, W. M. Czarnecki, M. Mathieu, A. Dudzik, J. Chung, D. H. Choi, R. Powell, T. Ewalds, P. Georgiev, et al., Grandmaster level in starcraft ii using multi-agent reinforcement learning, Nature 575, 350 (2019).
- [15] J. Degrave, F. Felici, J. Buchli, M. Neunert, B. Tracey, F. Carpanese, T. Ewalds, R. Hafner, A. Abdolmaleki, D. de las Casas, et al., Magnetic control of tokamak plasmas through deep reinforcement learning, Nature 602, 414 (2022)..
- [16] M. Bukov, A. G. R. Day, D. Sels, P. Weinberg, A. Polkovnikov, and P. Mehta, Reinforcement learning in different phases of quantum control, Phys. Rev. X 8, 031086 (2018).
- [17] Z. An and D. Zhou, Deep reinforcement learning for quantum gate control, EPL 126, 60002 (2019).
- [18] M. Dalgaard, F. Motzoi, J. J. Sørensen, and J. Sherson, Global optimization of quantum dynamics with alphazero deep exploration, NPJ Quantum Inf. 6, 6 (2020).
- [19] J. Mackeprang, D. B. R. Dasari, and J. Wrachtrup, A reinforcement learning approach for quantum state engineering, Quantum Mach. Intell. 2, 5 (2020).
- [20] F. Schäfer, M. Kloc, C. Bruder, and N. Lörch, A differentiable programming method for quantum control, Mach. Learn.: Sci. Technol. 1, 035009 (2020).
- [21] F. Schäfer, P. Sekatski, M. Koppenhöfer, C. Bruder, and M. Kloc, Control of stochastic quantum dynamics by differentiable programming, Mach. Learn.: Sci. Technol. 2, 035004 (2021).
- [22] R. Porotti, A. Essig, B. Huard, and F. Marquardt, Deep reinforcement learning for quantum state preparation with weak nonlinear measurements, Quantum 6, 747 (2022).
- [23] F. Metz and M. Bukov, Self-correcting quantum many-body control using reinforcement learning with tensor networks, arXiv:2201.11790 (2022).
- [24] M. Y. Niu, S. Boixo, V. N. Smelyanskiy, and H. Neven, Universal quantum control through deep reinforcement learning, NPJ Quantum Inf. 5, 33 (2019).
- [25] X.-M. Zhang, Z. Wei, R. Asad, X.-C. Yang, and X. Wang, When does reinforcement learning stand out in quantum control? a comparative study on state preparation, NPJ Quantum Inf. 5, 85 (2019).
- [26] T. Fösel, P. Tighineanu, T. Weiss, and F. Marquardt, Reinforcement learning with neural networks for quantum feedback, Phys. Rev. X 8, 031084 (2018).
- [27] R. Sweke, M. S. Kesselring, E. P. L. van Nieuwenburg, and J. Eisert, Reinforcement learning decoders for fault-tolerant quantum computation, Mach. Learn.: Sci. Technol. 2, 025005 (2020).
- [28] Y. Ashida and T. Sagawa, Learning the best nanoscale heat engines through evolving network topology, Commun. Phys. 4, 45 (2021).
- [29] P. Sgroi, G. M. Palma, and M. Paternostro, Reinforcement learning approach to nonequilibrium quantum thermodynamics, Phys. Rev. Lett. 126, 020601 (2021).
- [30] P. A. Erdman and F. Noé, Identifying optimal cycles in quantum thermal machines with reinforcement-learning, NPJ Quantum Inf. 8, 1 (2022).
- [31] V. Cavina, P. A. Erdman, P. Abiuso, L. Tolomeo, and V. Giovannetti, Maximum-power heat engines and refrigerators in the fast-driving regime, Phys. Rev. A 104, 032226 (2021).
- [32] P. A. Erdman, V. Cavina, R. Fazio, F. Taddei, and V. Giovannetti, Maximum power and corresponding efficiency for two-level heat engines and refrigerators: optimality of fast cycles, New J. Phys. 21, 103049 (2019).
- [33] P. Salamon and R. S. Berry, Thermodynamic length and dissipated availability, Phys. Rev. Lett. 51, 1127 (1983).
- [34] P. Abiuso and M. Perarnau-Llobet, Optimal cycles for low-dissipation heat engines, Phys. Rev. Lett. 124, 110606 (2020).
- [35] M. Scandi and M. Perarnau-Llobet, Thermodynamic length in open quantum systems, Quantum 3, 197 (2019)
- [36] F. Schlögl, Thermodynamic metric and stochastic measures, Zeitschrift für Physik B Condensed Matter 59, 449 (1985).
- [37] J. Nulton, P. Salamon, B. Andresen, and Q. Anmin, Quasistatic processes as step equilibrations, J. Chem. Phys. 83, 334 (1985).
- [38] G. E. Crooks, Measuring thermodynamic length, Phys. Rev. Lett. 99, 100602 (2007).
- [39] D. A. Sivak and G. E. Crooks, Thermodynamic metrics and optimal paths, Phys. Rev. Lett. 108, 190602 (2012).
- [40] M. V. S. Bonança and S. Deffner, Optimal driving of isothermal processes close to equilibrium, J. Chem. Phys. 140, 244119 (2014).
- [41] V. Cavina, A. Mari, and V. Giovannetti, Slow dynamics and thermodynamics of open quantum systems, Phys. Rev. Lett. 119, 050601 (2017).
- [42] S. Deffner and M. V. S. Bonança, Thermodynamic control —an old paradigm with new applications, EPL 131, 20001 (2020).
- [43] R. Kubo, The fluctuation-dissipation theorem, Rep. Prog. Phys. 29, 255 (1966).
- [44] J. Weber, Fluctuation dissipation theorem, Phys. Rev. 101, 1620 (1956).
- [45] C. Jarzynksi, A nonequilibrium equality for free energy differences, Phys. Rev. Lett. 78, 2690 (1997).
- [46] D. A. Hendrix and C. Jarzynski, A "fast growth" method of computing free energy differences, J. Chem. Phys. 114, 5974 (2001).
- [47] J. Hermans, Simple analysis of noise and hysteresis in (slow-growth) free energy simulations, J. Phys. Chem. 95, 9029 (1991).
- [48] P. Abiuso, H. J. D. Miller, M. Perarnau-Llobet, and M. Scandi, Geometric optimisation of quantum thermodynamic processes, Entropy 22 (2020).
- [49] A. Jenčová, Geodesic distances on density matrices, J. Math. Phys. 45, 1787 (2004).
- [50] A. C. Barato and U. Seifert, Cost and precision of brownian clocks, Phys. Rev. X 6, 041053 (2016).
- [51] K. Proesmans and C. V. den Broeck, Discrete-time thermodynamic uncertainty relation, EPL 119, 20001 (2017).
- [52] V. Holubec and A. Ryabov, Cycling tames power fluctuations near optimum efficiency, Phys. Rev. Lett. 121, 120601

(2018).

- [53] L. M. Cangemi, V. Cataudella, G. Benenti, M. Sassetti, and G. De Filippis, Violation of thermodynamics uncertainty relations in a periodically driven work-to-work converter from weak to strong dissipation, Phys. Rev. B 102, 165418 (2020).
- [54] P. Menczel, E. Loisa, K. Brandner, and C. Flindt, Thermodynamic uncertainty relations for coherently driven open quantum systems, J. Phys. A: Math. Theor. **54**, 314002 (2021).
- [55] J. Lu, Z. Wang, J. Peng, C. Wang, J.-H. Jiang, and J. Ren, Geometric thermodynamic uncertainty relation in periodically driven thermoelectric heat engine, arXiv:2201.02477 (2022).
- [56] J. Liu and D. Segal, Thermodynamic uncertainty relation in quantum thermoelectric junctions, Phys. Rev. E 99, 062141 (2019).
- [57] B. K. Agarwalla and D. Segal, Assessing the validity of the thermodynamic uncertainty relation in quantum systems, Phys. Rev. B 98, 155438 (2018)

.

## **New Journal of Physics**

The open access journal at the forefront of physics





#### **PAPER • OPEN ACCESS**

## Optimal control of dissipation and work fluctuations for rapidly driven systems

To cite this article: Alberto Rolandi et al 2023 New J. Phys. 25 073005

View the article online for updates and enhancements.

#### You may also like

- Non-stationarity and dissipative time crystals: spectral properties and finite-size
- Cameron Booker, Berislav Bua and Dieter Jaksch
- Independent-oscillator model and the quantum Langevin equation for an Aritra Ghosh, Malay Bandyopadhyay,

Sushanta Dattagupta et al.

- Thermal and Orbital Evolution of Low-Michaela Walterová and Marie Bhounková

## **New Journal of Physics**

The open access journal at the forefront of physics



Published in partnership with: Deutsche Physikalische Gesellschaft and the Institute of Physics



#### **OPEN ACCESS**

### RECEIVED 20 December 2022

20 December 202

REVISED 19 June 2023

ACCEPTED FOR PUBLICATION 29 June 2023

PUBLISHED

12 July 2023

Original Content from this work may be used under the terms of the Creative Commons Attribution 4.0 licence.

Any further distribution of this work must maintain attribution to the author(s) and the title of the work, journal citation and DOI.



#### **PAPER**

# Optimal control of dissipation and work fluctuations for rapidly driven systems

Alberto Rolandi<sup>1</sup>, Martí Perarnau-Llobet<sup>1</sup> and Harry J D Miller<sup>2,\*</sup>

- Département de Physique Appliquée, Université de Genève, 1211 Genève, Switzerland
- Department of Physics and Astronomy, The University of Manchester, Manchester M13 9PL, United Kingdom
- \* Author to whom any correspondence should be addressed.

E-mail: harry.miller@manchester.ac.uk

Keywords: stochastic thermodynamics, quantum thermodynamics, thermodynamic control

#### **Abstract**

To achieve efficient and reliable control of microscopic systems one should look for driving protocols that mitigate both the average dissipation and stochastic fluctuations in work. This is especially important in fast driving regimes in which the system is driven far out of equilibrium, potentially creating large amounts of unwanted entropy production. Here we characterise these optimal protocols in rapidly driven classical and quantum systems and prove that they consist of two discontinuous jumps in the full set of control variables. These jumps can be tuned to interpolate between processes with either minimal dissipation or minimal fluctuations, and in some situations allow for simultaneous minimisation. We illustrate our general results with rapidly driven closed quantum systems, classical bit erasure and a dissipative Ising chain driven close to a quantum phase transition.

Minimising dissipation is a central optimisation problem in stochastic and quantum thermodynamics [1], and is especially important for ensuring efficient control of microscopic machines operating out of equilibrium. Careful consideration is needed when choosing Hamiltonian protocols that drive small systems along non-equilibrium trajectories in finite-time, as generating too much dissipation leads to irreversibility [2] and thus hampers any thermodynamic performance. A key feature of microscopic systems, whether they be quantum or classical, is that they are also heavily influenced by stochastic fluctuations, hence thermodynamic quantities such as work and heat behave as random variables [3, 4]. Therefore from an optimisation perspective it is also desirable to ensure fluctuations around the mean dissipation are kept small in order to maintain precision and stability along a thermodynamic process. However, typically it is not possible to minimise the dissipation and fluctuations simultaneously and a compromise must be chosen. Current research aims to understand the interplay and unavoidable trade-offs between dissipation and fluctuations in classical-stochastic and quantum thermodynamic systems [5–9], and it remains an ongoing problem of how best to balance these two competing figures of merit in different scenarios.

With regard to dissipation, or equivalently the average excess work done to drive a system out of equilibrium, optimal processes are well characterised in slowly driven or linear response regimes where methods from thermodynamic geometry can be employed [10–14]. In this case a metric can be assigned to the control parameter space with minimum dissipation protocols achieved by driving the system along a geodesic path [15]. For classical stochastic systems operating in these close-to-equilibrium regimes the work fluctuation-dissipation relation holds [16, 17], implying that paths of minimal dissipation simultaneously minimise the resulting work fluctuations. While this is not always satisfied by non-classical systems due to the impact of quantum coherence [18], an alternative geometric approach has been recently developed that can determine minimum fluctuation protocols for slowly driven quantum systems [19, 20]. On the other hand, when operating much further from equilibrium over shorter timescales these geodesic paths are no longer relevant for minimising either of these quantities. It is of course desirable to understand how to optimise systems beyond linear response driving and where shorter operation times are needed. The central

aim of this paper is to establish a general optimisation principle for minimising both the average excess work and its fluctuations in rapidly driven small systems.

The study of driven Brownian particles first hinted at a key feature of minimum-dissipation protocols for fast driving; such protocols contain discontinuous jumps in the system control parameters or degrees of freedom [21]. This has been further evidenced in a range of other systems through either analytic or numerical treatments of finite-time thermodynamic optimisation problems [22–26]. More recently the optimality of these control parameter quenches has been proven in general with regard to maximising the power and efficiency of microscopic heat engines with fast operation cycles [27, 28], and furthermore proven optimal for minimising the average excess work done on classical stochastic systems rapidly driven from equilibrium [29]. In contrast to dissipation, little is known about how to minimise work fluctuations under rapid driving, nor is it known how these protocols compare to those with minimal dissipation. In this paper we will prove that protocols with minimal fluctuations also consist of instantaneous jumps in the systems control parameters. Our result applies in full generality to any quantum or classical system whose generator is independent of the control parameter velocities. While sharing the same general design principle as minimal-dissipation protocols, these control variables typically need to jump to a distinct point in the parameter space, meaning that average excess work and work fluctuations cannot be simultaneously optimised. Furthermore, and as we will illustrate, one practical advantage of this approach is that it enables us to optimise driving protocols for complex many-body systems where exact results are lacking.

The paper is structured as follows; in section 1 we derive general expressions for the average excess work and its variance for rapidly driven quantum systems, and in section 2 we present the general Euler–Lagrange equations for finding optimal protocols in this fast driving regime and show that all solutions consist of discrete jumps in the control parameter space. We then explore different scenarios where this optimisation scheme can be implemented; section 3 focuses on closed quantum systems, whereas section 4 concerns open quantum systems including erasure of a quantum dot and driving a classical and quantum Ising spin chain.

#### 1. Average excess work and fluctuations for fast driving

We will begin with a rather general treatment of a finite-dimensional quantum system subject to rapid time-dependent driving, which may be isolated or in contact with an environment. The Hamiltonian of the system is first parameterised by a set of d scalar variables  $\vec{\lambda}_t = \{\lambda_1(t), \lambda_2(t), \dots \lambda_d(t)\}$  that can be controlled in time:

$$H(\vec{\lambda}_t) = H_0 + \vec{\lambda}_t \cdot \vec{X}, \quad t \in [0, \tau], \tag{1}$$

where  $H_0$  denotes a fixed Hamiltonian in the absence of driving, and  $\vec{X}$  are a set of corresponding observables with  $\vec{X} = \{X_1, X_2, \dots X_d\}$  which may be assumed time-independent without loss of generality. As we wish to compare the behaviour of different choices of driving protocols  $\gamma : t \to \vec{\lambda}_t$ , it will be useful to define the set of protocols  $\gamma \in \mathscr{C}$  that have a fixed initial and final value:

$$\gamma: t \to \vec{\lambda}_t \in \mathscr{C} = \{ \vec{\lambda}_t \in \mathbb{R}^d \mid \vec{\lambda}_0 = \vec{\lambda}_A, \quad \vec{\lambda}_\tau = \vec{\lambda}_B \}. \tag{2}$$

For now we can assume the evolution is given by a Markovian generator of the form

$$\dot{\rho}(t) = \mathcal{L}_{\vec{\lambda}_{\bullet}}[\rho(t)]; \quad \rho(0) = \pi(\vec{\lambda}_{A}) \tag{3}$$

with a thermal initial condition, where

$$\pi(\vec{\lambda}) = \frac{e^{-\beta H(\vec{\lambda})}}{Z(\vec{\lambda})}; \qquad Z(\vec{\lambda}) := \text{Tr}\left(e^{-\beta H(\vec{\lambda})}\right) \tag{4}$$

is the corresponding Gibbs state at inverse temperature  $\beta$ . The most notable part of this assumption is that the generator is *independent of the velocity*  $d\vec{\lambda}_t/dt$ , and depends only on the local values of  $\vec{\lambda}_t$ . This is readily satisfied by isolated quantum systems evolving unitarily, adiabatically driven open quantum systems [30] and Markovian dynamics for classical/quasi-classical systems driven by scalar potentials. On the other hand, open quantum quantum systems driven non-adiabatically may not meet this requirement [31]. We also stress that while our system is initially thermal, we place no restriction on the final state after apply the Hamiltonian protocol (2).

The control protocol will result in some work done on the system since it is driven out of equilibrium. Due to both thermal and quantum fluctuations, the work W is a stochastic quantity and its statistics are described by a distribution P(W). In a closed, unitarily-driven system this distribution can be ascertained

from projective measurements the system's Hamiltonian at the beginning and end of the process [4, 32, 33]. For weakly-coupled open systems one can similarly determine the work distribution by monitoring a set of quantum jumps as the system exchanges energy with its environment [34, 35]. In any case, the average work  $\langle W \rangle$  and its variance  $\sigma_W^2 = \langle W^2 \rangle - \langle W \rangle^2$  are given by the following general form [18, 36]:

$$\langle W \rangle := \int_0^{\tau} dt \, \frac{d\vec{\lambda}_t^T}{dt} \, \text{Tr} \left( \vec{X} \rho(t) \right),$$
 (5)

$$\sigma_{W}^{2} := 2 \operatorname{\mathbb{R}\!\mathit{e}} \int_{0}^{\tau} dt \int_{0}^{t} dt' \operatorname{Tr} \left( \dot{H}(\vec{\lambda}_{t}) \overleftarrow{P}(t, t') \left[ \Delta_{\rho_{t'}} \dot{H}(\vec{\lambda}_{t'}) \rho_{t'} \right] \right), \tag{6}$$

where we denote  $\Delta_{\rho}A = A - \text{Tr}(A\rho)$  and

$$\overleftarrow{P}(t,t')[(.)] := \overleftarrow{\mathcal{T}} \exp\left(\int_{t'}^{t} d\nu \, \mathcal{L}_{\vec{\lambda}_{\nu}}\right)[(.)],\tag{7}$$

is the time-ordered propagator. As a quantifier for the degree of irreversibility associated with the process, the average *excess* work done on the system is defined as

$$\langle W_{\rm ex} \rangle = \langle W \rangle - \Delta F,$$
 (8)

where  $\Delta F = F(\vec{\lambda}_B) - F(\vec{\lambda}_A)$  is the change in equilibrium free energy,  $F(\vec{\lambda}) := -\beta^{-1} \log Z(\vec{\lambda})$ . The excess work disappears  $\langle W_{\rm ex} \rangle \to 0$  in quasistatic processes where the system is always in thermal equilibrium, which also implies absence of work fluctuations due to the work fluctuation-dissipation relation  $\beta \sigma_W^2/2 = \langle W_{\rm ex} \rangle$  holding valid in this limit [16, 17]. For non-equilibrium processes, both  $\langle W_{\rm ex} \rangle$  and  $\sigma_W$  will become relevant, and we expect their magnitudes to increase with the speed of the process (i.e. as  $\tau$  decreases). Our goal is then to investigate which protocols  $\gamma$  in (2) give the smallest values of average dissipation  $\langle W_{\rm ex} \rangle$  and work fluctuations  $\sigma_W$  respectively. In general, computing and optimising the work moments relies on knowing an exact solution to the dynamics (3). While this is not generally tractable, we will demonstrate that this control problem becomes considerably simpler in fast driving regimes (i.e. when the overall time  $\tau$  taken to go from  $\vec{\lambda}_A$  to  $\vec{\lambda}_B$  is small relative to the characteristic timescales of the system).

We first quantify precisely what we mean by a rapid protocol by defining a characteristic timescale  $\tau_c$  for the generator given by [28]

$$\tau_{c}^{-1} = \max_{\vec{\lambda}_{i} \in \mathscr{C}} ||\mathcal{L}_{\vec{\lambda}_{i}}||, \tag{9}$$

where we introduce a norm

$$||\mathcal{L}_{\vec{\lambda}}|| = \max_{\text{Tr}(O) < \infty} \frac{||\mathcal{L}_{\vec{\lambda}_t}[O]||_1}{||O||_1}$$
(10)

and  $||A||_1 = \text{Tr}\left(\sqrt{A^\dagger A}\right)$ . For a finite-dimensional unitary generator, this parameter is bounded by the operator norm of the Hamiltonian, while for systems undergoing non-unitary dynamics with a unique fixed point then  $\tau_c$  bounds the shortest relaxation timescale associated with the system. Overall, this gives us a definition of the fast driving regime which assumes that the total duration is short enough such that  $\tau \ll \tau_c$ . To see how this approximation impacts the work moments, let us rewrite the evolution in dimensionless time:

$$\dot{\tilde{\rho}}(s) = \tau \mathcal{L}_{\vec{\lambda}_s}[\tilde{\rho}(s)]; \quad \tilde{\rho}(0) = \pi(\vec{\lambda}_A), \quad s = \frac{t}{\tau} \in [0, 1]. \tag{11}$$

In these units the work done is

$$\langle W \rangle := \int_0^1 dt \, \frac{d\vec{\lambda}_s^T}{ds} \, \text{Tr} \left( \vec{X} \, \tilde{\rho}(s) \right).$$
 (12)

We can expand the solution to (11) as a Dyson series:

$$\tilde{\rho}(s) = \pi(\vec{\lambda}_A) + \sum_{n=1}^{\infty} \tau^n \int_0^s dt_n \int_0^{t_n} dt_{n-1} \dots \int_0^{t_2} dt_1 \, \mathcal{L}_{\vec{\lambda}_{t_n}} \mathcal{L}_{\vec{\lambda}_{t_{n-1}}} \dots \mathcal{L}_{\vec{\lambda}_{t_1}} [\pi(\vec{\lambda}_A)], \tag{13}$$

where  $0 \le t_1 \le ... \le t_n \le s$ . Consider the first two terms in the expansion,

$$\sigma(s) = \pi(\vec{\lambda}_A) + \tau \int_0^s dt' \mathcal{L}_{\vec{\lambda}_{t'}}[\pi(\vec{\lambda}_A)]. \tag{14}$$

From our definition of the characteristic timescale (9) we have

$$||\tilde{\rho}(s) - \sigma(s)||_1 \leqslant \mathcal{O}([\tau/\tau_c]^2). \tag{15}$$

Therefore we can approximate the state by  $\tilde{\rho}(s) \simeq \sigma(s)$  so long as  $\tau \ll \tau_c$ . This approximation should be contrasted with the slow driving regime that treats the opposite case,  $\tau_c \ll \tau$ . Assuming the dynamics has a thermal fixed point, a slow driving approximation implies that the system stays close to equilibrium at all times, i.e.  $\tilde{\rho}(s) \simeq \pi(\vec{\lambda}_s) + \delta \rho(\vec{\lambda}_s)$  with  $\delta \rho(\vec{\lambda}_s)$  a linear correction to the instantaneous thermal state [37]. In the present context, the Dyson series allows us to perform the inverse of this expansion, with rapid driving moving the system far from instantaneous equilibrium instead. We can use (15) to now approximate the excess work, yielding

$$\langle W_{\rm ex} \rangle \simeq k_B T S(\pi(\vec{\lambda}_A) || \pi(\vec{\lambda}_B)) + \tau \int_0^1 \frac{d\vec{\lambda}_s^T}{ds} \int_0^s dt' {\rm Tr} \left( \vec{X} \, \mathcal{L}_{\vec{\lambda}_{t'}}[\pi(\vec{\lambda}_A)] \right),$$
 (16)

$$=k_B TS(\pi(\vec{\lambda}_A)||\pi(\vec{\lambda}_B))+\int_0^\tau dt\,\frac{d\vec{\lambda}_t^T}{dt}\int_0^t dt'\,\vec{R}(\vec{\lambda}_{t'}),$$

where we define the relative entropy

$$S(\rho_1||\rho_2) = \text{Tr}(\rho_1 \log \rho_1) - \text{Tr}(\rho_1 \log \rho_2)$$
(17)

and the quantum initial force relaxation rate:

$$\vec{R}(\vec{\lambda}_t) := \left\langle \mathcal{L}_{\vec{\lambda}_t}^{\dagger}[\vec{X}] \right\rangle_A \tag{18}$$

where  $\langle (.) \rangle_A = \text{Tr}\left((.)\pi(\vec{\lambda}_A)\right)$  is an average with respect to the initial equilibrium state. We then do an integration by parts to obtain

$$\langle W_{\rm ex} \rangle = k_B T S(\pi(\vec{\lambda}_A) || \pi(\vec{\lambda}_B)) + \int_0^{\tau} dt \left[ \vec{\lambda}_B - \vec{\lambda}_t \right]^T \vec{R}(\vec{\lambda}_t). \tag{19}$$

The first term represents the excess work from a perfect Hamiltonian quench [38], while the second term gives the leading order correction for a protocol at finite speed. This expansion agrees with the results of [29] for classical Focker-Planck dynamics, now generalised to a fully quantum regime.

Turning attention now to the work fluctuations, we convert the expression (6) into dimensionless units, so

$$\sigma_W^2 = 2 \operatorname{\mathbb{R}} e \int_0^1 ds \int_0^s ds' \operatorname{Tr} \left( \dot{H}(\vec{\lambda}_s) \overleftarrow{\mathcal{T}} \exp \left( \tau \int_{s'}^s d\nu \, \mathcal{L}_{\vec{\lambda}_{\nu}} \right) \left[ \Delta_{\tilde{\rho}(s')} \dot{H}(\vec{\lambda}_{s'}) \tilde{\rho}(s') \right] \right), \tag{20}$$

where we can approximate the propagator using the Dyson series again, so that

$$\begin{split} \sigma_W^2 &\simeq 2 \ \mathbb{R}e \int_0^1 ds \int_0^s ds' \ \mathrm{Tr} \left( \dot{H}(\vec{\lambda}_s) \ \Delta_{\tilde{\rho}(s')} \dot{H}(\vec{\lambda}_{s'}) \tilde{\rho}(s') \right) \\ &+ 2\tau \ \mathbb{R}e \int_0^1 ds \int_0^s ds' \int_{s'}^s d\nu \ \mathrm{Tr} \left( \dot{H}(\vec{\lambda}_s) \mathcal{L}_{\vec{\lambda}_{\nu}} \left[ \Delta_{\pi(\vec{\lambda}_A)} \dot{H}(\vec{\lambda}_{s'}) \pi(\vec{\lambda}_A) \right] \right). \end{split}$$

Applying the Dyson expansion to a shifted observable yields

$$\Delta_{\tilde{\rho}(s)} A \simeq \Delta_{\tilde{\sigma}(s)} A = \Delta_{\pi(\vec{\lambda}_A)} A - \tau \int_0^s ds' \operatorname{Tr} \left( A \, \mathcal{L}_{\vec{\lambda}_{s'}}[\pi(\vec{\lambda}_A)] \right). \tag{21}$$

Using this expansion, the Dyson expansion of the state and converting back to original units of time we get

$$\sigma_{W}^{2} \simeq k_{B}^{2} T^{2} V \left(\pi(\vec{\lambda}_{A}) || \pi(\vec{\lambda}_{B})\right) - 2 \operatorname{\mathbb{R}e} \int_{0}^{\tau} dt \int_{0}^{t} dt' \int_{0}^{t'} d\nu \operatorname{Tr} \left(\dot{H}(\vec{\lambda}_{t}) \pi(\vec{\lambda}_{A})\right) \operatorname{Tr} \left(\dot{H}(\vec{\lambda}_{t'}) \mathcal{L}_{\vec{\lambda}_{\nu}} [\pi(\vec{\lambda}_{A})]\right)$$

$$+ 2 \operatorname{\mathbb{R}e} \int_{0}^{\tau} dt \int_{0}^{t} dt' \int_{0}^{t'} d\nu \operatorname{Tr} \left(\dot{H}(\vec{\lambda}_{t}) \Delta_{\pi(\vec{\lambda}_{A})} \dot{H}(\vec{\lambda}_{t'}) \mathcal{L}_{\vec{\lambda}_{\nu}} [\pi(\vec{\lambda}_{A})]\right)$$

$$+ 2 \operatorname{\mathbb{R}e} \int_{0}^{\tau} dt \int_{0}^{t} dt' \int_{t'}^{t} d\nu \operatorname{Tr} \left(\dot{H}(\vec{\lambda}_{t}) \mathcal{L}_{\vec{\lambda}_{\nu}} [\Delta_{\pi(\vec{\lambda}_{A})} \dot{H}(\vec{\lambda}_{t'}) \pi(\vec{\lambda}_{A})]\right),$$

$$(22)$$

where the first term is the relative entropy variance [39]:

$$V(\rho_1||\rho_2) = \text{Tr}\left(\rho_1(\log \rho_1 - \log \rho_2)^2\right) - S^2(\rho_1||\rho_2). \tag{23}$$

Let us first define the initial force correlation matrix  $G(\vec{\lambda})$ , with elements

$$\left[\mathbf{G}(\vec{\lambda})\right]_{jk} := \frac{1}{2} \left\langle \mathcal{L}_{\vec{\lambda}}^{\dagger} \left[ \left\{ \Delta X_j, \Delta X_k \right\} \right] \right\rangle_A, \tag{24}$$

where  $\{X,Y\} = XY + YX$  is the anti-commutator and we define shifted force observables

$$\Delta X_j := X_j - \langle X_j \rangle_{_{A}}. \tag{25}$$

We also need to introduce another correlation function given by

$$\left[\mathbf{B}(\vec{\lambda})\right]_{ik} := \left\langle \left\{ \mathcal{L}_{\vec{\lambda}}^{\dagger}[\Delta X_j], \Delta X_k \right\} \right\rangle_A. \tag{26}$$

Then the nested integrals in (22) can be converted into a single one using integration by parts twice:

$$\sigma_W^2 = k_B^2 T^2 V \left( \pi(\vec{\lambda}_A) || \pi(\vec{\lambda}_B) \right) + \int_0^\tau dt \left[ \vec{\lambda}_B - \vec{\lambda}_t \right]^T \mathbf{G}(\vec{\lambda}_t) \left[ \vec{\lambda}_B - \vec{\lambda}_t \right] + \left[ \vec{\lambda}_B - \vec{\lambda}_t \right]^T \mathbf{B}(\vec{\lambda}_t) \left[ \vec{\lambda}_t - \vec{\lambda}_A \right]. \tag{27}$$

As we saw with the average excess work, the first term here is what one would expect for work fluctuations via an instantaneous quench [38], while the two terms in the integral are leading order corrections for a finite speed protocol. The expressions (19) and (27) are our first main results, and will now form the basis for finding optimal protocols in the fast driving regime.

#### 2. Optimality of instantaneous jump protocols

Our aim is now to determine control protocols (2) that minimise the average excess work and the work fluctuations subject to a fixed initial and final Hamiltonian. For this it is useful to define the *short-term power savings* [29], defined as

$$P_{\text{save}} := \tau^{-1} \left( k_B TS \left( \pi(\vec{\lambda}_A) || \pi(\vec{\lambda}_B) \right) - \langle W_{\text{ex}} \rangle \right), \tag{28}$$

which quantifies any additional reduction to the rate of work done provided by the finite-time protocol beyond that of an instantaneous quench. In a similar fashion we also introduce the *short-term constancy savings*,

$$C_{\text{save}} := \tau^{-1} \left( k_B^2 T^2 V(\pi(\vec{\lambda}_A) || \pi(\vec{\lambda}_B)) - \sigma_W^2 \right). \tag{29}$$

This measures the reductions to the rate of work fluctuations from a short-time protocol. These are now the two objectives to maximise in our control problem. Using our short-time approximations to both the average excess work (19) and work fluctuations (27), a general optimisation principle becomes immediately apparent for this regime. Since the integrands appearing in (19) and (27) are each independent of the control velocity  $d\vec{\lambda}/dt$ , we can infer that optimal protocols will consist of an instantaneous jump from  $\vec{\lambda}_A$  to a point in the parameter space, remaining there for the total duration  $\tau$  and concluding with another instantaneous jump

to the final boundary point  $\vec{\lambda}_B$ . We will denote the control values that maximise  $P_{\text{save}}$  and  $C_{\text{save}}$  respectively by  $\vec{\zeta}$  and  $\vec{\Lambda}$ , which are determined by the solutions to the following *distinct* Euler–Lagrange equations:

$$\vec{R}(\vec{\zeta}) = \nabla_{\vec{\lambda}} \left( \left[ \vec{\lambda}_B - \vec{\zeta} \right]^T \vec{R}(\vec{\lambda}) \right) \Big|_{\vec{\lambda} = \vec{\zeta}}$$
(30)

and

$$\nabla_{\vec{\lambda}} \left( \left[ \vec{\lambda}_B - \vec{\lambda} \right]^T \mathbf{G}(\vec{\lambda}) \left[ \vec{\lambda}_B - \vec{\lambda} \right] \right) \bigg|_{\vec{\lambda} = \vec{\Lambda}} = \nabla_{\vec{\lambda}} \left( \left[ \vec{\lambda} - \vec{\lambda}_B \right]^T \mathbf{B}(\vec{\lambda}) \left[ \vec{\lambda} - \vec{\lambda}_A \right] \right) \bigg|_{\vec{\lambda} = \vec{\Lambda}}. \tag{31}$$

The maximal short-term power savings are then given by

$$P_{\text{save}} \leqslant P_{\text{save}}^* := \left[\vec{\zeta} - \vec{\lambda}_B\right]^T \vec{R}(\vec{\zeta}),\tag{32}$$

which is saturated via the jump protocol

$$\vec{\lambda}_t = \vec{\lambda}_A + [\vec{\zeta} - \vec{\lambda}_A]\theta(t) + [\vec{\lambda}_B - \vec{\zeta}]\theta(t - \tau), \tag{33}$$

where  $\theta(t)$  denotes the Heaviside step function. The optimality of such processes was proven in [29] for classical systems. We have here shown that the same result applies to quantum mechanical systems, provided that the dynamical generator (3) remains independent of  $d\lambda/dt$ . As a more significant result, we can now see that it is possible to reduce fluctuations using a similar instantaneous jump protocol, albeit with a different choice of point in the parameter space. The maximum short-term constancy savings are given by

$$C_{\text{save}} \leqslant C_{\text{save}}^* := \left[\vec{\Lambda} - \vec{\lambda}_B\right]^T \left(\mathbf{G}(\vec{\Lambda}) \left[\vec{\lambda}_B - \vec{\Lambda}\right] + \mathbf{B}(\vec{\Lambda}) \left[\vec{\Lambda} - \vec{\lambda}_A\right]\right),\tag{34}$$

which is saturated by jumping to  $\vec{\Lambda}$  instead, so that

$$\vec{\lambda}_t = \vec{\lambda}_A + [\vec{\Lambda} - \vec{\lambda}_A]\theta(t) + [\vec{\lambda}_B - \vec{\Lambda}]\theta(t - \tau). \tag{35}$$

In general the values of  $\vec{\zeta}$  and  $\vec{\Lambda}$  will not typically coincide, implying a trade-off between minimised excess work versus minimal fluctuations. This can remain the case even in quasi-classical regimes where only changes to the energy levels of the system are allowed, as well as fully classical systems that admit a phase space description. This should be contrasted with slow driving or linear response regimes, which allow for simultaneous optimisation of the average and variance due to the validity of the fluctuation dissipation relation in the absence of quantum friction [17, 18]. However, depending on the particular Hamiltonian parameters and dynamics it is still possible to find situations where  $\vec{\zeta} = \vec{\Lambda}$  and simultaneous optimisation is possible, as we will highlight in subsequent sections.

Before we proceed it is important to highlight some consistency requirements needed to implement a jump protocol. As we are restricted to operating in fast driving regimes, this places restrictions on the set of points one can jump to in order to ensure that the Taylor expansions used in (16) and (22) remain valid. In the appendix it is shown that errors associated with these approximations scale according to

$$|\langle W_{\rm ex}\rangle^{\rm true} - \langle W_{\rm ex}\rangle^*| \leqslant \Delta h(\vec{\xi}) \, \mathcal{O}(\tau^2/\tau_c^2),$$
 (36)

$$|(\sigma_W^2)^{\text{true}} - (\sigma_W^2)^*| \leqslant \Delta h^2(\vec{\Lambda}) \, \mathcal{O}(\tau^2/\tau_c^2), \tag{37}$$

where  $\langle W_{\rm ex} \rangle^{\rm true}$  and  $(\sigma_W^2)^{\rm true}$  denote the exact values of (5) and (6) with respect to the jump protocols, while  $\langle W_{\rm ex} \rangle^*$  and  $(\sigma_W^2)^*$  are the corresponding values with respect to the fast driving approximations (19) and (27). Furthermore, we introduce the Hamiltonian magnitude

$$\Delta h(\vec{\lambda}) := 2 \max \{ ||H(\vec{\lambda}) - H(\vec{\lambda}_A)||_1, ||H(\vec{\lambda}_B) - H(\vec{\xi})||_1 \}. \tag{38}$$

This tells us that one cannot jump arbitrarily far from the boundary points  $\vec{\lambda}_A, \vec{\lambda}_B$  as this would lead to a large  $\Delta h$  and hence invalidate the fast driving approximation. Therefore any freedom in setting the magnitude of  $\vec{\xi}$  and  $\vec{\Lambda}$  must take these bounds into account, discounting arbitrarily large values of both  $P^*_{\text{save}}$  and  $C^*_{\text{save}}$ . For the remainder of the paper we now demonstrate the utility of these jump protocols in a range of different types of system.

#### 3. Closed quantum systems

As a starting point we consider an isolated quantum system whose dynamics are given by the time-dependent Liouville–von Neumann equation:

$$\mathcal{L}_{\vec{\lambda}_t}[(\cdot)] = -\frac{i}{\hbar} [H(\vec{\lambda}_t), (\cdot)]. \tag{39}$$

The work statistics of quenched isolated systems are well studied, particularly in the context of many-body quantum systems [40, 41]. Our formalism can now be used to calculate the leading short-time corrections to the excess work and fluctuations arising when the (instantaneous) quenches are replaced by fast Hamiltonian ramps, and then subsequently minimise them using the appropriate jump protocols outlined in the previous section. For closed, finite dimensional systems it is clear that the characteristic time scale is  $\tau_c \sim \hbar/E_{\rm max}(\vec{\lambda})$ , where  $E_{\rm max}(\vec{\lambda})$  denotes the maximum energy eigenstate of  $H(\vec{\lambda})$ , and we set  $\tau \ll \tau_c$  to establish the fast driving regime. The relevant initial force relaxation rate and correlation functions are found to be

$$\vec{R}(\vec{\lambda}) = -\frac{i}{\hbar} \langle \left[ \vec{X}, H(\vec{\lambda}) \right] \rangle_A , \qquad (40)$$

$$\left[\mathbf{G}(\vec{\lambda})\right]_{jk} = -\frac{i}{2\hbar} \left\langle \left[\left\{\Delta X_j, \Delta X_k\right\}, H(\vec{\lambda})\right]\right\rangle_A, \tag{41}$$

$$\left[\mathbf{B}(\vec{\lambda})\right]_{jk} = -\frac{i}{\hbar} \left\langle \left\{ \left[\Delta X_{j}, H(\vec{\lambda})\right], \Delta X_{k} \right\} \right\rangle_{A}. \tag{42}$$

The short-time power savings are then

$$P_{\text{save}} := \frac{i}{\tau \hbar} \int_0^{\tau} dt \left\langle \left[ H(\vec{\lambda}_B), H(\vec{\lambda}_t) \right] \right\rangle_A \tag{43}$$

while the constancy savings are

$$C_{\text{save}} := \frac{i}{\tau \hbar} \int_0^{\tau} dt \left( \left\langle \left[ H(\vec{\lambda}_B)^2, H(\vec{\lambda}_t) \right] \right\rangle_A - \left\langle \left\{ H(\vec{\lambda}_A), \left[ H(\vec{\lambda}_B), H(\vec{\lambda}_t) \right] \right\} \right\rangle_A - 2 \left\langle H(\vec{\lambda}_B) - H(\vec{\lambda}_A) \right\rangle_A \left\langle \left[ H(\vec{\lambda}_B), H(\vec{\lambda}_t) \right] \right\rangle_A \right). \tag{44}$$

We can already see from (43) and (44) that if  $H(\vec{\lambda}_B)$  and  $H(\vec{\lambda}_A)$  commute, or  $\vec{\lambda}_t$  is chosen such that  $H(\vec{\lambda}_t)$  commutes with either  $H(\vec{\lambda}_B)$  or  $H(\vec{\lambda}_A)$ , then the integrand is exactly 0—which directly follows using the cyclic property of the trace. Therefore if  $\vec{\lambda}_t$  is a linear combination of  $\vec{\lambda}_A$  and  $\vec{\lambda}_B$  the first order correction vanishes. An immediate consequence is that a naive protocol that linearly interpolates between the initial and final Hamiltonian in a closed system is equivalent to a quench up to first order in driving speed. Similarly, it follows directly (and without approximation) from (39) that if  $H(\vec{\lambda}_B)$ ,  $H(\vec{\lambda}_A)$  and  $H(\vec{\lambda}_t)$  commute for all t then the state does not evolve in time and therefore the protocol is equivalent to a quench. But we can note that here we get the same result (up to first order) with a weaker assumption on the commutation relations between the Hamiltonians.

We now choose a jump protocol to maximise either variable, and a simple argument can be used to determine the optimal points  $\vec{\xi}$  and  $\vec{\Lambda}$ . First notice that both  $P_{\text{save}}$  and  $C_{\text{save}}$  are linear in the control variables, so that their gradients are independent of  $\vec{\lambda}$ :

$$\nabla_{\vec{\lambda}} P_{\text{save}} = \frac{i}{\hbar} \left\langle \left[ H(\vec{\lambda}_B), \vec{X} \right] \right\rangle_A, \tag{45}$$

$$\nabla_{\vec{\lambda}} C_{\text{save}} = \frac{i}{\hbar} \left( \left\langle \left[ H(\vec{\lambda}_B)^2, \vec{X} \right] \right\rangle_A - \left\langle \left\{ H(\vec{\lambda}_A), \left[ H(\vec{\lambda}_B), \vec{X} \right] \right\} \right\rangle_A - 2 \left\langle H(\vec{\lambda}_B) - H(\vec{\lambda}_A) \right\rangle_A \left\langle \left[ H(\vec{\lambda}_B), \vec{X} \right] \right\rangle_A \right). \tag{46}$$

The fact that these gradients are independent of  $\vec{\lambda}$  implies that the optimal points  $\vec{\xi}$  and  $\vec{\Lambda}$  are vectors pointing in the direction of the respective gradients, with the norm chosen as large as possible. However, as argued in the previous section there is a limitation to how big this norm can be: the larger this norm is chosen the larger the error of the approximation is. In particular, setting  $|\vec{\xi}| \gg |\vec{\lambda}_A|, |\vec{\lambda}_B|$  gives  $|\vec{\xi}| \propto \Delta h(\vec{\xi})$  while  $\tau_c \propto 1/|\vec{\xi}|$ . Comparing with our error bound (36) we see that in this case

$$|\langle W_{\rm ex} \rangle^{\rm true} - \langle W_{\rm ex} \rangle^*| \leqslant \mathcal{O}(|\vec{\xi}|^3 \tau^2),$$
 (47)

which clearly limits how large the norm can be chosen relative to the duration of the protocol. A similar argument applies to the constancy savings and norm of the optimal point  $\vec{\Lambda}$ .

We can make some further inferences about the relation between the different jumps  $\vec{\xi}$  and  $\vec{\Lambda}$ . It follows from the commutators in (45) and (46) that

$$\vec{\lambda}_A \cdot \nabla_{\vec{\lambda}} P_{\text{save}} = \vec{\lambda}_A \cdot \nabla_{\vec{\lambda}} C_{\text{save}} = \vec{\lambda}_B \cdot \nabla_{\vec{\lambda}} P_{\text{save}} = \vec{\lambda}_B \cdot \nabla_{\vec{\lambda}} C_{\text{save}} = 0, \tag{48}$$

which means that both gradients are orthogonal to  $\vec{\lambda}_A$  and  $\vec{\lambda}_B$ . As was said before, this implies that if the protocol consists of a linear combination of  $H_A$  and  $H_B$  then the correction will be zero. But if the Hamiltonian has  $d \leq 2$  controllable parameters it is impossible for  $\vec{\lambda}_t$  to be linearly independent from  $\vec{\lambda}_A$  and  $\vec{\lambda}_B$ . Therefore, regardless of the type of driving, with  $d \leq 2$  controllable parameters the correction is always zero.

It is interesting to consider what happens when we can control exactly three parameters, d = 3. Equation (48) constrains the gradients of (45) and (46) to be parallel, which implies a direct relation between the variation of power and fluctuations

$$dP_{\text{save}} = \pm \frac{||\nabla_{\vec{\lambda}} P_{\text{save}}||_{\vec{\lambda} = \vec{\xi}}}{||\nabla_{\vec{\lambda}} C_{\text{save}}||_{\vec{\lambda} = \vec{\lambda}}} dC_{\text{save}} , \qquad (49)$$

where the sign is positive if the gradients are oriented in the same direction and negative otherwise. If the sign is positive we can optimize fluctuations and excess work simultaneously with  $\vec{\xi} = \vec{\Lambda}$ , if the sign is negative we have a direct trade-off between savings in power and constancy.

#### 3.1. Driven qubit

As an illustrative example we can compute and optimize the excess work and work fluctuations of a qubit that is undergoing unitary evolution. The most general Hamiltonian for a qubit is

$$H(\vec{\lambda}) = J\vec{\lambda} \cdot \vec{\sigma} \,\,\,(50)$$

where  $\vec{\sigma} = (\sigma^x, \sigma^y, \sigma^z)$  is the Pauli vector, J is an energy scale and  $\vec{\lambda} = (\lambda^x, \lambda^y, \lambda^z)$  are dimensionless parameters that characterize the Hamiltonian. Using the property that  $(\vec{a} \cdot \vec{\sigma})(\vec{b} \cdot \vec{\sigma}) = (\vec{a} \cdot \vec{b})\mathbb{1} + i(\vec{a} \wedge \vec{b}) \cdot \vec{\sigma}$  we can find that the thermal state can be written in the following way

$$\pi(\vec{\lambda}) = \frac{e^{-\beta H(\vec{\lambda})}}{Z(\vec{\lambda})} = \frac{1}{2}\mathbb{1} - \frac{1}{2}\tanh(\beta J ||\vec{\lambda}||) \frac{\vec{\lambda} \cdot \vec{\sigma}}{||\vec{\lambda}||}.$$
 (51)

Using this equation with the fact that Pauli matrices are trace-less it is straightforward to obtain

$$P_{\text{save}} = -\frac{2J^2 \tanh(\beta J \|\vec{\lambda}_A\|)}{\tau \|\vec{\lambda}_A\|} \int_0^{\tau} dt \, \vec{\lambda}_t \cdot (\vec{\lambda}_B \wedge \vec{\lambda}_A), \tag{52}$$

$$C_{\text{save}} = -\frac{4J^3}{\tau} \left[ 1 - \tanh(\beta J \|\vec{\lambda}_A\|)^2 \left( 1 - \frac{\vec{\lambda}_A \cdot \vec{\lambda}_B}{\|\vec{\lambda}_A\|^2} \right) \right] \int_0^{\tau} dt \, \vec{\lambda}_t \cdot (\vec{\lambda}_B \wedge \vec{\lambda}_A) . \quad (53)$$

It is clear that the integrands are maximised simultaneously by choosing a jump protocol with  $\vec{\xi} = \vec{\Lambda} = \alpha \vec{\lambda}_A \wedge \vec{\lambda}_B$ , and hence we find the optimal values

$$P_{\text{save}}^* = 2\alpha J^2 \sin^2 \phi \|\vec{\lambda}_A\| \|\vec{\lambda}_B\|^2 \tanh(\beta J \|\vec{\lambda}_A\|), \tag{54}$$

$$C_{\text{save}}^* = 4\alpha J^3 \sin^2 \phi \, \|\vec{\lambda}_A\|^2 \|\vec{\lambda}_B\|^2 \left[ 1 - \tanh(\beta J \|\vec{\lambda}_A\|)^2 \left( 1 - \frac{\|\vec{\lambda}_B\|}{\|\vec{\lambda}_A\|} \cos \phi \right) \right], \tag{55}$$

where  $\phi$  is the angle between  $\vec{\lambda}_A$  and  $\vec{\lambda}_B$ . We can notice that  $\tanh(\beta J \| \vec{\lambda}_A \|)^2 \left(1 - \frac{\| \vec{\lambda}_B \|}{\| \vec{\lambda}_A \|} \cos \phi\right) < 1$  for all choices of  $\vec{\lambda}_A$  and  $\vec{\lambda}_B$ . Therefore we can optimize fluctuations and excess work simultaneously by choosing  $\alpha > 0$ . The magnitude of  $\alpha$  has to be chosen in such a way that that the error of the approximation (47) remains small. A sufficient condition is then given by choosing

$$0 \leqslant \alpha \ll \frac{1}{J\tau |\sin \phi| \|\vec{\lambda}_A\| \|\vec{\lambda}_B\|} \ . \tag{56}$$

New J. Phys. 25 (2023) 073005 A Rolandi et al

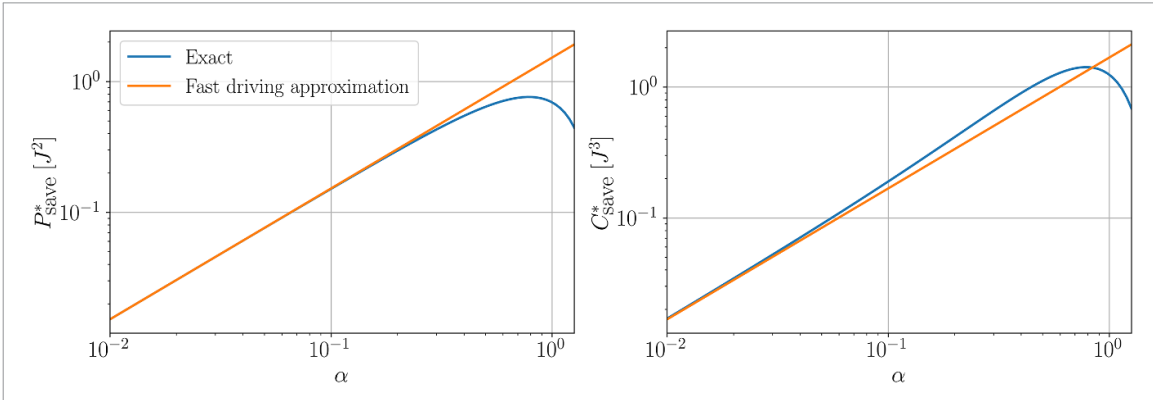


**Figure 1.** Comparison of  $P_{\text{save}}^*$  and  $C_{\text{save}}^*$  (in units of  $J^2$  and  $J^3$  respectively) in the exact case and fast driving approximation as a function of  $\alpha$  for a jump protocol with  $H_A = J\sigma^x$ ,  $H_B = J\sigma^z$  and  $J\tau = \beta J = 1$ .

This condition is illustrated in figure 1, in which we compare the results of (54) and (55) to the exact calculation of  $P_{\text{save}}$  and  $C_{\text{save}}$  for jump protocols in a qubit. The boundary conditions were set to  $H_A = J\sigma^x$  ( $\vec{\lambda}_A = \hat{x}$ ),  $H_B = J\sigma^z$  ( $\vec{\lambda}_B = \hat{z}$ ) and the relevant constants are set to  $\tau J = \beta J = 1$ . Then the condition of equation (56) becomes  $\alpha \ll 1$ , indeed we can see from the figure that as  $\alpha$  approaches  $\mathcal{O}(1)$  the approximation breaks down.

It is important to stress that for higher dimensional closed systems, simultaneous optimisation of  $P_{\text{save}}$  and  $C_{\text{save}}$  cannot always be guaranteed despite what we observe in the case of a qubit.

#### 4. Open quantum systems

We now move to open quantum systems. Our framework can be applied to any Markovian Lindblad equation of the form (3), in which the generator  $\mathcal{L}_{\vec{\lambda}_t}$  is independent of the velocity  $d\vec{\lambda}_t/dt$  and depends only on  $\vec{\lambda}_t$ . Here we illustrate it for the simple evolution:

$$\mathcal{L}_{\vec{\lambda}_t}[\cdot] = \frac{\pi(\vec{\lambda})\text{Tr}(\cdot) - (\cdot)}{\tau^{eq}},\tag{57}$$

which describes a decay of the state  $\rho$  into the instantaneous Gibbs state  $\pi(\vec{\lambda})$  with a timescale  $\tau^{eq}$ . This dissipative evolution naturally arises in collisional models [42] and also describes some systems weakly interacting with a reservoir with a sufficiently flat spectral density [22]. For this type of dynamics we find some more illuminating expressions for the various terms appearing in the leading corrections to the excess work and variance. Firstly, the initial force relaxation rate becomes

$$\vec{R}(\vec{\lambda}) := \frac{\langle \vec{X} \rangle_{\vec{\lambda}} - \langle \vec{X} \rangle_{A}}{\tau^{eq}},\tag{58}$$

where  $\langle (.) \rangle_{\vec{\lambda}} = \text{Tr}\left((.)\pi(\vec{\lambda})\right)$ . This demonstrates that  $\vec{R}(\vec{\lambda})$  quantifies the average rate at which each expectation  $\langle X_i \rangle$  changes from its initial value relative to the characteristic timescale  $\tau^{eq}$ . Furthermore, the correlation functions become

$$\left[\mathbf{G}(\vec{\lambda})\right]_{jk} = \frac{\mathcal{F}_{jk}(\vec{\lambda}) - \mathcal{F}_{jk}(\vec{\lambda}_A)}{\tau^{eq}} + \left(\langle X_j \rangle_{\vec{\lambda}} R_k(\vec{\lambda}) + \langle X_k \rangle_{\vec{\lambda}} R_j(\vec{\lambda})\right)$$
(59)

and

$$\left[\mathbf{B}(\vec{\lambda})\right]_{jk} = -\frac{2}{\tau^{eq}} \mathcal{F}_{jk}(\vec{\lambda}),\tag{60}$$

where  $\mathcal{F}_{ik}(\vec{\lambda})$  is the symmetric covariance defined as

$$\mathcal{F}_{jk}(\vec{\lambda}) := \frac{1}{2} \text{Tr}\left( \{ X_j, X_k \} \pi(\vec{\lambda}) \right) - \langle X_j \rangle_{\vec{\lambda}} \langle X_k \rangle_{\vec{\lambda}}. \tag{61}$$

This function defines a metric tensor on the manifold of control parameters, and was first introduced in [43] as a means of quantifying the geometric structure of thermal states. More recently this metric has been

shown to determine optimal protocols with minimal work fluctuations in slow driving regimes, achieved by traversing a geodesic path in the parameter space [18, 19]. In quasi-classical regimes where  $[X_j, X_k] = 0$  this metric becomes proportional to the well-known thermodynamic metric defined as the negative Hessian of the free energy [44]:

$$[X_j, X_k] = 0 \mapsto \mathcal{F}_{jk}(\vec{\lambda}) = -k_B T \frac{\partial^2 F}{\partial \lambda_j \partial \lambda_k}.$$
 (62)

This metric, which is equivalent to the fisher information matrix of the thermal state, can be used to determine geodesic paths with minimal excess work in slow driving and close to equilibrium regimes [15]. In the present context, we observe an interesting connection between the thermodynamic metric (61) and the work fluctuations in the complete opposite regime of rapid driving. However, minimal fluctuations are not given by following a geodesic path, but rather they are achieved by jumping to a point in the parameter space that maximises the balance (34) between the change in metric components, relaxation rates  $\vec{R}(\vec{\lambda})$  and displacements  $\vec{\lambda} - \vec{\lambda}_B, \vec{\lambda} - \vec{\lambda}_A$ . We will now explore the optimisation of three different systems: a driven quantum dot, and two Ising spin chains.

#### 4.1. Fast erasure of a single bit

A driven quantum dot interacting weakly with an environment is a paradigmatic example of a system that can be described by the simple dynamics (57) [22]. In that case the Hamiltonian is given by  $H(\epsilon) = \frac{1}{2}\epsilon\sigma^z$  with a single control variable  $\lambda_t = \epsilon(t)$  given by the energy gap of the two-level system. The optimal finite-time thermodynamics of such systems has been well studied with regard to minimising average dissipation in Landauer erasure [38, 45–49], including a recent experimental implementation in a driven single dot [50], as well as maximising average power and efficiency in heat engines [26, 51]. More recent numerical approaches have also been used to find optimal protocols that take into account the minimisation of work fluctuations [6, 52]. In the present context, the fast driving assumption allows us to obtain analytic results for these optimal protocols, which we now apply to a rapid bit-erasure process. The boundary conditions for erasure are then  $\epsilon_A = 0$  and  $\beta \epsilon_B \gg 1$ . We first note that the leading term of the expansion (16) yields:

$$\frac{S(\pi(\vec{\lambda}_A)||\vec{\lambda}_B))}{\tau} \approx \frac{1}{\tau} \left(\beta \epsilon_B - \ln(2)\right). \tag{63}$$

To characterise the first order correction, straightforward calculations provide the following expressions:

$$\tau^{eq}R(\epsilon) = \frac{1}{1 + e^{\beta\epsilon}} - \frac{1}{2} , \qquad (64)$$

$$\tau^{eq}G(\epsilon) = 0, (65)$$

$$\tau^{eq}B(\epsilon) = -\frac{1}{2} \,. \tag{66}$$

From this we can compute the power and constancy savings under the fast driving assumption  $\tau/\tau_c \ll 1$ :

$$P_{\text{save}} = \frac{k_B T}{\tau^{eq}} \int_0^1 ds \left(\beta \epsilon_B - \beta \epsilon(s)\right) \left(\frac{1}{2} - \frac{1}{1 + e^{\beta \epsilon(s)}}\right),\tag{67}$$

$$C_{\text{save}} = \frac{k_B^2 T^2}{2\tau^{eq}} \int_0^1 ds \, \beta \epsilon(s) (\beta \epsilon_B - \beta \epsilon(s)). \tag{68}$$

We now seek to find the optimal energy gaps to jump to in order to maximise either  $P_{\rm save}$  or  $C_{\rm save}$ . It will become clear in this case the power and constancy savings cannot be simultaneously maximised, and so the distinct gaps are denoted by  $\xi$  and  $\Lambda$  respectively. Maximising  $P_{\rm save}$  amounts to solving the following transcendental equation

$$\frac{1}{2} - \frac{1}{1 + e^{\beta \xi}} = \frac{(\beta \epsilon_B - \beta \xi) e^{\beta \xi}}{(1 + e^{\beta \xi})^2} \,. \tag{69}$$

In the limit of  $\beta \epsilon_B \gg 1$  we can solve it analytically up to terms  $\mathcal{O}(\beta^{-1}\epsilon_B^{-1}\ln{(\beta\epsilon_B)})$  and find the optimal jump  $\epsilon \mapsto \xi = \beta^{-1}\ln{(2\beta\epsilon_B)}$ . Maximum power savings are thus

$$P_{\text{save}}^* \simeq \frac{\epsilon_B}{2\tau^{eq}}.\tag{70}$$

For this power-optimised jump let us denote the resulting sub-optimal constancy savings by  $C_{\text{save}}^{\xi}$ :

$$C_{\text{save}}^{\xi} = \frac{\epsilon_B^2}{\tau^{eq}} \frac{\ln(2\beta \epsilon_B)}{2\beta \epsilon_B}.$$
 (71)

On the other hand, to maximise the constancy savings we need to choose a jump to  $\epsilon \mapsto \Lambda = \epsilon_B/2$  instead. This yields

$$C_{\text{save}}^* = \frac{\epsilon_B^2}{8\tau^{eq}}, \qquad P_{\text{save}}^{\Lambda} = \frac{\epsilon_B}{4\tau^{eq}},$$
 (72)

where the sub-optimal savings in power are denoted  $P_{\text{save}}^{\Lambda}$ . Clearly there exists a significant trade-off between these two choices of optimal protocol, with power-optimised jumps causing no improvement to the constancy while constancy-optimised jumps reducing the potential power savings by a factor of 1/2. Further comparison can be made with that of a naive linear driving  $\epsilon(t) = \epsilon_B t/\tau$ , which results in savings given by

$$P_{\text{naive}} \simeq \frac{\epsilon_B}{4\tau^{eq}}, \qquad C_{\text{naive}} = \frac{\epsilon_B^2}{12\tau^{eq}},$$
 (73)

where we again drop terms of order  $\mathcal{O}(\beta^{-1}\epsilon_B^{-1}\ln(\beta\epsilon_B))$ . Therefore we can see that choosing an optimal jump for the excess work leads to an improvement factor of 1/2, and choosing the optimal jump for the fluctuations gives an improvement factor of 3/2, each indicating significant improvements over a naive protocol. However, two unexpected observations here are that naive protocols are able to achieve larger savings in constancy than that of the power optimised protocol, and also achieve the same level of power savings to the constancy-optimised protocol. This emphasises that improvements to one objective do not necessarily translate into improvements of the other.

#### 4.2. Dissipative classical Ising chain

The strength of our approach is that it enables to deal with more complex systems, where exact solutions for minimising dissipation and/or fluctuations are lacking -in contrast to the previous example in section 4.1. This is illustrated now for an Ising chain weakly coupled to a bath with dynamics (57). We note that optimal driving protocols for classical spin chains have been devised in the slow driving regime [53–55], and now we complement such results by studying the opposite fast-driving regime. We first consider a classical spin chain,

$$H(\epsilon) = J \sum_{i=1}^{n} \left( \varepsilon \sigma_i^z - \sigma_i^z \sigma_{i+1}^z \right) , \qquad (74)$$

where J is the energy scale and  $\varepsilon$  is a dimensionless parameter which can be interpreted as the strength of an external magnetic field. We assume that  $\varepsilon$  can be controlled externally in time,  $\lambda = \epsilon$ , which results in work being done on the system. By assuming periodic boundary conditions we can compute the partition function per spin in the thermodynamic limit  $n \to \infty$  [56]:

$$\lim_{n \to \infty} \frac{1}{n} \ln Z = \beta J + \ln \left[ \cosh(\beta J \varepsilon) + \sqrt{\sinh(\beta J \varepsilon)^2 + e^{-4\beta J}} \right] . \tag{75}$$

The relevant force here is then the total  $X = J \sum_{i} \sigma_{i}^{z}$ . We now identify the following the relations

$$-\frac{1}{\beta}\frac{\partial}{\partial \varepsilon}\log Z = \text{Tr}(X\pi(\varepsilon)) , \qquad (76)$$

$$\frac{1}{\beta^2} \frac{\partial^2}{\partial \varepsilon^2} \log Z = \text{Tr} \left( X^2 \pi(\varepsilon) \right) - \text{Tr} \left( X \pi(\varepsilon) \right)^2 . \tag{77}$$

These allow us to compute the first order corrections to the excess work and the fluctuations per site of the protocol in the thermodynamic limit from (19) and (27), and employing the above expressions we obtain the initial force relaxation rates and correlation functions:

$$\tau^{eq}R(\varepsilon) = \frac{\sinh(\beta J \varepsilon_A)}{\sqrt{\sinh(\beta J \varepsilon_A)^2 + e^{-4\beta J}}} - \frac{\sinh(\beta J \varepsilon)}{\sqrt{\sinh(\beta J \varepsilon)^2 + e^{-4\beta J}}},$$
(78)

$$\tau^{eq}G(\varepsilon) = e^{-4\beta J} \left( \frac{\cosh(\beta J \varepsilon)}{(\sinh(\beta J \varepsilon)^2 + e^{-4\beta J})^{3/2}} - \frac{\cosh(\beta J \varepsilon_A)}{(\sinh(\beta J \varepsilon_A)^2 + e^{-4\beta J})^{3/2}} \right) + (\tau^{eq} R(\varepsilon))^2, \tag{79}$$

IOP Publishing New J. Phys. 25 (2023) 073005 A Rolandi et al

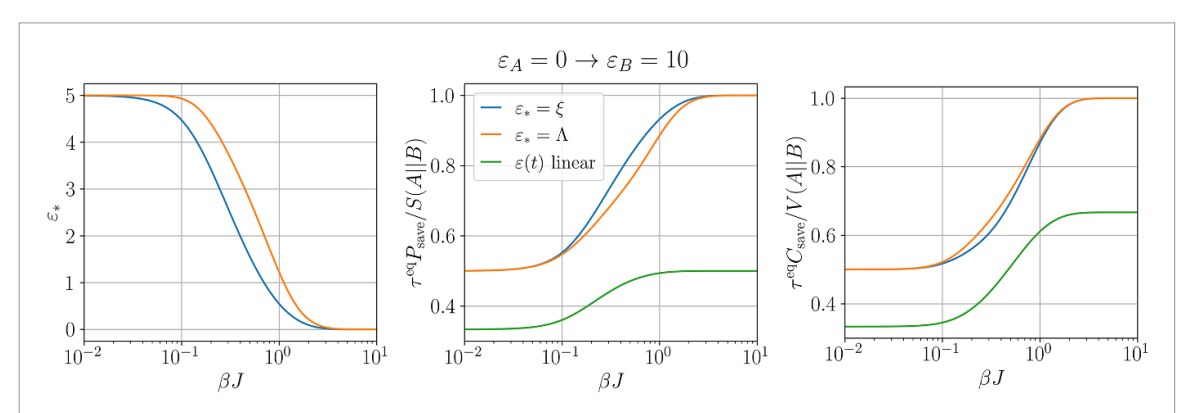


**Figure 2.** (left) Optimal value of  $\varepsilon_*$  for a protocol going from  $\varepsilon_A = 0$  to  $\varepsilon_B = 10$ . (centre and right) Relative power and constancy savings in three protocols going from  $\varepsilon_A = 0$  to  $\varepsilon_B = 10$ . We compare protocols that optimize excess work and fluctuations to a protocol that varies linearly the value of  $\varepsilon$ .

$$\tau^{eq}B(\varepsilon) = -2e^{-4\beta J} \frac{\cosh(\beta J \varepsilon_A)}{(\sinh(\beta J \varepsilon_A)^2 + e^{-4\beta J})^{3/2}}.$$
 (80)

It is now a case of substituting these into the two different Euler–Lagrange equations (30) and (31) to determine the optimal points  $\xi$  and  $\Lambda$  needed in each jump protocol, with solutions found numerically for a process that brings  $\varepsilon$  from  $\varepsilon_A=0$  to  $\varepsilon_B=10$  (i.e. turning on the magnetic field). In figure 2(left) we display the optimal field strength  $\varepsilon_*=\{\xi,\Lambda\}$  that maximises either the power or constancy savings. We can notice that in the limits of high and low temperatures they coincide, while we cannot maximise them simultaneously in between these regimes. In figure 2(centre) we plot the power savings  $P_{\text{save}}^*$  relative to the zeroth contribution  $k_B TS(\pi(\vec{\lambda}_A)||\pi(\vec{\lambda}_B))/\tau_c$ , while figure 2(right) displays the constancy savings  $C_{\text{save}}^*$  in units of  $k_B^2 T^2 V(\pi(\vec{\lambda}_A)||\pi(\vec{\lambda}_B))/\tau_c$ . Both plots show the relative savings depending on whether we choose to optimise the power or constancy, and this is also compared to the savings achieved by taking a naive linear driving  $\epsilon(t) = \epsilon_A (1-t/\tau) + \epsilon_B t/\tau$ . In this case we can see that there is only a modest difference between the  $\epsilon_A \mapsto \xi \mapsto \epsilon_B$  and  $\epsilon_A \mapsto \Lambda \mapsto \epsilon_B$  jump protocols, and they each perform considerably better than the naive approach, contrasting with what we observed for the driven quantum dot. This highlights the importance of optimal control in many-body open quantum systems.

#### 4.3. Ising chain in transverse field

We will conclude with a final example covering the remaining scenario of an open quantum system where the control is such that the Hamiltonian may not commute at different times, so that  $[H(\vec{\lambda}_t), H(\vec{\lambda}_{t'})] \neq 0$ . This non-commutativity implies the presence of quantum friction [57, 58], which is a distinctly non-classical contribution to the work done to drive the system that arises from allowing transitions between energy eigenstates. For this purpose we will consider a dissipative Ising chain with simple dynamics (57), though this time we apply a transverse field along the x-axis that can be controlled in time. We note that optimal driving protocols for this model has been considered in the slow driving regime [38], and the results presented here in the fast driving regime are hence complementary. In particular, we will focus on performing drivings close to a quantum phase transition, which has also been considered in several previous works [40, 59–61].

The Hamiltonian of the system is

$$H(g) = -J \sum_{i=1}^{n} \left( \hat{\sigma}_{i}^{z} \hat{\sigma}_{i+1}^{z} + g \hat{\sigma}_{i}^{x} \right) , \qquad (81)$$

where J is the energy scale and g is a dimensionless parameter which can be interpreted as an external (transverse) magnetic field. Clearly such a model will generate quantum friction as we vary the strength g in time. Assuming again periodic boundary conditions we can compute the spectrum of the system with a Jordan–Wigner transformation [62]. Then by taking the thermodynamic limit the partition function is given by

$$\lim_{n \to \infty} \frac{1}{n} \log Z = \int_0^{2\pi} dk \, \log \left[ 2 \cosh \frac{\beta \epsilon_k}{2} \right] \,, \tag{82}$$

where  $\varepsilon_k$  is the eigenenergy corresponding to the momentum k

$$\epsilon_k = 2J\sqrt{1 + g^2 - 2g\cos k} \,. \tag{83}$$

New J. Phys. **25** (2023) 073005 A Rolandi et al

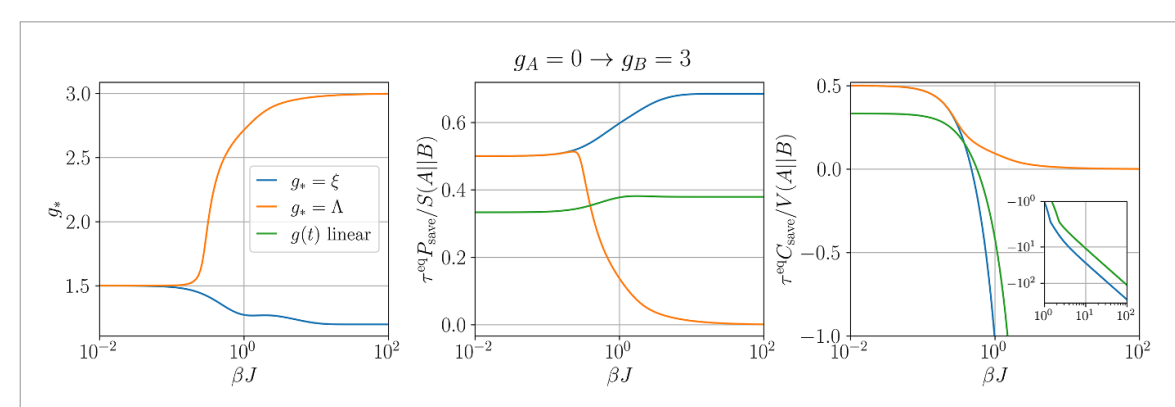


**Figure 3.** (left) Optimal value of  $g_* = \{\xi, \Lambda\}$  for a protocol going from  $g_A = 0$  to  $g_B = 3$ . (centre) Relative power savings in three protocols going from  $g_A = 0$  to  $g_B = 3$  and (right) relative constancy savings for the same three protocols. In each figure we compare these optimal protocols to one that varies linearly the value of g.

At zero temperature and g=1 this system presents a phase transition from an ordered ferromagnetic phase to a quantum paramagnetic phase. We will focus on studying protocols that take the system across this point by changing g at finite temperature. The relevant force this time is  $X = -J\sum_i \sigma_i^x$ , and we can use the relations

$$-\frac{1}{\beta} \left. \frac{\partial}{\partial g} \log Z \right|_{g=g_*} = \text{Tr}(X\pi(g^*)) , \qquad (84)$$

$$\frac{1}{\beta^2} \left. \frac{\partial^2}{\partial g^2} \log Z \right|_{g=g_*} = \text{Tr}\left(X^2 \pi(g^*)\right) - \text{Tr}\left(X \pi(g^*)\right)^2. \tag{85}$$

The first order corrections to the excess work and the fluctuations per site of the protocol are now computed within the thermodynamic limit, giving us

$$\tau^{eq}R(g_*) = -\frac{1}{2} \int_0^{2\pi} dk \,\dot{\epsilon}_k \tanh\frac{\beta \epsilon_k}{2} \bigg|_{g=g_*}^{g=g_*} , \qquad (86)$$

$$\tau^{eq}G(g_*) = \frac{J}{2} \int_0^{2\pi} dk \, \ddot{e}_k \tanh \frac{\beta \epsilon_k}{2} + \frac{\dot{\epsilon}_k^2}{2J} \cosh^{-2} \frac{\beta \epsilon_k}{2} \bigg|_{g=g_A}^{g=g_*} + (\tau^{eq} R(g_*))^2, \tag{87}$$

$$\tau^{eq}B(g_*) = -J \int_0^{2\pi} dk \, \ddot{\epsilon}_k \tanh \frac{\beta \epsilon_k}{2} + \frac{\dot{\epsilon}_k^2}{2J} \cosh^{-2} \frac{\beta \epsilon_k}{2} \bigg|_{g=g_A} , \qquad (88)$$

where  $\dot{\epsilon}_k = \frac{d\epsilon_k}{dg}$ . Substituting into the Euler–Lagrange equations (30) and (31) and solving numerically then determines the instantaneous jumps  $g_A \mapsto \xi \mapsto g_B$  and  $g_A \mapsto \Lambda \mapsto g_B$  for maximising the respective power and constancy savings. We set our boundary conditions to be  $g_A = 0$  and  $g_B = 3$  so that we turn on the transverse magnetic field and cross the phase transition point at g = 1. Similarly to the classical case, we also compare these optimal protocols to a 'naive' protocol in which the parameter is varied linearly in time,  $g(t) = g_A(1 - t/\tau) + g_B t/\tau$ .

In figure 3(left) we display the optimal fields strength of  $g_* = \{\xi, \Lambda\}$ , which noticeably coincide in the limit of high temperatures like we saw with the classical Ising chain. On the other hand at low temperatures they no longer coincide, indicating a distinctly non-classical feature of this example and demonstrating that simultaneous optimisation is no longer possible. In figure 3 we compare these two choices of protocol to linear driving and plot the resulting power savings (centre) and constancy savings (right). Since temperature is finite the phase transition is washed out but we can still observe a signature in the power and constancy savings occurring at lower temperatures, where we see that the two quantities move significantly further apart. One dramatic feature is the fact that optimising the power savings results in the constancy savings becoming significantly negative at lower temperatures beyond the phase transition, indicating a large growth in overall work fluctuations above that of an infinitely fast quench. On the other hand, if we choose to maximise the constancy savings we see that this drops drops to zero alongside the power savings at low temperatures. This indicates that the system is highly sensitive to the choice of protocol when driven close to a quantum phase transition.

#### 5. Discussion

We have derived approximations for the average excess work done (19) to rapidly drive a small system out of equilibrium along with the resulting work fluctuations (27). This has been derived under the assumption that (i) the dynamics can be described by a Markovian generator that is independent of the velocities in the time-dependent control parameters, and (ii) the duration of the process is short relative to the characteristic timescale of the dynamics,  $\tau_c \gg \tau$ . These approximations, which are based around the Dyson series, can be viewed as the inverse to the approximations used to treat the finite-time thermodynamics of slowly driven systems where  $\tau_c \ll \tau$  [17, 18, 37, 63]. Under these approximations we were able to prove that rapid processes that minimise either the average excess work or work fluctuations under fixed boundary conditions consist of two instantaneous jumps in the system control parameters, contrasting with the smooth geodesic paths that are optimal on slow driving and linear response regimes [15, 18], and bearing close similarity to exact results in stochastic thermodynamics [21, 22]. Protocols that minimise the excess work done jump from the initial configuration to a point determined from the Euler–Lagrange equation (30), stay there for the duration  $\tau$ then jump to the final boundary value. Protocols that minimise the work fluctuations follow the same pattern, but jump to an alternative point satisfying a different Euler-Lagrange equation (31). We have seen that in general, these points do no coincide which indicates a trade-off between the optimal values of the average and variance. While we have focused only on comparing these two distinct protocols, we can go further and reformulate this as a multi-objective optimisation problem. To do this one can use a *Pareto front* to quantify the family of protocols interpolating between the minimal-dissipation and minimal-fluctuation processes [6]. This is found from minimising the objective function  $\alpha \langle W_{ex} \rangle + (1-\alpha)\sigma_W^2 \, \forall \alpha \in [0,1]$ . By linearity, we can simply add (30) to (31) with respective weightings  $\alpha$  and  $1 - \alpha$  to get the corresponding Euler-Lagrange equation. Crucially, Pareto-optimal solutions will again consist of instantaneous jumps in the control parameters. This extends the results of [29] to show that jump protocols continue to be optimal when one also cares about keeping fluctuations minimal, while also extending this approach to the full quantum regime. In particular, it is worth emphasising that, beyond the standard scenario of a driven system in contact with a Markovian environment, our approach also applies to closed quantum driven systems where the form of minimally dissipative driving processes remain less explored [1, 64]. Our work also complements optimisations of power (and fluctuations) in quantum heat engines, where jump protocols were also typically found [27, 28, 52]. Due to its generality, our optimisation scheme can be used to improve the control of complicated chemical, biological and quantum many-body systems whenever short operation times are desired. This has been illustrated by minimising both excess work and fluctuations for a classical and quantum spin chain where an external magnetic field is rapidly changed in time. When driving the system close to a quantum phase transition, we found that optimising over driving protocols leads to substantial gains (see figure 3). It is interesting to combine and contrast these results with previous works considering the minimisation of dissipation in slowly driven many-body systems [38, 53–55].

A number of improvements and generalisations to our approach are warranted. For open quantum systems, it is important to note that protocols with non-commuting Hamiltonians may not adequately be described by adiabatic Lindblad equations such as (57) when operating in the fast driving regime [27, 28]. Hence, one should find a way to match our fast driving approximation to an appropriate Markovian master equation in situations where the system is weakly-coupled to a bath while allowing for fast, non-commuting Hamiltonian protocols. Interestingly, since non-adiabatic corrections can potentially lead to a dependence on the control velocities [31], this would imply that instantaneous jumps are not necessarily optimal in these cases. The approximations (19) and (27) will remain valid in any case, but terms appearing inside the first order corrections will now depend on the rates  $d\vec{\lambda}/dt$  and the Euler-Lagrange equations (30) and (31) will no longer hold. Moreover, this additional dependence means that solutions can generally consist of both discontinuous and continuous contributions to the optimal path, as is seen in exactly solvable models such as the driven Brownian particle [21]. Finding ways to determine these optimal protocols under more accurate treatments of the non-adiabatic dynamics will be crucial for understanding the impact of quantum fluctuations on the thermodynamics of rapidly driven systems. As we saw with the toy model in section 4.3, operating close to a quantum phase transition can have a significant detrimental impact on the work fluctuations along processes with minimal dissipation. For more realistic non-adiabatic dynamics, this motivates a more careful consideration of the full multi-objective optimisation problem in the presence of quantum fluctuations and will be left for future investigation.

#### Data availability statement

No new data were created or analysed in this study.

#### Acknowledgment

A R and M P-L acknowledge funding by the Swiss National Science Foundation through an Ambizione Grant No. PZ00P2-186067. H J D M acknowledges support from the Royal Commission for the Exhibition of 1851.

#### Appendix. Error approximation to fast driving expansion

Choosing the jump protocol  $\vec{\lambda}_t = \vec{\lambda}_A + [\vec{\zeta} - \vec{\lambda}_A]\theta(t) + [\vec{\lambda}_B - \vec{\zeta}]\theta(t - \tau)$  and using the fact that  $\dot{\theta}(t - t') = \delta(t - t')$ , we derive the following inequality:

$$\begin{split} |\langle W_{\rm ex} \rangle^{\rm true} - \langle W_{\rm ex} \rangle^*| &= \left| \int_0^1 ds \, \frac{d\vec{\lambda}_s^T}{ds} {\rm Tr} \left( \vec{X} \left( \tilde{\rho}(s) - \sigma(s) \right) \right) \right|, \\ &\leqslant \int_0^1 ds \, \left| \frac{d\vec{\lambda}_s^T}{ds} {\rm Tr} \left( \vec{X} \left( \tilde{\rho}(s) - \sigma(s) \right) \right) \right|, \\ &\leqslant \int_0^1 ds \, ||\dot{H}(\vec{\lambda}_s)||_1 ||\tilde{\rho}(s) - \sigma(s) \rangle||_1, \\ &\leqslant \left( ||H(\vec{\xi}) - H(\vec{\lambda}_A)||_1 + ||H(\vec{\lambda}_B) - H(\vec{\xi})||_1 \right) \mathcal{O}(\tau^2 / \tau_c^2), \\ &\leqslant 2 \max \left\{ ||H(\vec{\xi}) - H(\vec{\lambda}_A)||_1, ||H(\vec{\lambda}_B) - H(\vec{\xi})||_1 \right\} \mathcal{O}(\tau^2 / \tau_c^2), \\ &= \Delta h(\vec{\xi}) \, \mathcal{O}(\tau^2 / \tau_c^2) \end{split} \tag{A1}$$

where we used the triangle inequality followed by the trace bound  $|\text{Tr}(AB)| \le ||A||_1 ||B||_1$  and (15). A more involved procedure can be used to find the error approximation for the work fluctuations. First we define the truncated propagator appearing in the Dyson series (13),

$$\overleftarrow{M}(s,s')[(.)] := (.) + \int_{s'}^{s} d\nu \, \tau \mathcal{L}_{\vec{\lambda}_{\nu}}[(.)]. \tag{A2}$$

For a given operator *A* and  $0 \le s \le 1$ ,  $0 \le s' \le 1$ , consider the following norm

$$\mathcal{A}(s,s') := \left| \left| \overleftarrow{P}(s,s') [\Delta_{\tilde{\rho}(s')} A \, \tilde{\rho}(s')] - \overleftarrow{M}(s,s') [\Delta_{\sigma(s')} A \, \sigma(s')] \right| \right|_{1}. \tag{A3}$$

Expanding the propagators gives

$$\mathcal{A}(s,s') = \left\| \Delta_{\tilde{\rho}(s')} A \tilde{\rho}(s') - \Delta_{\sigma(s')} A \sigma(s') + \tau \int_{s'}^{s} d\nu \, \mathcal{L}_{\vec{\lambda}_{\nu}} [\Delta_{\tilde{\rho}(s')} A \tilde{\rho}(s') - \Delta_{\sigma(s')} A \sigma(s')] \right\|_{1} \\
+ \sum_{n=2}^{\infty} \tau^{n} \int_{s'}^{s} dt_{n} \int_{s'}^{t_{n}} dt_{n-1} \dots \int_{s'}^{t_{2}} dt_{1} \, \mathcal{L}_{\vec{\lambda}_{t_{n}}} \mathcal{L}_{\vec{\lambda}_{t_{n-1}}} \dots \mathcal{L}_{\vec{\lambda}_{t_{1}}} [\Delta_{\tilde{\rho}(s')} A \, \tilde{\rho}(s')] \right\|_{1} , \\
\leqslant \left\| \Delta_{\tilde{\rho}(s')} A \tilde{\rho}(s') - \Delta_{\sigma(s')} A \sigma(s') \right\|_{1} + \tau \left\| \int_{s'}^{s} d\nu \, \mathcal{L}_{\vec{\lambda}_{\nu}} [\Delta_{\tilde{\rho}(s')} A \tilde{\rho}(s') - \Delta_{\sigma(s')} A \, \sigma(s')] \right\|_{1}$$

$$+ \left\| \sum_{n=2}^{\infty} \tau^{n} \int_{s'}^{s} dt_{n} \int_{s'}^{t_{n}} dt_{n-1} \dots \int_{s'}^{t_{2}} dt_{1} \, \mathcal{L}_{\vec{\lambda}_{t_{n}}} \mathcal{L}_{\vec{\lambda}_{t_{n-1}}} \dots \mathcal{L}_{\vec{\lambda}_{t_{1}}} [\Delta_{\tilde{\rho}(s')} A \, \tilde{\rho}(s')] \right\|_{1} , \tag{A4}$$

where we used the triangle inequality for the trace norm. We next bound each of the three terms separately. Using the submultiplicavity of the trace norm, one has

$$\left| \left| \Delta_{\tilde{\rho}(s')} A \tilde{\rho}(s') - \Delta_{\sigma(s')} A \sigma(s') \right| \right|_{1} \leqslant 2 \left| \left| A \right| \right|_{1} \left| \left| \tilde{\rho}(s') - \sigma(s') \right| \right|_{1} = \left| \left| A \right| \right|_{1} \mathcal{O}(\tau^{2} / \tau_{c}^{2}) \tag{A5}$$

where we used (15). Similarly, using the definition of the characteristic timescale (9) one gets

$$\tau \left\| \left| \int_{s'}^{s} d\nu \, \mathcal{L}_{\vec{\lambda}_{\nu}} \left[ \Delta_{\tilde{\rho}(s')} A \, \tilde{\rho}(s') - \Delta_{\sigma(s')} A \sigma(s') \right] \right\|_{1} \leqslant \frac{\tau(s-s')}{\tau_{c}} \left\| \left| \Delta_{\tilde{\rho}(s')} A \tilde{\rho}(s') - \Delta_{\sigma(s')} A \sigma(s') \right| \right|_{1}, \tag{A6}$$

$$\leqslant \frac{2\tau}{\tau_{c}} \left\| A \right\|_{1} \left\| \tilde{\rho}(s') - \sigma(s') \right\|_{1},$$

$$= 2 \left\| A \right\|_{1} \mathcal{O}(\tau^{3} / \tau_{c}^{3}).$$

Furthermore,

$$\left\| \sum_{n=2}^{\infty} \tau^n \int_{s'}^{s} dt_n \int_{s'}^{t_n} dt_{n-1} \dots \int_{s'}^{t_2} dt_1 \, \mathcal{L}_{\vec{\lambda}_{t_n}} \mathcal{L}_{\vec{\lambda}_{t_{n-1}}} \dots \mathcal{L}_{\vec{\lambda}_{t_1}} \left[ \Delta_{\tilde{\rho}(s')} A \, \tilde{\rho}(s') \right] \right\|_{1} \leqslant \left\| |A| \right\|_{1} \mathcal{O}(\tau^2 / \tau_c^2). \tag{A7}$$

We can therefore conclude that

$$\mathcal{A}(s,s') \leqslant \left| \left| A \right| \right|_{1} \mathcal{O}(\tau^{2}/\tau_{c}^{2}). \tag{A8}$$

From here we can now bound the error in the fluctuations for the jump protocol  $\vec{\lambda}_t = \vec{\lambda}_A + [\vec{\Lambda} - \vec{\lambda}_A]\theta(t) + [\vec{\lambda}_B - \vec{\lambda}]\theta(t - \tau)$ , which we plug into

$$|(\sigma_{W}^{2})^{\text{true}} - (\sigma_{W}^{2})^{*}| = 2 \left| \mathbb{R}e \int_{0}^{1} ds \int_{0}^{s} ds' \operatorname{Tr} \left( \dot{H}(\vec{\lambda}_{s}) \left( \overleftarrow{P}(s, s') \left[ \Delta_{\tilde{\rho}(s')} \dot{H}(\vec{\lambda}_{s'}) \tilde{\rho}(s') \right] \right) - \overleftarrow{M}(s, s') \left[ \Delta_{\sigma(s')} \dot{H}(\vec{\lambda}_{s'}) \sigma(s') \right] \right) \right|. \tag{A9}$$

Following the same steps we applied in (A1) and combining this with (A8), it is straightforward to see that

$$|(\sigma_W^2)^{\text{true}} - (\sigma_W^2)^*| \leqslant \Delta h^2(\vec{\Lambda}) \ \mathcal{O}(\tau^2/\tau_c^2). \tag{A10}$$

#### **ORCID** iDs

Alberto Rolandi https://orcid.org/0000-0001-7667-9652

Martí Perarnau-Llobet https://orcid.org/0000-0002-4658-0632

Harry J D Miller https://orcid.org/0000-0001-6275-0446

#### References

- [1] Deffner S and Bonança M V S 2020 Europhys. Lett. 131 20001
- [2] Landi G T and Paternostro M 2021 Rev. Mod. Phys. 93 035008
- [3] Seifert U 2012 Rep. Prog. Phys. 75 126001
- [4] Esposito M, Harbola U and Mukamel S 2009 Rev. Mod. Phys. 81 1665
- [5] Pietzonka P and Seifert U 2018 Phys. Rev. Lett. 120 190602
- [6] Solon A P and Horowitz J M 2018 Phys. Rev. Lett. 120 180605
- [7] Horowitz J M and Gingrich T R 2020 Nat. Phys. 16 15
- [8] Holubec V and Ryabov A 2022 J. Phys. A 55 013001
- [9] Miller H J D and Perarnau-Llobet M 2022 arXiv:2205.03065
- [10] Salamon P and Berry R S 1983 Phys. Rev. Lett. 51 1127
- [11] Zulkowski P R, Sivak D A, Crooks G E and Deweese M R 2012 Phys. Rev. E 86 0141148
- [12] Bonança M V S and Deffner S 2014 J. Chem. Phys. 140 244119
- [13] Abiuso P, Miller H J D, Perarnau-Llobet M and Scandi M 2020 Entropy 22 1076
- [14] Brandner K and Saito K 2020 Phys. Rev. Lett. 124 040602
- [15] Sivak D A and Crooks G E 2012 Phys. Rev. Lett. 108 190602
- [16] Jarzynski C 1997 Phys. Rev. Lett. 78 2690
- [17] Speck T and Seifert U 2004 Phys. Rev. E 70 066112
- [18] Miller H J D, Scandi M, Anders J and Perarnau-Llobet M 2019 Phys. Rev. Lett. 123 230603
- [19] Miller H J D and Mehboudi M 2020 Phys. Rev. Lett. 125 260602
- [20] Mehboudi M and Miller H J D 2022 Phys. Rev. A 105 062434
- [21] Schmiedl T and Seifert U 2007 Phys. Rev. Lett. 98 108301
- [22] Esposito M, Kawai R, Lindenberg K and Van Den Broeck C 2010 Europhys. Lett. 89 20003
- [23] Aurell E, Mejía-Monasterio C and Muratore-Ginanneschi P 2011 Phys. Rev. Lett. 106 250601
- [24] Geiger P and Dellago C 2010 Phys. Rev. E 81 021127
- [25] Zulkowski P R and Deweese M R 2014 Phys. Rev. E 89 052140
- [26] Cavina V, Mari A, Carlini A and Giovannetti V 2018 Phys. Rev. A 98 012139
- [27] Erdman P A, Cavina V, Fazio R, Taddei F and Giovannetti V 2019 New J. Phys. 21 103049
   [28] Cavina V, Erdman P A, Abiuso P, Tolomeo L and Giovannetti V 2021 Phys. Rev. A 104 032226
- [29] Blaber S, Louwerse M D and Sivak D A 2021 Phys. Rev. E 104 022101
- [30] Albash T, Boixo S and Lidar D A 2012 New J. Phys. 14 123016

- [31] Dann R, Levy A and Kosloff R 2018 Phys. Rev. A 98 052129
- [32] Talkner P, Lutz E and Hänggi P 2007 Phys. Rev. E 75 050102
- [33] Roncaglia A J, Cerisola F and Paz J P 2014 Phys. Rev. Lett. 113 250601
- [34] Horowitz J M and Parrondo J M R 2013 New J. Phys. 15 085028
- [35] Elouard C and Mohammady M H 2018 Recent progress and outlook *Thermodynamics in the Quantum Regime* vol 195 (Springer) pp 363–93
- [36] Suomela S, Solinas P, Pekola J P, Ankerhold J and Ala-Nissila T 2014 Phys. Rev. B 90 094304
- [37] Cavina V, Mari A and Giovannetti V 2017 Phys. Rev. Lett. 119 050601
- [38] Scandi M, Miller H J D, Anders J and Perarnau-Llobet M 2020 Phys. Rev. Res. 2 023377
- [39] Guarnieri G, Ng N H, Modi K, Eisert J, Paternostro M and Goold J 2019 Phys. Rev. E 99 050101
- [40] Fusco L, Pigeon S, Apollaro T J G, Xuereb A, Mazzola L, Campisi M, Ferraro A, Paternostro M and Chiara G D 2014 Phys. Rev. X 4 031029
- [41] Arrais E G, Wisniacki D A, Roncaglia A J and Toscano F 2019 Phys. Rev. E 100 052136
- [42] Bäumer E, Perarnau-Llobet M, Kammerlander P, Wilming H and Renner R 2019 Quantum 3 153
- [43] Janyszek H 1986 Rep. Math. Phys. 24 11
- [44] Crooks G E 2007 Phys. Rev. Lett. 99 100602
- [45] Diana G, Bagci G B and Esposito M 2013 Phys. Rev. E 87 012111
- [46] Zhen Y-Z, Egloff D, Modi K and Dahlsten O 2021 Phys. Rev. Lett. 127 190602
- [47] Van Vu T and Saito K 2022 Phys. Rev. Lett. 128 010602
- [48] Zhen Y-Z, Egloff D, Modi K and Dahlsten O 2022 Phys. Rev. E 105 044147
- [49] Ma Y-H, Chen J-F, Sun C P and Dong H 2022 Phys. Rev. E 106 034112
- [50] Scandi M, Barker D, Lehmann S, Dick K A, Maisi V F, and Perarnau-Llobet M 2022 arXiv:2209.01852
- [51] Esposito M, Kawai R, Lindenberg K and Van Den Broeck C 2010 Phys. Rev. E 81 041106
- [52] Erdman P A, Rolandi A, Abiuso P, Perarnau-Llobet M and Noé F 2022 arXiv:2207.13104
- [53] Rotskoff G M and Crooks G E 2015 Phys. Rev. E 92 060102
- [54] Rotskoff G M, Crooks G E and Vanden-Eijnden E 2017 Phys. Rev. E 95 012148
- [55] Louwerse M D and Sivak D A 2022 J. Chem. Phys. 156 194108
- [56] Janyszek H and Mrugala R 1989 Phys. Rev. A 39 6515
- [57] Feldmann T and Kosloff R 2003 Phys. Rev. E 68 016101
- [58] Varizi A D, Cipolla M A, Perarnau-Llobet M, Drumond R C and Landi G T 2021 New J. Phys. 23 063027
- [59] Polkovnikov A 2005 Phys. Rev. B 72 161201
- [60] Dorner R, Goold J, Cormick C, Paternostro M and Vedral V 2012 Phys. Rev. Lett. 109 160601
- [61] Deffner S 2017 Phys. Rev. E 96 052125
- [62] Sachdev S 2011 Quantum Phase Transitions 2nd edn (Cambridge University Press)
- [63] Mandal D and Jarzynski C 2016 J. Stat. Mech. 2016 063204
- [64] Sgroi P, Palma G M and Paternostro M 2021 Phys. Rev. Lett. 126 020601